19/1/95
18.13.
5/2/96-20.59.
3/2 16.59

ProQuest LLC.
789 East Eisenhower Parkway
P.O. Box 1346
Ann Arbor, MI 48106 – 1346

PREDICTION OF THERMAL STRESS AND STRAIN GENERATED DURING THE QUENCHING OF LOW-ALLOY STEEL

COLIN ANDREW LEWIS

A thesis submitted in partial fulfilment of the requirements of the Council for National Academic Awards for the degree of Doctor of Philosophy

December 1990

Sheffield City Polytechnic in collaboration with AERE Harwell

ABSTRACT

The free edge of a quenched plate is subject to zero stress in a direction perpendicular to this edge. Therefore the thermal stresses set up in such a component must be modified in the vicinity of the edge in order to allow the required stress configuration to be produced. This is referred to as the 'edge effect' and its magnitude is conventionally estimated by the well-known Saint Venant Principle. However a detailed understanding of the variation in stress in such a specimen is not well understood and it has been the objective of the present programme to make a detailed elastic/plastic analysis of the stress generation process using a finite element method. To this end a disc specimen has been considered, so that both experimental and theoretical estimates of the stress fields are not influenced by the presence of sharp corners, which lead to a very complex stress system.

The stress generation process has been followed by a finite element axisymmetric model. The use of such a plane strain representation has been checked by comparison with a full 3 dimensional elastic analysis, at a very early stage in the process when plastic flow was not present. The results obtained by the two methods of calculation were in good agreement and justify the use of the plane strain model.

The finite element programme calculated the thermal history of the specimen by the Crank-Nicholson method, and the weighted mean technique was selected as the best method of smoothing the results. The effects of different element stress functions, and element size, as well as time and load steps have been studied and the optimum combination selected. Considerable difficulty had been experienced with the stability of the results, which was found to be due to limitations in the BERSAFE finite element package. The elimination of this problem led to a situation where successive stages in the stress generation process were calculated and examined with confidence, although great care was required to balance the time step with the thermal loading step.

The results from this model in the central region of the plate were in good agreement with those results reported by earlier workers.

The complex variation of stress distribution predicted by the model as the free edge is approached has been examined and justified against the classical governing equations. This includes non-linear decay of in-plane stresses and the development of axial and shear stresses near the edge of the plate. A further product of this work has been an evaluation of the development of plastic zones during the quench process.

Although the effect of the edge on the inplane stresses differs with axial position in the plate, the derivation of an overall edge correction factor (which is a mean ratio of average stress to the stress on the axis) provides a value which is consistent with the Saint Venant Principle. Therefore, it is concluded that the use of edge correction factors based on the linear decay of in-plane stresses from a position that is one plate's thickness from the edge is satisfactory for determining "real" body stresses from a finite difference model.

ACKNOWLEDGEMENTS

The author wishes to record his appreciation and thanks to Sheffield City Polytechnic and especially to Dr. A.J. Fletcher under whose direction this research was completed. Further thanks are extended to Dr. B. Hudson of AERE Harwell for his external supervision. Gratitude is also given to the personnel of the Rutherford and Appleton Laboratory Finite Element Group for their considerable help and assistance, as is appreciation for the helpful discussions with Dr. T.K. Hellen of the C.E.G.B. Reasearch Laboratories. Additional thanks is given to British Aerospace Space Systems Limited for support in the final preparation of this thesis. Lastly, but by no means least, my everlasting gratitude is given to my wife and family for their help and patience.

C O N T E N T S

1. INTRODUCTION

1.1 GENERAL

Residual thermal stress and strain is of importance to manufacturing processes where the use of a quenching operation is necessary to achieve particular physical and structural properties of a component. The thermal gradients and phase modifications which transpire when using liquid/gas quenchants or induction hardening techniques cause displacement within the component and thereby produce accumulative stress and strain which is retained in the structure at the end of the treatment. Invariably this state of internal stress/strain can lead to one or more of the following problems, depending upon the severity of quench and composition of material:-

(a) If the accumulative stress reaches that of the material's fracture stress, quench cracks may be formed either during or within a short period after the hardening process.

b) The bulk straining of the material causes varying degrees of distortion of components and as such can cause great difficulty in achieving critical dimensional tolerances.

(c) Even if cracking and gross distortion do not occur, the retained stress pattern within a part can cause further displacement and warping if that part undergoes selective machining after the hardening process. This is because the stresses must accommodate the loss of material which contained balancing forces and thus restore equilibrium.

(d) The residual stresses present in a component may change its in-service properties; e.g. surface tensile stresses can contribute towards the susceptibility of stress

corrosion cracking; also the stress magnitude and nature will modify the mean stress fatigue level of a component which may be for the good or detriment of the article depending on the form of dynamic loading applied during service.

The assessment and rectification of such problems in industry (e.g. the case carburising of automotive gears) is still based upon trial batch determinations. These trials indicate the required adjustments to either component dimensions and/or treatment parameters to achieve a satisfactory post treatment article. Unfortunately such practical assessments are time consuming, costly and rarely yield results which can confidently be applied to a full production run. This unreliability may be attributed to the large number of variables which contribute in a complex manner to the final stress distribution and which may alter during the time span of a manufacturing process.

If the manifestation of significant residual stresses and the accompanying effects can be theoretically predicted, this would save time and costs, increase yield and ultimately ensure an increased service life for components. The limiting factors for a theoretical prediction of internal stress are (as for the production method) the multiplicity of variables which in many cases are highly sensitive to the sample preparation and testing environment; yet the most difficult problem is encountered in obtaining accurate mechanical and physical property data of the material for a wide temperature range. Because most physical properties are temperature dependant, large quantities of data have to be experimentally determined which are not readily available due to such criteria being unique to a material of that particular composition.

These difficulties have, in the past, led to the formulation of theoretical models which are over simplified; but with the efforts of previous workers in providing much of the property

data and with the advancement in fast digital computers which can manipulate vast quantities of information, solutions with a sound fundamental basis are now possible for residual stress predictions.

In the development of recent theoretical models for residual stresses it had been necessary to eliminate some complicating factors without actually over simplifying the material behaviour; this was accomplished by modelling an air-hardenable material in the shape of a thin plate, which allowed the valid assumptions of plane stress conditions and a 100% Austenite/Martensite transformation on quenching. The model was then used to calculate internal stress in the 'infinite' plate region (remote from any edge effect) by a finite difference technique. The present work on modifying this model, which is detailed in this thesis, is to incorporate the influence of the plate's edges, and hence approach a more realistic mechanical situation. The classical approach to taking account of stress in the region of a free surface is defined by Saint Venant's Principle, which in its present form is an empirical statement that does not give detailed explanations for principle and shear stress re-distribution or generation in the area of interest.

The finite element technique which allows surface boundaries to be specified in 3 dimensional space, has been used for modelling the structure and validation of this model will be made by comparison of results for the centre of the plate against those from the finite difference solution and experimental determinations.

1.2 LIST OF SYMBOLS

Definitions of mathematical symbols are given below, and are consistant throughout the thesis unless redefined within the text or by reference to figures.

M_s, M_f = Start and finish temperatures of the martensite transformation.

X,Y,Z = Cartesian axes. (also used as subcripts)

u,v,w = Displacements in the cartesian axes.

r,H,z = Radial, hoop and axial directions in polar axes (also used as subscripts).

δ, σ = Principle Stress.

ε, ϵ = Principle Strain.

τ = Shear Stress.

ν = Poissons ratio.

E = Youngs modulus.

Δt, δt = Time increment.

θ, T = Temperature.

n = Order of diffraction)
λ = Wavelength) Barrett[20]
d = Interplanar distance)
θ = Bragg angle)

l, m, n = Direction cosines

$\sigma_{1(z_i)}$ = Corrected stress value)
$\sigma_{1m(z_i)}$ = Measured stress value)
z_i = Distance from lower surface to point of measurement) Kirk[24]
H = Original sample thickness)
dz = Thickness of layer removed)

$\sigma_x(z)$ = Actual residual stress in layer)
$\sigma_X(z)$ = Apparent residual stress in layer)
z = Layer thickness) Dai and Sato[25]
h = Plate thickness)
γ = Distance of layer from surface)

$\Delta\theta$ = Angular deflection)
S = Initial arc length of plate) Rai et al[28]
a = Layer thickness)

σ' = Mean stress of removed layer)
f' = Cross section removed)
f = Cross section remaining) Barrett[20]
Δl = Change in rod length) (Heyn & Bauer)
l = Original rod length)
d = Diameter of bore at step considered - Ford[30]
Δ_n^m = Correction of stress in nth layer due to previous removal of mth layer)
t = Plate thickness before removing nth layer) Andrews[4]
Δz = Layer thickness)
$\Delta e_x, \Delta e_y$ = Change of inplane strain after layer removal)
K_1, K_2 = Strain gauge constants)
α = Direction of maximum stress from gauge element number one) Beaney et al[39]
Y = Plate length measurement)
ΔV = Volume change due to transformation) Price[49]
A,q,k = known constants of partial differential equation) Crank & Nicholson[50]
w = function of distance in the X axis)
Θ_i^n = temperature at point n after i time intervals.)
α = coefficient of expansion.) Fletcher[57]
h = surface heat transfer coefficient.)
λ = thermal conductivity.)
K = elastic bulk modulus.)
G = elastic shear modulus.) Weiner[65]
S = bounding surface.)

2. PREVIOUS WORK

2.1 INTRODUCTION

The definition of residual stresses has been given by several authors 1, 2, 3, 4, 5 and can be stated simply as: "those stresses existing in bodies upon which no external forces are acting". Working from this definition Orowan[1] gave a comprehensive classification of the many types of internal stresses that is essentially accepted today, but with inconsistency of names for the various classes. First order residual stresses (also known as body stresses or macro-stresses) are those which act over long range distances comparable to the magnitude of the body, second order stresses have influences within the range of crystal dimensions, whereas third order stresses act only within interatomic distances. The latter two classes are frequently referred to as micro or tessellated stress, examples of which have been discussed by Laszlo[6] and Denton[2], e.g. principal textural inhomogeneities such as grain boundaries, dislocation glide and preferred orientation will give rise to micro-stress, as will structural transformations where there is a mismatch between parent and product lattices; also the third order residual stresses occur wherever solute atoms are straining the lattice.

It is generally accepted that the source of first order stresses which occur when quenching (as opposed to fabrication and machining processes) arise from three combined causes[7,8]:-

a. Thelning[3] shows the difference in cooling rate between the surface and centre of a 100mm diameter steel bar quenched from 850°C (Fig 2.1). This temperature difference within the body is the root cause of thermal stress generation and consequently the first step in any prediction must be an accurate calculation of the transient thermal history.

As a direct consequence of thermal gradients the differential contractions which take place in adjacent sub-layers of the body give rise to stress as equilibrium is maintained. The thermal elastic stresses generated by the temperature gradient in Fig. 2.1 are shown in Fig. 2 (curve a). Obviously the magnitude of these stresses are directly dependant on the material's coefficient of linear expansion.

b. If the stresses attained within a body exceed that of the yield stress, plastic deformation occurs[3,4]. This has the effect of leaving permanent strain within the material, even when its temperature has stabilised at ambient throughout the section (Fig. 2.2, curve c). This plasticity effect occurs most readily during the early stages of the quench whilst the high temperature yield stress is comparatively low. Orowan[1] and Denton[2] have made reference to the Bauschinger effect which implies that macro-stresses and textural micro stresses are inseparably inter-related, i.e. the deformation of grains during first yielding would change the yield characteristics of the material if reverse loading should occur at a later time.

c. The object of quenching a material is essentially to produce a hardened structure by causing an allotropic modification. The nature of phase transformation is bound to give a change in specific volume[9,10], which will generate stress from the interfacial boundary and give an overall dimension change. Although this is more correctly specified as transformation stress, it is produced under conditions where thermal contraction stresses are bound to arise, hence both may be referred to collectively as thermal residual stress[11]. The extent and complexity of residual stress created through transformation depends on both the constituent elements in the material and the rate of cooling, i.e. hardenability.

Thelning[3] shows how inherent hardenability influences the structures formed (Fig. 2.3); more than one phase is produced in many cases, and will have differing mechanical and physical properties. An example showing the effect of hardenability on residual stress has been given by Nelson et al[12] who case hardened plain carbon, boron and manganese steels; it was found that residual stress became more compressive as case depth increased (Fig. 2.4), although it was not understood if this effect was due to the volume ratio of phases present or the change in hardness gradient between case and core. The dimensional changes which accompany phase transformations can be readily observed by dilatometry experiments[10]. Figure 2.5 indicates that on fast cooling from austenitic temperatures there is an expansion occuring between the M_s and M_f temperature of the material.

If we consider the generation of thermal stress in a semi-infinite body, it will be noted that when superimposing the contribution from the above mentioned sources, the resulting stress may be entirely changed in nature and hence make the prediction of residual stresses a most difficult problem. Initially the temperature gradient in the body will give rise to tensile elastic stresses at the surface balanced by compressive elastic stresses in the core as the outer regions attempt to contract to a greater extent than the inner. As the temperature gradient becomes steeper, the yield stress of the material is exceeded and the centre and surface of the body plastically deform to give permanent strain[4]. At lower temperatures the stresses unload and eventually reverse, due to the increase in the rate of cooling at the centre relative to the surface. When the surface temperature falls to that of a transformation start, the specific volume increase effectively tries to expand this material to a greater degree than the thermal contraction so that the surface is placed in compression whilst the stress in the inner untransformed material becomes tensile. Plasticity can still occur at this stage but is more difficult due to the lower temperature yield properties of

the austenitic material and the very high yield point of the transformation product. In most cases by the time the centre of the body has cooled to the transformation temperature, the surface has completed its volume phase change and is again subject to a thermal contraction, thus when the centre transforms, its volume increase is constained and gives yet another stress reversal; the stress is now tensile at the surface and compressive in the centre.

Because thermal residual stresses are self equilibrating the stress distribution is usually symmetrical about the centre of the body: thus the relative magnitude of the stresses are dependant on the distance between this centre and a free surface[12] (Fig. 2.7). Buhler and Rose[14] have shown that a 10 mm diameter bar will have both a smaller temperature difference between its centre and surface, and a much shorter cooling time than a larger bar (Fig. 2.8A). This will affect the magnitude of the thermal stress generated during quenching and the transformation products which may also be expected to complicate the stress analysis. Therefore the geometry of a body, or more specifically its free surfaces, are considered to be of great importance[9]. The modification of the stress pattern is not only dependent on the specimen thickness, but also by the proximity of free surfaces in the other planes, e.g. the edges of a plate. Certain stress components within the body must reduce to zero as they approach a free surface to which they are perpendicular; this boundary condition invariably means a complex redistribution of the other component stresses, which as yet have not been examined.

Even when thermal stress generation is completely understood, there will be limits to the amount of control that may be exercised over this process, hence quenched material will still contain residual stress and strain. However post quenching and hardening processes are available[13], such as stress relief anneal, tempering and controlled plastic deformation, although these can only be applied to bodies

which have not undergone severe distortion or have not suffered quench cracking due to a grossly high stress level.

At the present time, when the stress generation process is imperfectly understood, theoretical studies are still of limited practical value and most industrial methods of studying this phenomenon are empirical. This review will therefore begin with a description of this empirical work, before going on to consider the details of the theoretical model of the stress generation process.

2.2 METHODS OF DETERMINING INTERNAL STRESS EFFECTS DUE TO HEAT TREATMENT AND SUBSEQUENT QUENCHING

2.2.1 Observation of Quench Cracks

In 1947 Thompson[9] realised that the size of a specimen markedly affected the tendency for quench cracking to occur. With large cross-sections, the surface residual stresses (or even transient stresses) could exceed that of the material's ductile limit, and might possibly contribute to premature martensite formation through the thermo-mechanical effect. Martensite lacks any appreciable ductility and once formed will be very sensitive to a further increase in thermal strain. Thompson argued that this is the most probable cause of quench cracking because at and around the fissures the breakdown of austenite has proceeded appreciably further than in the main body of the sample.

The first efforts to produce a standard specimen for measuring the quench crack sensitivity of steels were made by Chapman and Jominy[15] in 1953. After several attempts based upon specimens used for distortion measurements, they found that a test piece machined to the specifications shown in Fig. 2.8B, gave almost consistantly reproduceable results when specimens of SAE4340 steel were cracked, provided extreme care was taken in machining the notch. Other steels were then tested by the following procedure:-

a. Hold test specimen at an austenitising temperature long enough to eliminate any temperature gradient.

b. Quench into agitated oil or salt solution, with the thin section down.

c. After cooling, rough polish and examine for cracks at x50 magnification. Also carry out several Vickers hardness tests on the specimen.

d. Re-examine microscopically for cracks and repeat the hardness measurements.

In general the reliability of these tests were good, although in some instances specimens cracked whilst identical ones did not. In defence of this behaviour Chapman and Jominy stated these tests to be borderline cases, which were on the verge of cracking. The results gained from these experiments led to the following conclusions:-

a. The presence of non-metallic inclusions, through their effect as stress raisers, undoubtedly contribute toward cracking susceptability.

b. Quenching from a higher austenitising temperature is more likely to form cracks, although this finding is in direct conflict with the results of Jackson and Christenson[16]. It is suggested that the higher temperature gives a greater concentration of carbon in austenite which depresses the M_s temperature, thereby causing the transformation to occur under less ductile conditions. It is also probable that a greater thermal gradient produces a shallower rim of surface martensite whose low thermal conductivity would deter cooling of the core and thus generate sufficiently high thermal stresses to cause fracture.

c. Depending on the carbon content of an SAE steel there is a particular temperature below which a martensite transformation start will produce cracking. Therefore as the M_s temperature falls, lower carbon is necessary to prevent a failure, i.e. by reducing the amount of specific volume change even if this causes the introduction of other transformation products.

Essentially these conclusions mean that the ideal conditions to avoid quench crack problems require the use of low carbon steel with a high M_s temperature, which has been austenitised at a relatively low temperature.

An assessment of quench crack occurrence was undertaken by Kobasko et al[17] in 1970, and although a study of the effect of cooling rate during transformation was the major objective no attempt was made to explain the physical mechanisms which led to cracking. Small discs, cylinders and combination test samples of Si/Mn/S/P steels were quenched from 850°C into various media (hot, warm and cold water; saturated NaCl solution; a 12% NaOH solution) to achieve different cooling rates. The cooling rates during these tests were determined by differential thermocouples welded in the centre and at the surface of the samples. Quenching results were presented as a probability of distribution for cracking against the cooling rate measured at a core temperature of 350°C. The probability of cracking was determined from the ratio of the number of samples with cracks to the total number of samples. In the case of the cylindrical samples, the greatest probability of quench cracking was found to occur at a cooling rate of 300-350°C/sec, whilst undergoing transformation. Geometrical dependence of this probability was noted because a shift in the distribution curve was found when the specimen shape was changed, and the morphology of cracks in disc specimens were of the tangential type whilst in the cylinder/disc combinations cracks first appeared in the axial plane.

In a later paper Kobasko[18] suggests that quench cracks and self deformation may be considerably reduced by raising the temperature range of nucleate boiling so that transformation occurs as convective heat transfer begins, thus allowing the high thermal stress generation to take place whilst the structure is still predominantly supercooled austenite. The specimen surface during nucleate boiling is described by Kobasko as undergoing a "self-regulating" thermal process, i.e. it virtually remains at a constant temperature equivalent to the saturation temperature of the quenching medias. This may be disputed because it can be shown that the surface heat transfer coefficient is at a maximum during nucleate boiling (see below), and it may well be that this process has been confused with that of the vapour blanket stage. Nevertheless he has shown that by a change in the pressure of the quenchant it is possible to raise or lower the surface temperature of the test piece and consequently suppress or accelerate phase transformations. An increase in pressure will decrease the occurence of quench cracks.

The hoop cracks observed by Toshioka et al[19] were attributed to insufficient ductility in the radial direction. This again can be justified by the stiffness of martensite which is unable to accommodate high thermal strains which can be induced after transformation.

In the review of the previous work on quench cracking, there appears to be a consensus of opinion that to prevent this form of failure the nucleate boiling stage of cooling should be completed before transformation so that the stresses created by steep thermal gradients are absorbed by the much softer austenite, but that the change to convective heat transfer and the start of the transformation should be almost simultaneous and at a sufficiently high temperature for the martensite properties to withstand the volume change associated with its formation.

2.2.2 X-Ray Diffraction Techniques

It has been recognised since the mid 1920's that X-ray diffraction examination of materials which are under strain exhibit results which are peculiar to that form of structural distortion. A series of review papers by Barret[20] in 1934 gives a qualitative summary of various X-ray diffraction effects which have stemmed from internal stresses. All the effects are dependant on the diffraction of an X-ray beam at a specific angle by crystallographic planes according to the Bragg equation, $n\lambda = 2d \sin\theta$. There are sufficient differences in the methods to warrant a brief resume of each type.

a. The Laue method uses a heterogeneous beam of X-rays which are diffracted by a thin crystalline specimen, and the diffracted beams which emerge are registered on a photographic film or plate, which will show an array of "Laue spots". If the crystal is bent to cause internal strain, it provides a varying angle of incidence of the X-ray beam on the atomic planes, and this results in a spectra forming from the different wavelengths in the primary source. This effect may be clarified by the otpical analogy of reflection from curved mirrors and thus emphasises that the Laue method registers strains by virtue of the changes in orientation of reflecting planes. The characteristic appearance of a photogram from a bent crystal is of spots which are spread radially and constitute an "asterism". The magnitude of asterism is dependant on the size of spot struck by the X-rays and the degree of straining; it is rarely observed when the strain lies in the elastic range but a small amount may be caused by a reduction in lattice symmetry through non-uniform elastic shear, so great care should be taken in analysing results. It is during plastic deformation that the significant changes in crystal orientation take place which develop the asterism.

b. If the X-ray beam used in the analysis is monchromatic and the specimen used is polycrystalline the photographic pattern formed will be a series of rings. These rings are composed of adjacent spots which are produced by diffraction in singular grains. If grains are bent or rotated about the incident beam axis, the corresponding spots on the Debye rings will be elongated peripherally the full length of the Laue streak. Below the elastic limit of the specimen this peripheral widening is indicative of the internal stress, but, should this limit be exceeded the increased widening is then only representative of the distortion. It was found that a linear relationship exists between the peripheral width of spots and strain up to 40% of the latter. This method was proposed as a quantitative measurement of deformation, but is was necessary to calibrate the camera by applying known stresses to the material under the same temperature condition in which it was to be used, for the method could not measure stress directly. Using large specimens meant the diffracted Debye rings could only be registered by back reflection, and at this point it became clear that the results would only correspond to the surface layers penetrated by the incident beam. Even so, Regler made unsubstantiated claims of great accuracy for this technique, i.e. stress measurements of ± 1 N/mm^2. The major problems with peripheral spot widening analysis are that the results correspond to microstress rather than macro; no effects of biaxial stress have been considered; and with only surface penetration triaxial distributions of stress cannot be found.

c. Consideration of spot widening may be developed to include the whole Debye rings. An homogenously stressed specimen would show an overall line shift, but if this stress distribution is microscopically inhomogenous there will be a variable shift and a resultant line widening.

Unfortunately this phenomenae is, like the spot widening, so sensitive to micro stresses that little relation can be made to body stresses.

d. The most direct X-ray method for stress measurement is that employing the overall shift of diffraction lines. If all the reflecting grains are similarly stressed, the diffracted rays from all of them will superimpose to produce sharp lines displaced from their normal unstressed positions. The diffraction pattern of the interatomic spacings then becomes a strain gauge which measures macroscopic strains. When this idea was applied to a variably loaded steel ribbon in a forward reflection camera, the average reading for six diffraction lines showed a linear relation of interplanar distance to stress. Since the reflecting planes were approximately perpendicular to the direction of applied stress the change of interplanar spacing was approximately equal to the longitudinal strain. For bulk specimens, this experiment was repeated in a back reflection camera where the reflecting planes were parallel to the specimen surface and not perpendicular to the principal stress. The calculation of strain in this situation considered the principal beam to be in the z cartesian direction and the uniaxial tensional stress, σ_x, to be along the x axis. The strain in the Z direction was given by:

$\varepsilon_z = \frac{-\nu}{E}\sigma_x$, where ν was Poissons ratio and E was Youngs modulus, and the strain measured by the X-ray diffraction line shifts in the same direction was given by:

$$\varepsilon_z = \frac{d - d_o}{d_o}$$, where d_o = unstressed interplanar spacing

d = stressed interplanar spacing

Hence the macro stress, σ_x may be determined. Certain corrections were required in the calculation of the ε_z strains from the photogram, because in practice it is more convenient to place the X-ray beam at a slight angle to the specimen surface, and as can be seen it was also

necessary to know the interplanar spacing (d_0) for the unstrained condition. This may be readily achieved by removing the load if only externally applied forces are under consideration, but if residual stresses are to be examined d_0 can only be found by testing an annealed sample. To achieve any reasonable level of accuracy by the shifting of lines method the precision of determining interplanar spacing must be very high, because an error of ± 0.0001 Å in the latter will give an error of approximately ± 90 N/mm² in the former. This is known as the single exposure technique.

In 1966 a review of residual stress determination by Denton[2], follows the development of the line shifting X-ray technique. Using the previous position of the sample in the cartesian co-ordinate system, if it is accepted that plane stress conditions are observed at the free surface, the elastic strain normal to the surface is:-

$$\varepsilon_z = -\nu \frac{\sigma_x + \sigma_y}{E}$$

hence the sum of the principal surface stresses is given by:

$$\sigma_x + \sigma_y = -\frac{E}{\nu} \left\{ \frac{d_1 - d_0}{d_0} \right\}$$

A generalised set of equations have been given by Denton[2] and Andrews[4] for the state of principal stress and strain. These equations are derived from the ellipsoid of stress shown in Fig. 2.10, and are based on the direction cosines 1, m and n;

$$\sigma = l^2\sigma_1 + m^2\sigma_2 + n^2\sigma_3$$

$$\text{and} \quad \varepsilon = l^2\varepsilon_1 + m^2\varepsilon_2 + n^2\varepsilon_3$$

where $l = \sin\psi \cdot \cos\phi$, $m = \sin\psi \cdot \sin\phi$ and $n = \cos\psi$. For the surface conditions put $\sigma_3 = 0$ and $\phi = 90°$, the combination of these two equations and substituting l, m, n, ε_1 and ε_2 in terms of the principal stresses gives:

$$\sigma_\phi = \frac{d_\psi - d_{z1}}{d_{z0}} \cdot \frac{E}{1 - \nu} \cdot \frac{1}{\sin^2\psi} \qquad \text{.....2.1}$$

A simplification may be made to reduce the unknowns in this equation, by which d_{x0} (the unstrained lattice spacing) is put equal to d_{z1} (strained), which will cause the loss of little accuracy and allows an analysis on an annealed specimen to be dispensed with. This technique is known as the Two-Exposure method, because to determine the stress in a specific direction of the surface (say $\phi = 30°$) a perpendicular exposure will give d_{z1} and an oblique exposure (say $\psi = 45°$) will give d_{ψ} which provides the equation unknowns required to calculate σ_{ϕ}. If three arbitrary σ_{ϕ} values are found, the direction and magnitude of the principal stress may be determined from elasticity theory.

The "two exposure" equation was modified by Donachie and Norton[21] who compared the results from stressed and unstressed samples to see if there was any difference in their refracting powers. For an error of ± 10% they proposed that σ_{ϕ} could be calculated from a stress constant K and the change in the Bragg angle $\Delta\theta$;

$$\sigma_{\phi} = \frac{E}{1 + \nu} \cdot \frac{1}{\sin^2\psi\tan\theta} \Delta\theta = K\Delta\theta$$

Due to large errors it was considered that for reliability, the standard two-exposure equation (2.1) should be used because it made no assumption of K equality between a stressed and unstressed specimen.

A more reliable change to equation 2.1 was previously proposed by Hawkes[22]; this was based upon the substitution of the interplanar spacings by sin θ functions (permissable from the Bragg equation) to give:

$$\text{cosec } \theta_{\psi} = \sigma_{\phi} \left\{ \frac{1 + \nu}{E \sin \theta_z} \right\} \sin^2\psi + \text{cosec } \theta_z$$

As can be seen cosec θ_{ψ} is a linear function of $\sin^2\psi$, so that the gradient of the line plotted from several results will give the stress σ_{ϕ} when it is divided by the known factor in brackets. Obviously this will lead to greater

numerical accuracy because the results depend on measurement of the Bragg angles and not on a small difference in the interplanar change. This is known as the $\sin^2\psi$ technique.

Regardless of whether the single exposure, two-exposure, or sine technique is used the degree of accuracy attained relies on the operators ability to determine the exact position of the diffraction lines. It has been mentioned previously that crystallographic distortion causes line thickening of the Debye rings, so that the line positions used may be somewhat tenuous. To overcome this problem it has been concluded that the film method of recording diffracted X-rays must be discarded in favour of a diffractometer technique which has an electronic counter that locates exactly the peak intensity of a broad diffraction line[23]. Further sources of error noted by Denton are:-

a. although the X-ray penetration is very shallow it may still be deep enough to invalidate the assumption that there is zero axial stress

b. it is assumed that E and ν are constants whilst in reality they vary considerably with crytallographic direction.

The necessary use of a diffractometer in the stress determinations of hardened steels is re-affirmed by Kirk[24], who also states that such methods are quicker that the use of film and allow computer analysis of the data obtained. Although Kirk reiterates the theoretical foundations of the $\sin^2\psi$ and two-exposure techniques already given, he makes an important comment on the choice of reflecting planes from which results will be taken. If the Bragg equation is differentiated to give:

$$\Delta\theta = - \frac{\Delta d}{d} \cdot \tan \theta$$

the substitution of relevant values into this relationship will give a much larger $\Delta\theta$ for a big θ value than for a small

θ value when the lattice strain remains constant; therefore the best line shift results will be achieved using crystallographic planes that have a large Bragg angle. Reference is also made by Kirk to the problems of successively removing layers of material and performing step wise X-ray analysis to determine stresses in the interior of the specimen. The method of layer removal should not induce additional stresses, but it is recognised that the removal of material will certainly cause a redistribution of stress in the remaining body. The correction necessary to allow for this change was given for a rectangular plate specimen:

$$\sigma_{i(z_i)} = \sigma_{lm(z_i)} + 2\int_{z_i}^{H} \sigma_{lm(z)} \cdot \frac{dz}{z} - 6z_i \int_{z_i}^{H} \sigma_{lm(z_i)} \cdot \frac{dz}{z^2} .$$

Layer removal and diffractometer stress determinations have been performed by Dai and Sato[25] on longitudinal and transverse sections of band saw blades. They compared the results of an X-ray analysis of the back and front surface as the layers of material were successively removed from one surface. The few assumptions made are:-

a. isotropic properties

b. axes of principal residual stresses coincide with axes of symmetry, and

c. principal stresses are constant in each layer.

Comparison of their methods with measurement by a strain gauge (see section 2.2.3) showed very good agreement (Fig. 2.11). The main conclusion reached in this step-wise technique is that the front surface method has the advantage that it is able to obtain the residual stress on the initial surface directly with small errors, because the correction formulas have only integral terms unlike the back surface method which contains differential terms that may give a considerably larger error. Unfortunately the front surface

method requires a fine surface finish before analysis after each layer has been removed.

Stahlkopf and Egan[26] show that the single X-ray analysis technique is a very versatile method. The necessity to determine stresses within pipeworkings in the nuclear industry has led to the development of a portable X-ray rig which can test components in situ. Although this has been termed a single exposure technique, the determination of the 2θ angle of the Debye ring on both sides of the incident beam gave sufficient data to allow substitution into the double exposure equations.

Well into the mid 1970's the work on stress analysis by X-ray methods was still striving to obtain the factors which determine whether the measured strains are indicative of micro or macro stresses. Macherauch and Wolfstieg[27] give three good examples of alloys which show varying amounts of micro and macro stresses when examined using the $\sin^2\psi$ method. They suggested that the form of stress evaluated on a plastically deformed specimen depends to a large extent on the type of material and the amount of heterogeneity.

The past work performed on X-ray residual stress measurement has shown it to be a versatile instrument in this field of analysis, particularly if only surface stresses are required and the technique must be non destructive. As shown, there are several ways in which the measurement may be made, each based upon sound mathematical solutions, but the major problems which have to be realised are:

a. the interpretation of the class of stresses measured, and

b. the introduction of errors by the method of layer removal, if sub-surface analysis is required.

The latter problem is not confined to X-ray techniques but also applies to the mechanical methods, and as such will be discussed in greater detail in the following section.

2.2.3 Material Removal Methods

During the review of X-ray stress analysis methods, reference to layer removal has been made as a means by which the variation of stress through the section may be measured. In those particular cases the removal of material was purely a means of disclosing sub-surface points, yet in fact it constitutes a whole branch of residual stress analysis. The action of removing material causes a redistribution of stress and strain to accommodate the lost body forces and hence maintain equilibrium. This redistribution of stress leads to a distortion of the remaining body which is related to the stress in the removed layer, and may be measured by either resistance strain gauges or optical equipment. It is therefore necessary to consider the various methods of layer removal, along with their relative attributes and mathematical development.

2.2.3.1 Electrolytes and Chemical Etchants

Preliminary comments made by Barrett[20] on the uses of chemical etchants for material removal urged caution due to the possible lack of uniformity in the reaction and the possibility of a weakening of the underlying structure by the acid attack. These reservations were also made by Denton[2], but he pointed out that the attraction of such a stress-free method had prompted other authors to use it, with encouraging results when a weak (10%) acid solution was employed. Comparable results were also obtained by electrolytic etching of copper samples in a phosphoric acid.

Although Dai and Sato[25] used X-rays for their primary analysis technique, they also removed material in a step-wise procedure with a H_3PO_4/CrO_4 electrolyte which produced a

surface finish within one micron roughness and free of oxide films. Selective removal was achieved by masking with laquer. It is possible by this method to have a continuous assessment of the stress profile, e.g. the rate of material lost at any time is known from the electrolysing parameters, and any curvature produced from the plate can be measured by a telescope and mirror arrangement, with the latter connected to the sample. A comparison is given in this paper of the derivation of actual stress from the amount of material removed at various points; the final equations for principal residual stress being:

a. Stress determination at new surface

$$\sigma_x(z) = \sigma_x(z) + 2\int_0^z \frac{\sigma_x(\zeta)}{h - \zeta}\, d\zeta$$

$$- 6(h - z)\int_0^z \frac{\sigma_x(\zeta)}{(h - \zeta)^2}\, d\zeta$$

b. Stress determination at opposite side of plate to the layer removal

$$\sigma_x(z) = \frac{-(h - z)}{2} \cdot \frac{d\delta x}{dz} + 2\delta x$$

$$- 3(h - z)\int_0^z \frac{\delta x(\zeta)}{(h - \zeta)^2}$$

These derivations were based upon variations of stress components within the plate produced by membrane forces and bending moments caused by the removal of stressed layers; it should be noted that the removal of material containing a positive stress gives a compressive stress at the back surface.

Further work on the layer removal method incorporating electrolytes was performed by Rai et al[28] on 2.5 mm thick mild steel plates. By relating the angular deflection to a change in radius of curvature of the remaining plate, the following equation was proposed for the average stress (σ) in a removed layer of thickness (b):

$$\sigma = \frac{E.b^2.\Delta\theta}{b.S.a}$$

The results obtained from this experiment are shown in Fig. 2.12, but Rai has not compared them with those for other techniques or even assessed the experimental/mathematical sources of error. Although it was remarked that compressive residual stresses of the same magnitude as the materials yield stress were found, no attempt was made to explain the stress profile.

It has been proposed that surface residual stresses in ultra-high strength steels may be quantitatively examined by etching in a variation of Fry's re-agent[29]. This re-agent produces characteristic furrows in the metal, which run approximately perpendicular to the direction of the tensile surface stresses. The furrow spacing varies according to the magnitude of the stress. It is thus stated that once the etching process has been calibrated for a material, complex etch patterns can be analysed and residual stresses mapped out in direction and magnitude. As yet the mechanisms of "stress etching" are not fully understood and it has been applied mostly within the fracture mechanics field.

2.2.3.2 Mechanical Techniques and Modified Sachs "Boring Out".

In the first of the abstracts by Barrett[20] a good outline is given to the development of mechanical stress analysis techniques up to the mid 1930's. The different methods fall into two basic categories of measurement:

a. Measurement of the dimensional change to a body when material is removed from a specific area

b. Measurement of the bending of a strip when it is cut from the object.

Methods in (b) above require the cutting of a "tongue" from a tube or parting off and splitting of a ring, and depend upon the measurement of the change in radius of curvature to give an indication of the elongation and compression of surface

fibres. Unfortunately stresses calculated in this way have been found to be inaccurate and not easily reproduceable. The early methods which fall into category (a) assumed either radial and tangential or only axial stresses in rods and cylinders. One such method is to turn concentric rings from a tube and then calculate σ_r and σ_H by using elasticity theory and the change in the diameter of each ring. If the ring expands, it is under compressive stress whilst still part of the tube.

Barrett described the Heyn and Bauer experiment as the first of the layer removal techniques by which successive layers were turned from a rod and at each stage the removed stresses in the axial direction were mainfest by the change in the rod length (all other stresses assumed zero) to achieve equilibrium. The governing equation in this instance was:

$$\sigma' = E.\frac{f}{f'}.\frac{\Delta l}{l}$$

Where σ' = Mean stress of removed layer

The previously mentioned examples and others[20, 30] are specialised cases of a more generalised technique of layer removal developed by Sachs. The Sachs boring out technique as described by Barrett[20] and Ford[30] includes the following method:

The unit longitudinal strain $\lambda = \frac{l - l_i}{l_i}$ and the unit circumferential strain $= \frac{D - D_i}{D_i}$ are plotted against the cross-sectional area A, of the remaining metal, and a smooth curve drawn through the points.

If $A_i = \frac{\pi D_i^2}{4}$ $\quad A = \frac{\pi}{4}(D_i^2 - d^2)$

$\psi = \lambda + \nu\delta$ and $\theta = \delta + \nu\lambda$, then

(1) Longitudinal stress at diameter D

$$\sigma_l = \frac{E}{1 - \nu^2} \{(A_i - A)\frac{d\psi}{dA} - \psi\},$$

(2) Circumferential stress at diameter D

$$\sigma_c = \frac{E}{1 - \nu^2} (A_i - A) \frac{d\theta}{dA} - \frac{(A_i + A)}{2A} \theta, \text{ and}$$

(3) Radial stress at diameter D

$$\sigma_r = \frac{E}{1 - \nu^2} \frac{A_i - A}{2A} \theta$$

where l_i and D_i = initial length and diameter of cylinder

l, D = length and external diameter

$\frac{d\psi}{dA}$ and $\frac{d\theta}{dA}$ are obtained by drawing tangents to the curves of ψ and θ versus A.

Typical results for internal stress in a cold drawn brass rod examined by the boring out method are shown in Fig. 2.13. Since no assumptions about a special type of stress distribution (i.e. plane stress) are made, the Sachs approach is more accurate and indicates that the earlier methods involve errors of up to 40%. The implicit assumptions of the Sachs method have been summarised by Denton[2] as:

1. The metal is effectively isotropic and has a constant value of Young's modulus and Poissons ratio.

2. The residual stresses are distributed with rotational symmetry about the axes of the bar/tube.

3. The tube formed by boring is circular in section and all wall surfaces are concentric.

4. The specimen is sufficiently long to prevent lateral bending.

Denton[2] also discusses the advantage of performing an analysis by half boring and half turning a specimen, so that extrapolation for the stresses in the remaining material which is too small to machine, will be between two known values.

The basic Sachs equations and technique have been modified by several authors such as Cepolin[31] and Andrews'[4], for specific applications. The former used the Sachs technique to determine residual stresses in a welded half inch thick plate of Hastelloy N steel, but the calculation considered the tangential and radial components only and assumed the geometry to be such that plane stress conditions occurred. The maximum tangential stress measured was of the order of 350 MN/m^2, and did not appear to be affected by variations in the heat input during welding. However such a conclusion may be questioned since the heat input affects thermal gradients and hence the thermal stress component.

Andrews'[4] modified the use of the Sachs equations in the determination of stresses in thin plates when material was removed from one surface and the changes in strain measured on the other. Since forces and moments must be in equilibrium and considering geometrical factors (Fig 2.14) he determined that the stress in each layer (corrected for previous layer removal) is given by: $\sigma_1 = S(1)$,

$$\sigma_2 = S(2) - \Delta_2^1, \quad \sigma_3 = S(3) - \Delta_3^1 - \Delta_3^2, \quad \sigma_4 = S(4) - \Delta_4^1 - \Delta_4^2 - \Delta_4^3$$

where

$$\Delta_n^M = \frac{\Delta\sigma x}{z_2}_m \cdot (z_1)_m - (n - m)\Delta z + \frac{\Delta \dot{z}}{2}$$

and

$$S(n) = \frac{\Delta\sigma x_n (t - \Delta z_n)^2}{(2t + \Delta z_n)\Delta z_n}$$

The subsiduary variables are found from,

$$z_1 = \frac{(t - \Delta z)(4t - \Delta z)}{6t}$$

$$z_2 = t - \Delta z - z$$

$$\Delta\sigma x = \frac{E}{1 - \nu^2} \quad (\Delta ex + \nu \Delta ey)$$

where, S(n) = stress in the n^{th} layer without correction

Few authors have used the Sachs method for investigating residual thermal stresses in thin plates, but the proposed modifications of Andrews have been followed by Price[11] who examined quenched EN30B material. The residual stress profiles he recorded for 20 mm thick x 120 mm square plates showed good agreement with predicted results in the case of a water quench, but the correlation was far from satisfactory in the use of oil quenched samples. Although it was noted that strain gauge "drift" was a difficult problem to overcome (because it is not possible to re-calibrate after the test has begun) other sources of error may well have had a much greater effect. Thus Price allowed 15 minutes lapse time between the grinding operation and the taking of readings from the strain gauge, so as to allow stabilisation of the system. However, according to Shreiber[31], not only does the test system require a settling period, but the test piece material needs a much longer relaxation to allow strain redistribution. Even though Shreiber's experiments were conducted on case hardened materials, and the layer removal was by electro errosion, he claims there was a considerable increase in axial stress with a corresponding decrease in tangential stress if the test samples were stored for up to 24 hours after a layer had been removed. This is unrealistically long, because it would take a very long period to deal with a specimen during which the gauge drift would invalidate the measurements.

Obviously grinding can be a very severe operation which induces residual stress in addition to those which are to be measured. Little comment is made about this problem in most

work on thermal stresses, apart from the usual caution that grinding parameters should be of a "gentle" nature. A more detailed assessment of this operation has been covered by several authors from an engineering stand point[32, 33, 34, 35].

There is strong evidence that stresses induced by grinding originate from thermal friction, burnishing and the cutting action of abrasive grains. The residual stress arising from thermal effects are of a tensile nature (up to 200 MN/m^2) and tend to be at a maximum perpendicular to the direction of wheel travel, whilst the burnishing effect only contributes an insignificant compressive component. By far the greatest contribution to the stress is induced by the cutting action of the grains, which causes a large compressive stress (above 400 MN/m^2 under normal grinding conditions) due to the necessary plastic loading. Because of the magnitude of the latter source of stress, the principal direction lying parallel to the travel of the wheel is compressive (up to 0.1 mm deep) with only small amounts of tensile thermal stress to either side in the perpendicular direction. Nowikowski et al[36, 37] have run large series of experiments to determine the optimum conditions for low stress grinding, which are:

1. Use a soft and open (H, I, J grades) grinding wheel which should be course dressed frequently to maintain sharpness.

2. The wheel speed should be as low as 700 m/min, whilst the table speed should not be slower than 16 m/min.

3. The down feed rate should be in steps of approximately 0.015 mm, reducing progressively to complete the layer removal with a step of 0.0025 mm.

4. The coolant fluid should be a highly sulphurised oil.

Only the last point is open to criticism from the point of view of residual stress determination. Dolle and Cohen[38] state that by using a mild coolant (oil rather than water) the heat created during machining can offset the compressive cutting stress by allowing dynamic recovery of dislocations.

2.2.3.3 Centre Hole Air Abrasive

In an attempt to overcome the adverse effects of layer removal by grinding, use is made of the 'centre hole technique[39, 40], which is based upon measurements of the redistribution of stress that occurs in the area immediately surrounding a small hole. The hole is bored in the centre of a strain gauge rosette (Fig 2.15) and consequently at this point the radial body stresses must fall to zero at the wall of the hole (Fig 2.16). Relaxed strains, which are the fundamental measurement of this method, depend on the hole depth, but these reach a maximum when the hole depth is equal to its diameter. Although millers and cutters are used to produce the hole, the relative size of the material removed makes this the least destructive mechanical method of residual stress determination, and from an industrial point of view, it can be used for the in situ testing of, for example, welds and bulk structures.

The equations which give the maximum and minimum principal stresses in the plane parallel to the strain gauge are:

$$\sigma \text{ max} = \frac{1.E}{k_1.2}\left[\frac{\varepsilon_1 + \varepsilon_3}{1 - \frac{\nu k_2}{k_1}} + \frac{1}{1 + \frac{\nu k_2}{k_1}}\sqrt{(\varepsilon_1 - \varepsilon_3)^2 + \{2\varepsilon_2 - (\varepsilon_1 + \varepsilon_3)\}^2}\right]$$

$$\sigma \text{ min} = \frac{1.E}{k_1.2}\left[\frac{\varepsilon_1 + \varepsilon_3}{1 - \frac{\nu k_2}{k_1}} - \frac{1}{1 + \frac{\nu k_2}{k_1}}\sqrt{(\varepsilon_1 - \varepsilon_3)^2 + \{2\varepsilon_2 - (\varepsilon_1 + \varepsilon_3)\}^2}\right]$$

Direction of σ max from gauge element one,

$$\alpha = \tfrac{1}{2} \tan^{-1}\left[\frac{2\varepsilon_2 - (\varepsilon_1 + \varepsilon_3)}{\varepsilon_1 - \varepsilon_3}\right]$$

The constant $\nu k_2/k_1$, which replaces Poisson's ratio, and the overall calibration factor $1/k_1$, which is dependent on the hole diameter for any particular gauge format, are determined by the use of a stress relieved sample in the externally applied uniaxial stress field. It has been found that the constant is in most cases a value of 0.3.

Unfortunately, when the hole is bored by cutters, reamers or drills, mechanical and thermal stresses are created that are similar to those found in the grinding process, giving errors of 10%. It has been found that the reliability of the results are susceptible to two other factors:

1. If the stresses present in the bulk material are greater than 50% of the yield stress, plasticity may occur at the hole edge and cause serious errors in the strain relaxation readings.

2. The governing equations are only applicable to an axisymmetric arrangement, so the hole must be perfectly concentric with the gauge. This makes the maintenance of hole alignment whilst machining very difficult.

The centre hole may also be produced by the air abrasive technique. Bush[40] and Beaney[41] describe air jet machining (AJM) as a jet of high velocity air (directed at the centre of the strain gauge) which contains a suspension of abrasive particles (usually 50μm $A10_2$ powder) that erodes the target material without leaving any form of machining residual stress. Bush claims the use of AJM improves the accuracy of centre hole analysis of toughened steel to an error within 6%. This is an encouraging improvement, but further work by Beaney showed that the abrasively formed hole tapers towards the bottom and also tends to be rounded at the top edge and bottom corners; to overcome this the fluid jet needs to be mounted in a slowly trepanning head. Such a modification

then complicates the technique and increases the time required to a level comparable with that consumed by the alignment of reamers.

Up to the later 1970's the centre hole technique had only been used for the determination of surface stresses. Obviously if a further analysis was performed by grinding off a layer after each centre hole test (to effectively gain access to sub-surface material) nothing would be gained in accuracy because of the grinding stresses so induced. Consequently, Owens[42] and Beaney[43] returned to mechanical boring through the section of a test sample: they made a 20 mm hole, down which they fixed axial strain gauges which measured the relaxed strains as a circular trough was trepanned out around the original hole. Owens professed particular concern at the errors induced in this analysis, although the operator error is minimal (-30×10^{-6} m/m strain) since the use of a mechanical boring technique has once again introduced the associated cutting and thermal stresses. Owens also theoretically checked the constants and calibration factors required for sub-surface analysis and complex stress and geometry situation by the use of a finite element program. This work indicated that the aforementioned parameters do not remain constant with steep sub-surface stress gradients.

2.2.4 Distortion Effects

In addition to the development of residual stresses and possibly the occurence of cracks, a quenching operation will also cause an overall distortion in a specimen. Murray[44] has classified this distortion in terms of two dimensional changes:-

1. Volume change (inherent distortion) resulting from transformation dilations, and

2. Warpage shape change due to uneven cooling of complex geometries.

A review produced by BISRA[45] gives a concise list of the more important factors which contribute to distortion. The volume change, which is closely related to the carbon content of a material, is directly responsible for major distortion, but depth of hardening is dependant on section size, quench severity and chemical heterogeneity (such as case carburisation), all of which may alter the thermal gradients and dilatation profiles. Non-symmetrical parts with greatly varying section size (e.g. a thin web between two adjacent thick rims) will cool with differing temperature gradients leading to different transformation products and ultimately buckling of the thinner part.

To determine the relative importance of factors controlling distortion in case-hardened steels, Hopkins[46] used a modified "Navy-C" specimen which is similar to the "crackability" specimen proposed by Chapman and Jominy (Fig 2.8) except that the notch is replaced by a gap of 10 mm. Hopkins tested two casts of EN35 steel, whilst Murray[44] conducted similar experiments (varying quenching media) on SAE-4817. Typical values of distortion recorded were in the range of 0.25-7.00% of the gap distance, but it is apparent that results obtained from a "Navy-C" type specimen are only useful for comparative work, because the change in gap distance is dependant on the major diameter and size of eccentric bore, and hence is not a fundamental measurement of the dimension change in the component. The conclusions from these two pieces of work are:

a. Even slight variations in chemical composition have a major effect on distortion tendency (up to 25% between two casts of the same material).

b. A higher surface carbon content after case hardening gives a higher distortion.

c. As the case depth is increased, distortion increases until the former is approximately one millimetre, after which the distortion decreases with increasing case depth.

d. In the case of pearlitic and ferritic structures only carbon content has an effect on distortion, whereas with bainite and martensite structures there is a linear relationship between transformation temperature, t_{50} (temperature of 50% transformation as determined by Murray in dilatation experiments), and the degree of distortion. According to Murray this relationship is the most important for hardened materials, because as t_{50} is depressed the amount of distortion observed greatly increases.

e. Direct quenching after the carburising treatment causes less distortion than when subsequent heat treatment is performed.

f. All the above factors are complicated by different transformation temperatures caused by the carbon gradient in the case.

The last named problem is amplified by Mocarski[47] who describes how the non-uniformity of carbon composition can alter the transformation sequence. In low alloy steels the high carbon case will transform at a lower temperature and with a larger volume change than the core, thus although the surface is naturally cooler than the core it is possible that the core may transform first. This effect is less pronounced with high alloy steels because the transformation temperature is relatively low at all carbon contents. Obviously the degree of distortion will vary under these circumstances. Thus a low temperature case that is involved in a large volume change with a rigid transformed core, will give

different levels of distortion to a high temperature case transformed with a small volume change over a soft austenitic core.

Llewellyn and Cook[48] decided that the distortion indicated by the gap change in a Navy-C specimen were unrepresentative of the true geometrical changes in carburised components. In preference, they used a washer-like specimen which closely related to a gear blank. Measurements were carried out at several positions of the outside and bore diameters and through thicknesses of such specimens made from EN352, CM607 and CM80 steel. After carburising at 925°C and furnace cooling to 840°C specimens of each material were quenched in water or oil, or air cooled. Re-measurements of the dimensions using a Societe Genevoise Universal Measuring Machine (accuracy of ± 0.001 mm) gave the results shown in Fig 2.17. The general trend observed was that distortion increases with increasing severity of quench; but in contradiction to Murray[44] and Mocarski[47] that the carbon depression of M_f in steels of low hardenability reduces the overall change. Hardenability was shown to have a marked effect on absolute geometry, because as it increased progressive contractions take place in the bore and external diameters with a compensating increase in thickness.

Price[49] conducted similar distortion measurements on water quenched plates (17 x 119 x 119 mm) of EN30B steel, using a Societe Genevoise machine. The pre and post quenching measurements were made across the plate perpendicular to the locations shown in Fig 2.18. Hence lateral distortion was given by:

$$\%\Delta Y = \frac{Y_Q - Y_A}{Y_A} \times 100$$

Q = quenched
A = annealed

Direct distortion measurement by this simple method was shown to contain inaccuracies due to the mechanical influence of the free edges. By measuring through thickness distortion (Fig 2.19) Price was able to estimate the area of "infinite" plate where the constant axial strain could be directly related to the changes in length and width by assuming zero axial stress. Then by incorporating the term $\frac{\Delta V}{3}$ to give the linear change due to transformation volume increase, he was able to calculate the true in plane strain (ε_x) from the measured through thickness distortion (ε_z) using:

$$\bar{\varepsilon}_x(\text{calculated}) = -\tfrac{1}{2}\{\varepsilon_z(\text{measured}) - \frac{\Delta V}{3}\}$$

2.3 SEMI-INFINITE BODY APPROACH TO THERMAL STRESS PREDICTION DURING QUENCHING

The calculation of thermal stresses are bounded by time and space domains, the latter being three dimensional. Much of the work reported in this area has reduced the mathematical complexities by limiting the number of degrees of freedom within each domain (e.g. the assumptions of unidirectional heat flow, plane stress/strain and other boundary conditions which reduce variables to zero), thus enabling solutions by standard numerical difference methods.

2.3.1 Temperature Distributions in a Body

The first step in the prediction of residual stress and strains is to determine the thermal history of the material. As shown by Crank and Nicolson[50] this requires the solution of a non-linear partial differential equation such as Fick's Law of transient heat conduction:

$$\frac{\partial\theta}{\partial t} = K\left(\frac{\partial^2\theta}{\partial x^2}\right) - q\frac{\partial w}{\partial t}$$

where the last term incorporates secondary heat generators or heat sinks. This equation has an infinite space domain and can only apply to a physical structure if the solution

contains applied constraints with respect to x, such as a specified power law of heat transfer at a free surface and a zero temperature gradient at the body centre.

Crank and Nicolson reviewed two methods of solution proposed by D. R. Hartree and then gave a third method which they developed:

Method 1 The time derivative is replaced by a finite difference ratio, which gives an ordinary differential equation in x and θ.

Method 2 The linear dimension x is divided into finite intervals with θ at each point expressed as values determined from neighbouring points to give a first order equation in time. The explicit form of this finite difference method[51] for a one dimensional problem is:

$$\frac{\theta_i^{n+1} - \theta_i^n}{\Delta t} = \alpha_{td} \frac{\theta_{i+1}^n - 2\theta_i^n + \theta_{i-1}^n}{(\Delta x)^2} \qquad \ldots\ldots 2.2$$

where α_{td} = thermal diffusivity
and by chosing the finite intervals to give:

$$\frac{\alpha_{td}\Delta t}{(\Delta x)^2} = \tfrac{1}{2} \qquad \text{(Schmidt modulus)}$$

the solution simplifies to the Schmidt formulation:

$$\theta_i^{n+1} = \frac{(\theta_{i+1}^n + \theta_{i-1}^n)}{2} \qquad \ldots\ldots 2.3$$

An equivalent implicit formulation of this problem is given by replacing the θ^n values on the right hand side of equation 2.2 by θ^{n+1} values.

Method 3 This is a combination of the previous two methods, i.e both derivatives are replaced by finite difference ratios, then the solution proceeds in finite steps of time. As can be seen in equation 2.4, the difference terms use all of the implicit and explicit temperatures in a truncated series:

$$\frac{\theta_i^{n+1} - \theta_i^n}{\Delta t} = \frac{1}{2(\Delta x)^2} (\theta_{i+1}^{n+i} + \theta_{i+1}^n) - 2(\theta_i^{n+1} + \theta_i^n) + (\theta_{i-1}^{n+1} + \theta_{i-1}^n) \quad \ldots\ldots 2.4$$

as with the explicit formulation, by setting $\Delta t/(\Delta x)^2 = 1$ the Crank - Nicolson method becomes simplified to:

$$\theta_i^{n+1} = \tfrac{1}{4}(\theta_{i+1}^{n+1} + \theta_{i+1}^n + \theta_{i-1}^{n+1} + \theta_{i-1}^n) \quad \ldots\ldots 2.5$$

A series of analyses on simple problems using all three methods, showed that convergence to a stable solution is dependant on the refinement of finite intervals in x, and the increase in the number of finite time steps over a given period.

Jaeger[52] employed the Schmidt formulation to predict the heating of a semi-infinite slab, using various power laws of heat transfer at the surface boundary. His results showed no inherent accumulative or oscillatory errors. This is true provided that $\alpha_{td}\Delta t/(\Delta x)^2 \leq \frac{1}{2}$, since coarse Δx values only lead to errors of the order of $(\Delta x)^2$ [53]. By comparison with the Crank - Nicolson method, Jaeger concluded that the Schmidt technique is not appreciably inferior to the former and can be justified in terms of reduced computation requirements.

Ideally the governing equations for surface boundary conditions would interface more easily with the general heat conduction formulations and also allow thermal gradients exterior to the structure if they were expressed as finite difference terms themselves. This modification to the Schmidt technique is given by Aparci[54], where the co-ordinates of the finite increments are such that the surface of a structure falls in the centre of the first

element. The ambient temperature of the surrounding media ($\theta\infty$) is positioned at a distance of λ/h from the surface, and by assuming a constant $\frac{d\theta}{dx}$ between $-\lambda/h$ and $\frac{\Delta x}{2}$, θ_1^{n+1} in the media may be found from finite differences without assuming a value for the surface temperature. To maintain accuracy $\lambda/h > \Delta x$. This method also simplifies the finite difference terms used when applying the $\frac{d\theta}{dx} = 0$ boundary condition at the central position of a symmetrically stressed structure.

Application of the modified Schmidt formulation has been adequately demonstrated by Katayama and Saito[55], who predicted thermal gradients in semi-infinite plates for several different heat flux conditions at the surface and with a composite structure of two materials of different conductivity. They show systematically the ease with which the various boundary conditions may be expressed as difference equations.

Wood and Lewis[56] compared the time marching schemes that may be used to solve the transient heat conduction equation, on a four element beam with heat flow constrained to the axial direction. Their model coupled finite difference schemes involving time with finite elements (see later) involving space. Stability of the time step was dependant on,

$$\Delta t < \frac{2}{(1 - \emptyset)\mu_i} \qquad \text{where } \mu_i = \text{eigen value}$$

For a backward difference method ($\emptyset = 1$) there is therefore no inherent oscillatory error, whilst for the Crank-Nicolson method ($\emptyset = \frac{1}{2}$) which uses central differences, "noise" can occur if:

$$\Delta t_{crit} > \frac{128}{(2n - 1)^2\pi^2} \qquad \text{where } n = \text{degrees of freedom}$$

However if Δt_{crit} is small and one of the suggested weighted average methods for damping is used, it was concluded that the Crank-Nicolson formulation is the preferable technique for transient temperature analysis.

Fletcher[57], using the Schmidt method predicted the thermal history of EN30B plates quenched from 850°C with both constant and variable surface heat transfer coefficients. He was able to complete the analysis using equation 2.3 and the following two equations which describe the initial and subsequent boundary conditions and allow the determination of θ_o^1 and θ_{t+1}^1 (Fig.2.20).:-

$$h(\theta_o^s - \theta^\infty) = \frac{2\lambda(\theta_o^s - \theta_o^1)}{\Delta x}$$

$$\theta_{t+1}^1 = (\theta_t^2 - \theta^\infty)\left(\frac{\lambda}{h} - \frac{\Delta x}{2}\right)/\left(\frac{\lambda}{h} + \frac{\Delta x}{2}\right) + \theta^\infty$$

The boundary equation for the plate centre was, $\theta_t^j = \theta_t^{j+1}$

Forty-one elements were used to sub-divide the half thickness of a 49 mm plate (dictated by the stability criterion) and thus many time steps were required for the whole calculation when the Schmidt modulus was equated to $\frac{1}{2}$. Although these predicted results were not confirmed by experimental values, subsequent work by Price and Fletcher[58] showed that similar predictions for a 40 mm plate of EN30B gave good correlation with experimental results obtained when the plates were quenched in water and oil.

2.3.2 Themoelastic/Plastic Stress Analysis

The calculation of residual stresses by classical thermoelastic methods is well documented in standard texts[59, 60, 61, 62]. The complete solution to a three dimensional problem would yield 6 stress components $(\sigma_{xx}, \sigma_{yy}, \sigma_{zz}, \sigma_{xy}, \sigma_{yz}, \sigma_{zx})$, ,6 strain components $(\varepsilon_{xx}, \varepsilon_{yy}, \varepsilon_{zz}, \varepsilon_{xy}, \varepsilon_{yz}, \varepsilon_{zx})$ and 3 displacement components (u, v, w) which must satisfy the following equations with prescribed boundary conditions:

Equilibrium equations,

$$\frac{\partial \sigma_{xx}}{\partial x} + \frac{\partial \sigma_{xy}}{\partial y} + \frac{\partial \sigma_{xz}}{\partial z} + X = 0$$

$$\frac{\partial \sigma_{xy}}{\partial x} + \frac{\partial \sigma_{yy}}{\partial y} + \frac{\partial \sigma_{yz}}{\partial z} + Y = 0$$

$$\frac{\partial \sigma_{xz}}{\partial x} + \frac{\partial \sigma_{yz}}{\partial y} + \frac{\partial \sigma_{zz}}{\partial z} + Z = 0$$

Stress-Strain relations,

$$\varepsilon_{xx} = \frac{1}{E}\{\sigma_{xx} - \nu(\sigma_{yy} + \sigma_{zz})\} + \alpha T$$

$$\varepsilon_{yy} = \frac{1}{E}\{\sigma_{yy} - \nu(\sigma_{zz} + \sigma_{xx})\} + \alpha T$$

$$\varepsilon_{zz} = \frac{1}{E}\{\sigma_{zz} - \nu(\sigma_{xx} + \sigma_{yy})\} + \alpha T$$

$$\varepsilon_{xy} = \frac{1}{2G}\sigma_{xy};\ \varepsilon_{yz} = \frac{1}{2G}\sigma_{yz};\ \varepsilon_{zx} = \frac{1}{2G}\sigma_{zx}$$

Strain-Displacement relations,

$$\varepsilon_{xx} = \frac{\partial u}{\partial x};\ \varepsilon_{yy} = \frac{\partial v}{\partial y};\ \varepsilon_{zz} = \frac{\partial w}{\partial z}$$

$$\varepsilon_{xy} = \tfrac{1}{2}\gamma_{xy} = \tfrac{1}{2}\left(\frac{\partial u}{\partial y} + \frac{\partial v}{\partial x}\right)$$

$$\varepsilon_{yz} = \tfrac{1}{2}\gamma_{yz} = \tfrac{1}{2}\left(\frac{\partial v}{\partial z} + \frac{\partial w}{\partial y}\right)$$

$$\varepsilon_{zx} = \tfrac{1}{2}\gamma_{zx} = \tfrac{1}{2}\left(\frac{\partial w}{\partial x} + \frac{\partial u}{\partial z}\right)$$

The latter twelve relations are sometimes combined into compatibility equations which contain stress components alone. When boundary conditions for a free body are prescribed the sum of the stress components in any principal direction must be zero and in the case of a thin plate with a temperature distribution only as a function of its thickness (z) we may assume stresses exist only in the plane of the plate

viz $\quad \sigma_{xx} = \sigma_{yy},\ \sigma_{zz} = \sigma_{xy} = \sigma_{yz} = \sigma_{zx} = 0$

Even when simplified by such assumptions, the governing field equations require a solution which is invariably achieved by numerical difference methods.

Other formulations of thermoelastic stress analysis which have been frequently used are the approximate variational stress function techniques, whereby a global function of stress (Green's or Airey's) defines a stress variation whose second order partial differentials give the desired stress, strain and displacement components. These stress functions (geometric and exponential) are obviously more complex to solve, on account of the multiple levels of integration and differentiation required.

Russell[63] was one of the first to attempt a prediction of residual stresses whilst taking into consideration metallurgical aspects, such as transformation progress with respect to position. He used the Schmidt graphical method to solve the heat conduction equation in the case of a cylinder made from a carbon steel of eutectoid composition which had been quenched from 750°C. The calculation of thermal history included a heat generation term associated with a phase transformation (but this parameter was only estimated) and the thermal properties were unaffected by temperature. The model assumed a fast cool followed by isothermal transformation in successive steps as the temperature was reduced. No pro-eutectoid or metastable phases were accounted for. Although the austenite decomposition was incorporated in the temperature analysis (latent heat) the corresponding volume expansion was not included in the stress determinations. The equations proposed assumed only elastic stress, and an infinitely long cylinder (plain strain) and no shear stress, but allowed Young's Modulus and Poisson's ratio to vary as the temperature fell. The principal stresses were given by the following equations:

$$\sigma_z = \frac{\alpha E}{1 - \nu} \left\{ \frac{f_2(b)}{f_1(b)} - T \right\}$$

$$\sigma_r = \frac{\alpha}{r^2 f(b)} \left\{ f_1(r) f_2(b) - f_2(r) f_1(b) \right\}$$

$$\sigma_\theta = \sigma_z - \sigma_r$$

where

$$f_1(r) = \int_0^r \frac{Er}{1-\nu}\,dr, \quad f_2(r) = \int_0^r \frac{ETr}{1-\nu}\,dr, \qquad b = \text{outer radius}$$

The results showed tensile and compressive stresses at the surface and centre respectively at all times, and it was stated that their magnitude was sufficient to cause plasticity. No experimental evidence was given to substantiate this model.

Hirone[64] also worked on infinitly long cylindrical steel ingots, and used the assumption that at all temperatures above M_f the material would behave plastically and below M_f it would be elastic. Expansion due to transformation was obtained from a dilatation curve. Although no experimental stress analysis was undertaken, the model indicated a distinct increase in mid-radial tensile stress as the austenitisation temperature was increased.

A determination of residual stress in a free plate of thickness 2h was made by Weiner[65] who used the Prandtl-Reuss theorem. The plate was considered to be an elastic/perfectly plastic body with all properties independant of temperature, and the plate's edges were assumed to be free of tractions. Heat was introduced at one face and then allowed to disperse within the plate but all other surfaces were insulated. The strain relations used were:

mean values $$\dot{\varepsilon} = \frac{1}{3K}\dot{\sigma} + \alpha\dot{T}, \quad \sigma = \frac{1}{3}\sigma_{ii}$$

deviatoric values $$\dot{e} = \frac{1}{2G} \cdot S_{ij} + \mu S_{ij};$$

with an upper bound on elastic stress which allowed the use of an explicit calculation. During heating of the specimen plastic flow was predicted initially at both major surfaces but the dispersion of the heat through the plate caused unloading of the initial stresses. If the initial heat input was large enough, the stresses reversed and eventually produced further plastic flow. The residual stress distribution was a tensile surface/compressive centre, which is the reverse of the distribution at the initial stage of the quench.

Several examples of suitable methods of solution have been given by Boley[66], in the case of a beam of length 2L, depth 2c and width b, with a two dimensional stress distribution T(x,y). The axial stress is given by,

$$\sigma_z = - \alpha E T + (1/A)\alpha E \int T dA + (y/I)\alpha E \int T y dA$$

where $A = 2cb$, $I = 2c^3b/3$

Mura[67] considered 0.3% carbon steel cylinders water quenched from 600, 750 or 900°C. His model assumed that the material was perfectly plastic (zero yield stress) above an arbitrary temperature, T_o (he used 600 and 500°C), perfectly elastic below T_o with constant properties, no volume change due to plastic flow and no shear stresses. As the transient analysis progressed each new strain was equated to the previous plastic strain plus any transformation volume increase, plus the new thermal strain calculated during the current time step. With an infinitely long cylinder, plane strain conditions applied, and stresses were calculated for the three principle directions. The surface of the cylinder was always compressive, and at a maximum in the case of the quench from 750°C. Reasonable agreement was found with experimental values derived by the Sachs method, although the latter were slightly lower than the theoretical values predicted after the quenches from 600 and 700°C.

Mura also attempted to predict the residual thermal stress in bearing rings of composition 1% C, 0.45%Cr, 0.28%Ni that had been quenched from 840°C in oil.

Unfortunately the results obtained from either of the models used did not give good agreement with the experimentally determined values. It may be concluded that the size of structure used was too small in the axial direction to allow the model to be free of edge effects at any point.

Symmetrically cooled plates were investigated by Landau[68] who used a viscoelastic/perfect plastic model based upon the Maxwell body, with a Von Mises yield criterion dependent upon the temperature. Temperatures were determined from an explicit finite difference solution of the unsteady heat conduction equation using the assumption of a zero gradient at the plate centre and a condition of $\partial T/\partial x = - \lambda T$ at the surface. The plates were thin enough to allow plane stress conditions to be assumed. It was found that the introduction of viscoelasticity into the model had negligible effect on the residual stresses, although the temperature dependence of σ_f considerably increased the level of such stresses. The development of plastic regions with varying rates of heat extraction showed that at low quench rates, plasticity would only occur at the surface. This model was developed for slowly varying heat rates, thus the solution took no account of transformations.

Toshioka et al[69] considered a bar of an air hardenable carbon/chromium/molybdenum steel. They assumed this material was virtually non-elastic in the austenitic region and would produce a completely martensitic structure on quenching. Figure 2.21 shows the type of strain induced by a particular temperature distribution. Experimental measurements of the temperature gradients during the quench allowed the

determination of a temperature gradient coefficient (A), which was then used in the following relation:

$$\tau_r = (1 - A(r/R)^2)T_o$$

where, A = 0.9 in the case of water quenched material
T_o = centre temperature
R = outer radius

Transformation strain was incorporated in the model by the equation,

$$\varepsilon = \Delta\varepsilon\left\{1 - \frac{(T - T_f)^2}{T_s - T_f}\right\},$$

but this does not compare well to the true relation between fraction transformed and temperature. The position of the boundary between the elastic and plastic zones was determined by consideration of the volume, internal stress and pressures. The relationship between principal stress and τ was given by the equilibrium equation,

$$\frac{r}{R} \cdot \frac{d\sigma r}{dr} = 2d\tau$$

The surface stresses in a 100 mm diameter bar oil quenched from 850°C, were tensile at temperatures above M_s and below M_f but were compressive during transformation, due to a volume increase. The surface tensile stress was at a maximum when the centre had just completed transformation. This maximum increased as the severity of the quench increased up to the point where the stresses due to the temperature gradient alone, were greatly in excess of the transformation stress. As the change in dominant mechanism occurred the tensile peak moved towards the plate centre.

A further investigation into transformation strain showed that a larger dilatation would greatly increase the magnitude of residual stresses, whereas a displacement in the temperature range over which dilation occurred has a smaller effect. It may be concluded that the value of $\Delta\varepsilon = \varepsilon_{T_{ms}} - \varepsilon_{T_{mf}}$ is of greater importance than the values of T_{ms} and T_{mf}. No detail of experimental work was given in support of this model.

Dilatations vary according to the product of austenite decomposition, hence the relative contribution for each product is of great importance when considering multiphase transformations, as did Hildenwall and Ericsson[70], who modelled carburised, infinitely flat plates. The thermal properties of their material (EN352) were estimated from the volume fraction of the various phases present at each stage. The thermal history was determined by a finite difference solution of the transient heat conduction equation, and the predicted temperatures were in good agreement with measured values at the centre of an austenitic steel cylinder. However despite this agreement the values of surface heat transfer coefficient used differ by up to an order of magnitude from those determined later by Price and Fletcher[58]. At all stages of the stress calculation the mechanical properties were dependent upon the structure which was estimated from TTT diagrams that had been obtained from several continuous cooling curves. The previous stress history was not considered to effect transformations, but plastic flow after a stress reversal was influenced by the Bauschinger effect. Work hardening was incorporated as a single linear coefficient determined from tensile tests at various temperatures of steels with various structures. Surface residual stresses (Fig 2.22) are compressive and of the order of 900 N/mm^2. The maximum compressive stress appears to occur at a specific carbon content but the point in the plate at which it occurs is dependent upon surface carbon content and case depth. No experimental work was carried out to support the theoretical calculations.

Fletcher[57] modelled the generation of thermal stress and strain in an air hardenable plate of EN20B. An explicit finite difference solution of the transient conduction equation was used to calculate temperature distributions, with a variable surface heat transfer coefficient to simulate several quenching conditions that varied from slow oil to brine. He used linear relations between temperature and both Young's modulus and the flow strain of austenite. Transformation strain was assumed to be 1.5%, with the volume fraction linear between 310-150°C. Perfect plasticity was another assumption. The calculation followed the following stages:

a. Calculate the displacement of individual elements introduced in a small time increment due to changes in temperature and microstructure

b. Determine the elastic stress associated with (a) under conditions of complete constraint,

$$\Delta\sigma^{n}_{t+1} = \frac{Ee(\theta^{n}_{t+1} - \theta^{n}_{t})}{1 - \nu} \quad ; \; n = 2, \ldots\ldots J$$

where e = coefficient of expansion.

c. Add incremental elastic stress to previous stress, and adjust all values until the zero net body force condition applies.

d. All points exceeding the yield stress are reduced to σ flow.

e. Distribute force generated as a consequence of yielding uniformly throughout the elastic regions and apply Von Mises yield criterion. Iteration of this process until unbalanced force $<$ ± 25N, to give the corrected stress values.

f. The original strain values are adjusted to take account of the change in elastic stress

$$(\Delta\varepsilon^{n}_{t+1})p = (\Delta\sigma^{n}_{t+1})p/1.5E \; ; \; n = 2 \ldots J$$

The results obtained showed an initial tensile stress at the surface and a corresponding compressive stress at the centre. Plastic flow occurred at an early stage in the quench, particularly at the surface. The subsequent reduction in the cooling rate at the surface relative to the centre caused unloading and eventually stress reversal at both surface and centre, which took place before the M_s temperature was reached at the former position. When transformation began at the surface the volume increase enhanced the magnitude of the compressive stress, which was accompanied by a simultaneous increase in flow stress. As the transformation front moved towards the centre unloading and reversal of the stress occurred at this point. This was accompanied by unloading of the compressive stress at the surface, followed by the generation of a tensile stress. This work confirmed that in general the residual stresses were increased as the surface heat transfer coefficient increased. Several examples of the relationship between stress and strain at the surface and centre are given which clearly showed the loading and reversal cycles. No experimental work was reported.

Fletcher and Price[49] followed up the above work by using improved mechanical and thermal property data, e.g. work hardening coefficients to give stresses above the original yield value, and the modelling of a dilatometry curve by linear and polynomial relations to give exact transformation volume increases instead of the change in the room temperature lattice parameter previously used. As a consequence of these modifications no plasticity was predicted during the formation of martensite, even when a water quench was used. After such a quench there was a maximum tensile residual stress predicted just below the surface with a compressive stress at the centre. This stress

pattern was reversed in the case of an oil quench and the stress levels were of a much smaller magnitude. The relationship between stress and strain during the oil quench (Fig. 2.23) show the effect of a persistant vapour blanket at low temperature.

The modified Sachs technique was used to determine the stresses present in quenched plates 40 mm and 20 mm thick, and the results obtained were corrected for the effect of the free edge on the stress distribution to allow comparison with the predicted results. The correction factor, based on the profile of the plate after it had been quenched, was larger than the value suggested by the Saint-Venant Principle (see below). There was reasonably good agreement between the predicted and measured stresses after a water quench (Fig. 2.24) but as can be seen the stress distributions after an oil quench were in conflict (Fig. 25). It was suggested that the discrepancy in the latter case may be due to stress relaxation effects.

Much work has been performed to incorporate viscous processes and transformation plasticity into the prediction of residual stresses. Abbasi and Fletcher[118] introduced stress relaxation and creep into a finite difference model which gave improved agreement with the experimentally derived stress distributions in an oil quenced plate. Further work by Fletcher and Soomro[119] took into account the initial stress situation with respect to the rate of stress relaxation; its incorporation into the predictive model gave even further improvement in the oil quench results. Transformation plasticity is the occurance of plastic deformation at stresses which are below the material's yield strength. Denis et al[120] reported that as trasnformation from austenite progresses, after 25% of the phase change the plastic strain in the transformation zone increases linearly and is a function of the material flow stress and the specific volume variation of the phase change. Abassi and Fletcher[121] introduced the transformation plasticity

phenominae into their model by extending the viscoelastic-plastic model, developed for stress relaxation, to include the effect of stress on the characteristics of the martensite trasnformation. To accomplish this modification, stress dilatometry data was introduced into the mathematical model by using the concept of a reduction in yield stress or by the use of an additional transformation strain. Both methods improved the correlation between the calculated and experimentally determined residual stress and strain obtained after an oil quench. However, the introduction of any or all of the above modifications for viscous processes and transformation plasticity produced a reduced level of agreement in the case of water quenched materials.

Of the many parameters which are used in a residual stress model some have been investigated to determine the affect of their variation. Allen and Fletcher[122] have studied the effects of surface roughness on quenchant characteristics and subsequent residual stresses and strains. It was concluded that stress is not a function of surface roughness, but that residual strains may vary by significant amounts (±0,05% absolute) as the surface finish is changed in the range 120 to 600 grade. Similarly Fletcher and Soomro[123] assessed the dependance of residual stresses and strain on the transofrmation temperature range; the latter would be changed practically by variations in the material composition. It was found that with increasing martensite transformation start temperature (M_S), strain also increased but not stress. The conclusion of this work was that close control of material composition is to be preferred, and that the best material integrity will be achieved by a composition which gives a lower M_S.

2.4 THE SAINT-VENANT PRINCIPLE AND THE EFFECTS OF A FREE EDGE ON THE STRESS DISTRIBUTION

The main problem associated with the use of thermal stress predictions made by the infinite plate model in real bodies

is the decay in the stress perpendicular to a free surface as that surface is approached. This leads to the generation of a complex stress system in the vicinity of the edge where the assumption of plane stress conditions applicable in the interior is invalid.

The first comments on the effect of stress decay were made by Saint Venant in 1885 who said:

> "The self-equilibrating difference between actual tractions and those contemplated in theory is not appreciably felt except in the short regions equivalent to the dimension of application".

This in effect says that if an equal and opposite force opposes the inplane force at the edge to reduce it to zero, the change in stress distribution in the plate is only apparent within a plates thickness of that edge. This statement known as Saint Venant's Principle is purely qualitative and there have been many attempts to verify and improve it. Invariably the problem is approached by consideration of a self equilibrating stress applied to a part or whole surface of a large body rather than the attenuation of internal stress towards an edge, but the one is in fact just an inverse application of the other.

Goodier[71] justifies the principle by consideration of the conservation of energy. He examined the case of a small loaded area on a large body and by discussion of the strain energy he shows that the work done by this elastic traction is not appreciable at distances from that area which are large compared with its linear dimension. This argument however, depends on the manipulation of the units of each algebraic term and proof that the difference between the total work done by the traction and the strain energy per unit volume (that it implies) is in fact a unit volume. This is self evident and not necessarily a proof of the Saint Venant Principle.

Taking this argument a stage further Goodier[72] upheld the Saint Venant Principle in a situation where non-equilibrating forces were applied to the ends of a rigidly fixed body. He used strain energy conservation to show that the stresses and strains induced would only be appreciable within a limited distance of the loaded ends (comparable to its thickness), because equilibrium is attained by forces in the rigid attachment, which experiences shear stresses.

According to Von Mises[73] the statically equivalent loads which are applied to bodies will only abide by the Saint Venant Principle if they are perpendicular to the surface or edge concerned. If this is true it may not be applied to finite bodies with three dimensional stress variations. It is shown by Von Mises, and later by Sternberg[74], that under certain circumstances the edge effect in a three dimensional system can extend to distances equal to the second order of strain (ϵ^2) applied at the edge. Both workers stated that in special classes of bodies such as "thin" plates or "long" cylinders the Saint Venant Principle would still be valid.

Two papers by Horvay[75, 76] give the first indication of the variation of the principal and shear stresses as the edge is approached. This is achieved by developing a variational stress function for the applied stress at the edge, but it is necessary to describe the self equilibrating force in a mathematical relation, which in this case was a parabolic relationship between stress and perpendicular distance from the adjacent surfaces. The proposed stress variation near an edge of a square body is exponential, but the effected region is larger if the adjacent surfaces are divergent (e.g. a wedge shape). The variational stress function (ϕ_σ) given by a parabolic stress at the boundary of a square shape is:

$$\phi_\sigma = \frac{2}{3\sqrt{(35)}}\ h^2\ \hat{\sigma}\ f_2(y)\, g_2(x)$$

where

$$f_2(y) = \frac{3\sqrt{(35)}}{16} (1 - y^2/h^2)^2$$

$$g_2(x) = e^{-\alpha_2 x/h} \{\cos(\beta_2 \cdot \frac{x}{h}) + \frac{\alpha_2}{\beta_2} \sin(\beta_2 \cdot \frac{x}{h})\}$$

$$\alpha_2 + i\beta_2 = 2.0751 + i\ 1.1429$$

$\hat{\sigma}$ = maximum tensile stress at the edge

α_2 = attenuation constant

$\alpha_2 + i\beta_2$ = complex roots of the Euler-Lagrange equation which represents the variation of strain energy with distance from the edge

h = half thickness of plate

From this function (ϕ_σ) the principal and shear stress may be calculated, viz:

$$\sigma_x = \partial^2\phi/\partial y^2 , \quad \sigma_y = \partial^2\phi/\partial x^2 , \quad \tau = - \partial^2\phi/\partial x \partial y$$

The change in stress predicted by this process is shown in Fig. 2.26. This shows the generation of perpendicular and shear stresses in the edge region, even though the applied stress function acted only in the x direction, and complete decay is achieved at a point approximately the structure thickness from the edge.

The Saint-Venant Principle has been applied to temperature functions[60, 77, 78] which are self equilibrating in both steady state and transient analyses. For the transient case the temperature $T_{(x, y)}$ at a given distance from the heated surface is found from:

$$T_{(x, y)} = \frac{2cQ(y)}{K} \int_0^{t'} \sqrt{(\frac{1}{\pi t'})} \exp - (4\pi^2 t' + x^2/16c^2t') \, dt'$$

where,

$$Q_{(y)} = Q_o \cos \frac{\pi y}{c} \quad , \qquad \int_{-c}^{c} Q_{(y)}\, dy = 0$$

$$t' = Kt/(4c^2), \quad t = \text{time}, \quad K = \text{material constant}$$

This is comparable with the stress analysis of Horvay since it involves a solution that requires an exact definition of the load function ($Q_{(y)}$) and is dependent on the magnitude of maximum load (Q_o = maximum heat input). Again it is shown that the decay of the applied load, be it mechanical or thermal, is an exponential function.

With respect to thermal stress[60, 61] in thin plates with a through thickness temperature variation ($T_{(z)}$), the equilibrium, compatibility and boundary equation have been combined to give:

$$\sigma_{yy} = \sigma_{xx} = \frac{-E\alpha T}{1 - \nu} + c_1 + c_2 z \quad ,$$

where the constants c_1 and c_2 are determined by the boundary conditions which give zero resultant force and moment of σ_{xx} and σ_{yy} over the edge of the plate. This however only holds true for positions well away from the plate edge. Saint Venant's Principle could be used in this situation by the superimposition of a stress distribution on the edge, equal in magnitude but opposite in sign to the "infinite plate" stresses. This would create significant shear stress terms in the edge region (known as "the shear lag effect") as has been suggested by Horvay[76].

The only mathematical treatment given by Boley and Weiner[60] that involved the effect of edges on stress was in a proof of Saint Venent's Principle. The equations derived for this proof were produced by the application of a force (F) on the end of a bar of thickness 2b and width t viz:

$$F_{(x)} = 0.93\ bt\tau_{(x)} = Fe^{-(2.15(x/2b))}$$

This gives an approximate solution for forces $F_{(x)}$ (Fig. 2.27) and shear stress $\tau_{(x)}$ at a point in a body within the edge region. When x = 2b, F_x/F approaches zero, which concurrs with Saint Venant. When a more exact solution which takes account of the effect of the applied force F is required, the variational stress function technique of Horvay[76] should be employed.

Unfortunately Horvay's models were not three dimensional, the stress functions are complex to solve and become prohibitively difficult in transient analysis, due to high computation costs. Therefore to resolve this problem a numerical method of solution of second order partial differentials in three dimensions is required: the finite element technique is such an example.

2.5 THE FINITE ELEMENT TECHNIQUE

2.5.1 Fundamental Theory of Finite Element Stress Formulation

The analysis of field problems by finite elements has been described in several texts[79, 80, 81, 82] and in many papers[83, 84, 85]. Although this method was originally devised for stress analysis problems it is actually a mathematical technique[86] that converges to an exact solution for variational functions in a domain which is split up into finite elements connected by nodes.

The fundamental technique is based upon the minimisation of the potential energy[87] of the variational function (X) with respect to an unknown parameter (δ), which in the case of stress analysis is a nodal displacement field. Minimisation of energy occurs when the differential, is equated to zero, as is given by the general equilbrium equation:

$$\{\frac{\partial \chi}{\partial \delta}\} = (K)\ \{\delta\} - \{F\} = 0$$

where (K) = Stiffness matrix

{F} = Load vector

{δ} = Displacement vector

this gives the relation

$$\{F\} = (K)\ \{\delta\}$$

The sequence used in the solution of this equation, when the displacement method is employed, is as follows:

a. Sub-division of the continuum into finite elements.

b. Evaluation of individual element stiffness matrix (K^e) and equivalent nodal forces (F^e);

$$K^e = \int_{V_e} (B)^T DB\ dV \quad , \quad F^e = \int_{V_e} (N)^T p.dV + \int_{S_e} (N)^T q.dS \quad ,$$

where, p = body forces per unit volume

q = applied surface tractions

V_e = element volume

S_e = element surface loaded area

(B) = strain matrix, (discussed later) = $\sum_{e=1}^{m} (B_i)$

D = elastic constant matrix, typically for plane stress

$$\frac{E}{1 - \nu^2} \begin{bmatrix} 1 & \nu & 0 \\ \nu & 1 & 0 \\ 0 & 0 & \frac{1 - \nu}{2} \end{bmatrix}$$

N = shape function of the element (discussed later)

c. Assembly of all the element stiffness and load items into an overall stiffness matrix and load vector[88],

$$(K) = \sum_{e=1}^{m} (K^e) \quad , \quad (F) = \sum_{e=1}^{m} (F^e)$$

d. The introduction of the above into the general equilibrium equation and the solution of the resluting linear simultaneous equation for the unknown variables δ^e.

e. Determination of the strain ($\epsilon = B\delta^e$) and stress ($\sigma = D\epsilon$) in each element

As can be seen, this procedure is based on matrices and vectors that volve individual elements, but each of these contains subsets for the individual nodes which lie in each element, e.g. the displacement vector $\{\delta^e\}$ for an element when partitioned gives under plane stress conditions:

$$\delta^e = \begin{bmatrix} \delta_1 \\ \delta_2 \\ \vdots \\ \delta_n \end{bmatrix} \quad \text{, where } \delta_i = \begin{bmatrix} u_i \\ v_i \end{bmatrix} \quad ; \; u_i \text{ and } v_i = \text{cartesian components of nodal displacement for node i.}$$

Likewise partitioning can be performed for the other functions

$$F^e = \begin{bmatrix} F_1 \\ F_2 \\ \vdots \\ F_n \end{bmatrix} \quad , \quad F_i = \begin{bmatrix} P_{xi} \\ P_{yi} \end{bmatrix}$$

$$\epsilon = \begin{bmatrix} \epsilon_x \\ \epsilon_y \\ \gamma_{xy} \end{bmatrix} = \begin{bmatrix} \partial u/\partial x \\ \partial v/\partial y \\ \dfrac{\partial u}{\partial y} + \dfrac{\partial v}{\partial x} \end{bmatrix} = B\delta^e \qquad \ldots\ldots 2.6$$

The most important function in this analysis is the shape function[88 89], N, which is a property of the element type used and describes the ability of nodal points to be displaced according to an algebraic function (linear, parabolic, cubic) of the spatial co-ordinates, i.e. if a strain gradient exists across an element the relative positions and displacements of its constituent nodes are

determined by this shape function. This too may be partitioned to give $N = (N_1, N_2, \ldots N_n)$ where $N_u = f(I)$ and I is a square identity matrix (r x r) with r degrees of freedom per node. Convergence to a suitable solution is only possible if the shape function allows constant strain and continuous displacement between adjacent elements. When a choice is made of elements for a structure it is advisable to remember that the more degrees of freedom available in an element the fewer degrees of freedom are required overall for convergence. This is because the structure requires fewer elements to model the displacement variation.

The identity matrix of the shape function is expressed in terms of the U and displacements, and is substituted into equation 2.6 to give the nodal subset B_i of the strain matrix B:

$$B_i = \begin{bmatrix} \frac{\partial N_i}{\partial x} & 0 \\ 0 & \frac{\partial N_i}{\partial y} \\ \frac{\partial N_i}{\partial y} & \frac{\partial N_i}{\partial x} \end{bmatrix}$$

In this manner the element strains are expressed in terms of the nodal displacement.

This general description of the finite element method can be modified to describe many geometric models and alternate variation functions[87], e.g.

a. Axisymmetric models, which have 2 x 2 identity matrices like those of the plane stress models, but the strain matrix contains a non-differential term for the hoop strain, which is a linear function of the radial displacement,

b. Three dimensional models, which have 3 x 3 identity matrices, and the nodal displacement functions δ_i have a third term.

c. Thermal models, where the unknown parameter δ in the variational function is temperature instead of nodal displacement.

d. Plasticity models.

Much work has been undertaken on the modification of the finite element analysis method to enable elastic-plastic calculations[90, 91, 92, 93] to be carried out. Several flow sequences have been proposed in the literature for the segregation of the total strain into elastic and plastic components during the progressive application of the load by small increments. All of these sequences require a full elastic analysis at the first load increment, after which the derived stresses are used in one of the following procedures:

a. The stresses are scaled up to produce yielding at the point of maximum equivalent stress: this is followed by successive increments of load with the summation of the increments of plastic strain at these nodes which are in the plastic region

b. The stresses are used to determine the increment of plastic strain, that is then treated as an initial strain ϵ_o. This is in turn used to modify the stress estimate e.g $\{\sigma\} = (D)\ (\{\epsilon\} - \{\epsilon_o\})$ before the next load increment is applied. After each load increment the energy of the system is minimised.

Obviously the conditions which govern the ability of the finite element method to converge to a successful solution are:

1. The degrees of freedom and order of the algebraic displacements in the shape function. For simple elements considerable mesh refinement will be required for complex or severe load variations. Weighted averages at nodes or average stress between the elements at whose boundaries the nodes lie in will reduce irregularities in the results.

2. The size of the load increment in plasticity and other non-linear analysis.

3. The size of the time step in field problems such as transient thermal analysis.

2.5.2 Transient Temperature Analysis of a Body by Finite Elements

Wilson and Nickel[94] have shown how the heat conduction equation can be reduced to an equivalent set of first order, ordinary differential equations expressed in terms of nodal temperatures. The position of the nodes is again determined by the arrangement of elements into which the continuum has been divided. In the case of a transient analysis certain of the matrix functions are time dependant so the solution technique requires that the time period be split into a series of finite time increments (Δt).

The general field relation which gives rise to the set of simultaneous equations with unknowns $\{\theta_i\}$ is:

$$(\bar{K})\{\theta_i\} = \{Q_i\} \text{ or } (\bar{K})\{\theta_i\} + (C)\{\dot{\theta}_i\} = \{Q_i\}$$

where, $(\bar{K})$ = conductivity matrix (analogous to the stiffness matrix) for time step.

$= (K) + \frac{2}{\Delta t}(C)$

(C) = heat capacity matrix

$\{\theta_i\} = \frac{1}{2}\{\theta\}_t + \frac{1}{2}\{\theta\}_{t-\Delta t}$ = column vector of unknown nodal point temperatures; defined in a backward difference form with respect to time.

$\{Q_i\} = \frac{1}{2}\{Q\}_t + \frac{1}{2}\{Q\}_{t-\Delta t} + \frac{2}{\Delta t}(C)\{\theta\}_{t-\Delta t}$

= thermal force vector (analogous to the equivalent nodal force vector F).

t = present time

$\{\theta_i\}$ = thermal gradient vector

Obviously the matrices and vectors are assembled from sets for individual elements which are integral functions of (α_m) and $\langle b_m \rangle$ with respect to element volume. These terms are comparable to the shape function and strain matrix in stress analysis. The subsets of $(\bar{K})$ and $\{Q_i\}$ which represent surface elements also contain an integral term with respect to surface area, which incorporates the surface heat transfer coefficient (h);

$$q = h \times (\theta_e - \theta)$$

where, q = heat flux across the boundary layer

θ = surface element temperature

θ_e = temperature beyond the layer

Boundary conditions are applied by the specification of temperatures at nodal points.

This technique was applied to a one dimensional heat flow problem, which involved a constant heat flux applied to a semi infinite solid. Comparison with an exact solution (Fourier analysis) showed excellent agreement at all times (Fig. 2.28), although variation in the time step proved to have a considerable effect on the rate of convergence (Fig. 2.29).

Zienkiewicz and Parekh[95] formulated a similar finite element programme which also carried out transient temperature analysis, but this technique was based upon the use of a central difference scheme (Crank-Nicolson) for the derivation of field matrices and vectors. The elements used were 'isoparametric', which means that the shape functions, N (or thermal equivalent), of an element is defined by curvilinear co-ordinates (ε η ζ) with the origin at the element centre; this obviously is a different co-ordinate system to that used in the total structure, (x, y, z) and the two are related by:

$x = (N)\{x\}^e$, $y = (N)\{y\}^e$, $z = (N)\{z\}^e$, where $\{x\}^e$ etc.

are the nodal co-ordinates.

The values at individual nodal points of the unknown function Φ (temperature or displacement) is obtained by:

$$\Phi = \Sigma N_i \Phi_i = (N)\ \{\Phi\}^e$$

In the case of elements with three or four nodes per side, the function variation along the boundary, is parabolic or cubic respectively. Figure 2.30 shows the comparison of results obtained with simple (linear) and isoparametric (cubic) elements in a quarter plate model with heat transfer at a centre hole. This shows that the use of higher order elements can produce accurate answers with a smaller number of total degrees of freedom, and that mesh refinement in areas of high thermal gradients is advantageous.

Saliman and Fakhroo[96] used the finite element method to determine the temperature distribution in a rectangular ingot during cooling by a two dimensional heat flow. They assumed no thermal gradient in the longitudinal direction, but specific heat and conductivity varied as the temperature fell. Simple triangular elements were used to mesh a segment of the ingot and surrounding mould. Although the process of cooling in the mould is not as severe as during a quench the starting temperatures of the mould and ingot are nevertheless greatly different, yet no mesh refinement was used close to this boundary. This could account for the discrepancy found between calculated and measured temperatures at the interface between mould and metal during the initial cooling stages. However at later times, the calculated and experimental results showed good agreement.

It has been demonstrated by Comini et al[97 98], that good temperature prediction can be achieved with simple elements, even when the model is complicated by non-linear variations in boundary conditions and physical properties. This was shown in a calculation of the temperature distribution during the cooling and solidification of a liquid. The effects of latent heat were approximated to a very high degree by rapid variations in the heat capacity { (C) } within a narrow temperature range, and the integral solution of subsets was based upon the Crank-Nicolson central difference method, which assumes that the temperature varies linearly in the small time interval between $t - \Delta t$ and $t + \Delta t$.

2.5.3 Prediction of Thermal Stress in a Structure of Finite Dimensions

Modification of the standard finite element technique of stress analysis to take into account thermal loads has been adequately described in many papers[99 100 101]. Inclusion of these loads can be performed in numerous ways that depend upon the choice of the integral functions used in the stiffness matrix ($\bar{K}$) and equivalent force vector {F}, i.e. the equilibrium field equation can be based upon minimisation of potential energy or virtual work. It is common to treat the apparent thermal strains $\{\epsilon_o\}$ as an initial strain increment,

$$\{\varepsilon_o\} = \frac{E}{1 - \nu} \begin{bmatrix} \alpha T \\ \alpha T \\ 0 \end{bmatrix} \qquad \text{where } \alpha = \text{coefficient of expansion}$$

which is incorporated in the thermal force vector {F},

$$\{F\} = \int \left(\int (B)^T \{\varepsilon_o\} dV\right)$$

This is then used in the assembled field equation,

$$\{F\} = (K)\ \{\delta\}$$

Stress increments are given by $\{\sigma\} = (D)\ (\{\varepsilon\} - \{\varepsilon_o\})$.

One of the earliest workers to apply the finite element method to thermal stress analysis was Webber[102]. He considered the plane stress model of a flat, thin plate with equivalent heat sources applied at opposing ends (which were free of tractions) to give a longitudinal temperature gradient. Only a thermo-elastic analysis was performed on a 24 element mesh of a quadrant of the structure, with the results given as displacements in the thickness direction. Figure 2.31 compares the results obtained with

a. elements with variable temperature, and
b. elements of uniform temperature,

with these obtained by an exact energy method. This indicates that the solution can develop errors in the proximity of boundaries if the functional variation (N) of the elements are not of a high enough order.

Gurney[108] used a pseudo finite mesh to analyse the effect of localised heating and cooling at the centre of a 38 cm diameter plate. The structure was not meshed as a continuum, but was idealised as a 'cobweb' of radial and circumferential tie bars. Only the yield stress varied with temperature. Although the peak temperature used in the model was 700°C, volumetric changes due to transformation on cooling were ignored. It may be concluded from this work that the onset of plasticity depends on the peak temperature and yield stress of the material at high temperature. Since the results were only given up to a maximum radius of 7.5 cm the attenuation of stress at the plate edge cannot be commented upon, although it is highly probable their magnitude would be negligible at this distance from the heat source.

The water and oil quenching of 0.38% carbon steel bars was analysed by Toshioka[103]. A quadrant of the cylinder was divided into a mesh of triangular axisymmetric elements (Fig. 2.32); with the element size biased to give smaller elements in the areas of largest function change. All the

properties used (thermal and physical) were temperature dependent. Although the axial stresses generated during a water quench were given on a plane at the centre of the cylinder, no comment was made upon the change in axial stress as the end of the structure was approached. However, the change in dimensions of the bar were shown along the whole length of the specimens and these results suggest an edge effected region somewhat smaller than the diameter of the bars. Toshioka suggested that a convex type of plastic deformation was produced by a shrinking case while a concave type was produced by a shrinking core, so that the final shape would depend on which mechanism predominated in a particular instance. This would depend upon the magnitude of the temperature gradient and the rigidity of the structure.

It is generally accepted now that changes associated with transformations and variability of the surface heat transfer coefficient are of great importance in the field of thermal stress prediction. However as late as 1980 a model was presented[104] of the stress generation process in quenched plates of mild steel which did not take into account either finite surface heat transfer coefficients or dilation of the structure when a phase change occurred. The yield stress (σ_F) was allowed to vary with temperature (T) according to experimental values. A plate quadrant was modelled by 12 square unrefined isoparametric elements with 8 nodes per element, and plane stress conditions were assumed. The finite element programme calculated the component stresses (σ_x and σ_y) after each time increment, and at each node an effective stress ($\bar{\sigma}$) was determined by means of the yield criterion:

$$\bar{\sigma} = \sqrt{(\tfrac{1}{2}\{\sigma_x^2 + \sigma_y^2 - \sigma_x\sigma_y + 3\tau_{xy}^2\})}$$

Then if $\bar{\sigma} > \sigma_F(T)$ the node was assumed to be plastic. The whole formulation of this model was crude in terms of both the assumptions and meshing of the structure; not

surprisingly it was found that the calculated values were very much smaller than those determined by experiment.

By far the most work performed on thermal stresses by the finite element method has been conducted in the research group led by Inoue. The majority of this work has aimed to modify a basic finite element program[105] to include the effects of phase transformations as realistically as possible.

Originally Taira and Inoue[105] considered a carbon steel shaft of 190 mm diameter x 380 mm long, whose central portion was heated by induction and then water quenched. The shaft was modelled as an axisymmetric body made up of simple triangular elements (Fig. 2.34): the mesh obtained is an excellent example of element refinement. The thermal history of the structure was determined by a finite difference technique and unknown parameters such as heat transfer coefficients were arbitrarily adjusted to give results which matched experimentally determined temperature distributions. A linear work hardening coefficient was included but neither it nor the yield stress varied as the temperature changed. Only residual stresses caused by plastic straining were considered and although transformations were ignored in this work, the authors claimed good agreement with experimental results obtained by means of a Sach's technique; however no experimental details were given. Yielding in tension was predicted at the surface just below the induction coil with compressive stresses further down the shaft. These compressive stresses fell to zero just before the end of the shaft, but it is impossible to say how much of this attenuation is due to the edge effect as opposed to the additional reduction due to the distance from the localised thermal load.

Inoue[7] then attempted to incorporate phase transformations into the model by consideration of the strains induced through dilatations. He considered a 0.43% carbon steel cylinder (60 mm diameter) water quenched from 870°C. In this and any further work by the Inoue group, no mesh of the structures have been shown, but examination of the 6 x 6 elasticity matrix suggests a three dimensional formulation. The boundary conditions for the thermal analysis were experimentally determined temperatures at the surface and the centre. This would automatically impose surface heat transfer conditions. The coefficient of expansion which was used to follow the dilatation curves was taken to be a function of both temperature (T) and cooling rate (T) whilst the dependence of elastic properties on temperature was considered unimportant relative to the much greater effect of temperature on the yield stress. The transformation product at any point in the cylinder was defined by comparison of the maximum cooling rate (T_{max}) with upper and lower critical limits on this parameter. Thus:

$\dot{T}_{max} < 50^{o}C/sec \rightarrow$ pearlite

$50^{o}C/s < \dot{T}_{max} < 180^{o}C/s \rightarrow$ bainite + martensite

$180^{o}C/s < \dot{T}_{max} \rightarrow$ martensite

Typical volume expansions for these three microstructures were incorporated in the program. Figure 2.35 shows the predicted and experimentally determined results which are in good agreement. It should be noted that the radial stress falls to zero at the cylinder surface, but no detail has been given concerning the axial stress variation along the axial direction, particularly towards the ends of the cylinder.

In later papers the Inoue group modified this analysis to include creep during tempering and heat generation on transformation[106]. This latent heat was dervied from the mass fraction of phases present[107] and the effect seemed to

improve the accuracy of predicted cooling curves when compared with those obtained experimentally but the stress analysis based on this modification gave erratic results which did not correspond with experimental values. The next development[108] was the adoption of 6 curves from the continuous cooling/transformation diagram of a 0.43% carbon steel, along with corresponding dilatometry data, to enable all types of microstructures to be included. In this latter program all properties had a linear temperature dependence, but it was realised that little work hardening would occur in the hardened condition. Again stresses were only shown at a central plane in a water quenched cylinder, although radial distortions were given for the whole section (Fig 2.36). The predicted and experimental distortions did not agree, although both sets of results indicate an edge effected region which is less than the diameter of the cylinder.

The above model has been developed to follow phase nucleation and growth[109], and even the occurrance of carbide in the structure[110]. During the latter stages of this model development, the results appeared to show adequate agreement with both the Sachs and X-ray stress determination experiments, but no practical details were given.

In none of the finite element models discussed above has consideration been given to the effect of variations in

a. the time step used in the temperature calculation

b. the incremental load step used in the plasticity calculation

c. mesh size

It can only be assumed that these variables were critically examined and that optimum conditions were applied to the final analysis.

Schroder[124] employed an axisymmetric finite element model to investigate the residual stresses in quenched cylinders of various lengths and diameters. He recognised the complications of free surfaces at the ends of the clyinders, and therefore performed analyses on specimens of short length, i.e. circular plates, to establish the stress modifications in this region. His initial analyses imposed a quadratic temperature distribution across the radius of the cylinders with a temperature difference of 100 K from axis to edge; only elastic stresses were considered. The results of this work predicted an axial stress distribution which decayed to zero at the end of the cylinder, with tangential stresses on the axis that became more compressive ($-230\ N/mm^2$) close to the end before unloading to a value at the free surface ($-120\ N/mm^2$) which was substantially different to that found well away from the end ($-120\ N/mm^2$). These models also showed that radial and axial displacements only varied in the regions adjacent to the ends of the cylinders. Further detailed analyses included ideal elastic-plastic behaviour, multi-transformation products and coating from all surfaces of the cylinder. However, only a constant heat transfer coefficient was employed of $3000\ w/m^2K$, which is not truly representative of a coolant's quenching characteristics. Schroder[124] concluded that global cooling (as opposed to only radial cooling) changed the magnitude of the stresses but not their distribution unless phase transformation occurred. and that plastic deformation begins at the ends of the cylinders before growing into the section. Consideration of X-ray experiemental methods with surface removal techniques, to measure residual stresses in specimens, was dismissed as inadequate for obtaining data at the ends of the cylinder. Overall the work presented by Schroder[124] shows specific analytical examples to prove the importance of the edge effect in quenched cylinders, but does not attempt to quantify this phenomenae or suggest the correction factors which could be applied to simpler analysis techniques.

2.6 CONCLUSIONS FROM PREVIOUS WORK

The finite element technique has been utilised to calculate the principal stresses and strain, and the overall dimension changes in quenched bodies. Although this technique has been extended to determine the complex variation in stress which occurs near traction-free edges in a body of finite dimensions, little attempt has been made to understand or explain these variations. This analysis method is ideally suited to quantifying the extent of the "edge effect" and thereby allowing the generation of correction factors which could be applied to simpler and cheaper analysis techniques.

3. EXPERIMENTAL DETERMINATION OF THERMAL STRESS AND STRAIN IN THE REGION ADJACENT TO THE EDGE

3.1 EXPERIMENTAL DETERMINATION OF DISTORTION

3.1.1 Sample Preparation

The specimens used in the determination of residual stress and distortions (after quenching) were taken from a billet of En30B steel and machined into discs of 120mm diameter and 20mm thickness with flat parallel faces. A hole was drilled and tapped in the edge of each disc for the attachment of an eye bolt to facilitate handling during the quenching process. The eye bolts were also machined from En30B to prevent errors associated with differential expansion. As in previous work[49] En30B was chosen because it is an air hardenable steel which can be expected to transform totally to martensite during the quench without retaining undesirable diffusional transformation products. Two segments of the original billet were submitted for chemical analysis to verify the material constituents against the British Standard for En30B (see table below).

SPECIFICATION

C	Si	Mn	S	P	Ni	Cr	Mo
0.26-0.34	0.10-0.35	0.40-0.60	0.05 MAX	0.05 MAX	3.9-4.3	1.1-1.4	0.2-0.4

ANALYSIS RESULTS

C	Si	Mn	S	P	Ni	Cr	Mo
0.30	0.29	0.58	0.022	0.01	4.23	1.4	0.23

After machining to size the test specimens were lightly polished to remove mechanical abrasions and then cleaned in alcohol. To prevent gross scaling during subsequent heat treatments the plates were then coated with a thin nickel flash by electro-deposition, to a nominal depth of 0.05mm (<0.5% of the total plate thickness).

Stress relief annealing of the samples at 630°C for 2 hours followed by a slow furnace cool ensured a stress free state prior to the commencement of the quench process. This annealing cycle was performed in an argon atmosphere to further ensure a minimisation of oxidation.

Throughout these preparatory operations and during subsequent heating/quenching treatments sample plates were tested for hardness, nickel coat integrity and microstructure.

3.1.2 Initial Plate Measurements

After 24 hours repose time in the metrology laboratory, to allow temperature stabilisation, the annealed plates were marked out (lightly scored) according to figure 3.1-1. All measurements of diameter and thicknesses were made in a Genevoise Universal Measuring Machine. Before using this equipment it was necessary to determine the feeler constant and assess the operator performance for repeatability. This involved the use of a calibrated slip gauge.

The specimen was placed on the Genevoise revolving table with an intermediate (smaller diameter) raised platform to enable access to the plate lower edge. Centring of the plate was achieved by the use of a dial gauge and the positioning of the "eyebolt hole" at 0° was performed manually by alignment of the "A" scorelines with the microscope cross wires. Measurements across the diameter of the plate were then taken

at the 85° and 355° positions at various levels through its thickness. These levels were at the top, bottom and at 5mm intervals (positions E to I in figure 3.1-1) measured on a vernier scale.

Due to the limitations of the Genovoise machine it was not possible to perform through thickness measurements at all points, but it was possible to make reference measurements at A, B, C and D (figure 3.1-1) by the following method:-

1. The plate was stood vertically with a traverse line (A-B) nominally parallel to the the machine bed.

2. The microscope was focussed on the cross score.

3. It was checked that the faces of the plate were parallel to the machine transverse axis by movement of the stylus.

4. The thickness of the plate was measured at the reference point with the stylus just inside the edge.

5. The table was rotated 180° for determination of the opposing reference point.

6. The above procedure was repeated for the reference points on the other traverse line (C-D).

With these known reference points it was then possible to traverse the plate with a travelling vernier, using slip gauge blocks to give fixed steps across the diameter. Although the plate was nominally levelled on a plasticine base prior to commencing these measurements it was evident that some form of correction factor would be necessary when determining the true through thicknesses across the traverse. Such a correction factor was derived from the geometry shown in figure 3.1-2, where A and B are the known reference thicknesses. N is the measurement increment and C_n is the actual vernier deflection at that point. By inspection;

$$C_{1\ TRUE} = \frac{(A-B)}{2}$$

Correction factor for levelling = $C_1 - \frac{(A-B)}{2}$

Thus the thickness of the plate at any point, N, was calculated by:-

$$THICKNESS_N = A - 2\left\{C_N - \frac{(11-N)}{10}\left[C_1 - \frac{(A-B)}{2}\right]\right\}$$

3.1.3 Quenching

After the geometry of the annealed plate had been determined it was prepared for quench hardening by fixing in an insulation mounting shown in figure 3.1-3. This mounting was constructed from mild steel and served two purposes;

a. to retain the kaol insulation wool in close contact with the edges of the plate, to prevent heat loss from this surface and thereby produce unidirectional heat flow.

b. to provide a means of locating the plate precisely in the guide channels of the quench tank

As the forces which cause thermal distortion may be small in magnitude the plate must be unconstrained, so the insulation and mounting had to exert no appreciable traction on the plate whilst at the same time maintaining its position. This was achieved by using two lock nuts on the En30B eyebolts (handling aid) which located against the mounting frame. This eyebolt was screwed directly into the plate.

The plate complete with eyebolt, insulation and mounting frame were placed in a muffle furnace at 850°C for 1½ hours after the plate reached this soak temperature as determined

by a surface mounted thermocouple.

The quench tank to be used (figure 3.1-4) was filled with water at 20°C and of sufficient volume to possess a quenchant thermal mass much larger than that of the plate specimen. A pair of quide rails suspended centrally in the tank ensured that the plate mount could be positioned exactly in the centre of the water volume and held vertically during the quench. The frame supporting these rails also held two electric motors which drove paddles at 50 r.p.m. The paddles were to agitate the water and thereby prevent localised heating of the quenchant.

After the plate had soaked in the furnace for the required period it was swiftly removed and immediately quenched in the water tank according to the configuration described above. Several minutes was allowed to ensure thermal equilibrium before the plate was removed from the tank and its mounting frame. It was then dried, lightly descaled and finally placed in the metrology laboratory for a further 24 hours before remeasurement could take place.

3.1.4 Remeasurement

Post quench measurements of the dimensions of the plate samples followed the procedure detailed in 3.1.2, with additional corrections made for the blistered nickel surface by performing a TAYLSURF traverse. This enabled surface roughness values above the mean plate surface to be subtracted from the apparent through thickness measurements. The corrected plate dimensions could then be compared with the initial measurements to determine the distortion which was associated with the quenching process.

3.2 SAMPLE MORPHOLOGY

In parallel with the primary task which determined residual distortion and stresses, other plates were examined at intermediate stages of the experimental procedure to assess the integrity of the nickel plate, as well as the variation in the microstructure and hardness of the plate.

3.2.1 Surface Examination

Prior to sectioning, the plate samples were examined visually and at 400X magnification on an Optomax system. Subsequent to plating but prior to the anneal the surface nickel flash was seen to be continuous, smooth and lusterous. There was evidence of a few small pits in this coating, and the corners of the samples had been slightly radiussed by the plating process.

After the stress relief anneal a grey oxide film had formed on the nickel, and the surface had become noticably rougher although it still appeared to be continuous. After quench hardening the visual appearance of the sample had changed little, but the rough texture of the nickel flash was more prominent.

3.2.2 Sectioning and Sample Preparation

To enable an examination of the microstructure and to perform hardness measurements in a lateral direction it was necessary to section two sample plates. Both plates were annealed together, then one was sectioned whilst the other was hardened prior to sectioning.

Sectioning of the plates, as shown in figure 3.2-1, was undertaken with a diamond slitting wheel and abasive disc, using a water soluble coolant. Great care was taken not to over-heat the samples or cause mechanical damage to the nickel plating. However, a small amount of burnishing was

observed on the hardened specimens. After mounting, all the microsections were polished back beyond the region effected by the sectioning process, to a final finish of 1um. The annealed sections were etched in 2% nital, whilst the hardened sections had to be swabbed with 4% picral to produce a satisfactory etch.

3.2.3 Microstructure of the Plate and Nickel Coating

At a magnification of X1000 the annealed specimens proved to have a fine uniform pearlite microstructure across the plate section. A clear boundary was observed at the nickel interface, without evidence of diffusion. Closer examination of the nickel flash disclosed many pits and some plate intrusions; a few rare blisters were also observed. Even so, this protective coating remained continuous because the pits did not penetrate through to the steel, all surface intrusions were filled with nickel, and the blisters were not perforated.

After quench hardening the plate structure had transformed to a uniform martensitic structure (viewed at X2500 magnification) across the specimen section. Some grain boundary penetration into the steel by nickel diffussion was observed for a few microns below the nickel flash. This protective layer maintained its integrity throughout the quench process, with no greater evidence of discontinuities than that discovered after the anneal. It is interesting to note that the nickel flash had undergone thinning on those faces which were open to the furnance atmosphere, compared to the edge which was insulated.

3.2.4 Hardness Traverse Across Plate Before and After Quenching

After removal of the nickel flash by gentle polishing, hardness values were determined for annealed and quenched plates according to the format shown in figure 3.2-1. The through-thickness traverse was performed on a microsection

sample taken from the plate centre, whilst the surface analysis was made on the lower half off-cut of the sectioned plate.

In the annealed condition the surface of the plate possessed a hardness range between 40.7 to 43.2 VPN, while in the interior the hardness lay between 39.8 - 41.0 VPN. The corresponding values in the hardened plate were 420-586 VPN and 575 VPN respectively. The dispersion of hardness values in either sample was random; no particular region or depth within the plate displayed a trend for a greater hardness than any other position.

The conclusions to be drawn from the above results are that the adopted experimental procedure for determining residual distortion and stress;

(a) produces a uniform microstructure which is annealed and hardened throughout the section,

(b) does not create varying properties within the samples

(c) maintains the integrity of the nickel flash which is used to prevent oxidation/decarburisation.

3.3 DETERMINATION OF RESIDUAL STRESS USING THE CENTRE HOLE AIR ABRASIVE TECHNIQUE

3.3.1 Introduction

The objectives of the work which includes an investigation of the effect of an edge on the bulk stresses of a plate sample, inhibits the use of a thin layer removal technique across the plate. Such a method has been employed in previous work, but only provides averaged data for the inplane stresses across the whole plane of the plate. To identify the axial component and modified radial stresses which are generated locally near the edge it was necessary to use an alternative

method of analysis. The best available analysis method for this purpose was the centre hole air abrasive technique.[40,41].

3.3.2 Test Procedure

A standard En30B plate, 120mm diameter by 20mm thickness, had four 20mm flats machined on the edge prior to nickel plating. These flats (or faces) were positioned in the four quadrants of the plate at 45° to the plate axes (figure 3.3-1). After the plate had undergone the anneal and quenching operations, a strain gauge rosette (TML.FRS-2-11) was bonded to each of these small faces.

Gauges AD and CB were positioned on the centre line of the plate, whilst gauges DB and CA were off-set 3mm above and below the centre line respectively. Such gauges contain a strain-senstitive alloy in the form of a foil grid (figure 3.3-2) which exhibits a change in resistance when subjected to a micro-strain. The resistance is measured using a Wheatstone bridge and the corresponding strain is derived from a calibrated gauge factor. Each rosette foil contains three gauge grids radially positioned around a centre hole. The composite strain results from these three gauges can be used to calculate the magnitude and direction of principal stresses.

With the plate now prepared as described above, strain gauge measurements were taken during the formation of a small hole made at the centre of each rosette gauge. These holes were 2mm diameter by 4mm deep, and were produced by a high velocity jet of air containing alumina abrasive particles. The air jet was provided from a trepanning head which ensured the holes had parallel sides as opposed to a tapered profile. This machining technique would not have induced additional stresses into the plate, but the residual stresses which were present in the removed material close to the plate edge were released and manifest as a strain on the surrounding gauges.

4. THEORETICAL PREDICTION OF THERMAL STRESSES IN THE REGION ADJACENT TO THE PLATE EDGE

From a practical point of view the model used for stress prediction in the edge affected region was a circular plate. This removes the complicating factors of sharp corners where the stress system is very complex. To prevent any other complications such as three dimensional heat transfer and transformation products other than martensite, the principle model considered only unidirectional heat extraction through the upper and lower surfaces of this plate (i.e. insulated edges), which has the properties of an air hardenable steel. This steel, En30B (835M30), whose chemical specification is shown in the table below has sufficient hardenability[111] for all the plates considered to transform completely to martensite during water quenching.

MATERIAL	C%	Mn%	Si%	Ni%	Cr%	Mo%	Fe
835M30	0.30	0.72	0.42	4.83	1.25	0.28	BALANCE
830A31	0.31	0.44	0.20	3.40	1.26	0.47	BALANCE

4.1 CLASSICAL FIELD EQUATIONS AND JUSTIFICATION OF THE CHOICE OF ELEMENT

The equilibrium equations and strain displacement relations which govern a system defined in cylindrical co-ordinates[60] are shown in Figure 4.1-1. In a structure such as a symmetrically loaded circular plate there cannot be a tangential stress gradient in the hoop direction, and any displacement in that direction is only as a consequence of expanding arcs as displacement takes place in the radial direction. Because of these constraints the boxed terms in Figure 4.1-1 are reduced to zero. From compatibility considerations, it is obvious that the sides of the element must remain parallel to the same radial plane under all

conditions, hence the shear stresses $\epsilon_{r\theta}$ and $\epsilon_{z\theta}$ are zero. The remaining stress components and their terms are therefore valid and are found in the strain matrix (ϵ)for an axisymmetric finite element[79]

$$\epsilon = \begin{bmatrix} \epsilon_z \\ \epsilon_r \\ \epsilon_\theta \\ \epsilon_{rz} \end{bmatrix} = \begin{bmatrix} \frac{w}{z} \\ \frac{u}{r} \\ \frac{u}{r} \\ \frac{u}{z} + \frac{w}{r} \end{bmatrix}$$

Where ϵ_z, ϵ_r, ϵ_θ, ϵ_{rz} = strain components
r, z = radial and axial directions
u, w = radial and azial displacements

Therefore the plate model was sub-divided into a mesh of axisymmetric finite elements, for the purpose of predicting the temperature distributions during quenching and the subsequent transient thermal stresses, as described below.

4.2 TEMPERATURE ANALYSIS

4.2.1 Finite Element Formulation

The calculation of the plate's thermal history during water quenching was performed using the Berkeley finite element programme, FLHE[112]. This employs a Crank-Nicolson scheme for solving the transient heat conduction equation, and hence the temperatures at a given time are equated to those at a preceding calculation time. The transient heat flow is governed by:-

$$\left((G)_t + \frac{2}{\Delta t}(P)_t\right)\{\Phi\}_t = \left(-(G)_{t-\Delta t} + \frac{2}{\Delta t}(P)_{t-\Delta t}\right)\{\Phi\}_{t-t} + 2\{F\}_t - \frac{\Delta t}{2}$$

where (P) = heat capacity matrix

(G) = conductivity and heat transfer matrix

{F} = thermal loading vector

{Φ} = nodal temperature vector (unknown)

t and Δt = time and time step increment

The set of equations that are to be solved is given by:-

$$(P)\ \{\partial \Phi\ \partial t\} + (G)\ \{\Phi\} = \{F\}$$

For a finite element analysis each of the terms in the above equation is a matrix consisting of individual parameters for every node in the model. As an analysis progresses, those matrices which contain temperature dependant data, such as surface heat transfer values, needs to be modified. This updating of data was performed after discrete time steps in the analysis but certain approximations were necessary because the temperatures at time, t, were unknown. The approximations used for updating properties were:-

$$\{\Phi\}_t = \{\Phi\}_{t - \Delta t} \text{ and } 2\{F\}_{t - \Delta t/2} = \{F\}_t + \{F\}_{t - \Delta t}$$

In this programme, an initial temperature of 850°C was prescribed to all nodes, and the upper surface boundary condition was applied by specifying a surface flux as a function of temperature. The absence of fluxes on the other boundaries infers perfect insulation or a plane of symmetry, i.e. $d\Phi/dz = o$. The time steps to be used were defined at the beginning of the analysis which required a prior knowledge of the likely change of surface flux with time, and had to be small enough to prevent instabilities in the solution. The early time steps originally used were of the order of 0.1 seconds.

The solutions to the temperature vector at each step were down loaded into the computer memory for subsequent use as the thermal history in the stress calculation.

4.2.2 Finite Elements, Meshes and Smoothing Procedures

The finite element type chosen to describe the plate was an axisymmetric isoparametric element (EX16) with four corner nodes, four midside nodes and with a shape function that allows quasi-quadratic temperature variation in any plane. As a first analysis, a single column of 20 equal sized EX16 elements were used to describe an upper segment of the plate (10mm thick) with the bottom of the column corresponding to its centre plane. It was unnecessary to examine an entire plate quadrant at this stage, as the heat flow to be considered was unidirectional.

Improvement of this simple model was obtained in two ways;

a. Mesh refinement at the surface, where the expected temperature gradient was most severe. This was achieved by a linear bias in element thickness towards the surface without increasing the number of elements (Fig. 4.2-1).

b. Treatment on the calculated temperatures by two smoothing procedures.

The first smoothing procedure employed was to produce a weighted average of the results,

$$\Phi^{*}_{t} = 0.25\ (\Phi_{t-1} + 2\Phi_{t} + \Phi_{t+1})$$

but this modification could only be performed after the first estimate of the temperature solution had been completed using FLHE. The second smoothing procedure used the same weighted averaging technique after the first three time increments to produce an average second value. However as each new set of temperature values were calculated these were successively averaged, using the previously averaged temperatures (Φ^{*}_{t-1}).

This latter procedure produced results that closely correlated with results obtained by an exact analytical method. Hence they were adopted in all further analyses.

4.2.3 Thermal Property Data

All thermal data supplied to the finite element programme was temperature dependent, and was introduced as specific values at particular temperatures. At intermediate temperatures linear interpolation was carried out between the relevant pairs of values. The values used for thermal conductivity (λ), specific heat capacity (C_p) and density (ρ) are shown in the table below, and have been taken from the information available on 830A31 steel[113], which is very similar to 835M30.

Thermal Properties of 835M30 Steel

TEMP. °C	THERMAL CONDUCTIVITY W/m°C	SPECIFIC HEAT CAPACITY J/Kg°C	DENSITY Kg/m^3
20	25.58	450.0	7843
223	26.14	840.0	7800
328	22.83	620.0	7900
850	27.15	635.0	7630

The variation of surface flux with temperature for water quenching was derived from the surface heat transfer (h) information derived by Price [11],

$$\text{surface flux} = h(\Phi - \psi)$$ where Φ = quenchant temperature, ψ = surface temperature

The variation of the surface flux is controlled by the successive stages of surface heat transfer during the quench, ie vapour blanket, nucleate boiling, and liquid contact stages. See table below:-

TEMP. °C	SURFACE FLUX W/mm²
20	0
94	-0.1014
275	-2.7335
381	-4.8753
827	-1.2201
850	-1.2201

4.3 THERMAL STRESS ANALYSIS

4.3.1 Finite Element Thermoelastic-plastic Formulation

The finite element programme used to calculate thermal stresses[114 115] is based upon the assumption that the total strain increment $\{\epsilon\}$at any point in the structure equals the sum of the elastic, plastic and thermal strains[116],

$$d\{\epsilon\} = d\{\epsilon_e\} + d\{\epsilon_p\} + d\{\epsilon_\theta\}$$

The stress increment $d\{\sigma\}$ is given by

$$d\{\sigma\} = [D]\, d\{\epsilon_e\}$$

where (D) is the modulus matrix. The relationship between total strain $\{\epsilon\}$ and the nodal displacement vector $\{u\}$ for the element containing that point is given by

$\{\epsilon\} = (B)\ \{u\}$, where (B) is a matrix of shape functions and boundary conditions specific to the type of finite element being used.

If H' is the instantaneous slope of the uniaxial stress-plastic strain curve, the plastic modulus matrix is readily obtained from;

$$[D_p] = [D] \frac{\partial F}{\partial \{\sigma\}} \left(\frac{\partial F}{\partial \{\sigma\}}\right)^T [D] \left[H' + \left(\frac{\partial F}{\partial \{\sigma\}}\right)^T [D] \frac{\partial F}{\partial \{\sigma\}} \right]^{-1}$$

Defining the plastic stress increment by $d\{\sigma_p\}$ gives the relations;

$$d\{\sigma\} = d\{\sigma_e\} + d\{\sigma_p\}$$

$$d\{\sigma_p\} = [D]\, d\{\epsilon_p\}$$

and $$d\{\sigma_p\} = [D_p]\, (d\{\epsilon\} - d\{\epsilon_e\})$$

Thus, the plastic stress increment can be determined from the total strain, which in turn is dervied from the incremented displacements and the plastic modulus matrix.

The Von Mises yield criterion is defined as;

$$F = \sqrt{}\, (3\bar{\sigma} - Y) = o$$

in which σ is the equivalent stress and in three dimensional space is given by;

$$\bar{\sigma}^2 = \frac{1}{6}\left[(s_x - s_y)^2 + (s_y - s_z)^2 + (s_z - s_x)^2\right] + \tau_{xy}^2 + \tau_{yz}^2 + \tau_{zx}^2$$

where s_x, s_y and s_z are deviatoric stress and τ_{xy}, τ_{yz} and τ_{zx} are the accompanying shear stresses.

Analogous to the equivalent stress is the equivalent plastic strain defined by;

$$\epsilon_p = \int d\epsilon_p\, dt$$

over the strain history[116].

Due to the requirement of incompressibility, the plastic strain increments are deviatoric:

$$(d\epsilon_p)^2 = \frac{2}{9}\left[(d\epsilon_{px}-d\epsilon_{py})^2 + (d\epsilon_{py}-d\epsilon_{pz})^2 + (d\epsilon_{pz}-d\epsilon_{px})^2\right] + \frac{1}{3}\left[d\gamma_{pxy}^2 + d\gamma_{pyz}^2 + d\gamma_{pzx}^2\right]$$

Where $d\epsilon_{px}$, $d\epsilon_{py}$ and $d\epsilon_{pz}$ = Plastic strain increments in the x, y and z axes.

$d\gamma_{pxy}$, $d\gamma_{pyz}$ and $d\gamma_{pzx}$ = Plastic shear strain increments.

When formulating the finite element solution, the maintenance of equilibrium was expressed using the principle of virtual work as

$$\int_V [B]^T \{\sigma\} dV = \{R\}$$ where $[B]^T$ = transform of the strain/shape function matrix

where the integration is over the structural volume (V); {R} is the external load vector due to thermal processes.

An increase of load of d{R} will effect a stress increase of d{σ}, resulting in a new equilibrium condition:

$$\int_V [B]^T d\{\sigma\} dV = d\{R\}$$

The attainment of equilibrium is ensured by using the initial stress method which gives,

$$\int_V [B]^T d\{\sigma\}\, dV - \int_V [B]^T d\{\sigma_p\}\, dV = d\{R\}$$

The first integral is the elastic stiffness matrix (K_o) and

$$[K_o]\, d\{u\} = d\{R\} + d\{S\}$$

Here, at any stage of iteration within a load increment, the current state of plastic stress increment is used to assess the equivalent nodal force vector, d{S}, from which a re-solution gives an improved set of displacements.

A suitable sequence of load increments has to be defined (10 were used) and convergence to a satisfactory solution was assessed by comparing the ratio of the amount of unbalanced load remaining at the end of the load step to the total load applied during that time increment. Convergence was assumed to be complete when this value was <1%.

In plasticity, at any point in the loading sequence, the amount of thermal strain present has to be considered in increments as is the case for mechanical loading. The relationship between time and the load steps has to be defined. If the total load to be applied is R_T, and the load still to be applied after initial yielding is R, then the load level at this initial yielding is R_o when $R + R_o = R_T$. If the increments of load used after first yield are R_i, i = 1, N, then the time t taken to correspond to load increment i is given by:

$$t = \left[\sum_{j=1}^{i=1} \Delta R_j + \tfrac{1}{2} \Delta R_i + R_o \right] \left[\frac{t_2 - t_1}{R + R_o} \right] + t_1$$

where $t_1 \leq t \leq t_2$ and (t_1 to t_2) is the required total time span. Thus, at the given load increment i, the temperatures used will correspond to a time representing the midpoint of load increment i. The elastic load R_o uses temperatures at $t = t_1$. For the first load increment, t is given by

$$t = \left[\frac{R_o + \frac{1}{2} R_1}{R + R_o} \right] (t_2 - t_1) + t_1$$

The temperature changes during each load step can be used to obtain the current thermal strains at each element Gauss point, and would also be used to update the plastic material properties which have a temperature dependance.

Unfortunately, in BERSAFE the elastic material properties, which are temperature dependent, are based on temperatures obtained from the record of temperature-time history produced from the FLHE analysis; thus if violent temperature changes occur, it is necessary to frequently repeat the whole loading process.

4.3.2 En30B Material Properties

All of the mechanical property data used in this programme was temperature dependent. As with the thermal properties, the programme interpolates linearly between specified mechanical property values, see figures 4.3-1 and 2. The values for Young's modulus and Poisson's ratio were taken from reference[113]. The coefficient of linear expansion was taken across the 850°-200°C temperature range by determining the gradient of the dilatometer curve for 835M30 steel[11] at several points. This enabled the volume expansion due to the martensite transformation to be included in the value of this property. The variation of yield stress and work hardening coefficient[11] with temperature were obtained from seven stress-plastic strain curves. This data was introduced into the programme by the use of 20 stress-strain data points on each curve.

4.3.3 Creation of the Finite Element and Initial Steady State Elastic Analysis

The first step in the discretisation of a structure by finite elements is the identification of the smallest segment which is representative of the entire body. In the case of a circular plate with symmetrical loading, an upper quadrant (Fig. 4.3-3) fulfils this requirement. Regardless of the methods by which the upper quandrant may have been meshed, it was representative of the entire plate when the following boundary conditions were applied;

a. Zero radial displacement for any node lying on the plate axis.

b. Zero axial displacement for any node lying on the plate's plane of symmetry (centre plane).

With these specified in the programme, the corresponding unknown displacement vectors were set to zero in a direction perpendicular to the boundaries.
As was stated earlier, for this particular problem the use of axisymmetric elements was justifiable. To be consistent with the element type used in the thermal analysis, and to contend with quadratic temperature and displacements, the EX16 axisymmetric isoparametric elements were used. By using axisymmetric elements the fundamental vectors and matrices to be assembled were of the following forms.

a. The displacement field, $u = \begin{Bmatrix} u \\ v \end{Bmatrix} = (IN_1, IN_2, \ldots\ldots IN_8)\delta^e$

where I = 2 x 2 identity matrix

$N_1 = (a_1 + b_1 r + c_1 z)/2\Delta$, etc. = quadratic shape function for node one.

Δ = the element area

b. The strain matrix

$$B_i = \begin{bmatrix} 0 & \frac{\partial N'_i}{z} \\ \frac{\partial N'_i}{\partial r} & 0 \\ \frac{1}{r}N'_i & 0 \\ \frac{\partial N'_i}{\partial z} & \partial N'_i \end{bmatrix} = \frac{1}{2\Delta} \begin{bmatrix} 0 & c_i \\ b_i & 0 \\ a_i/r + b_i + c_i z/r & 0 \\ c_i & b_i \end{bmatrix}$$

c. The strain vector (initial thermal strain),

$$\epsilon_o = \begin{bmatrix} \epsilon_{zo} \\ \epsilon_{ro} \\ \epsilon_{\theta o} \\ \gamma_{rzo} \end{bmatrix} = \begin{bmatrix} \alpha\theta^e \\ \alpha\theta^e \\ \alpha\theta^e \\ 0 \end{bmatrix}$$

d. The elastic matrix,

$$D = \frac{E(1-\nu)}{(1+\nu)(1-2\nu)} \begin{bmatrix} 1 & \frac{\nu}{1-\nu} & \frac{\nu}{1-\nu} & 0 \\ & 1 & \frac{\nu}{1-\nu} & 0 \\ & & 1 & 0 \\ & \text{Symmetric} & & \frac{1-2\nu}{2(1-\nu)} \end{bmatrix}$$

The first mesh (mesh A) constructed of EX16 elements was a 10 x 12 structure which represented the plate upper quadrant of 7.5 mm thickness x 15mm radius. The elements were of equal size without refinement in any part of the mesh. This mesh was analysed elastically at a very early time point (0.05 sec) when the water quench had reduced the surface temperature to 812°C.

The BERSAFE finite elements package, which was used to analyse the plate, has a limitation on the total number of Gauss (internal integration) points that can exist in a single model. This in turn limits the number of elements that can be used, ie 250 of the EX16 type. A high element density is required in the regions of severe temperature and stress gradients but with a limited number of elements a large bias towards one boundary would create a mesh with some elements which have a high aspect ratio. The use of high aspect ratio elements, or failure to provide a sufficiently high element density had proved to cause instabilities in the analysis solution.

With these restrictions it was not possible to generate an ideal mesh of the plate structure, therefore an invesitigation of several element types and mesh configurations was undertaken to reach the best compromise between these conflicting requirements.

To justify the use of a two dimensional axisymmetric mesh the same quadrant size was meshed using EX60 elements, which are a three dimensional equivalent of the EX16 type, i.e. one midside node per edge in addition to the corner nodes. The first attempt to perform this descritisation for an entire quadrant in three dimensions (Fig. 4.3-4) proved to give a relatively coarse mesh by the use of sixty elements. Refinement of that mesh to give a higher quantity of elements across a radial plane (Fig. 4.3-5) resulted in such a large number of superfluous elements that it would obviously be an inefficient model to analyse. The alternative to this approach was to mesh a 5° wedge which lies in the upper quadrant. This presented problems due to the poor aspect ratio of certain elements if the radial and axial dimensions for each were equal. The aspect ratio of an element is the ratio of its longest to shortest dimension, and should not exceed 6:1 if a stable solution is to be achieved. By biasing of these elements in a 2:1 proportion against the edge and surface (Fig. 4.3-6) an acceptable mesh (B) was produced with the added benefit of refinement towards the areas of highest expected stress gradients. This mesh was analysed under the same conditions as mesh A.

As a further refinement and comparison, both the axisymmetric and three dimensional models were re-analysed with an element bias of 3:1 against the surface and edge (meshes C and D respectively), but with the radius increased to 20 mm to ensure the results at the centre would definitely be free from edge effects. This increase was necessary because the only sure method of confirming the validity of the model was by comparing the centre plate results with those of an infinite plate analysis which used the same conditions and properties[49].

To investigate the effect of element area on the results, the dimensions of mesh c were reduced, e.g. the quadrant dimensions were set to 3.75 mm x 10mm radius. This mesh (E) is shown in Figure 4.3-7. Although this scaling caused a change in the temperature distribution, a time point was chosen to give a similar stress level to the previous models so that the effect of the element area change could be assessed.

Mesh E was then analysed for a later time point where the surface temperature during water quenching had fallen to 670°C. Under these conditions, plasticity would have occurred so the analysis was made by the transient elasto-plastic formulation already given. The procedure used was to split the time step from 0-0.75 seconds into 10 equal load increments, perform an original elastic analysis at the first increment using property values corresponding to these temperatures, then march forward in time calculating the additional strain $\epsilon = \epsilon_E + \epsilon_p$ and new stresses at each load increment until the end of the time step.

The same size structure as mesh E was analysed under identical conditions by a mesh of triangular axisymmetric elements (Fig. 4.3-8) to make a comparison of results for different element types.

Although the general refinement of the structure to give mesh E appeared to give stable results which compared well with previous work[49], a stage had been reached where the size of this theoretical model (10 x 3.75mm) could not be compared against experimental results due to the practical problems of determining stresses in handling very thin plates. Because of this situation, the geometry of mesh E was scaled up to a size which would represent a plate of 20 mm thickness x 30mm radius, the localised refinement of elements was set to a bias of 6:1 against the surface and edge, and 3 additional columns of elements were introduced across the radius (mesh F) as shown in figure 4.3-9. Elasto-plastic analysis were performed on this mesh, but over much smaller time steps

(0.01, 0.02, 0.04, 0.08, 0.16 seconds) to allow for the loss of general refinement caused by employing a larger plate.

With this 10 x 15 element mesh (F) the only other methods available to improve the stability of the model was to either uprate the number of internal integration (Gauss) points per element or increase the overall number of elements in the mesh. The matrix assembly routines of the finite element programme to be used had a maximum capacity of one thousand Gauss points per structure. All the elements so far used, employed an integration rule of 2 (2 x 2 Gauss points/element) but if an integration rule of 3 were to be adopted, the number of available elements for meshing would only be 111. This was sufficient to mesh the plate quadrant with 11 element columns along the radius, although the aspect ratios of the top centre elements were close to the upper limit of 6:1. Such a mesh was analysed for a time step of 0.16 seconds (final surface temperature = 790°C), along with a mesh of 240 elements (15 x 16) which had the original integration rule of 2. The results from these models were not significantly different from those predicted by mesh (F), hence the latter was adopted during the main calculation programme.

4.3.4 Calculation of Thermal Stresses

The primary analysis of the calculation of thermal stresses by finite elements was performed using a 10 x 15 element arrangement. This was applied to the unidirectional water quench of a 30mm radius by 20mm thick disc of EN30B steel (mesh F described in the previous section), The rim of the disc (ie the edge) was assumed to be perfectly insulated. To establish a comparison between this model and the more realistic quenching of a component a second analysis was performed on a 13 x 17 element model using a plate of identical dimensions but with biaxial heat transfer (ie no

insulation on the rim). This simulated quenching of the plate from both the edge and parallel surfaces involved the application of surface heat transfer conditions to both of these boundaries.

More elements were used in this analysis to achieve an improved mesh refinement close to the plate edge, which would now be subject to more severe thermal and stress gradients, because it was necessary to maintain an acceptable aspect ratio for individual elements. This analysis was continued until 14 seconds of the quench had elapsed.

To establish the effect of plate dimensions, on the generation of stress, two further analyses of unidirectional quenched plates were conducted. These employed 10 x 15 elements and maintained a plate thickness of 20mm but the radius varied between 15 and 60mm.

A fifth and final analysis (again unidirectional heat transfer) was performed using a 32mm radius plate with a 2mm radius hole through the centre. This model had a mesh of 10 x 15 elements and displayed an edge effect on both radial boundaries.

These latter three models were only continued for the first 0.4 seconds of the quench.

5. RESULTS OF EXPERIMENTAL DETERMINATION OF RESIDUAL STRESS AND DISTORTIONS AFTER QUENCHING.

5.1 SHAPE OF PLATE AFTER QUENCHING

5.1.1 Machine Calibration

Prior to measurement of the dimensions of the plate in either the annealed or quenched conditions, calibration of the Genovoise feeler gauge was undertaken by repeated measurements of a slip gauge standard (10.0001 mm). Ten sample readings from this gauge gave the most probable value of the feeler constant (K) which is given in the table below along with the associated confidence limits.

	ANNEALED PLATE	QUENCHED PLATE
FEELER CONSTANT (K)	4.1120 mm	4.1122 mm
STANDARD DEVIATION	6.146×10^{-4} mm	9.274×10^{-4} mm
95% CONF. LIMITS	1.390×10^{-3} mm	2.097×10^{-3} mm

5.1.2 Transverse Dimension Variations

After allowing for surface roughness corrections, the transverse dimensions of the plate, as determined before and after the quench process, were used to calculate distortion values. These distortion values (shown in figure 5.1-1) were obtained perpendicularly to the face at points along two orthogonal lines on the face which are vertical (A-B) and horizontal (C-D) with respect to the plate orientation in the quench tank. Such results, which show an overall contraction in the plate in the transverse direction, are comparable with those reported in previous work by Fletcher and Price[49]. In both cases the region of the plate face which is apparently under the influence of the edge is within a distance of approximately one plate thickness of the edge.

However, the square plate of Fletcher and Price exhibits a mean distortion of approximately -0.7% whilst the circular plate used in the present work has a mean distortion of approximately -0.45%. This anomaly may be attributed not only to the difference in the two plate geometries but also to the difference in the aspect ratios. The present quench sample was 120mm diameter by 20mm thick, whilst that used by Fletcher and Price was 120 mm square by 17 mm thick.

5.1.3 Longitudinal Dimension Variations

The distortion along the plate diameters (shown in Fig. 3.1-1) which occurred during water quenching are given in the table below:-

DIAMETER POSITION		MEAN DISTORTION %
(TOP SURFACE)	E	0.4222
	F	0.3436
(CENTRE PLANE)	G	0.2986
	H	0.3718
(BOTTOM SURFACE)	I	0.4278

The combination of these results with those in the transverse direction shows that the plate has assumed a "dog bone" shape as a consequence of the thermal strain generated during the quench.

With a mean diametrical change of +0.37% and a mean through thickness change of -0.45%, the plate has sustained a volume increase of +0.29% during quenching.

5.2 CENTRE HOLE AIR-ABRASIVE STRESS DETERMINATION

5.2.1 Variation of Strain Measurements During Drilling

During the abrasive forming of each of the four holes on the plate edge, it was observed at the very early stages that low

magnitude tensile strains were registered on the strain gauge rosettes. These were indicative of low magnitude compressive residual stresses in the surface layers of the plate edge, but this phenomena was registered for such a short period that quantitive evaluation of these stresses was not possible. Throughout the remaining period of the hole formation only compressive strains were observed on the strain gauge elements of the four rossettes.

5.2.2 Stress Measurements on Completion of Drilling

The results of the residual stress measurements were calculated from the measured strains on each gauge by the following equations

$$\sigma_1 = \frac{1.E}{k_1.2}\left[\frac{\varepsilon_1 + \varepsilon_3}{1 - \frac{\nu k_2}{k_1}} + \frac{1}{1 + \frac{\nu k_2}{k_1}}\sqrt{(\varepsilon_1 - \varepsilon_3)^2 + \{2\varepsilon_2 - (\varepsilon_1 + \varepsilon_3)\}^2}\right]$$

$$\sigma_2 = \frac{1.E}{k_1.2}\left[\frac{\varepsilon_1 + \varepsilon_3}{1 - \frac{\nu k_2}{k_1}} - \frac{1}{1 + \frac{\nu k_2}{k_1}}\sqrt{(\varepsilon_1 - \varepsilon_3)^2 + \{2\varepsilon_2 - (\varepsilon_1 + \varepsilon_3)\}^2}\right]$$

$$\alpha = \tfrac{1}{2}\tan^{-1}\left\{\frac{2\varepsilon_2 - (\varepsilon_1 + \varepsilon_3)}{\varepsilon_1 - \varepsilon_3}\right\}$$

where K_1, K_2 = gauge constants

ν = poissons ratio

E = Young's Modulus

α = Angle between gauge 1 and the principal stress; σ_1 (+ve is clockwise)

$\epsilon_1, \epsilon_2, \epsilon_3$ = relaxed strains

σ_1, σ_2 = Principal stresses

The calculated results are given in the table below:-

ROSSETTE	σ_1 N/mm²	σ_2 N/mm²	α
AD central	+598	+381	-10°
CB central	+554	+335	- 5°
CA below	+411	+346	-40°
DB above	+377	+124	+45°

These residual stresses and their directions represent mean values over the hole depth of 4mm. Because the residual stress levels are below 50% of the yield stress of martensite the total error in the measurement system is ±8%.

On the central plane of the plate, in both measurement positions AD and CB, the principal stress is effectively in the axial direction with the secondary stress in the hoop direction. Within the accuracy of the experimental technique the measured values for these two positions, which are on the same plane, are consistant. The remaining two positions, CA and DB, were displaced below and above the centre line of the plate respectively, with CA close to the handling bolt and DB diametrically opposing. In both cases the experimentally determined principal stresses have rotated up to 45° away from the axial and hoop directions of the plate, and the stress levels are no longer consistant, with those at DB being much lower than at CA. Although these two positions are nominally identical and might be expected to display similar stress characteristics, it should be noted that CA is 3mm from the centre plane whilst DB is only 2.5mm from this datum. This physical discrepancy was due to the error involved when manually attaching strain gauge rossettes, and may be directly responsible for the variation in measured stress values because of the stress gradients associated with axial position.

6. FINITE ELEMENT THERMAL STRESS ANALYSIS RESULTS

6.1 TRANSIENT TEMPERATURE DISTRIBUTIONS

The initial analysis produced the relationships between temperature and time at each nodal point as described earlier in section 4.2 (unidirectional water quench of a 20 mm thick En30B disc). The results were found to agree with those of Price and Fletcher[58] who used an explicit finite difference method. At no time during this simulation were "background noise" or non-covergent instabilities observed.

The full relationships between time and temperature at four points in the plate are shown in figure 6.1-1. These clearly show the initial higher cooling rate of the plate surface (NODE 471) compared to it's centre (NODE 1).

Figure 6.1-2(a) shows the predicted relationships between time and the temperature of the plate surface (T), along with the difference in temperature between surface and centre (T) during the early stages of the quench. These are compared with the surface heat transfer coefficient (h), which was used to characterise the heat transfer between plate surface and water quenchant.

These thermal relationships are associated with the following thermal phenomena:-

1. In the first 0.10 seconds of the quench a continuous vapour blanket forms around the plate surface, thereby restricting heat transfer.

2. As the vapour blanket breaks up at 827°C and the onset of nucleate boiling occurs, the rate of heat loss at the surface increases and the temperature just below the surface drops rapidly before any corresponding change occurs in the centre layers.

3. The highest rate of temperature drop (330°C/s) corresponds to full nucleate boiling which occurs at ~ 380°C (1.7 seconds).

4. After nucleate boiling the liquid contact stage begins with a consequent drop in the surface heat transfer coefficient because this is a much less vigorous mechanism for convection. The lower surface flux is accompanied by a lower rate of temperature drop just below the surface.

5. In the early seconds of the quench the surface temperature has fallen rapidly in response to the changes in surface flux, whilst the centre plane temperature has only reduced slowly. After 2.6 secs a maximum temperature difference of 540°C has been achieved between surface and centre.

6. After 2.6 secs the temperature gradient through the plate gives rise to a high level of heat transfer from the centre. Subsequently the rate of temperature drop at the centre plane is larger than at the surface and hence with increasing time the temperatures of the two planes are convergent as ambient is approached (time = 65 secs).

The temperature distributions which relate to each of the times discussed in section 6.2 are shown in Fig. 6.1-2b.

6.2 THERMAL STRESS EVOLUTION

6.2.1 Elastic stresses and the onset of plasticity (0-0.2S)[125]

The effect of a free edge on the distribution of stress in a quenched plate is most readily examined in the very early stages of the quench, before the complications produced by plastic flow and stress reversals have appeared. Thus, the results shown in Figs. 6.2-1 to 6.2-8 are those obtained at the first incremental point of the loading sequence of the

first calculation. This occurred after only 0.02s, when the surface and centre temperatures were 830 and 850°C respectively. Well away from the edge (that is, one-and-a-half plate thickness distant) the associated stress distribution is identical to that predicted by the infinite-plate plane-stress model, in which a relatively large radial stress exists at the surface and a smaller compressive radial stress occurs towards the centre. The hoop stress is identical to the radial stress at the same point and the axial stress is always zero.

As the edge is approached the radial stresses decay until, at the edge, they become zero.

As is clear from the equations of equilibrium the decay is accompanied by changes in the hoop stress as well as the development of axial and shear stresses. These changes are initially considered just after the start of the quench when all the stresses are elastic.

Figure 6.2-2 shows that the rate of decay of the radial stress depends on position within the plate. At the surface this stress begins to decay at about one plate thickness from the edge; the initial rate of decay is small but it becomes progressively greater as the edge is approached (Fig. 6.2-3). In a direction just below but parallel to the surface, the tensile radial stress well away from the edge (GF in Fig. 6.2-2) is lower than at the surface, but the rate of decay is unchanged. Consequently the stress becomes zero some distance from the edge (at a point on AB in Fig. 6.2-2), after which it becomes slightly compressive before returning to zero (at a point on BC). The stress reversal becomes more pronounced as the distance of the section from the surface increases, and the magnitude of the maximum compressive stress may be greater than the original tensile stress present before the start of the decay process (compare points D and E). The tendency for the stress to become more negative during the approach to the edge persists even when

the original stress (on line GF) is also negative. Therefore, in such cases there is an initial increase, rather than a decay, in the radial stress. Eventually, at a point very close to BC, the radial stress falls abruptly to zero, to comply with the boundary conditions at the free edge (Fig. 6.2-2).

Along lines close and parallel to the centreline, the compressive stress decays steadily but reaches zero a short distance from the edge. It then becomes slightly positive, before returning again to zero at the edge itself (Fig. 6.2-4).

This set of very complex results is the consequence of several factors:

a. the requirement that the radial stress reaches zero at all points on the edge (BC),

b. the marked variation in the level of stress found at points well away from the edge (for example, GF in Fig. 6.2-2) before decay begins, with a consequent variation in the amount of decay required as the edge is approached,

c. the requirement that the net force on any section perpendicular to the surface must be zero; this would account for the stress reversals associated with most longitudinal sections and the delay in the decay process in sections close to the midplane between surface and centre,

d. the requirement that the rate at which the radial stress decays is related to other stress components through the equations of equilibrium.

These are of course additional to the compatibility requirements of the plate, which has shrunk at different rates in different parts of the structure.

At points on GF in Fig. 3 the radial and the hoop stresses are equal (Fig. 6.2-1). As the radial stress decays towards the edge, the hoop stress changes in a similar but not identical fashion (see Fig. 6.2-5), although there is no requirement for the latter to reach zero at the edge. However, the equation of equilibrium shows that the rate of change in the radial stress is related to either the development of a difference between the hoop and radial stresses or the development of a shear stress gradient perpendicular to the surface. Hence, there is usually a small discrepancy between the hoop and radial stresses present at each point (see e.g. Figs 6.2-3 and 4). In addition, the net hoop force on any radial section must be zero. Thus, over most of the section there is a net compressive force which has to be compensated for by tensile forces at all points along the edge. At the corner B this stress is substantial, since the hoop stress at the surface never falls to less than half its value at F.

Despite the differences already mentioned, the overall pattern of hoop stress resembles quite closely the corresponding radial-stress distribution (compare Figs. 6.2-4 and 5).

Under the plane-stress conditions found more than one-and-a-half times the plate thickness from the edge (along FG), there is zero axial stress at all points (Fig. 6.2-6). Likewise, there can be no axial stress normal to the plate surface which is not constrained. Over most of the section a small compressive axial stress is generated, which gradually becomes more negative towards the central plane. There is, however, a requirement that the net axial force on any section parallel to the surface plane must be zero,

so a limited region of relatively high tensile stress exists close to the edge. A typical example of the change in axial stress as the edge is approached is shown in Fig. 6.2-4 which refers to the central plane of the plate.

There is a further constraint on the axial stress since the central plane is a plane of symmetry and must not therefore be subject to a net bending moment. The difference in length of lines parallel to the plate surface induced by the temperature gradient could be accommodated by the bending of the whole quarter-plate section shown in Fig. 1, particularly at points close to the edge, where such accommodation is not produced by radial stresses. Therefore the axial stresses produced along the central plane (CG) must be such as to maintain continuity with the plate on the other side of the plane; that is, the axial stresses must prevent any bending of the central plane that might be produced as a consequence of the thermal gradient perpendicular to the surface.

Over most of the edge-affected region the shear stress is compressive, but immediately adjacent to the edge there is a thin wedge-shaped region where the shear stress is tensile (Fig. 6.2-7). The apex of this wedge is on the edge close to the junction B with the surface. The regions of most intense shear are also close to the edge, with the most compressive stress adjacent to the junction and the most tensile stress in a lens-shaped region in the centre of the above-mentioned wedge. The shear stresses at points well away from the edge (on FG) and at points along the central plane are zero, as are the same stresses at points at the surface and edge, except immediately adjacent to the corner B. A line along which the stress is zero occurs between X and Y in Fig. 6.2-7.

Although at this stage in the quench the deformation of the plate is elastic at all points, the variation in equivalent stress within the plate is a useful indication of the points at which plastic flow would be generated.

For an infinite plate the maximum equivalent stress would be at the surface, and this is true also over much of the edge-affected region of a finite plate. However, in the latter case the surface equivalent stress falls to about half its original value by the time the junction with the edge is reached (Fig. 6.2-8). With minor variations, this stress falls rapidly as the perpendicular distance from the surface is increased.

Therefore one would expect the onset of plastic flow to occur at a point on the surface at least one plate thickness from the edge and at a value of equivalent stress identical to that predicted by an infinite-plate model.

As the temperature gradient increases the general level of stress rises, although the pattern of stress distribution is very similar to that obtained at the shorter time. However, after 0.2s the yield stress is exceeded and flow occurs in the vicinity of the plate surface between the points X and F in Fig. 6.2-9. The surface and centre temperatures are now 792 and 850°C, respectively. Flow occurs first at F, but the plastic zone then spreads quickly along the surface as far as X; at the same time it moves a short distance inward from the surface towards the central plane.

Although the general stress pattern is little changed by the initial onset of plastic flow, its major consequence is to maintain the stress level found near the centre of the plate (in the surface layers) much closer to the edge (Fig. 6.2-9). This retarded decay of the radial stress component is accompanied by an initial rise in the hoop stress before it falls to a value close to that observed before plasticity began.

A comparison of the radial stress map (Fig. 6.2-10) at a time of 0.2 seconds with the earlier map at 0.02 seconds (Fig. 6.2-2) shows that the same features are present as described above at the earlier time.

The greater temperature gradient through the plate section inevitably causes a higher stress gradient throughout the surface and edge region of the model, as is apparent from the higher values of the iso-stress lines. However this effect has been suppressed in the subsurface layers where the occurrance of plastic strain has prevented a large rise in tensile stress. It can also be observed that with the increase of temperature gradient and onset of surface plasticity the maximum compressive stress zone (D in Fig. 6.2-2) has now moved towards the free corner of the plate. This shift of the zone towards the edge is to be expected because the edge region is not yet plastic, and hence a greater increase in stress has taken place during this period which must be balanced across the section to maintain equilibrium.

As with the early elastic results the hoop stresses at 0.2s (Fig. 6.2-11) are virtually coincident with the radial stresses away from the edge of the plate. Again these two components differ in that the hoop stress does not have to decay to zero at the free edge. It can be observed that with increasing time and temperature gradient the maximum hoop stress is developing close to the corner B. This feature may be explained by the fact that the corner is a unique point in the section since it is common to both edge and surface. Hence both radial and axial stresses become zero at this point. Therefore the hoop component is the only available stress at this point that can satisfy the boundary conditions, the equations of equilibrium and the equations of continuity.

The proportion of the plate model which is subject to axial stresses (Fig. 6.2-12) and shear components (Fig. 6.2-13) at 0.2 secs is similar to the region observed at the earlier time point where the stresses were elastic. Near the centre of the plate plane-stress conditions exist whilst an axial component is generated as the edge is approached.

In line with the general increase in radial and hoop stresses under the increasing thermal load, the axial stresses are also higher in magnitude at this later time, whilst still maintaining a zero net axial force on any plane parallel to the surface. Because the in-plane stresses of the plate are still tensile at the surface and compressive at the centre there is a tendancy for the plate section to be in a state of shear. This tendancy is overcome close to the plate axis entirely by the balancing of inplane stresses, whereas the requirement for decaying radial stress as the edge is approached produces a need for a tensile axial stress at the edge to maintain continuity across the centre plane. It should be observed that just as the maximum compressive radial stress is moving towards the free corner, the maximum and minimum axial stresses are also tending to occur in this same region.

6.2.2 Period of maximum heat transfer and most extensive plastic zones (0.2 - 2.8S)

From the onset of plasticity (0.2s) until 2.8 seconds into the quench is the period during which the greatest number of changes occur to the thermal stress components. The generation of plastic zones and movement of the plastic boundaries during this time are displayed in Fig. 6.2-14. A summary of the main events which occur over this period are given below:-

a. 0.2 - 0.6s

The plastic zone (A') near the surface has propogated from the central axis to the edge to create a front parallel to the surface. The width of this plastic zone increases as the quench continues as shown in Fig. 6.2-14a. After 0.6 seconds the surface temperature has dropped to 706°C, and the plastic zone occupies the quarter of the plate closest to the surface.

b. 0.6 - 0.8s

Although the plastic front in the bulk of the plate continues to move in towards the centre plane whilst remaining parallel to the surface, the section of the zone closest to the edge has run ahead of the main front and has begun to fragment (B', Fig. 6.2-14b). The surface temperature is now 662°C and the centre plane temperature has also begun to fall (848°C).

c. 0.8 - 1.0s

By the time the surface and centre temperatures reach 615°C and 844°C respectively, the plastic zones lie in four distinct areas (Fig. 6.2-14c). The zone across the surface layer (A') is shrinking as a consequence of unloading of the stresses; a plastic zone towards the corner of the plate (C'), which is a second fragment of A', has a front which is travelling towards the centre plane. This movement and fragmentation occurs because unloading of the stress is taking place on one side of the zone while new plastic flow is being generated on the other. The plastic zone on the edge (B') is growing and moving towards the centre plane; while a new plastic zone (D') has been established on the central plane and close to the central axis of the disc.

d. 1.0 - 1.2s

The yield stress in the surface layers has now risen above the equivalent stress level at this point, because of the lower temperature (560°C). Therefore although the stresses are still rising they have become elastic without unloading. The growth of the plastic zone at the plate centre (D') has caused it to amalgamate with those at the edge (B' and C') (Fig. 6.2-14d). Thus there is now one large plastic zone along the central plane (E').

The width of this zone is steadily increasing.

e. 1.7s

The maximum surface heat transfer has been achieved, of 4.5 W/mm², which corresponds to the most vigorous nucleate boiling mechanism.

f. 1.8s

The surface of the plate (350°C) becomes elastic at all points and remains so throughout the remainder of the quench because the rise in yield stress as the temperature becomes lower is always higher than that achieved by the thermal loads. At this time the surface tensile stresses begin to unload. The plastic zone in the central layers (E') begins to retreat slowly towards the centre plane (Fig. 6.2-14e). This continues up to 2.8 seconds.

g. 2.6s

The martensite transformation begins at the plate surface as the temperature falls just below 290°C.

h. 2.8s

With the surface at 280°C and the plate centre at 820°C the maximum difference in temperatures between surface and centre occurs. The changes to the distribution of the three stress components during the 0.2 to 2.8s time span can best be observed by examination of the contours shown in Fig. 6.2-15. The radial and hoop stresses well away from the edge effected region (Fig. 6.2-15a) are coincident and display a stress distribution perpendicular to the surface which still closely resembles that produced at the beginning of the quench process.

There are still tensile surface and compressive centre stresses to give zero net hoop/radial forces through the section. The very large temperature gradient in a direction perpendicular to the surface has created much higher stresses (~ 150N/mm² just below the surface) but the presence of plastic flow has restricted this stress in the surface layers of the plate closest to the axis. It can be observed that as the highest rate of cooling is now moving from the surface to the centre of the plate the stresses in these two regions are beginning to unload prior to a stress reversal. This effect is accentuated at the surface where the volume increase associated with the martensite transformation is beginning to occur. The radial stress along the surface has changed significantly with increasing time (Fig. 6.2-15b); thus whereas the initial onset of plastic flow (0.2 seconds) had apparently delayed the decay of the radial stress as the edge is approached, the rise of the flow stress as the temperature falls has produced an elastic radial component and re-established the "edge-effect" over distances up to one plate thickness away from the edge. The radial stress now rapidly decays to zero and becomes signficantly compressive before returning to zero again at the edge. The profile of the radial stress along the centre plane has changed little from the early time point (Fig. 6.2-15C); except for a general increase in stress level across most of this plane and the start of unloading at the point where the central plane and axis coincides.

As previously stated, the relationship between hoop stress and position along the axis is identical to that of the corresponding radial stress. On moving along the surface of the plate from the axis position the hoop and the radial stresses diverge as the latter decays. The hoop stress falls to a smaller extent but then rises back almost to its original value before falling again at the edge (Fig. 6.2-15b).

The complexity of the relationship between hoop stress and position towards the plate corner is associated with the dominance of this component in this part of the structure, where the other stress components are approaching zero. Thus this component is responsible for continuity in the presence of the temperature gradient. Along the centre plane the hoop stress, unlike its behaviour at the start of the quench, now departs significantly from the radial stress profile. Hence it becomes substantially more compressive before it reverses to produce a tensile component at the edge (Fig. 6.2-15c).

The axial stress distribution which exists in the plate after 2.6 seconds into the quench is similar in form to that described at the earlier time, with the exception that the stress gradient close to the edge is reduced, (Fig. 6.2-15c). During the early part of the quench in which plastic zones developed at the edge, the level of axial stress along the edge quickly rose to and maintained a general level of $\sim 40 N/mm^2$, and only decayed to zero as the surface was approached. However, after unloading of the stress at points on the edge near to the corner this axial stress became modified, to show a compressive stress in this region and tensile stress at other points on the edge (Fig. 6.2-15d).

The equivalent stress across the plate radius shows little variation at this stage (Fig 6.2-15b), whilst the equivalent stress along the axis or edge is close to the absolute value of the most dominant stress component (fig 6.2-15a,d). Of course the plastic zone boundary (Fig 6.2-14e) follows the equivalent stress contours.

6.2.3 Stress Reversals and the Martensite Transformation (2.8 - 4.0S)

Four seconds after the start of the quench the temperature at the plate centre has dropped to 770°C and the upper surface has fallen to 250°C. The initiation of the martensite transformation, at 289°C, causes a 1.5% increase in volume near the surface of the plate which substantially modifies the stress fields in the body.

The relationships between radial and hoop stress and position along the axis of the plate (Fig. 6.2-16(a)) display an abrupt stress reversal close to the plate surface. This small zone of compressive stress near the surface is due to the formation of martensite and the associated dilation of the structure. The maximum stress produced in this zone is below the yield stress of the material. All three stress components in the section of the plate adjacent to the transformation front have changed little during the previous 1.2 seconds of the quench, (Fig. 6.2-16 a. and b.) and it can be observed that a small plastic layer has formed below the transformation front in the austenite. Closer to the centre plane the stresses have begun to unload which causes most of this region to become elastic (Fig 6.2-17).

The stress fields during the very early part of the quench could be simply explained by the surface temperature gradient through the plate, but as the quench process has progressed up to 4 seconds the plate has undergone temperature gradient changes, plasticity, and surface transformation to give a radial stress diagram which displays a considerable increase in complexity (Fig. 6.2-18). The decay of radial stresses as the edge is approached in a direction parallel to the surface can vary greatly, depending on the depth below the surface; five such planes have been chosen (Fig. 6.2-18) to display these differences in behaviour:-

A-B Along the surface plane (also shown in Fig. 6.2-16c) the compressive stress observed near the axis increases considerably from 200 to 320 N/mm² as the edge is approached and only decays to zero in the material immediately adjacent to this boundary. This means the peak stress observed in that part of the plate transformed to martensite occurs close to the plate corner.

C-D This plane lies in the austenite region and passes through the small plastic layer. The radial stresses decay directly to zero at the edge in a fashion which is similar to that displayed in the tensile region at the beginning of the quench. The decay begins at approximately one plate's thickness from the edge.

E-F This plane lies along the zero stress line near the axis of the plate. The radial stress component does not remain at zero all along E-F, but as the edge is approached a small tensile component is first generated before it finally falls back to zero some small distance before the edge.

G-H Along this plane the radial stress decays abruptly to zero a considerable distance from the edge.

I-J The modification of the radial stress along the centre plane (Fig. 6.2-16b) shows first a small increase in the compressive stress followed by a steady decay in this stress to zero at the edge.

In general it is true to say that the decay of the radial component to zero at the edge is usually preceeded by an increase in the absolute level of this stress. The exceptions are the regions which are effected by plastic flow or points close to a zero stress plane near the axis of the body.

This complex stress pattern, which has been generated after 4.0 seconds, is a result of the requirements that the net radial forces and bending moments on any section in the plate must be zero and that the forces perpendicular to a free boundary shall also always be zero.

By comparison with the radial stress the hoop component displays a much more consistent level across the various planes of the plate (Fig. 6.2-19). In the surface layer where martensite has formed the hoop stress remains almost constant along the plane from axis to edge except for an abrupt 50% reduction immediately before the edge is reached. This observation is also true for the sub-surface layers (up to 3mm deep), which incorporates the plastic zone ahead of the transformation front. On any plane parallel to those referred to above but at a depth of more than 3mm, the hoop stress behaves in a fashion similar to the radial component but with two distinct differences;

1. the initial increase in the compressive stress level as the edge is approached is somewhat larger, and

2. although the hoop stress decays at the edge there is no requirement for it to be zero, so that a small compressive or tensile value usually remains at this point.

Throughout the 3.0 to 4.0 second period of the quench process the level of radial and hoop stresses have steadily risen up to typical values of -200 and -300 N/mm^2 at the plate surface, but this is not true of the axial component (Fig. 6.2-20). During the early stages of the quench (0.2S) axial stresses of 40 N/mm^2 existed, but even after the creation of the more severe temperature gradients after 4 seconds the maximum axial stress is only -80 N/mm^2. Again it can be observed that on the central plane close to the edge a tensile axial stress is required to maintain material continuity across the plane of symmetry,

and that a small region of compressive stress exists further into the plate which ensures net zero force and bending moments on any plane close to the centre line. The compressive axial stress which formed close to the plate corner earlier on in the quench (~2.6s) is now principally responsible for the small plastic zone which is expanding from the edge just below the transformation front. It is interesting to note that after a period of 4.0 seconds, the proportion of the plate which experiences axial stress zones is considerably less than during the earlier periods.

Figure 6.2-21 which refers to the equivalent stress after 4 seconds shows a series of iso-stress contours that in general, remain virtually parallel to the plate surface. Only very close to the edge is there evidence of deviation from this condition. It can be seen that the combination of the hoop and axial components, near the plate corner on the edge, have produced the high stress region which has exceeded the austenite flow stress and caused the growth of a plastic zone just below the transformation front.

6.2.4 Period of Maximum Absolute Stress Generation (4.0 - 12.0S)

In the period 4.0 to 12.0 seconds, at the end of which the surface and centre temperatures have reached 165 and 425°C respectively, the maximum absolute stresses associated with the quench process occur with substantial plastic zones once again formed in the austenite region of the plate.

The very severe stresses which are created in some parts of the plate during this period are the consequence of two phenomenae whose effects are additive;

1. As already observed, the expansion due to the formation of martensite creats a compressive surface layer which must be balanced by tensile forces elsewhere in the section.

2. Even if transformation had not taken place, the steepest temperature gradient and largest rate of temperature change has now moved away from the plate surface into the interior, thereby creating a reverse situation from the initial part of the quench, i.e. the centre layers are now contracting faster than the surface layers and consequently the stress distribution due solely to the thermal gradient must reverse to compressive and tensile stresses at the surface and centre respectively. This reversal to tensile stresses at the centre occurs after 4.8 seconds, which is a natural progression from the unloading compressive stresses observed at 4.0 seconds.

As time progresses the combination of these two phenomenae give increasing stress levels which reach a maximum after approximately 11.2 seconds, thereafter the surface stresses begin to unload once again.

The small plastic zone which remains along the centre plane at 4.0 seconds is completely replaced by elastic values after 4.8 seconds, when the plastic front finally disappears at the plate centre. Similarly, the narrow plastic enclave associated with the high radial/hoop stresses in the austenite just ahead of the transformation front, has also disappeared. This latter effect is due to the increasing yield stress of austenite as the temperature drops.

As time progresses from 4.8 seconds onwards the very small plastic zone which had formed at the plate edge (adjacent to the transformation front) grows into the plate both laterally and vertically (Fig. 16.2-22 a). In the period between 9.6 and 12.0 seconds this plastic zone expands towards the centre plane of the plate because the radial and hoop components have completed their stress reversal and have risen to the point where tensile flow occurs (Fig. 16.2-22b) in this region.

However a small elastic field remains on this plane at the outer edge. The edge of the plastic zone nearest the surface retreats towards the central plane as the martensite transformation progresses from the surface (Figure 6.2-22b).

Now that the transformation is well established and the peak rate of temperature change now occurs below the surface of the plate, the radial component contours (Fig. 6.2-23) are the reverse of those observed at the beginning of the quench. Examination of figure 6.2-24 shows that the overall radial stress pattern in the plate has become simplified after the complex changes which took place between 2.8 and 4.0 seconds. The rate of decay of the tensile radial component as the edge is approached is consistent throughout the central region, and tends to zero some small distance from the edge as shown specifically on the centre plane in Fig. 6.2-23b. The radial stress decay in the compressive layers immediately below the surface is followed by a reversal of this stress to a significant tensile value before it again decays to zero at the edge (Fig. 6.2-23c); thus a tensile zone is formed in the vicinity of the plate corner. At this stage a region within which the radial stresses are decaying from the value observed at the axis, is approximately one plate's thickness from the edge. This corresponds to the extent of the region of the plate affected by the free edge.

As with the radial component the hoop stress has now re-established a fairly consistant rate of decay in the edge region, regardless of depth below the surface. Whereas at 4.0 seconds the hoop stress remained at a constant level until very close to the edge, it now decays steadily towards zero, but at a slower rate than the radial component, as can be seen in the case of the surface layer in Fig. 6.2.-23c. As is always the case with the hoop stress, a significant value always remains at the edge, although this is usually a small fraction of that existing at an equivalent position on the axis.

At this particular time the decay is from a high tensile stress of 225 N/mm² near the mid radial position to a compressive stress of -50 N/mm² at the edge. The overall hoop stress map of the plate quadrant (Fig. 6.2-25) is relatively simple, viz:-

a. The surface material, which is in compression, has a high stress gradient to a depth of 3mm.

b. The maximum stress of -900 N/mm² occurs at the centre of the plate surface

c. A large proportion of the plate section adjacent to the centre plane is a region of tensile stress of >200 N/mm² which reverses to give a compressive region close to the edge.

d. A small zone of tensile hoop stress exists at the point where the transformation front meets the edge. This point on the edge is also associated with an axial stress change which will be discussed later.

At the beginning of this period (~4.8 seconds) the axial stress where the centre plane meets the edge has reversed from a tensile to a compressive value; this occurs concurrently with the opposite reversal of the radial stress further along the plane. Comparison of the axial stress map after 12.0 seconds (Fig. 6.2-26) with that after 4.0 seconds (Fig. 6.2-20) shows that this component has reversed at all points. It is observed that along the edge of the plate the axial stress changes from tensile to compression at a point on the same plane as that at which the hoop and radial stresses reverse from compressive to tensile. This plane coincides with the transformation front. Obviously, as the dominant component, the axial stress is the major contributor to the plastic flow which occurs near the edge ahead of the transformation front whilst within the martensite material the maximum tensile axial stress of 300 N/mm² is generated

just away from the corner. Despite these zones of high stress close to the edge, the axial stress is low over the greater part of the specimen.

The equivalent stress diagram (Fig. 6.2-27) 12.0 seconds into the quench shows a similar distribution to that presented after 4.0 seconds, except that the general stress levels are now much higher and that the stress gradient in the surface region that has transformed to martensite is particularly large. It can be seen that the inner half of the section is stressed to a relatively consistent value of 150 N/mm² where the material is still austenitic. This zone is associated with the large plastic region, which covers most of the untransformed region.

6.2.5 Latter Stages of the Quench Process (12.0S Onwards)

17.0 seconds after the start of the quench the temperature on the centre plane has fallen to the martensite start point (289°C). This is associated with the following :-

a. The plastic zone has completely disappeared on account of the large increase in flow stress associated with the formation of martensite. The last evidence of plastic behaviour is at the point where the centre plane meets the edge. From 17.0 seconds until the end of the quench all the stresses in the plate will be elastic.

b. At this time the tensile radial and hoop components in the centre region of the plate begin to unload due to the expansion associated with the martensite transformation. After 21.0 seconds the unloading of these components becomes a stress reversal which is the last to occur before the end of the quench. An opposite effect has occurred in the case of the axial component on the centre plane near the edge; it has reversed from a compressive to tensile value during the time period 17 to 21 seconds.

After 30.0 seconds the last vestige of nucleate boiling has given way to full liquid contact which at the surface of the specimen produces a low surface heat transfer flux of only 0.2 W/mm². The analysis was terminated at 65.0 seconds when the surface and centre temperatures had fallen to 58°C and 69°C which were below the M_f temperature. From previous work on an infinite plate it is known that no further significant changes take place to the stresses after this point in the quench.

6.2.6 Residual Stresses (65S)

The residual radial and hoop stress along the specimen axis are shown in Fig. 6.2-28a. These residual stress profiles are the same as those predicted by a semi infinite plate model. Both stress components are the same at any particular point along the axis, and where it reaches the surface and central planes these stresses are -500 N/mm² and -100/Nmm² respectively. At an intermediate point 3mm below the surface the stress reached a peak value of 270 N/mm².

The variation in the radial stress as the edge is approached is similar along both the surface and centre planes (figures 6.2-28 b. and c.); and is typical of the stress profile along the central plane observed at the beginning of the quench. With departure from the central axis on either plane the stress begins to decay towards zero almost immediately. A zero value of radial stress exists 6mm away from the edge on both the centre and surface planes, but these components then rise to tensile values of 20 and 50 N/mm² respectively before again decaying to zero at the edge. The overall radial stress distribution can be seen in figure 6.2-29 and can best be described by subdividing into the following planar regions:-

A-B As at the surface (AA) the planes in this region have a compressive stress at the plate axis, which decays to zero and then becomes tensile before

again falling to zero at the edge. With increasing depth into the plate (from A to B) the stress levels and gradients along the planes become smaller, the initial crossing of the zero stress axis is closer to the plate axis, and the final decay to zero is achieved at points progressively further from the edge.

B-C Point B on the plate axis is the zero stress cross over position from compressive to tensile residual stresses. Between points B and E on the axis there are tensile residual stresses, but the manner in which these decay to zero at the edge differs depending upon depth below the surface. In those layers lying in the B to C region the tensile stresses remain constant at points up to 10mm from the plate axis and then decay to zero in the vicinity of the edge. The zero stress value is reached at a point further away from the edge on planes closer to the C-C plane, but in all cases a compressive radial stress is then generated (~50 N/mm^2 in the zone centre) before this component again falls to zero at the edge. This compressive zone is bounded by the edge of the plate and the zero iso-stress contour which runs from the plate corner into the plate.

C-D Here the stress decays abruptly to zero at a point about 10mm from the axis and then remains there until the edge is reached.

D-E In this region the tensile stresses at the axis have decayed to zero and become compressive at positions along the planes, which are much closer to the axis than is the case in B-C region. This position is approximately 24mm from the axis on the D-D line, but becomes progressively closer with increasing depth until it occurs at ~12mm

from the axis, just above the E-E line. Throughout this region the compressive stresses then decay back to zero very close to the edge.

E-F The E point on the axis corresponds to zero radial stress; closer to the central plane than this point the stresses on the axis are compressive. Within this zone (E-F) the decay of radial stress as the edge is approached follows a similar profile to that described above in the case of the central plane (figure 6.2-28c). However the zero point and zone of tensile stress occurs progressively further away from the edge as the central plane is approached.

Within 15mm of the axis throughout the section the residual hoop stresses produced in the plate (figure 6.2-30) are generally similar to the distribution of radial stresses. Only in the outer annulus of the plate do the hoop and radial stress profiles differ significantly; there is of course no requirement for the hoop stress component to be zero at the edge which is the radial boundary condition. Nevertheless; the hoop stress does decay as the edge is approached (figure 6.2-28b) and is similar to that of the radial component, but along the plate surface this decay rate is slower and does not reverse thus maintaining a small compressive stress at the edge. Along the centre plane and within the edge affected region there is a considerable difference between the profiles of the hoop and radial components (figure 6.2-28c); at the former position the decay of the hoop stress is retarded but the subsequent reduction to zero is sudden. In the outer anulus the hoop stress becomes compressive again and returns to its original level at the edge.

A zone with highly tensile hoop stresses (up to 150 N/mm²) exists at the edge 3mm below the corner, which has developed from the embryo zone first observed 12.0 seconds after the start of the quench. This area corresponds to the region where the change in the radial stresses varies markedly as discussed in the previous section.

In common with the radial stress variation on the centre plane, the corresponding axial stress also displays a high degree of similarity to that observed at the beginning of the quench (fig. 6.2-28c). There is a high tensile component of 160 N/mm² at the plate edge on the centre plane which quickly reverses to a compressive value ($\sim$ -50 N/mm²) in the annulus of material 6mm away from the edge. This compressive zone then decays to zero further along the plane (towards the axis) and reverses yet again to give a small tensile value. As described at earlier time points in the quench, the combined effect of these tensile and compressive regions of axial stress give a net zero force perpendicular to the central plane. Examination of the total residual axial stress pattern (figure 6.2-31) shows that the high tensile values of this component are concentrated in the 3mm of material adjacent to the plate edge. The peak axial stress value of 250 N/mm² occurs on the edge, approximately 3mm below the corner, and thus coincides with the region of highest hoop stress on this boundary. The high axial stress gradient which exists near the edge is adjacent to a much larger region of lower compressive values which covers half of the radial distance towards the axis of the plate; this region does not extend to the plate surface because at this boundary the axial component must be zero.

It should be noted that as at earlier times, the highest absolute axial stress (compressive at the end of the quench) occurs on the centre plane. The residual axial component is zero or of an insignificant value compared to the other components over 90% of the plate section.

Overall consideration of the residual radial, hoop and axial stress components give the impression that the edge affected region is confined to the outer half of the disc. In keeping with the infinite plate model, the stresses in the inner section abide by the following constraints.

$$\sigma_{RADIAL} = \sigma_{HOOP}$$

$$\sigma_{AXIAL} = \tau_{SHEAR} = 0$$

An examination of the shear stress distributions (figure 6.2-32) indicates a substantial influence of the edge all along the outer surface of the plate. This arises because the generation of shear stresses is related to the radial and axial stress gradients, as described by the equilibrium equations **shown in Figure 4.1-1.**

Two distinct areas of shear stress are observed at the end of the quench;

1. A positive area with iso-stress contours essentially parallel to the plate surface culminating in a maximum stress of 40 N/mm² approximately 3mm below the surface and in the mid radial position.

2. A negative area of approximately equal absolute magnitude through the plate section in the region adjacent to the plate edge. The maximum compressive stress in this zone occurs towards the plate corner.

These two zones are in close proximity along a 30° line from the corner and it is here that the highest shear stress gradient is observed. The centre area of the plate is clearly free from shear stresses, and along the edge (particularly close to the central plane) where the axial stress component is dominant and the radial stress had decayed to zero, there is little evidence of a resultant shear stress. When this final shear stress profile is compared to that observed after 0.2s into the quench (fig. 6.2-13), it is evident that although the general levels are now higher and the sense of the stress in individual areas are now reversed, there are certain points of similarity;

a. The shear stresses exist in two distinct areas, one with negative and one with positive values. One traverses the section close to the edge whilst the other is located towards the plate surface

b. The highest shear stress gradient occurs in the edge region towards the corner of the plate.

c. The two stress regions are separated by a zero iso-stress contour which passes from the corner towards the centre of the plate.

The residual equivalent stress map (figure 6.2-33) is related to the principal stresses by the Von Mises equation. It is evident that the equivalent stress is dominated by the radial and hoop components (figures 6.2-29 and 30) in the region surrounding the plate axis whilst the axial component (figure 6.2-31) is the major influence at the edge. Plane stress conditions exist (i.e no edge effect) only where the in plane stresses do not vary with radial position. From examination of the residual stress maps it can be seen that plane stress conditions generally hold true for the plate within 10mm of the axis, except for the layers between 3 and 5mm below the surface where the iso-stress contours are not parallel to the plate surface, and therefore indicate an absolute value for σ_{AXIAL} and τ_{SHEAR}.

6.2.7 Relationship Between Stress and Strain During the Quench at Specific Positions in the Plate

The relationships between stress and strain predicted at the four corners of the plate quadrant under consideration are shown in figures 6.2-34 and 35. These positions are:

NODE	POSITION
1	Plate Centre
31	Edge Centre
471	Surface centre
501	Corner

The results shown in figure 6.2-34 agree with those of previous work[49], that employed a plane stress model. Here one stress component is zero and the other two are equal, so only one stress and strain parameter is required to specify the mechanical history at these points.

Thus the relationship between stress and strain on the plate axis show the following characteristics:-

a. An initial stage where tensile plastic flow occurs at the surface node (471) and compressive plastic flow occurs at the centre (node 1). This lasts until the mean temperature gradient across the plate reaches a maximum.

b. A subsequent period where the stresses unload and reverse. This is a accentuated by the transformation of the material at node 471 to martensite, with a consequent increase in the compressive stress, on account of the associated dilation of the material. The stresses are now elastic at node 471 but there is plastic flow in tension at node 1.

c. Finally there is a second period of stress unloading, as the centre (node 1) is transformed to martensite.

At the corner where the surface and edge meet (node 501) the only non zero stress component is the hoop stress, which accommodates the changes in volume produced during the quench in a similar manner to the radial and hoop stresses in the middle of the surface. Figure 6.2-35 shows a very similar pattern to the results reported at node 471. In the centre of the edge (node 31) the significant component is the axial stress (Figure 6.2-36). The relationship between this and the axial strain follow the reverse pattern to that obtained from the hoop and radial stresses and strains at the corresponding point on the axis (node 1). Since each position has a similar thermal history and volume change this result is to be expected, because a dilation in the axial direction is the equivalent to a compression in the other principal directions and vice versa. Thus the observed strains at these positions accommodate the same dimensional changes.

6.3 EDGE CORRECTION FACTORS FOR THE UNIAXIAL QUENCH MODEL

A full stress analysis, of the type reported above is a very expensive and time consuming operation. There is a need for a simple means of allowing for the variation in stress in the vicinity of a free edge, so that a simpler analysis away from the edge may be modified. This would allow stresses to be predicted in a variety of relatively complex components. A suitable correction factor would be the best means of achieving such a result. For example, a correction factor might be obtained by comparing the stress at some point on the axis with the mean stress in the edge affected region along a line parallel to the surface (Fig 6.3-1). A ratio of these two values provides a correction factor which can be applied to infinite plate results and thereby generate values which are applicable to a finite body. The following tables show the derivation of such correction factors which apply to the present specimen after 0.02, 4.0, 12.0 and 65.0 seconds after the start of the quench.

6.3-1 EDGE CORRECTION FACTORS AT 0.02 SECONDS (EARLY ELASTIC STRESSES) - Fletcher and Lewis[125]

DISTANCE FROM SURFACE, MM	STRESS ON PLATE AXIS MN/M²	AVERAGE RADIAL STRESS / STRESS ON PLATE AXIS	AVERAGE HOOP STRESS / STRESS ON PLATE AXIS
9.61 CENTRE	-2.7	0.54	0.65
8.70	-2.7	0.56	0.67
7.79	-2.7	0.58	0.70
6.89	-2.7	0.64	0.73
5.98	-2.7	0.70	0.77
5.07	-2.7	0.73	0.85
4.15	-2.4	0.76	0.88
3.25	-2.0	1.20	1.50
2.26	-0.5	0.30	
1.35	4.0	0.60	0.82
0.45 SURFACE	22.0	0.74	0.91
MEAN		0.67	0.85
STANDARD DEVIATION		0.21	0.23
OVERALL MEAN		0.76	

6.3-2 EDGE CORRECTION AT 4.0 SECONDS (PLASTIC STRAINS, STRESS REVERSALS AND THE MARTENSITE TRANSFORMATION)

DISTANCE FROM SURFACE, MM	STRESS ON PLATE AXIS MN/M²	AVERAGE RADIAL STRESS / STRESS ON PLATE AXIS	AVERAGE HOOP STRESS / STRESS ON PLATE AXIS
10 CENTRE	-50.0	0.85	0.87
9	-50.0	0.82	0.87
8	-50.0	0.74	0.86
7	-45.0	0.69	0.89
6	-41.0	0.62	0.87
5	-30.0	0.57	0.82
4	-20.0	0.08	0.45
3	25.0	1.13	1.15
2	115.0	0.78	0.94
1	125.0	0.75	0.94
0 SURFACE	-200.0	1.10	0.99
MEAN		0.74	0.88
STANDARD DEVIATION		0.27	0.16
OVERALL MEAN		0.87	

6.3-3 EDGE CORRECTION AT 12.0 SECONDS (FURTHER PLASTICITY AND PEAK STRESS GENERATION)

DISTANCE FROM SURFACE, MM	STRESS ON PLATE AXIS MN/M²	AVERAGE RADIAL STRESS / STRESS ON PLATE AXIS	AVERAGE HOOP STRESS / STRESS ON PLATE AXIS
10 CENTRE	200.0	0.63	0.83
9	200.0	0.66	0.83
8	200.0	0.68	0.83
7	200.0	0.71	0.83
6	200.0	0.72	0.86
5	200.0	0.73	0.82
4	200.0	0.64	0.74
3	120.0	0.20	0.27
2	-250.0	0.56	0.76
1	-640.0	0.63	0.74
0 SURFACE	-900.0	0.61	0.77
MEAN		0.62	0.75
STANDARD DEVIATION		0.14	0.16
OVERALL MEAN		0.69	

6.3.-4 EDGE CORRECTION AT 65.0 SECONDS (RESIDUAL STRESS CONDITION)

DISTANCE FROM SURFACE, MM	STRESS ON PLATE AXIS MN/M²	AVERAGE RADIAL STRESS / STRESS ON PLATE AXIS	AVERAGE HOOP STRESS / STRESS ON PLATE AXIS
10 CENTRE	-100.0	0.57	0.81
9	- 80.0	0.58	0.83
8	- 60.0	0.59	0.76
7	- 10.0	0.38	2.50
6	50.0	0.25	0.22
5	100.0	0.33	0.46
4	210.0	0.42	0.57
3	230.0	0.52	0.64
2	100.0	0.96	0.89
1	-200.0	0.23	0.49
0 SURFACE	-500.0	0.46	0.62
MEAN		0.48	0.80
STANDARD DEVIATION		0.19	0.57
OVERALL MEAN		0.64	

An overall factor for the whole plate has been determined at each time by averaging the factors which apply to each successive plane and then averaging the results for the radial and hoop components. This approach is probably acceptable because, in general, at the points where there are major discrepancies between the actual and the mean ratios, the initial axis stresses tend to be <10% of the maximum stress occurring on the axis; thus such discrepancies are not very significant. These anomolies are most apparant where the stress changes from a tensile to compressive sense or visa-versa. By considering both the radial and hoop stress components all the stresses in the plane of the plate are included. The overall factor is therefore applicable to the single stress on the axis which includes both hoop and radial stress.

When applying such correction factors to a set of infinite plate results it should be recognised that the factors derived are dependant on the particular aspect ratio of the modelled plate which has a specific ratio of edge affected

region to specimen radius. However an increase in the radius does not change the edge affected region so it is easy to recalculate the factor appropriate to the new dimensions, and the correction factors thus generated should be closer to unity. If the radius becomes smaller than the extent of the edge affected region a plane strain condition is being approached, and the analysis would be performed in a different way.

6.4 BIAXIAL HEAT TRANSFER ANALYSIS

6.4.1 Transient Temperature Distribution

The predicted relationships between time and temperature at various positions in a water quenched 60mm diameter 20mm thick plate are shown in figure 6.4-1a). This analysis simulated heat removal from both the plate surface and edge. The positions of the nodal points referred to in the figure are as follows:-

- Node 1 at the plate centre
- Node 35 on the centre plane at the plate edge
- Node 690 at the centre of the plate surface
- Node 724 at the plate corner

The effect of heat transfer from all external boundaries of the plate shows that the edge (node 35) now has a cooling curve similar to that of the surface (node 690). As expected, the mean cooling rate of the plate corner (node 724) is very severe (nucleate boiling had commenced by 0.005 seconds) and has had the overall effect of cooling the upper surface of the plate somewhat faster than in the one dimensional quench analysis. The distance between nodes 35 and 725 is small so the rate of cooling at the former is only slightly lower than at the latter. The various temperature gradients along the specimen boundaries at different times are shown in figure 6.4-1 b to e.

6.4.2 Thermal Stress Evolution

The initial elastic stresses generated in the two dimensional heat flow model (at 0.0005 s) are very similar to those predicted in the earlier unidirectional heat flow analysis. Along the central axis of the plate the radial and hoop stresses are coincident (fig 6.4-2a), with a low magnitude compressive stress below the surface which rises sharply to a tensile (+27 N/mm^2) value at a depth of 1.5mm of the below surface. This simple profile is caused by the initial contraction of the surface as cooling begins. Examination of the stress distribution along the surface (fig 6.4-2b) shows the first difference between the unidirectional and two dimensional heatflows. Although the radial and hoop components are superimposed across most of this boundary and the radial stress drops to zero at the edge, the hoop value now rises at the edge as a consequence of the more severe contraction strains produced by the higher rate of cooling now sustained at the plate corner. Further evidence of differences between the two analyses can be seen along the central plane of the plate (fig. 6.4-2c). As in the unidirectional heat flow case the compressive radial stress decays to zero at the plate edge but does not overshoot to a tensile value just prior to the final decay. Because the radial component cannot sustain the thermal strains close to this free edge a tensile axial stress is generated to maintain continuity which then becomes compressive a small distance into the plate before decaying to zero in the bulk of the material. This phenomenon is directly comparable with the unidirectional heat flow case and has been described in an earlier section. However, the hoop component now displays a significantly different profile in the outer region of the central plane. The hoop stress does have an equivalent compressive value to the radial component within the bulk of the plate, but as the edge is approached it no longer decays to a small tensile value (close to zero) but equates with the axial stress profile which sharply rises to a maximum value at the plate edge.

This situation is analogous to the stress profile along the axis of the plate where tensile hoop and radial stresses at the cooled surface are balanced by compressive stresses in the plate centre; likewise, tensile hoop and axial stresses at the cooled edge are balanced by compressive stresses elsewhere along the same plane.

0.25 seconds after the start of the quench nucleate boiling has commenced on all free surfaces which in general have cooled to ~ 775°C. The plate corner and adjacent material has cooled to approximately 650°C. Along the axis of the plate (Fig. 6.4-3a) the stress profile is similar to that obtained after 0.0005 seconds but the actual radial and hoop stress values have increased until plasticity has occurred in a region within 2mm of the surface of the plate (> 30 N/mm^2). Examination of the results across the plate surface (Fig. 6.4-3b) show that the radial component persists closer to the edge before decaying to zero when plasticity has occurred. Along the surface and along the centre plane (fig 6.4-3c) the general stress levels are increasing with time. Examination of stress distributions on parallel planes at intermediate positions below the plate surface has shown that the maximum values of the axial stress (zero at the surface) and the penetration of the compressive axial zone towards the plate axis is a function of the depth of the plane below the upper surface. Of course the axial stress must decay to zero at the surface (to which it is perpendicular) as shown in figure 6.4-3d, just as the radial component must decay to zero at the edge. Hence the corner of the plate is a unique position where only hoop stresses can support thermal contractions, and so this component rises to a high tensile value which is greater than any component elsewhere in the plate.

After 1.0 second into the quench both stress components away from the edge of the plate have increased to -35 N/mm^2 at the centre and 90 N/mm^2 at the surface (figure 6.4-4a).

The plastic zone close to the plate axis has penetrated to a depth of 3mm, but the nature of the stress distribution within 1mm of the surface suggests that the yield stress, which increases as the temperature falls, has exceeded the equivalent stress of the material in this upper layer. Well below the surface there is evidence that the axial stress component, which is associated with the edge effect, has penetrated to the plate axis. 1.0 second after the start of the quench the corner of the plate has cooled to 235°C, and hence the martensite transformation has begun in this region. Figure 6.4-4b shows that as a consequence of the volume expansion associated with the transformation the radial stress along the plate surface reverses to a compressive value before decaying to zero at the corner. Likewise, the tensile hoop component, which is dominant at the plate corner, has begun to reverse. Along the plate centre plane (figure 6.4-4c) the radial stress decays to zero well before the edge, whilst the hoop stress now becomes more compressive before reversing to overlay the axial component. These stresses show that as at the surface, the edge now has a thick elastic outer layer with an adjacent plastic annulus that penetrates 1mm into the plate. This figure confirms that a small axial stress now exists at the plate centre.

After the quench time has increased to 2.0 seconds the centre of the plate surface and its edge (at 327°C and 312°C respectively) are now cooling faster than the corner (at 158°C); i.e. 280°C/s compared to 77°C/s. With this temperature profile the martensite transformation has spread from the corner to affect nearly all of the free boundaries of the plate. The radial and hoop stresses at the centre of the plate (figure 6.4-5a) have remained static during the previous 1 second time step, but at a point on the axis some distance from the central point they become more compressive ($-50 N/mm^2$) before reversing to a tensile value ($+160 N/mm^2$) at the surface.

Along the surface of the plate (figure 6.4-5b) the radial and hoop stresses both still maintain this stress level for a distance of 21mm along the radius towards the edge, but after this point the radial component drops to a compressive value of ~-400N/mm² before again rising to a tensile level prior to decaying to zero at the edge. The hoop component still shows a drop at the plate edge, but this is to a higher value than seen at 1.0 second. From figure 6.4-5a there can now be seen evidence of axial stresses at both the plate surface and centre. As along the axis of the plate, the stress distributions along the centre plate (figure 6.4-5c) show that the hoop stress becomes more compressive before rising to join the axial stress within a few millimeters of the edge; these two components then become highly tensile as before, but drop back slightly on the boundary. The stress profiles along the edge of the plate (figure 6.4-5d) are very similar in form to those across the surface of the plate except that the axial component now takes the place of the radial stress. The hoop stress is tensile at points away from the corner but becomes highly compressive as this point is approached, whilst the axial stress changes from tensile to compressive and back again to tensile before decaying to zero at the corner. Because both the surface and edge are being cooled in this analysis it is not unexpected that the stresses in the boundary layers are behaving in a similar manner.

After 5.6 seconds of the quench the centre of the plate (at 688°C) is now cooling faster than the outer surfaces which are now all martensitic. The combined effect of the position of the highest temperature gradient moving towards the plate centre and the volume expansion associated with the transformation at the surface has causes a complete reversal of the radial and hoop stresses at points along the centre axis (fig 6.4-6 a). The majority of this section is now tensile (~ 100 N/mm²) whilst the martensitic surface layers have become highly compressive (~ 700 N/mm²).

This large change in stress at the surface can also be seen in figure 6.4-6 b where the radial and hoop components at the surface but away from the edge have changed from + 170 N/mm² to a level in the range -700 to -1100 N/mm² along this boundary. The radial stress still decays to zero at the corner and the compressive hoop stress at this point has become yet more compressive during the period 2.0 to 5.6 seconds. Along the centre plane of the plate (figure 6.4-6 c) there has been a complete reversal of all stress components; radial, hoop and axial. The radial and hoop values are tensile and equivalent in value out to ~ 18mm radial distance, at which point the radial stress drops to zero and the hoop stress rises just prior to becoming highly compressive at the edge. As may be expected, because the bulk stresses within the plate are of a reversed nature in comparison with the start of the quench the axial stress generated towards the edge to maintain continuity in a region where the radial stress cannot support the thermal strains, has itself reversed. After being close to zero in the bulk of the plate the axial component becomes significantly tensile (+200 N/mm²) before falling to a highly compressive value (-1200 N/mm²) at the edge. In this outer region of the plate the hoop and axial stresses are closely associated and essentially take up the same profile. In common with all the other plate sections at the 5.6 seconds, the outer edge of the plate (fig 6.4-6 d) displays a general stress reversal. Both the hoop and axial components have become compressive in the material adjacent to the centre plane (-950 and -1250 N/mm² respectively). This axial stress then decays to zero and becomes tensile before again dropping to zero at the corner.

After 9.8 seconds the centre of the plate (node 1) has cooled to 494°C, the surface point on the central axis (node 690) is at 177°C, the edge centre (node 35) is at 133°C, and the corner (node 724) is at 98°C. In the latter position the martensite transformation is virtually complete.

Along the axis of the plate (fig 6.4-7a) the stress distributions are similar to those at 5.6 seconds, except the magnitude of the stresses has increased and the compressive outer layer has penetrated to 2.5mm below the surface. This stress distribution is very similar to that produced in the case of unidirectional heat flow (fig 6.2-23a) and suggests that remote from the plate edge the generated thermal stresses are dominated by the plane stress condition and the surface cooling. Also, along the surface of the plate (fig 6.4-7b) the stress distributions are very similar to those obtained after 5.6 seconds. This is essentially the same situation as is found in the unidirectional situation (fig 6.2-23c) although in the two-dimensional heat flow case the hoop and radial components become more compressive before dropping in value as the corner is approached, and there is a higher compressive hoop value at the corner. These differences may be attributed to the completion of the martensite transformation and more severe temperature gradient which exist at the edge in the case of two dimensional heat flow heat flow. As elsewhere in the plate the stress distribution along the centre plane and the edge (figs 6.4-7 c and d) have changed little during the time period 5.6 to 9.8 seconds except for a general increase in magnitude. Comparison of the unidirectional and two dimensional heat flow cases show qualitative similarities, i.e. tensile radial and hoop stresses away from the edge with the generation of a tensile axial component which then reverts to compression at the boundary. The differences between the results of the two analysis on this plane are the absolute values of the individual components, such as the hoop stress which posseses a maximum of +400 N/mm^2 and a minimum of -600 N/mm^2 at the edge in the two dimensional case compared to +220 N/mm^2 and -50 N/mm^2 respectively in the unidirectional case. When comparing these profiles it can be observed that in the edge region of the two dimensional heat flow case the axial and hoop stresses become coincident (like the radial and hoop in the interior of the plate) which is not the situation for the unidirectional heat flow analysis.

This phenomenae, apart from the general increase in stress levels, has proved to be a characteristic which is peculiar to the two dimensional heat flow results throughout the quenching process.

6.5 COMPARATIVE ANALYSIS

The primary analysis results (section 6.2) for a water quenched plate of 20mm thickness and 30mm radius can be compared with three further sets of results;

a. for two plates which differ only in the radial dimension, i.e. 60 and 15mm, and

b. for a 30mm radius plate with a 2mm radius hole through the centre.

For these plate models the temperature distributions with time are identical to that calculated for the original 30mm radius plate. To enable comparison the results for the 30mm plate are shown along the axis, edge, surface and centre plane for initial elasticity at 0.02s in figure 6.5-1 and for the onset of plasticity at 0.2s in figure 6.5-2.

6.5.1 Plate Diameter Variations

The results for the 60mm radius plate are very similar to that for the 30mm plate. The early elastic results at 0.02 (figure 6.5-3) and those at 0.2s (figure 6.5-4) along the surface and centre plane show identical stress profiles as for the primary analysis (fig 6.5-1 c,d and 6.5-2 c,d). In both cases that part of the plate which is under the influence of the edge, i.e. where axial stresses are generated and the radial/hoop profiles decay or change from the interior values, is identical. This statement holds true when comparing the results along the surface, or centre plane. The only difference which can be detected between

these two sets of results is that at the earliest time (0.02s) the 60mm plate has a slightly higher hoop stress ($2N/mm^2$ = +10%) at the corner, node 501. This difference disappears with the onset of plasticity. Overall, these results were to be expected, because the increase in radius has effectively increased that part of the plate unaffected by the edge, where a plane stress situation prevails.

Conversely the 15mm radius plate has a greatly reduced infinite body section of the plate and although the stress distributions in the edge regions are similar to those in the 30mm plate the much smaller radial distance has allowed the edge effected zones to penetrate to the central axis and interaction with the diametrically opposing zone has caused a modification of the stress profiles. This phenomenae is not readily observed along the surface of the plate (figures 6.5-5a and 6.5-6a) where edge effects are less dominant, hence the 15mm radius plate has a stress distribution on this plane which is almost identical to the results obtained from the 30mm radius plate except that the hoop component is 10% lower at the corner while the stresses are elastic. However, along the central plane of this smaller plate the stress modifications referred to above are very evident. Figure 6.5-5b shows that the radial and hoop components have a value of $-1.6\ N/mm^2$ at the axis which is lower than the corresponding values (2 to 2.7 N/mm^2) in the 30mm radius plate (figure 6.5-1d) at an equivalent position from the edge. As the edge is approached in the small plate the radial and hoop stresses decay towards zero with greater similarity than in the larger model, and the radial component does not now overshoot to a tensile value but remains at zero in the region adjacent to the edge. At this boundary the hoop stress is now $1.5\ N/mm^2$ as opposed to $0.5\ N/mm^2$ in the 30mm plate. The biggest variation between the stress distributions can be seen in the axial stress generation.

Whereas this component had a maximum compressive region of ~-1.5 N/mm² at a distance of 9mm away from the edge before it decays to zero at the axis of the 30mm radius plate, in the 15mm radius plate this peak compressive value is 3.0 N/mm² which remains constant along the centre plane right up to the axis.

For both plates the axial stress values at the edge are identical. At the later time of 0.2s, when plasticity has commenced (figure 6.5-6b), the differences between the two stress distributions along the centre plane are similar to those described above for the earlier time when the stresses were elastic, except the difference in absolute stress values is not as great.

6.5.2 Plate with a Centre Hole

The introduction of a 2mm radius hole through the centre of the plate has created a free edge close to the axis of the component. Examination of the results, described below, has shown some instabilities and inaccuracies in the model including significant radial stresses at the edge of the hole, which are due to insufficient refinement of the mesh in this critical region. However, this inaccuracy has not affected the sense of the stress distributions from which general conclusions can be made. The stress distribution observed after 0.2 seconds of the quench display exactly the same characteristics as at the earlier time point of 0.02 seconds, hence only the former will be presented.

The stress distributions along the edge of the hole from centre plane to surface (figure 6.5-7a) show a hoop stress distribution which is essentially the same as along the axis of a plate which has no hole, except the maximum compressive value near the plate centre and the peak tensile value at the surface are now a little higher because the radial stress component is unable to sustain any thermal strains along this boundary and should be zero.

Because the hole is a free edge a tensile axial stress has generated along its length and is at a maximum of 10 N/mm² at a depth of 3mm below the plate surface and then decays to zero where the two boundaries meet. This is directly comparable with the axial stress profile along the outer edge of the plate (figure 6.5-2b) although the stress levels are considerably lower.

It might be expected that the predicted stress distribution would show a similar edge effect in the region close to the hole as was observed at the outer radius of the plate for all the preceeding analyses. Along the surface of the plate (figure 6.5-7b) this tendancy can be seen as a symmetrical stress profile between the edge of the hole and edge of the plate. Without model instabilities the radial stress would decay to zero at the hole edge (node 471). However, examination of the results along the centre plane (figure 6.5-7c) indicate that different equilibrium and compatibility factors are governing the stress profiles close to the hole compared to the outer edge. With allowances for model inaccuracies it can be seen that the radial stress should decay to zero as the hole is approached, and that as in the case where the hole is absent the continuity of material across the central plane is maintained by a tensile axial stress. Both the radial and axial stress distributions suggest that the edge affected region is smaller in the case of the central hole than it is at the periphery of the plate. This phenomenoe may be explained by the axisymmetric nature of the model, where close to the hole the stress tensors are near a concave boundary with a very small radius of curvature and thus more bulk material surrounds a descrete point at a given distance from the hole than for an equivalent point an an equal distance from the outer edge. The biggest difference between the two edge effects can be seen in the hoop stress distribution; as the outer edge is approached it decays to zero from a compressive value then reverses to a small tensile value at the boundary, but as the hole is approached the hoop stress becomes distinctly more compressive.

This difference may arise because the hoop stress is a function of radial displacement, therefore any radial movement of material away from the plate interior at a free boundary, would produce a tensile hoop stress at the outer edge and a compressive hoop stress at the inner hole.

7. DISCUSSION

7.1 GOVERNING EQUATIONS

The equilibrium equations given in figure 4.1-1 refer to an axisymmetric body that is not subject to external forces. These equations state the relationship between the principal and the shear stress gradients which must be satisfied at all points throughout the volume, hence the internal forces produced between the parts of the body are in equilibrium. The implication of these relationships for an axisymmetric plate are:

- radial stresses must balance in any plane parallel to the plate axis.

- axial stresses must balance in any plane parallel to the central plane

- hoop stresses must balance in the plane of a radial section.

For the purpose of the present work, described in previous chapters, both the internal loading (as a consequence of residual thermal strains) and the model geometry are axisymetric. Therefore the first two of the above statements can be modified to say:

- radial stresses must balance on any line parallel to the plate axis

- axial stresses must balance on any radial line which is parallel to the central plane.

Even with known boundary conditions it is not possible to determine the state of stress in a plate by simply solving the differential equations of equilibrium. To obtain a solution it is also necessary to consider the

deformation of the body. A principal stress cannot be solely related to its corresponding strain component without taking account of the strain components in the other axes. Therefore, to maintain continuity of material, the existence of continuous displacement functions and hence compatible strain components must be derived for the given geometry. Definition of such relations produce compatibility equations in terms of first and second order stress differentials. Compatibility equations for the axisymetric case have been given in figure 4.1-1.

Definition of the boundary conditions along with the equilibrium and compatibility equations enable a full solution of the stress field. Generally the stress components vary over the volume of a body, and when they arrive at a boundary they must be such as to be in equilibrium with the external forces on that boundary, so that the external forces may be regarded as a continuation of the internal stress distribution. For the axisymmetric, water quenched plate models the boundary conditions are defined below;

a. No external forces are applied to the plate, hence any principal stress which is normal to a free boundary must be zero at that point. Consequently the radial stress must be zero at the plate edge, and the axial stress must be zero at the plate surface.

b. On axes of symmetry such as the centre plane and central axis, which are the remaining two boundaries of the model, the bending moments, stress and shear stress gradients must also be zero.

7.1.1 Stress in the Infinite Plate Region

Well away from the circumference of the plate where plane stress conditions are known to exist the radial and hoop components (σ_r and σ_θ) must be equal, whilst the axial and shear stresses (σ_A and τ_{rz}) are zero at all points. From the first equilibrium equation (a),

$$\frac{\partial \tau_{rz}}{\partial z} \quad \text{and} \quad \frac{\sigma_r - \sigma_\theta}{r} = 0$$

Therefore, $\frac{\partial \sigma_r}{\partial r} = 0$ (and consequently $\frac{\partial \sigma_\theta}{\partial r} = 0$)

This means that σ_r and σ_θ remain constant on any plane which is parallel to the central plane of the plate. By equating the two consistency equations c and d, and removing all terms which are known to be zero, we find;

$$\frac{\partial^2 \sigma_r}{\partial z^2} = \frac{\partial^2 \sigma_\theta}{\partial z^2}$$

Therefore σ_r and σ_θ can vary through the plate thickness to accommodate internal loading due to thermal strain, and the two components change by an equal amount so that they are always equivalent to each other and are consistant with plane stress conditions.

7.1.2 Stress in the Edge Effected Zone

Let the radial position r_1 represent the limit of the plane stress condition, past which the internal stresses become affected by the edge and where σ_r does not remain constant as r changes.

Hence $\frac{\partial \sigma_r}{\partial r}$ is no longer equal to zero in the first

equillibrium equation (a) and this must then be offset by the other terms in this expression to maintain equilibrium. On entry to the edge affected region, σ_r and σ_θ were equal so a small change in radius, dr, will produce a value of $\sigma_r - \sigma_\theta$ that will be of the same order as $d\sigma_r$,

then equilibrium cannot be unless a shear stress gradient is generated in the edge affected region. Expressed mathematically this is;

$$\frac{\sigma_r - \sigma_\theta}{r} \simeq \frac{\partial \sigma_r}{r+\partial r} \neq \frac{\partial \sigma_r}{\partial r} \quad \therefore \frac{\partial \tau_{rz}}{\partial z} \neq 0$$

At the plate edge where $\sigma_r = 0$, it is clear that the shear stresses (τ_{rz}) must be zero and examination of the governing equations show that only the hoop and axial components remain to support the thermal strains at this boundary.

7.1.3 Stresses at the Plate Corner

In the upper region of the edge effected zone, which is closely bounded by both the surface and edge at the plate corner, the radial, axial and shear stresses must drop to zero (boundary condition), hence the hoop component will become the major term in all of the governing equations. The compatibility equations suggest that with a dominant hoop component the stress and shear stress gradients will be severe in this region.

7.2 RESIDUAL STRESSES IN THE EDGE EFFECTED REGION OF THE PLATE MODEL

7.2.1 Radial Stress Decay and the Development of Axial Stresses

The predictive modelling has shown that regardless of the thermal history of a quenched plate and the occurrence of transformations within its structure, the radial stresses which exist well away from the edge always decay to zero at that edge to fulfil the necessary boundary conditions. This modification of the in-plane stress distribution is always accompanied by the generation of an axial stress in the edge region, which is essential for the maintenance of material continuity in the presence of thermal and transformation strains which can no longer be supported by the radial component.

Whether the radial stress decays from a tensile or compressive value, which exists in the interior (away from the edge) of the plate, is entirely a function of the transient stress distribution through the thickness of the section that has been generated as a consequence of the thermal gradients and transformation boundaries which arise from the quenching operation. This radial stress irrespective of its nature near the plate axis or whether the plate surface or centre plane is considered, is modified by the edge region and finally becomes zero with one of the characteristic distributions described below;

a. the stress falls directly to zero at the plate edge from the value sustained at the plate axis.

b. the stress at the plate axis initially rises in absolute value as the edge is approached, then falls directly to zero at the edge

c. as in a. or b., but the decay of radial stress overshoots the zero value some millimetres in from the edge to a small value of the opposite sense before finally dropping back to zero at the edge. This is the situation for the final residual stress pattern.

At any particular time in the quench the radial stress decay in the surface layers may display a different distribution to that observed in the central layers. However, the change from one type of decay distribution to another on any specific plane is associated with an identifiable event in the quench process, such as the onset of the martensite transformation or the movement of the maximum temperature gradient in the section of the plate. Both of these phenomena also cause a reversal of the infinite body stresses.

The distance from the edge at which the radial stress begins to decay (edge effected region) depends upon three factors; position in the plate, plasticity, and time into the quench. It has been observed from the quench analyses that the edge effected region is smaller in the surface layers of the plate than at the centre, and in general these regions penetrate further in from the edge as the quench proceeds (discussed further in section 7.6). The occurrence of plastic flow does not change the type of radial stress decay, but modifies the distance from the edge at which this component varies from the plane stress value. This is adequately demonstrated when comparing the radial stress decay along the plate surface between 0.02 and 0.2 seconds into the quench. The application of the yield criterion to elastic stresses reduces these values to that of the current yield stress, therefore the infinite body stress persists closer to the plate edge (see fig 7.2-1).

The generation of axial stresses in the edge region of the plate always displays the same characteristic distribution along a radial plane, and throughout much of the quench the tensile or compressive nature of this component is directly related to the nature of the radial stress which exists close to the plate axis on the same plane. Where a compressive radial stress decays to zero at the edge this is accompanied by the development of a tensile axial stress at this boundary, and visa-versa when a tensile radial stress decays. This statement holds true for the first half of the quench where the stress diagrams of the plate axis has just two distinct regions, e.g. a tensile surface and compressive centre, but in the latter stages and for the residual stress situation the axial component is entirely tensile along the plate edge although a tensile radial stress region is sandwiched between two compressive zones on the plate axis.

Regardless of the nature of the axial stress at the plate edge it always falls quickly to zero a few millimetres distance in from this boundary and overshoots to a small

value of the opposite sense before again dropping to zero. This crossing of the zero point may occur several times as the distance from the edge increases and each successive rise is to a smaller absolute value than the preceding contour, hence the axial stress profile has the appearance of an attenuating waveform.

The generation of an axial stress at the plate edge can easily be explained by the examination of a simple thermal stress situation. Where the surface of the plate is much cooler than the centre, the upper layers (which are attempting to contract) are in tension and in equilibrium with the central layers which are in compression. In a semi-infinite body this equilibrium can be fully satisfied by the plane stress components (σ_R and σ_H) but in the edge region where the boundary condition necessitates radial stress decay, there is a tendency for the contracting surfaces of the plate to shear away from the centre plane. Obviously a cleaving of the plate along its centre plane does not occur, thus continuity of material must be maintained by the generation of other stress fields. As indicated by the equilibrium equations, shear and axial stresses can be produced to ensure continuity of the body. The "cleaving" effect is overcome by shear in the material which, accompanied by a tensile axial stress, effectively holds the two halves of the plate together on the centre plane at the edge. The shear and axial stresses required to achieve this continuity must themselves be in equilibrium along any plane and at the extreme edge, where σ_R is zero, the bending moment produced is higher than that required further into the plate (where σ_R still has an absolute value), hence the axial stress must reverse away from the edge to maintain the equilibrium requirement and ensure that the sum of the bending moments on that plane is zero.

As with the decay of radial stresses the development of the axial component is dependant upon distance from the plate surface and time into the quench.

Close to the corner of the plate, at which point σ_z must be zero, the axial stress gradients are high but penetrate only a short radial distance into the plate, whereas further down the edge towards the centre plane the axial stress gradients are smaller but penetrate further into the plate towards its central axis. Therefore the edge effected zone with respect to axial stress generation tends to lie in a triangulated area which is bounded on two sides by the edge and central plane. At the conclusion of the quench operation the dominating residual axial stresses lie in the outer anulus of the plate within a few millimetres of the edge.

7.2.2 Implications for the Hoop Stress

The variation of the hoop stress in the edge effected zone of the plate differs slightly between the single and two dimensional heat flow cases. For the case where heat removal was only simulated from the upper surface, the hoop component is closely related to that of the radial and axial stresses excepting that the former does not have a requirement to drop to zero at the edge. Throughout the quench the hoop stress would decay from the central axis value, but would either maintain a substantial proportion of that value at the edge or have a profile which passed through zero to give a value of the opposite sense at the boundary. As with the radial stress, the hoop component may sometimes increase its value before decaying towards the edge. In general, the hoop stress begins its decay closer to the edge than the accompanying radial stress, and the characteristic distributions are not usually identical at the same time point, e.g at 2.6 seconds the radial stress on the centre plane decays directly to zero at the edge, whereas the accompanying hoop stress initially increases its compressive value before decaying through zero to leave a tensile stress at the edge (fig. 6.2-15c). Close examination of all the results for the single heat flow analysis shows that the hoop stress profiles reflect a combination of the radial and axial

stress profiles in the layers away from the surface of the plate, that is to say that within a few millimetres of the edge the hoop stress gradients are virtually identical to that of the axial stress whilst it more nearly resembles the radial stress profiles in the intermediate region between this outer anulus and the infinite body region of the plate.

In the two dimensional heat flow case, close to the centre plane of the plate the hoop and axial components in the edge region not only have identical stress gradients but also have superimposed profiles. Thus, near the edge the hoop and axial stresses are equivalent, just as the hoop and radial stresses are equivalent, in the infinite body section of the plate.

It is clear that the hoop stresses in the majority of the edge effected region are generated as a consequence of the other two principle stresses/strains and as dictated by the equilibrium and consistency equations. This may be expected because in the axisymmetric coordinate system used for this analytical modelling the hoop strains and stresses are a function of radial displacement rather than hoop displacement. It is only in the extreme corner of the plate where neither radial or axial stresses can exist (because of the boundary conditions) that the hoop stress alone is the dominant component, but again the stresses observed at this point are a consequence of cumulative radial distortion as opposed to localised thermal strain in the hoop direction.

7.3 DEVELOPMENT OF PLASTIC ZONES

It is due to the occurrence of plastic flow during the quench process, that residual stresses remain in the plate when thermal equilibrium has been achieved. If the initial transient stress distributions had not induced plastic strain, the later stress reversals would only have caused unloading to leave a stress free plate at the end of the quench.

The present work has shown that the development of plastic zones in a finite model geometry is far more complex than had previously been believed from work with semi-infinite models, where the generation of plastic strain is independent of position in the plane of the plate.

Near the axis of the plate, where plane stress conditions exist, the radial and hoop components are equal and plastic flow occurs when they attain the value of the uniaxial yield stress. However, towards the edge extensive regions of high axial stress are liable to occur. This tends to be the most significant component in this part of the plate and regions of very high axial stress nucleate one of the plastic zones that develop during cooling. However, the position at the edge is complicated by the possibility of significant hoop stress components and at the point where the edge meets the face (surface) the axial stress falls to zero. At this point (the plate corner) the only stress component is the hoop stress and it is this component that is responsible for plastic flow.

Although plastic zones form and subsequently disappear at specific points in the plate, after formation they quickly develop until they cover large parts of the plate section. Obviously, as has been pointed out above, the dominant stress component within such a zone will change as position within the plate changes.

Plastic zones tend to grow rapidly from their point of nucleation in a direction parallel to the plane of the plate. Their growth in a direction perpendicular to this tends to be slow. Therefore in many instances the plastic zone boundaries tend to lie in a direction parallel to the plane of the plate and the zone extends over most or all of the distance from axis to edge. This penomenae can be readily observed in Figure 6.2-14a where the plastic zone A'

nucleates at the centre of the plate surface, then rapidly develops towards the edge before growing axially into the plate at an equal rate across most of the section. Similar behaviour can be seen for plastic zones nucleated at the centre of the plate (zones D' and E' in Figures 6.2-14c and d). This means that despite the decay in the radial stress as the edge is approached plastic flow persists. Therefore the assumption that the presence of the edge prevents plastic flow is incorrect, since axial and hoop components provide the necessary stress.

During the course of the quench, three plastic zones develop. The earliest along the surface, the next towards the central plane and finally, as martensite forms, a third in the austenite, nucleated just ahead of the martensite/austenite boundary at a point on the edge. The development of these zones will be discussed in the order given.

In the early stages the equivalent stress is highest at a point where the plate axis emerges at the surface (point A in Figure 6.2-8). Tensile plastic flow begins at this point (Figure 6.2-14a) and as the contours of equal equivalent stress lie almost parallel to the surface this plastic zone spreads rapidly towards the corner (point B in Figure 6.2-14a). In contrast, movement of the plastic zone boundary into the interior is slow, on account of the rapid reduction in the equivalent stress in a direction perpendicular to the surface. Consideration of Figure 6.2-10 shows that the radial stress is maintained until a point very close to the corner (B) is reached where the equivalent stress value is maintained by an increase in the hoop component. Of course there is no axial stress in this point of the plate. After 0.8 seconds the plastic zone reaches its greatest penetration and subsequently it reduces in size until it disappears at a point (A), where it had been initiated. The yield stress of the material is rising continually as cooling continues, so it is this rather than a

reduction in equivalent stress that is responsible for the disappearance of this plastic zone. The shrinkage of this plastic zone involves complications. Since after 0.8 seconds the zone boundary immediately adjacent to the edge rapidly retreats to the plate corner whilst the boundary a few milimetres from the edge continues to grow into the interior of the plate for a short period (Figure 6.2-14b) before it too shrinks back towards the plate surface.

The second plastic zone is found in the interior of the plate and begins to form after 0.8 seconds. It is nucleated at three separate positions at approximately the same time, although they subsequently grow and merge to form a single zone. One begins at a point on the edge (B' in Figure 6.2-14b), a second begins close by (C' in Figure 6.2-14c) and a third is nucleated at the centre of the plate, (D' in Figure 6.2-14c). As the quench continues the two regions near the edge move towards the mid-plane, whilst the third extends rapidly from the centre along the mid-plane until it merges with the other two. Thus, after 1.2 seconds the plastic zone extends over the whole section of the plate, with the elastic/plastic boundary parallel to the plate surface. Obviously, over such a large area the dominant stress components vary, being hoop and radial at the central point and predominantly axial at the edge. All this region is autstenitic and at the high temperatures involved the yeild strength is low. However, as the temperature falls and the difference in temperature between surface and central planes continues to increase, this plastic zone begins to shrink until it disappears at points along the central plane but falls very suddenly at points approximately midway between the surface and the central plane. The same figures show a high equivalent stress towards the surface, but the colder and hence stronger material in this part of the plate does not yield. However it is interesting that slightly later, after 3.2 seconds, Figure 6.2-17 does show a very narrow region of plastic flow in this region of high equivalent stress.

At a later time point (~4.0 seconds) when the plastic zones discussed above have disappeared, a new zone begins to develop from the edge region immediately below the martensite transformation front. The plastic boundary of this zone moves into the plate in a direction at 45° to its edge (fig 16.2-22a) and eventually fills the central half of the section, with the exception of an outer anulus on the centre plane which is the last area to become plastic. Unloading of the stresses along the upper boundary occurs as the transformation front progresses. By the time the transformation front has reached the mid-section plane (5mm from the surface and centre planes) the plastic zone begins to recede away from the edge just below the martensite region and finally disappears at the plate centre. The development of this final plastic zone is somewhat different from that sugggested by the semi-infinite body analysis. This calculation which applies along the central axis suggests that this plastic zone formed adjacent to the martensite/austenite interface at ~10.0 seconds and extended towards the centre of the plate as the quench continued and the martensite region moved further into the section. The present analysis has shown that this zone forms some six seconds earlier at the edge and midway between the corner and midplane before penetrating to the axis and then moving back to a point on the edge close to its intersection with the central plane (Figure 6.2-22a). The correspondance between the contours of equivalent stress and the plastic zone after 12 seconds of the quench can be seen in Figures 6.2-17 and 6.2-22b. The stress components responsible are predominantly the positive radial and hoop stresses but the compressive axial stress predominates towards the edge.

Such results show that the geometry of the plate has a substantial effect on the development of plastic zones, and that the presence of a free boundary greatly modifies the development of these zones from the position found in quenched infinite plates.

7.4 RELATIONSHIPS BETWEEN STRESS AND STRAIN

The relationships between stress and strain are governed by the generalised form of Hookes Law. In the general case these equations cannot be represented graphically except by the relationship between equivalent stress and strain. However, at certain positions in the plate simpler relationships occur which allow the individual components to be illustrated and which gives an insight into the way the stress and strain build up during the quench. Four such points have been identified and are considered here. These include the centre of the plate, the point on the surface where the axis emerges, the corner and the centre of the edge (nodes 1, 471, 501 and 31 in Figures 6.2-34, 6.2-35 and 6.2-36). In the first two cases plane stress conditions prevail and there is only one relationship between stress (hoop and radial) and strain. In the third case, the only relationship is between the hoop stress and strain, and in the fourth, the most meaniningful relationship is between axial stress and strain. In this last case a hoop stress also exists but it remains relatively small throughout the quench, so its effect is relatively insignificant.

All along the surface a similar type of relationship between stress and strain is obtained, with an initial tensile plastic strain, followed by compressive stress with no plastic deformation. At node 471 the stress is provided by both hoop and radial components, but at node 501 the radial stress has decayed, so only the hoop stress is present. After 1.8 seconds the difference in temperature between the surface and central plane is at a maximum and the tensile strain is likewise a maximum, although its value varies from 0.43% to 0.25% between the centre of the surface and the corner. The magnitudes of the maximum stress components are similar at both points. Thus the differences in the amount of strain and the change in the stress components is the main difference obtained along the surface; obviously the corner is subject to much less strain than the rest of the surface.

Likewise, during the subsequent compressive stage, both positions are subjected to maximum absolute stresses very late in the quench, although some time remains to allow a certain degree of unloading of these stresses. In neither case does the stress become tensile before the end of the quench. This is of practical importance since it is on the surface that cracks are most likely to be initiated, so a compressive stress field in this region would prevent their growth. The strain along the surface of the plate at the end of the quench is reasonably consistant at ~0.2%.

There is a superficial resemblance between the stress and strain relationships at the centre of the plate (node 1) and the centre of the edge node 31). Both points are subject to an initial plastic flow followed by an unloading and reversal of the stress components, and then a second period of plastic flow occurs (these are referred to as plastic flow stages 2 and 3 in the previous section). However the situation of the relationships along the central plane is more complex than along the surface, since at intermediate positions all three stress components have significant magnitudes. Even at node 31 (Figure 6.2-36) there is some hoop stress that has been omitted from the figure due to its insignificant value.

Because the axial stress and strain acts in a direction perpendicular to the other principal stresses and strains, the sense of the axial components is always the opposite of the radial and hoop components. This allows the maintenance of compatibility of the elements into which the plate is divided. This relationship between the axial and in-plane components is well illustrated in Figures 6.2-34 and 6.2-36 for nodes 1 and 31 respectively, and shown more globally by comparison of Figures 6.2-18, 19 and 20. Consideration of Figure 6.2-14d shows that the plastic regions that develop along the central plane are continuous despite the change in the components of stress responsible for this strain.

The two periods of plastic flow tend to counteract one another, so that the magnitude of the final strain is comparatively small, with compressive values at the edge and tensile values at the centre of the plate. The origin of the plastic zone towards the surface and the first plastic zone towards the central plane is the initial creation of the temperature gradient in the plate. The second plastic zone towards the central plane is caused by the formation of martensite at the surface and the movement of the phase interface towards the centre.

Two types of stress/strain relationships have been developed in the above discussion. Neither vary to any great degree with respect to radial position, except that the stress levels are lower in the edge effected region of the plate's surface. The first type of relationship occurs in the vicinity of the surface while the second occurs towards the central plane of the plate. The essential difference between the two types is that the second relationship is associated with plastic flow after the first stress reversal, and this can occur in those parts of the structure which is still austenitic and therefore has a low yield stress.

7.5 CORRELATION BETWEEN ANALYTICAL, EXPERIMENTAL AND PREVIOUS RESULTS.

7.5.1 Residual Stresses

7.5.1.1 Analytical and Previous Results

In previous work, Fletcher and Price [49] modified their experiementally determined stress results by an edge correction factor based upon the Saint Venant Principle to enable comparison with the calculated results obtained from an infinite plate model. It was assumed that the in plane stress and strain values which are independant of radial position away from the plate edge reduce linearly to zero at

the edge, and the radial point at which the reduction begins is either one plate's thickness from the edge or at a distance determined from the practical measurement of the variation in plate thickness in the vicinity of the edge. Application of these factors gave reasonable correlation between experimental and calculated stresses. Similarly, to compare the results of the present calculations with those obtained from the infinite plate model, the former must also be modified by an edge correction factor.

One factor to be employed has been determined in section 6.3 (table 6.3-3) where the following relationship was predicted in a unidirectionally water quenched plate of 30mm radius and 20mm thickness;

$$\frac{\text{Average in-plane stress within whole plate}}{\text{Average in-plane stress at the plate axis}} = 0.64$$

, where the average in-plane stress means in this instance the average of the radial and hoop components.

Hence to convert from the average in plane stresses of a finite plate model and compare them with the results of an infinite plate model they should be factored by the reciprocal of 0.64, which is 1.5625. This "correction" has been performed for the present results, taken from the final stress maps in section 6.2, and they are shown in figure 7.5-1 along with the results of Fletcher and Price for comparison. The significance and validity of these correction factors are discussed in section 7.6 below. Overall, the absolute stress levels as predicted by the finite element model used in the present work are lower than the corresponding values generated by the infinite plate model. However, the finite element results more closely resemble the stress levels predicted experimentally by Fletcher and Price.

The largest discrepancy in the correlation of analytical and previous results is the relationship between stress and position below the plate surface. The zero stress and peak tensile stress planes in the finite element model are displaced over 1mm deeper into the section than reported in the work by Fletcher and Price[49] although it should be noted that the stress gradients are essentially the same. These differences may be attributed to the fact that in the finite element model the axial and shear stresses arising from the edge effect had penetrated well into the plate (towards the axis) by the conclusion of the quench analysis, and the strain energy associated with these components would by necessity modify the final in-plane stress distribution.

7.5.1.2 Analytical and Experimental Results

The attempt to measure experimental stresses on the edge of a quenched plate and then to correlate these against results from the finite element model has not been successful except for the purpose of drawing certain conclusions about the chosen approach.

Table 7.5-1 shows the measured stresses on the edge of a plate (see chapter 5) which were determined by the method described in Chapter 3. This table also shows the span of stresses at equivalent points as determined by the finite element models using either unidirectional or two dimensional* heat flow problems. A span of stresses is presented because these exist over the 4mm distance in from the plate edge, which is equivalent to the hole depth in the practical determination.

FOOTNOTE : *It should be noted that although the two-dimensional heat flow results beyond 14 seconds have not been formally presented in this text (due to model instabilities requiring refinement) the analysis had been continued to the conclusion of the quench and it is these results presented in table 7.5-1 for the purpose of comparison.

TABLE 7.5-1 Practical and Analytical Stress Results on the Edge of a Water Quenched 20mm Plate.

POSITION/ COMPONENT	MEASURED STRESS N/mm^2	CALCULATED STRESS N/mm^2	
		1-D Heat Flow	2-D Heat Flow
		(EDGE)	(EDGE)
CENTRE AXIAL	+575	0 to +160	-600 to +250
HOOP	+358	-50 to -90	-370 to +320
3mm Off-Set AXIAL	+377 to +411	0 to +180	No results
HOOP	+124 to +346	-150 to 0	No results

It is clear that the measured stresses do not correlate with those stresses calculated assuming the unidirectional heat flow condition. Certainly one major source of error stems from the machined flats on the edge of the plate, to which the strain gauge rosettes were attached. This meant the plate geometry had been significantly changed, although it was believed initially that this would only have a minor effect.

Not only would this have modified the stresses in a region of high stress gradients, but each strain gauges was lying on a plane that did not correspond to a constant radial position across its width. This lack of axial symmetry would expose the strain gauges to a stress system which cannot be readily correlated against the analysis of an axisymmetric model. Proof of this point was given by the experimental results which showed that the principal stresses measured had directions which were rotated from the axial direction by anything from 5° to 45°.

A further source of discrepancy between the two sets of data is that transformation plasticity was not incorporated in the stress calculations. It is also clear from inspection of the analytical results that a complex stress system of widely varying magnitudes and sense exists within the 4mm anulus adjacent to the edge of a quenched plate. The air abrasive technique can only attempt to average the stresses in the

material removed and although the initial testing indicated a compressive stress in the outer most layer the technique was incapable of quantifying this observation.

Assuming that the above sources of error and practical limitations of the centre-hole air-abrasive technique are responsible for the general lack of correlation between the experimental and analytical results, it is interesting to note that there is greater similarity with the calculated stresses that were obtained using two-dimensional heat flow results in terms of (i) the higher absolute values of the stresses, and (ii) the axial and hoop components having the same sense. These two observations are strong characteristics of the two-dimensional heat flow results and are also characteristic of the experimental results. However, many of these observations are contrary to those obtained using unidirectional heat flow figures. It may therefore be that although the experimental configuration during quenching attempted to create unidirectional heat flow from the plate by employing insulation around its edge, that this technique is not wholly successful and significant cooling of the edge does occur thereby giving rise to a greatly modified stress pattern in this region.

7.5.2 Stress and Strain Profiles

The axis of the plate is 1.5 times the plate thickness from the edge. Therefore it is to be expected that the edge will have no effect on the state of stress at the plate axis, so that the results obtained on this line by the present finite element model should be very similar to those obtained by the infinite plate model of Fletcher and Price[49], particularly as the same relationship between surface heat transfer coefficient and temperature occured in each case. A comparison shows that the two sets of results are relatively close although some discrepancies exist.

At the surface of the plate both models predict a peak tensile stress of ~200 N/mm², but the finite element model suggests this occurs at a temperature of 355°C with a strain of ~ 0.5%, whilst the infinite plate model[49] predicts that this occurs at 386°C with a strain of ~0.65%. Similar discrepancies at the points of unloading and stress reversal are continued throughout the remainder of the quench, and have further increased by the time that the peak compressive stress has occurred. The finite element model predicts a stress of -925 N/mm² for a strain of -0.1% at 170°C compared to the prediction of -1200 N/mm² for a strain of +0.1% at 236°C by the infinite plate model.

Similarly, at the centre of the plate the initial peak compressive stress, prior to the first unloading, varies between the two models. In the finite element model this occurs with a strain of -0.34%, whilst the infinite plate model predicts a strain of -0.55%; the temperature and stress levels are identical for both analyses at any time point. Again, as at the surface, the strain discrepancy at the plate centre continues throughout the quench analyses; the peak tensile stress in the finite element model occurs with a strain of +0.25% as opposed to +0.5% in the infinite plate model.

Figure 7.5-1 illustrates the state of residual stress at the end of the quench along the plate axis as predicted by the two models. Both show a maximum tensile stress at a point intermmediate between surface and centre with compressive stress zone at the latter position. However at the surface the finite element model predicts a substantial compressive stress that has decayed little during the latter part of the quench while the infinite plate model predicts that this stress unloads to a very much smaller value (close to zero). Hence the finite element model predicts a larger zone of compressive stress at the surface compared to the infinite plate model. This discrepancy is due to a relatively modest movement of the tensile region towards the plate centre in

the finite element case and appears to be associated with small differences in the predicted temperature distributions in the later stages of the quench. The differences have practical significance since compressive zones at the surface can prevent crack growth from surface flaws.

7.5.3 Distortion Comparisons.

The diametric distortions (mean in-plane strains) on the centre plane and surface, as measured in the current work and also by Fletcher and Price, can be compared with the overall displacement of edge nodes from the finite element model. The practical determination of distortion was based upon measurement of the plate at ambient temperatures before austenitisation of the samples and after the quenching operation. Because the finite element model only calculated values of strain which relate to cooling from the austenitisation temperature, to enable comparison with practical results, it was necessary to correct the final displacements by adding the linear changes associated with heating the plate from 20°C to 850°C. This correction also incorporated the volume change of the austenite transformation. The distortion values to be compared as shown below in table 7.5.-2.

TABLE 7.5-2 EXPERIMENTAL AND CALCULATED DIAMETRIC DISTORTIONS IN A WATER QUENCHED, 20mm THICK PLATE

POSITION	MEASURED DISTORTION %		CALCULATED DISTORTION%	
	CURRENT WORK	FLETCHER & PRICE [49]	INITIAL VALUES	CORRECTED FOR HEATING
SURFACE PLANE	+0.42	+0.45	-0.33	+0.38
CENTRE PLANE	+0.30	+0.30	-0.36	+0.35
MEAN VALUES	+0.36	+0.375	--	+0.365

The correlation between the two sets of measured distortion is very good, however the calculated distortions are lower at the surface and higher at the centre plane (by approximately the same amount). The correlation between experimental and calculated results is much closer when the mean diametric distortions through the thickness are compared. Even so the agreement between all three sets of results is good.

Throughout section 7.5 where the finite element results have been assessed against those of previous models and the results of experimental work, it has been found that the former model has predicted much lower strains and slightly lower stresses on the axis of the plate. Because the average diametric distortions are in agreement with those values from other sources it is clear that the stresses and strains generated in the edge effected region of the plate (including axial and shear components) modify the stresses and strains in the plate central region in a complex manner. However, this effect has been complicated by the differences in the predicted temperature distributions between the two models (in the later stages of the quench) because prediction of strain values is dependant on the time/temperature/flow stress parameters which are intimately linked in the modelling philosophy.

7.6 EDGE CORRECTION FACTORS

The results obtained using the unidirectional heat transfer model have been used to produce edge correction factors that have been presented in section 6.3. By using these factors, which are calculated as a ratio of the average in-plane stress components at a particular position to the stress at the same position on the plate axis, it is possible to convert the results from the infinite plate model to those which would be predicted in a plate of finite dimensions. The advantage of using this correction factor is that the infinite plate method is a cheaper, and comparatively simpler, analytical tool.

The relationship between quenching time and the average edge correction factor is shown in figure 7.6-1. The pronounced increase in edge correction factor near the start of the quench is consistent with the observation that with the onset of plasticity the edge effected region penetrates a smaller distance from the edge into the plate than is the case later in the quench. This phenomenon has been separately addressed in section 7.2. The figure shows that the edge correction factor (ECF) reaches a maximum at approximately 4 seconds which coincides with the peak plastic stress/strain at the centre of the plate. From this time on the stresses at the plate centre begin to unload, no further plastic zones are formed in the plate section and the ECF reduces to a level which is close to that proposed by the Saint Venant Principle. In the latter case the edge affected zone is assumed to extend one plate thickness from the edge and the inplane stress falls linearly to zero in this region.

For the 60mm diameter by 20 mm thick plate, which was the primary analytical model, the end-of-quench ECF was 0.64. The effect of this factor on the distribution of radial stress near the plate edge is shown in figure 7.6-2, and is compared with the linear relationships derived from the Saint Venant Principle and assumed by Fletcher and Price [49]. There are three reasons why the analytically derived profile differs from that of the other ECF's;

(a) The finite element model shows that the radial stress does not decay linearly in the edge region.

(b) The specific edge correction varies with depth in the plate.

(c) The overall mean ECF takes account of the hoop stress which does not decay in the edge region by the same amount as the radial component.

The magnitude of the edge affected region is approximately equal to the plate thickness. Beyond this distance from the edge the stresses remain constant with position along the radius of the plate. On this basis the ECF for the uniaxial heat flow model has been recalculated for increased plate diameters by taking the stress levels over the additional radial distance to be equal to that observed on the plate axis. This has the effect of raising the mean stress level on any plane and thereby increasing the overall ECF by a corresponding amount. The relationship between ECF calculated by this means and the diameter to thickness ratio of the plate is shown in figure 7.6-3; curves based upon the Saint Venant Principle and the factor determined by Fletcher and Price are also shown in this figure for comparison.

It is clear that the edge correction factors for various plate dimensions closely agree with the Saint Venant Principle, but differ by a significant amount from the relationship used by Fletcher and Price. The ECF calculated from the finite element model was based upon the mean stress levels taken along a single line on a vertical plane through the plate and are valid for the correction of infinite plate model data.

However, the stresses and strains measured experimentally from a plate are an average of the stresses and edge effects in both axes of the plane of the plate; therefore in this situation the correction factor to enable comparison with finite difference generated results should be based upon an average across the whole plane which encompasses all edge boundaries. Expressing these two types of correction factors mathematically we have:-

For a circular plate where, Plate diameter = D
Annular thickness of edge effected zone = t

1) To correct infinite plate stresses to the true average in-plane stresses of a finite plate;

$$ECF = \frac{D-t}{D}$$

2) To compare experimentally measured stresses with infinite plate model results;

$$ECF = \frac{D^2}{D^2-2Dt+2t^2}$$

It is clear from figure 7.6-3 that the finite element results give edge effects which are commensurate with the Saint Venant Principle, for which t=one plate thickness. In the case of the Fletcher and Price work t=1.5 x plate thickness. Although the relationships in figure 7.6-3, discussed above, have been based upon type 1 ECF's, it also shows a Saint Venant curve which is of the type 2. This curve is very close to that shown for the Fletcher and Price values of type 1, and leads to the conclusion that the Saint Venant Principle with the type two correction factor would have given good correlation between their practical and analytical results.

In fact, for a square plate * the type 2 Saint Venant ECF is 1.421, which would have given better agreement with the mean longitudinal strains derived from the measured thickness at the plate centre than the actual correction factor which was adopted. The overall conclusion from this comparative work is that the Saint Venant Principal is valid when compared against realistic geometry modelling and that its application to an edge correction factor is also valid provided that it is employed according to the cases 1) and 2) defined above.

FOOTNOTE : * 120mm X 120mm x 20mm.

Other analyses performed with different boundary conditions yielded insufficient results to make generalised statements about applicable edge correction factors. The model with a central hole had highly modified hoop stress profiles and a reduced edge effect near this boundary, whilst in the two dimensional heat flow analysis significant axial stresses had penetrated to the plate central axis by 2 seconds into the quench whilst the hoop stress at the edge was always observed to be coincident with the axial component. In both models the edge correction factor would be much more complex than in the uniaxial heat flow analysis and it is clear that in the 2 dimensional heat flow case the identification of an edge effected zone is much more difficult because a 3 dimensional stress system exists throughout the plate section.

8 CONCLUSIONS AND SUGGESTIONS FOR FURTHER WORK

The finite element model has shown that a complex 3-dimensional stress field exists in the edge effected region of a quenched plate. The general characteristics of such a stress field are;

(a) Radial stresses which exist in the main body of the plate decay non-linearly to zero at the edge, but may overshoot to a small value of the opposite sense before finally dropping to zero at the free boundary.

(b) Axial and shear stresses are developed in the edge region where the decaying in-plane stresses can no-longer sustain the induced thermal strain. The axial stress maintains material continuity across the centre plane of the plate.

(c) Hoop stresses in the edge region may also decay in a similar fashion to the radial component, but will not become zero at the plate edge. In the case of a 2 dimensional heat flow model, the hoop stress in the outer regions of the edge effected zone becomes coincident with the axial stress.

(d) At the plate corner, where both the radial and axial components are zero, the hoop stress is of a level commensurate with the stresses on the plate axis and may actually be the highest stress within the plate.

Generally, the edge effect observed, in terms of stress profile and the distance from the edge at which the above characteristics are observed, is dependent upon axial position in the plate and the time into the quench.

A major event during the quench process is the occurrence of plasticity. Plastic zones can be generated either from the plate axis or edge, and will grow to cover the whole plate

section. During unloading of the stresses they will also shrink to single points within the edge affected region. The assumptions made by Fletcher and Price about the reduction in strain in the edge affected zone are inconsistant with the actual extension of the plastic zone to the edge of the plate.

Generation of plastic stress is dependant on the equivalent stress value at any point in relation to the von Mises criterion, but the equivalent stress may be dominated by one or more of the constituent components. Therefore plastic zones developed at the edge of the plate are a consequence of the axial stress, whilst plasticity near the plate axis is dependant on the in-plane stresses. Examination of the stress fields during the development of plastic zones showed that plasticity has a transient effect on the extent of the edge region of the plate, whereby the edge effected zone is temporarily smaller than is the case during the remainder of the quench.

Characteristic relationships between stress and strain have been described for specific points on the finite element model of the water quenched, 20mm thick plate. The relationships observed on the axis of the plate are in good agreement with the results of Fletcher and Price [49] with the exception of absolute strain values after the first stress reversal. The characteristic relationship for in-plane components remains the same along the plate surface from axis to plate corner, whereas the stress/strain relationship for the axial component on the edge of the centre plane displays strains of the opposite sense when compared to the relationship for in-plane components at the plate centre. This latter characteristic is to be expected when continuity of material is considered.

The derivation of a mean edge correction factor to enable the prediction of stresses and strain in a finite body from the results of a finite difference analysis have validated the Saint Venant Principle. Edge correction factors determined from the finite element model would give virtually identical results to those that would be generated if the correction factor used was based upon the linear decay of in-plane stresses from a position one plate's thickness in from the edge. This statement is true, regardless of the aspect ratio of the plate.

To follow on from the results of the present work an additional analysis should be performed to simulate a different quenching medium and therefore establish if the characteristics of the edge effected zone, and the consequent edge correction factor, is insensitive to this parameter. An axisymmetric finite element model of the 2 dimensional heat flow problem should also be optimised to give stable results throughout this much more severe analysis case. Results from such a model would give a better understanding of the stress/strain relationships, plastic zone generation and determination of edge correction factors for a situation which is truly representative of a component that receives global cooling during a quench operation. Such a model should also include the effect of transformation plasticity and the change of surface heat transfer coefficient around the plate, both of which will modify the predicted generation of stress during the quench.

9 REFERENCES

1. OROWAN E — Symposium on Internal Stresses, Institute of Metals, 1947 p 47-59.

2. DENTON A A — Metallurgical Reviews, Vol.11, 1966, p 1-23.

3. THELNING K E — "Steel and its Heat Treatment", Bofors Handbook, 1967, Butterworths.

4. ANDREWS K W — "Physical Metallurgy. Techniques and Applications" Vol. 2, 1973, George Allen and Unwin.

5. TALL L — Int. Conf. The Welding Inst. "Residual Stresses in Welded Structures", 1977, p 49-62.

6. LASZLO F — Journ. Iron & Steel Inst. 1943, p 173-205.

7. INOUE T, TANAKA K — Int. Journ. Mech. Sci. Vol. 17, 1975, p 36\-367.

8. DENIS S, SIMON A, BECK G

9. THOMPSON F C — Symposium on Internal Stresses, Inst. of Metals, London, 1947, p 227-233.

10. READ-HILL — "Principles of Physical Metallurgy".

11. PRICE R F — PhD Thesis, Dept. of Metallurgy, Sheff. Poly. 1978.

12. NELSON D V, RICKLEFS R E, EVANS W P — Soc. Auto Eng., Fatigue & Eval. Commt. 1969, p 1-9.

13. EVANS E B — Soc. Auto Eng., 1968, p 1-6.

14. ROSE A — Harterei Techn. Mitt, 21 No.1 1966, p 1-6.

15. CHAPMAN R D, JOMINY W E — Metal Progress, 1953, p 67-72.

16. JACKSON C E, Trans. Am. Inst. Min. Met. Eng., Vol. 158, p 125

17. KOBASKO N I Met.Sci. Heat Treatment, Vol. 11, 1970, p 900-901

18. KOBASKO N I Met. Scie. Heat Treatment, 1975, p 287-290.

19. TOSHIOKA Y, FUKAGAWA M, SAIGA Y CHRISTENSON A L J.I.S.I. Japan, Vol. 59, 1973, p 308-312.

20. BARRETT C S Metals & Alloys, Vol. 5, 1934, p 131-225.

21. DONACHIE M J, NORTON J T Proc.Soc.Exper. Stress Anal. Vol. 19, 1962, p222

22. HAWKES G A Brit. J. Appl. Phys. Vol. 8 1957, p 229.

23. CULLITY

24. KIRK D "Strain", April 1970, p 75-80.

25. DOI O, SATO Y Bull. Jap. Soc. Mech. Eng. Vol. 14, 1971, p 383-391.

26. STAHLKOPF K, EGAN G R, DAU G Inst. Conf. The Welding Inst., London, 1977, p 321-335.

27. Macherauch E, Wolfstieg U Matl. Sci. & Eng., Vol. 30, 1977, p 1-13.

28. RAI J K, MISHRA A, RAO U R K Int. J. Prod. Res., Vol. 16, 6, 1978, p 463-467.

29. BENSON D K Met. Trans., Vol.3, 1972, p 2547-2550.

30. FORD H Symposium on Internal Stresses, Inst. of Metals, London, 1947, p 3-11.

31. SHREIBER G K, IVANOV G A Indus. Lab., 1972, p 460-461.

32. KISHI K, EDA H Trans. J. Jap. Inst. Met., Vol. 13, 1972, 0 412-418.

33. SCHREIBER E Hart. Tech. Mitt,(BISITS13783) Vol. 28, 1973, p 186-199.

34. BIEDERMAN R R, REYNOLDS C C — Soc. Man. Eng., MR75-120, 1975, p 1-7.

35. WAKABAYASHI M, NAKAYAMA M — Bull. Jap. Soc. Prec. Eng. Vol. 13, 1979, p 75-81.

36. NOWIKOWSKI L J — Soc. Aut. Eng.J., 1961,p 41-45

37. UNKNOWN — Manuf. Eng. 1976, 77, (4), p 38;39, p 38-39.

38. DOLLE H, COHEN J B — Met. Trans. (A), Vol. 11A, 1980, p 159-164.

39. BEANEY E M, PEOCTOR E — Strain, 1974, p 7-14.

40. BUSH A J, KORMER F J — ISA Trans., Vol 12, (3) 1973 p 249-259.

41. BEANEY E M — Strain, 1976, p 99-106.

42. OWENS E M — BSSM - I.Prod.E.Inter.Conf. at Univ.of Aston, Sept.,1980, p 1-21.

43. BEANEY E M — Brit.Soc.Strain Measur. 14th Ann.Conf. 1978, p 1-19.

44. MURRAY I D — Auto.Eng. Vol.55, 1965 p 186-192

45. BISRA — Brit.Iron Steel Res.Assoc. MG/N/150/58, 1958, p 1-7.

46. HOPKINS A D, HOLLAND N H — Journ.ISI, Vol.4, 1962, p 308-316

47. MOCARSKI S — Indus.Heat., May 1974, p 58-70

48. LLEWELLYN D T, COOK W T — Metals Tech. Vol.5, 1977, p 265-278.

49. FLETCHER A J, PRICE R F — Metals Tech, 1981, p 427-446.

50. CRANK J, NICOLSON P — Procs.Camb.Phil.Soc. Vol 43, 1947, p 50-67.

51. DUSINBERRE G H — "Heat Transfer Calculations by Finite Differences", 8, 1961, Scranton, Pa, International

52. JAEGER J C — Procs.Camb.Phil.Soc., Vol. 46 1950, p 634-641.

53.	ADAMS J A, ROGERS D F	"Computer Aided Heat Transfer Analysis", New York, McGraw-Hill 1973
54.	APARCI V S	"Conduction Heat Transfer", Reading Mass., Addison-Wesley, 1966.
55.	KATAYAMA K, SAITO A	Bull.of JSME, Vol.12, No.52, 1969, p 857-864.
56.	WOOD W L, LEWIS R W	Int.Journ.for Num.Meth. in Eng. Vol.9, 1975, p 679-689.
57.	FLETCHER A J	Metals Tech. 1977, p 307-316.
58.	PRICE R F, FLETCHER A J	Metals Tech. 1980, p 203-211.
59.	TIMOSHENKO S P, GOODIER J N	"Theory of Elasticity" 1970 McGraw-Hill
60.	BOLEY B A, WEINER J H	"Theory of Thermal Stresses" 1960, John Wiley & Sons.
61.	JOHNS D J	"Thermal Stress Analysis", 1965 Pergamon Press
62.	MANSON S S	"Thermal Stress and Low Cycle Fatigue", 1966, McGraw-Hill
63.	RUSSELL J E	Symp.on Internal Stresses. Inst. of Metals, 1947, P95-106
64.	HIRONE T, TSUYA N	528th Rep. of Research Inst. for Iron, Steel & other metals 1948 p 169-173.
65.	WEINER J	Journ.Appl.Mech., Vol.23 1956, p 395-402.
66.	BOLEY B A	Journ.of the Aeron.Scis., Vol.23,1, 1956, p 67-75.
67.	MURA T	Res.Rpts.Faclt.Eng.Maijf Univ. No.10, 2, 1957, p 14-27.
68.	LANDAU H G, WEINER J H, SWICKY E E	Journ.Appl. Mech., 1960, p297-302.
69.	TOSHIOKA Y, FUKAGAWA M,	Trans. I.S.I.J. Vol.12, 1972 p 6-15
70.	HILDENWALL B, ERICSSON R	

71.	GOODIER J N	Phil.Mag.Ser.7, Vol.23, 1937 P 607.
72.	GOODIER J N	Journ.Appl.Phys., Vol 13, 1942, p 167-171.
73.	MISES R V	Bull.An.Maths.Soc., Vol 51, 1945, p 555-562.
74.	STERNBERG E	Quart. of Appl. Math., Vol.11, 4, 1954, p 393-402.
75.	HORVAY G, SCHENECTADY N Y	Journ.Appl.Mech., 1953, p 87-94.
76.	HORVAY G	Journ. Mech. Phys. of Solids, Vol 5, 1957, p 77-94.
77.	BOLEY B A	Proc.3rd.U.S.Mat.Cong., 1958, p 259-264.
78.	BOLEY B A	Quart.Appl.Maths., 1960, p 205-207.
79.	ZIENKIEWICZ O C	"The Finite Element Method", 1977, McGraw-Hill.
80.	HINTON E, OWEN D R J	"Finite Element Programming", 1977, Academic Press.
81.	NORRIE D H, DEVRIES G	"An Introduction to Finite Element Analysis", 1978, Academic Press.
82.	ROCKEY K C et al	"The Finite Element Method", 1975, Granada.
83.	PIAN T H H, TONG P	Int.Journ.Nun.Meth.Eng., Vol 1, \969, p 3-28.
84.	ODEN J T	Int.Journ.Num.Meth.Eng.Vol. 1969.
85.	RICHARDS T H	Methods and Practice for Stress and Strain Analysis, 1979, p 128-135.
86.	EDUARDO R De ARANTES E OLIVERA	Int.Journ.Solids.Struct., Vol4 1968, p 929-952.
87.	ZIENKIEWICZ O C	Appl.Mech.Rev., Vol.23, 1970, p 249^256.
89.	ERGATOUDIS I, et al	Int.Journ.Solids.Struct., Vol. 4, 1968, p 31-42.

90.	MARCAL P V	Int.Journ.Mech.Sci., Vol 7 1965, p229-238.
91.	MARCAL P V, KING I P	Int.Journ.Mech.Sci., Vol 9 1967, p 143-155.
92.	YAMADA Y, et al	Int.Journ.Mech.Sci., Vol 10 1968, p 343-354.
93.	ZIENKIEWICZ O C, VALLIAPPAN S, KING I P	Int.Journ.Num.Meth.Eng., Vol 1 1969, p 75-100.
94.	WILSON E L, NICKELL R E	Nuc.Eng.Design, Vol.4, 1966, P 276-286.
95.	ZIENKIEWICZ O C, PAREKH C J	Int. Journ.Num.Meth.Eng., Vol.2, 1970, p 61-71.
96.	SOLIMAN J I, FAKHROO E A	Journ.Mech.Eng.Sci., Vol.14 No.1, 1972, p 19-24.
97.	COMINI G, et al	Int.Journ.Num.Meth.Eng. Vol.8, 1974, p 613-624.
98.	LEWIS R W	Proc.F E Symp.Atlas Comp.Lab. March, 1974, p 43-56.
99.	GRILL A, SORIMACHI K	Int.Journ.Num.Meth.Eng. Vol.14, 1979, p 444-505.
100.	LEWIS R W, BASS B R	Journ.Heat Trans., 1976, p 478-484.
101.	BEER G, MEEK J L	Univ.Queensland, Aust.No.CE 10 1980, p 1-27.
102.	WEBBER J P H	Journ.Strain Anal., Vol.2 1967, p 43-51.
103.	TOSHIOKA Y	I.S.I.J., 1976, p 154-164.
104.	RAI J K, MISHRA A, RAO U R K	Int.Journ.Mach.Tool DES.RES. Vol.20, 1980, p 1-8.
105.	TAIRA S, INOUE T, UEDA H	Proc.14th Jap.Congr.Matl.Res., Sept. 1970, p 165-169.
106.	INOUE T, HARAGUCHI K, KIMURA S	Trans. I.S.I.J., Vol.18, 1978, p 11-15.
107.	UEMURA K, NAGAKE S, INOUE T	Journ.Soc.Matl.Sci.Jap., 1978 p 24-29.
108.	HASHIMOTO S, INOUE T, YAMADA T	Journ.Soc.Matl.Sci.Jap., 1978, p 422-426.

109.	KISHINO T, NAGAKI S, INOUE T	Journ.Soc.Matl.Sci.Jap., 1979 p 861-867.
110.	MONKAWA M, NAGAKI S, INOUE T	Journ.Soc.Matl.Sci.Jap., 1980 p 1173-1179.
111.	BRITISH STANDARDS	En30 steels (Properties)
112.	FULLARD K	C.E.G.B. Research Dept. RD/B/N2865, 1974.
113.	B.S.C. RESEARCH REPORT	PGM/6757/-/73/A
114.	HELLEN T K, FLACK V	C.E.G.B. Research Dept. RD/B/NA057, 1977.
115.	HELLEN T K, HARPER P G	C.E.G.B. Research Dept. RD/B/N3597, 1976.
116.	HELLEN T K	Unpublished.
117.	HELLEN T K	Private communication.
118	ABBASI F, FLETCHER A J	Matl. Sci. and Technol., October, 1985 p 770-779.
119	FLETCHER A J, SOOMRO A B	Matl. Sci. and Eng. 82 (1986) p 101-115.
120	DENIS S, et al	Matl. Sci. and Technol., October, 1985 p 805-814.
121	ABBASI F, FLETCHER A J	Matl. Sci. and Technol., October, 1985 p 830-837.
122	ALLEN F S, FLETCHER A J	Matl. Sci. and Technol., April, 1987 p 291-298.
123	FLETCHER A J, SOOMRO A B	Matl. Sci. and Technol., July, 1986 p 714-719.
124	SCHRODER R	Matl. Sci. and Technol., October, 1985 p 754-764
125	FLETCHER A J, LEWIS C A	Matl. Sci. and Technol., October, 1985 p 780-785

FIGURE 2.1

TEMPERATURE GRADIENTS IN A
COOLING BODY

FIGURE 2.2

DEVELOPMENT OF THERMAL STRESSES
(Transformation Stresses Not Included)

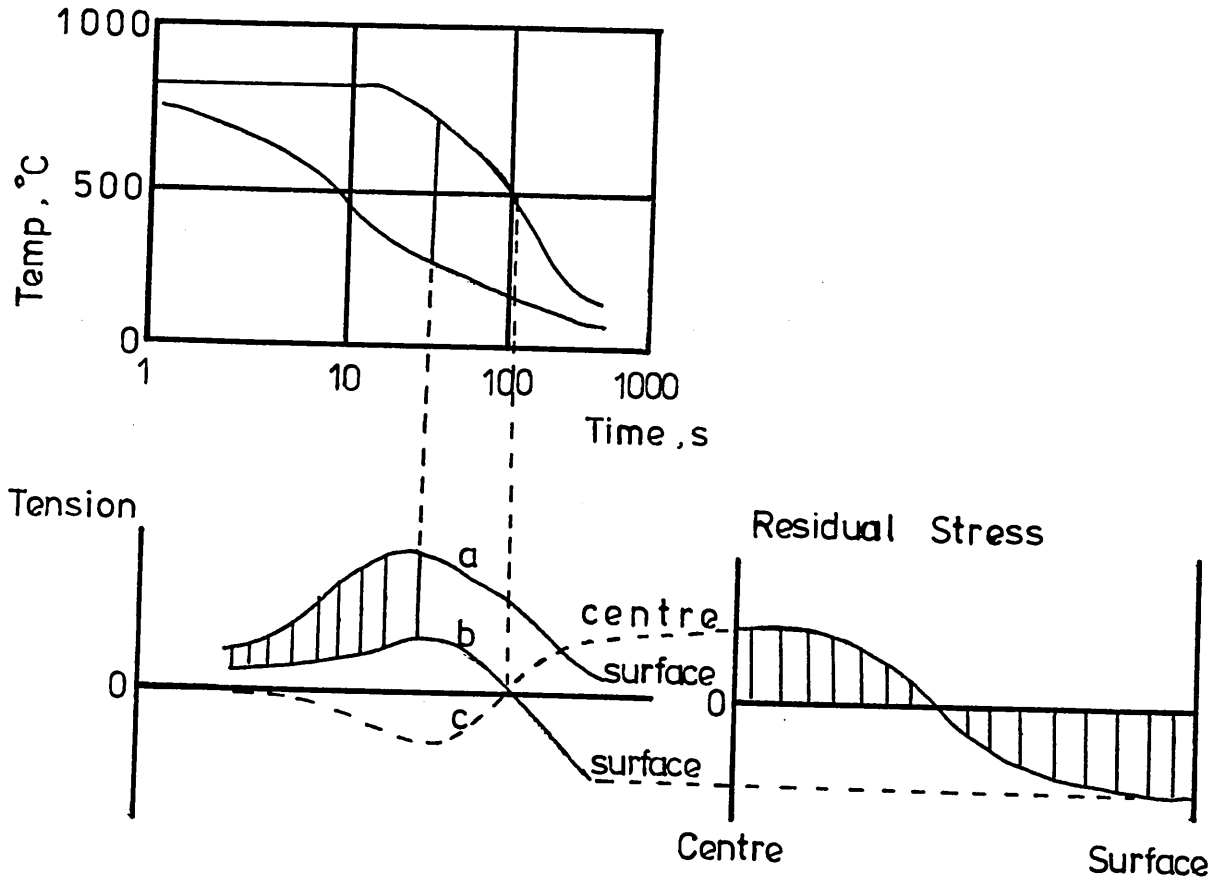
1000
500
0
Temp., °C
1
10
100
1000
Time, s
Tension
a
b
c
0
centre
surface
surface
Residual Stress
0
Centre
Surface

FIGURE 2.3

HARDENABILITY INFLUENCE ON THE STRUCTURES FORMED IN A COOLING BODY

FIGURE 2.4

EFFECT OF HARDENABILITY ON PEAK RESIDUAL STRESS

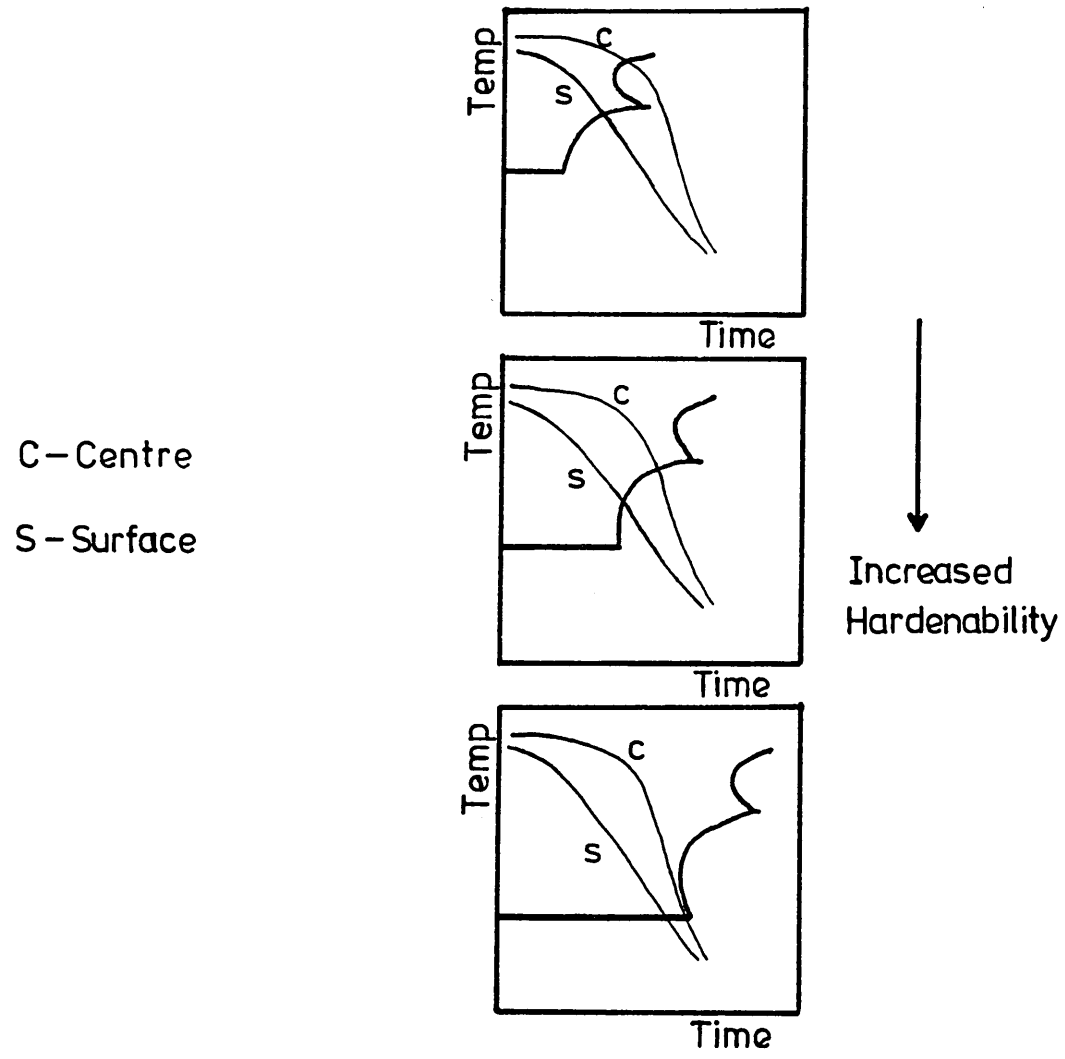
C – Centre
S – Surface
Temp
C
S
Time
Temp
C
S
Time
Increased
Hardenability
Temp
C
S
Time

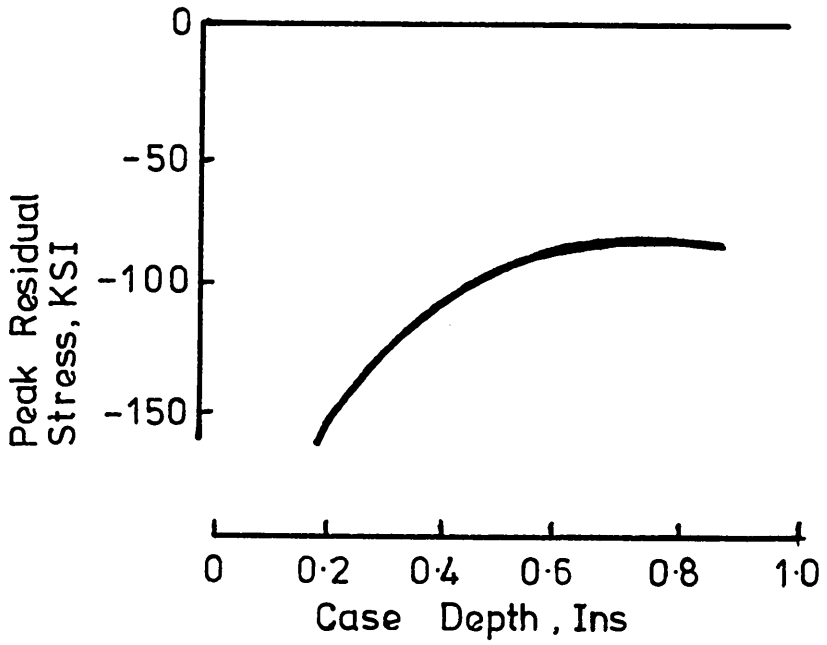
0
-50
-100
-150
Peak Residual
Stress, KSI
0
0·2
0·4
0·6
0·8
1·0
Case Depth , Ins

FIGURE 2.5

A TYPICAL DILATION CURVE FOR STEEL, SHOWING VOLUME EXPANSION ON COOLING DUE TO TRANSFORMATION

FIGURE 2.6

SPECIFIC VOLUMES OF STEELS

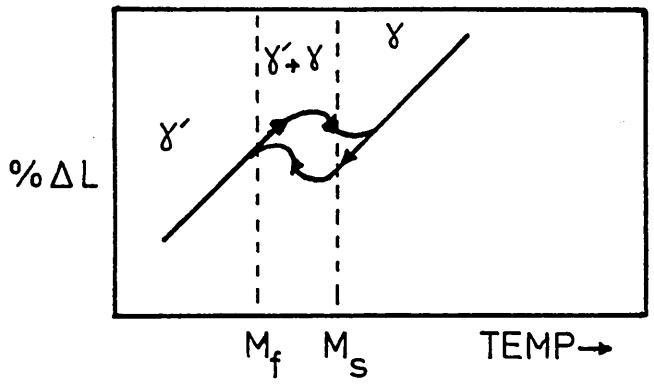
γ'+γ
γ
γ'
%ΔL
M_f
M_s
TEMP→

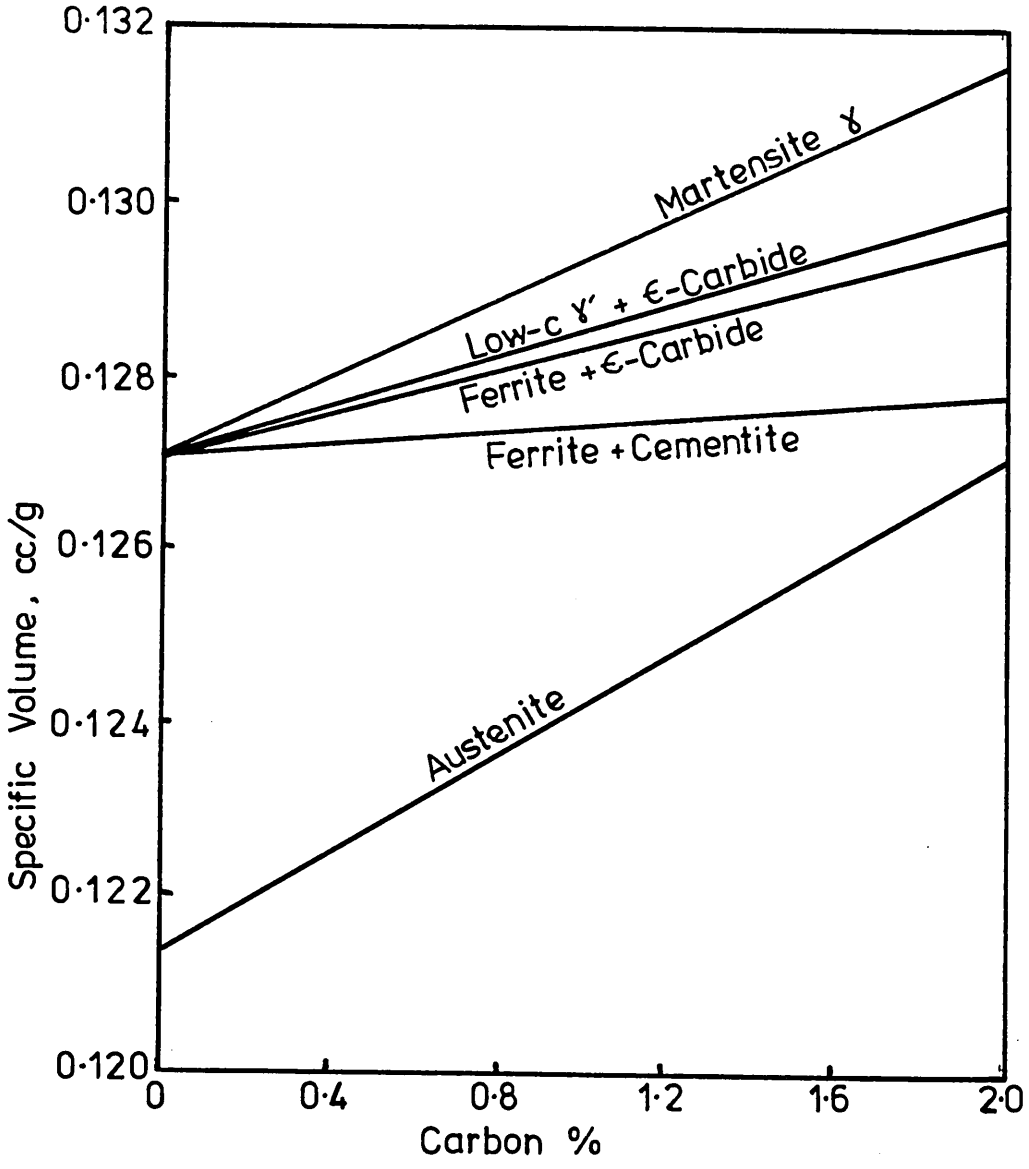
0·132
0·130
0·128
0·126
0·124
0·122
0·120
Specific Volume, cc/g
Martensite γ
Low-c γ' + ε-Carbide
Ferrite + ε-Carbide
Ferrite + Cementite
Austenite
0
0·4
0·8
1·2
1·6
2·0
Carbon %

FIGURE 2.7

THE EFFECT OF SIZE ON THE SURFACE RESIDUAL STRESSES IN WATER QUENCHED SAE 1045 CYLINDERS

FIGURE 2.8a

THE EFFECT OF SIZE AND TRANSFORMATION ON RESIDUAL STRESSES IN QUENCHED DIN 22 STEEL

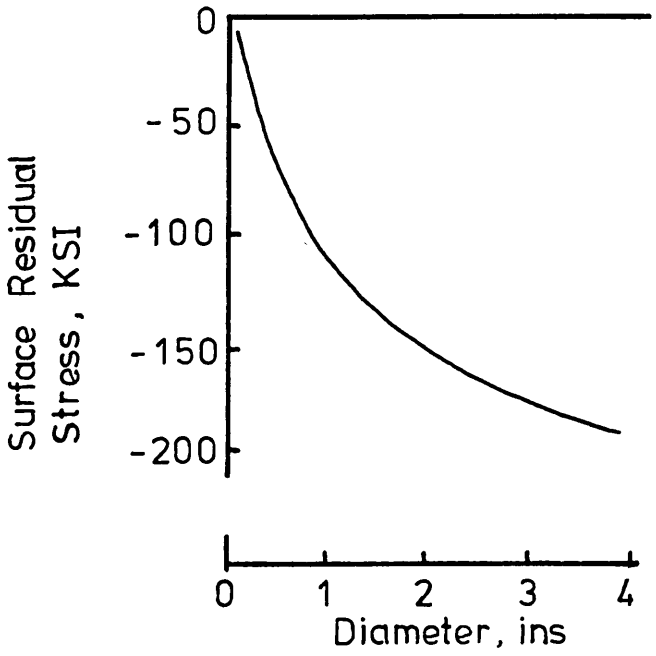

s - Surface

c - Centre

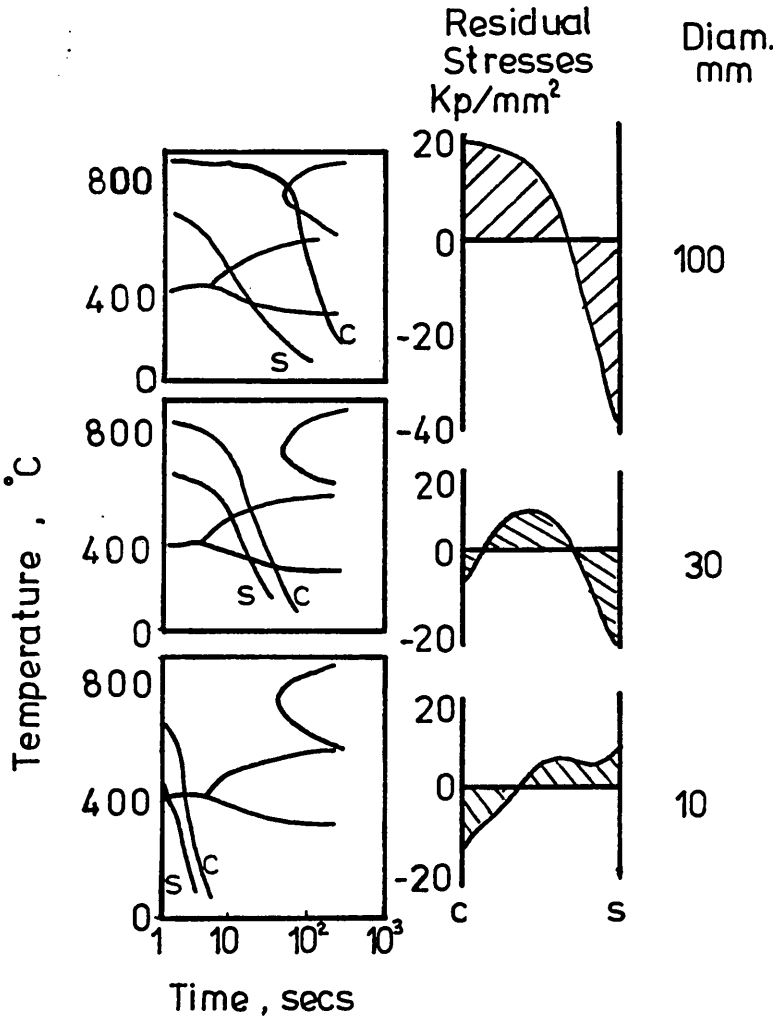

FIGURE 2.8b

THE CHAPMAN AND JOMINY
"CRACKABILITY TEST SPECIMEN"

FIGURE 2.9

QUENCH CRACK PROBABILITY
OF 40KH STEEL

FIGURE 2.10

ELLIPSOID OF STRESS

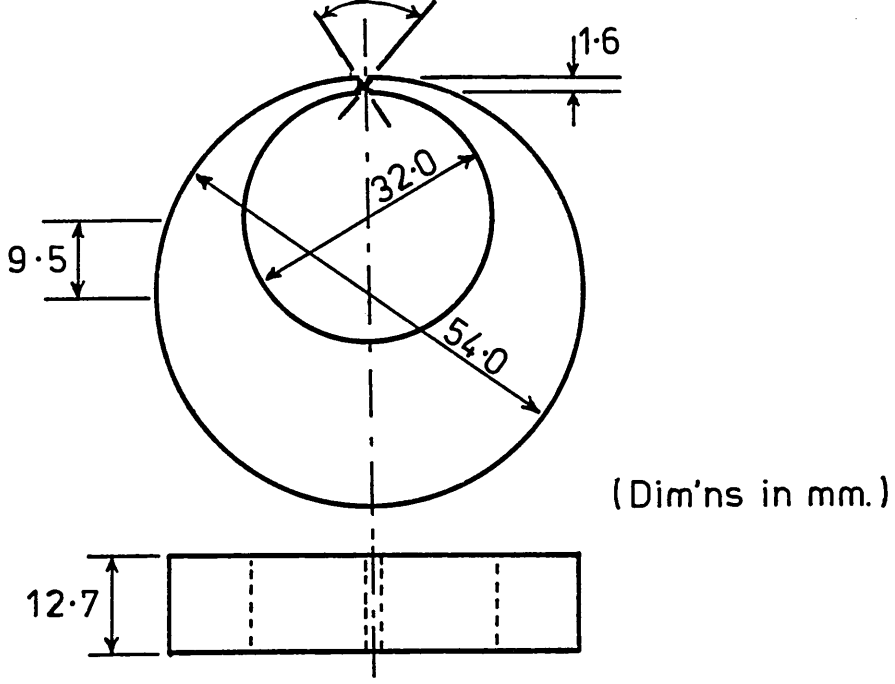
1·6
32·0
9·5
54·0
12·7

(Dim'ns in mm.)

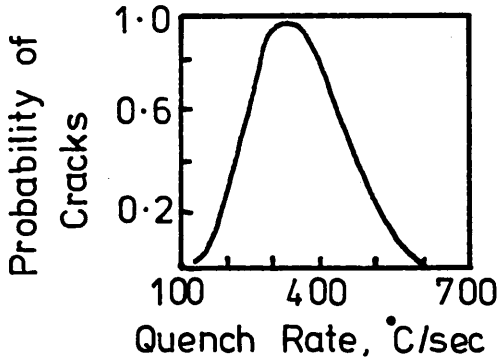
Probability of Cracks
1·0
0·6
0·2
100
400
700
Quench Rate, °C/sec

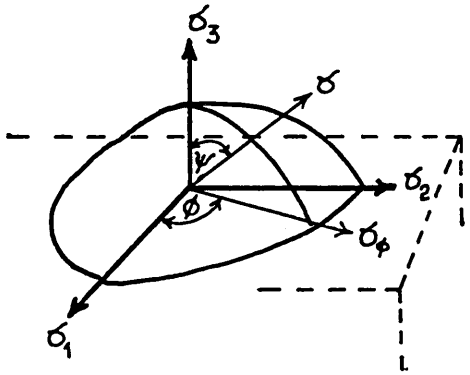
σ3
σ
ψ
σ2
φ
σφ
σ1

FIGURE 2.11

COMPARISON OF X-RAY STRESS ANALYSIS AGAINST STRAIN GAUGE RESULTS

FIGURE 2.12

RESIDUAL STRESS ANALYSIS OF QUENCHED MILD STEEL BY A LAYER REMOVAL - DEFLECTION TECHNIQUE

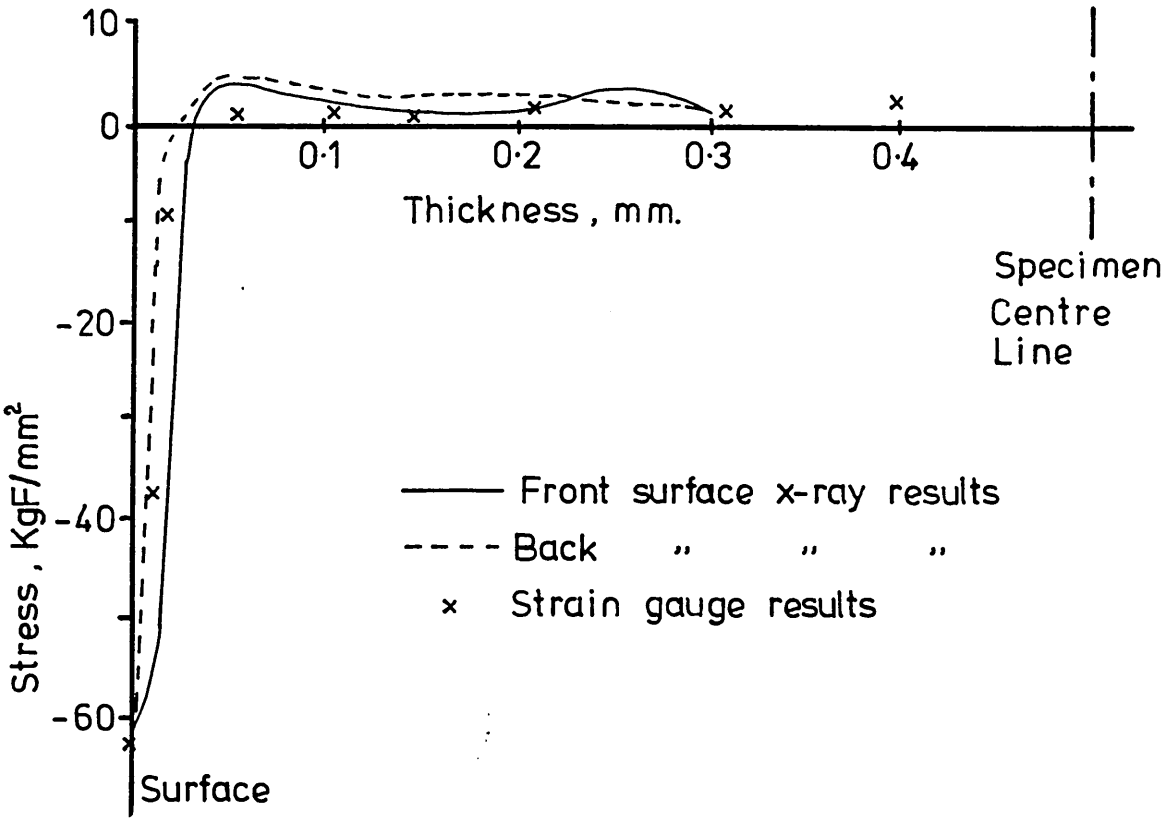
10
0
-20
-40
-60
Stress, KgF/mm²
0·1
0·2
0·3
0·4
Thickness, mm.
Specimen Centre Line
Surface
Front surface x-ray results
Back " " "
Strain gauge results

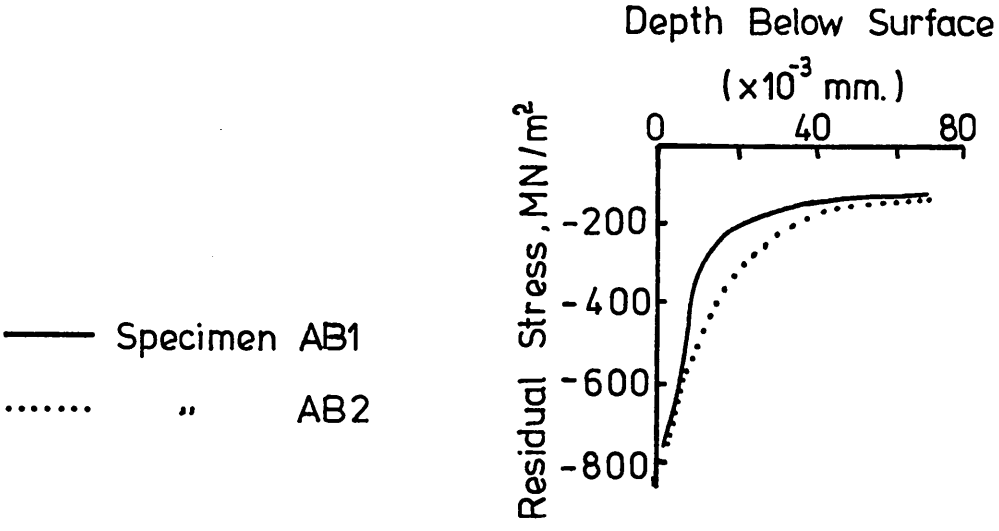
Depth Below Surface
(x10⁻³ mm.)
0
40
80
Residual Stress, MN/m²
-200
-400
-600
-800
Specimen AB1
" AB2

FIGURE 2.13

RESIDUAL STRESS IN A COLD DRAWN BRASS ROD BY THE SACHS BORING-OUT METHOD

FIGURE 2.14

CROSS-SECTION OF STRIP USED FOR DERIVING THE LAYER REMOVAL METHOD OF RESIDUAL STRESS ANALYSIS

FIGURE 2.15

A STRAIN GAUGE ROSETTE
(ϕ = 8.89mm. TO SCALE)

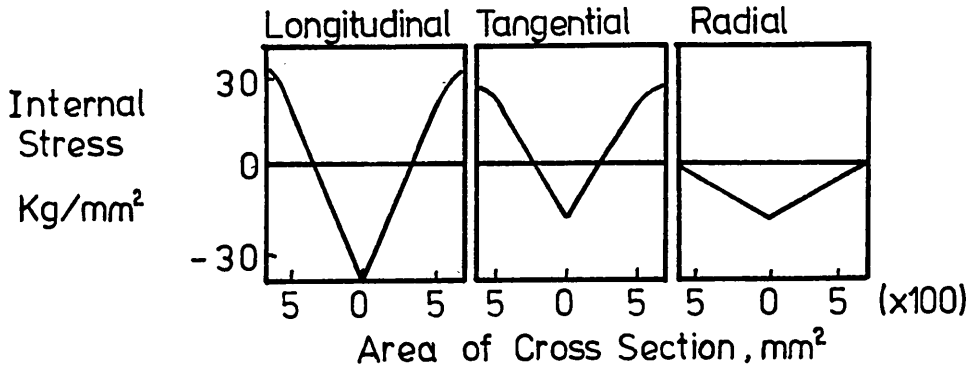
Longitudinal
Tangential
Radial
Internal Stress
Kg/mm²
30
0
-30
5 0 5 5 0 5 5 0 5 (x100)
Area of Cross Section, mm²

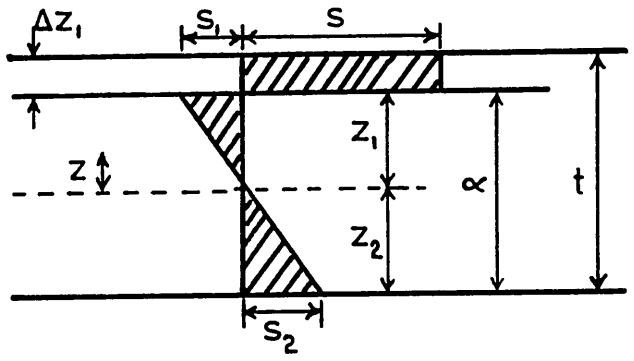
ΔZ1
S1
S
Z1
Z
∝
t
Z2
S2

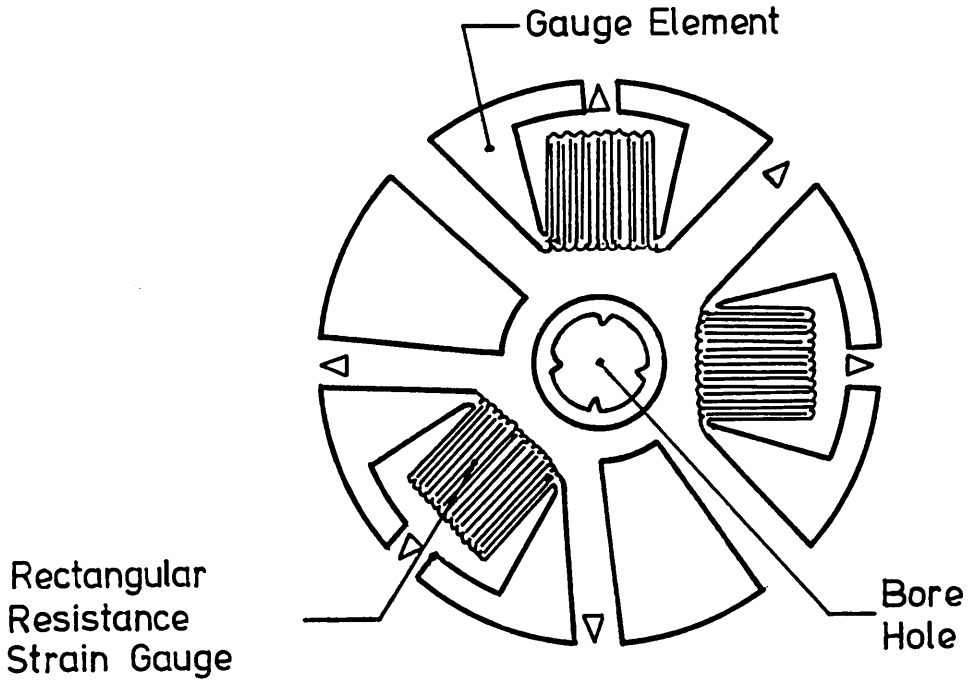
Gauge Element
Rectangular Resistance Strain Gauge
Bore Hole

FIGURE 2.16

ELASTIC RADIAL STRESS RELAXATION IN THE CENTRE HOLE BORING TECHNIQUE

FIGURE 2.17

GENERAL TRENDS OF DIMENSIONAL CHANGE DURING QUENCHING OF CM80, CM60 AND EN352 STEEL CYLINDERS

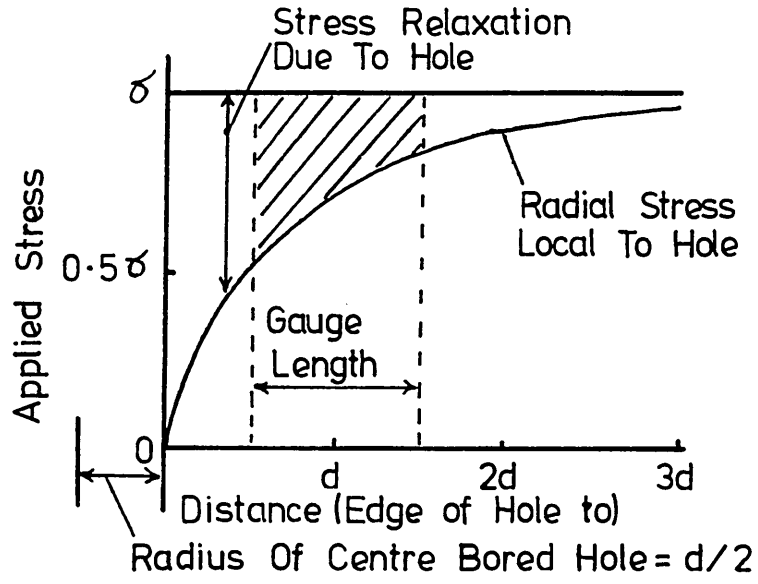
Stress Relaxation
Due To Hole
σ
0·5σ
0
Applied Stress
Radial Stress
Local To Hole
Gauge
Length
d
2d
3d
Distance (Edge of Hole to)
Radius Of Centre Bored Hole = d/2

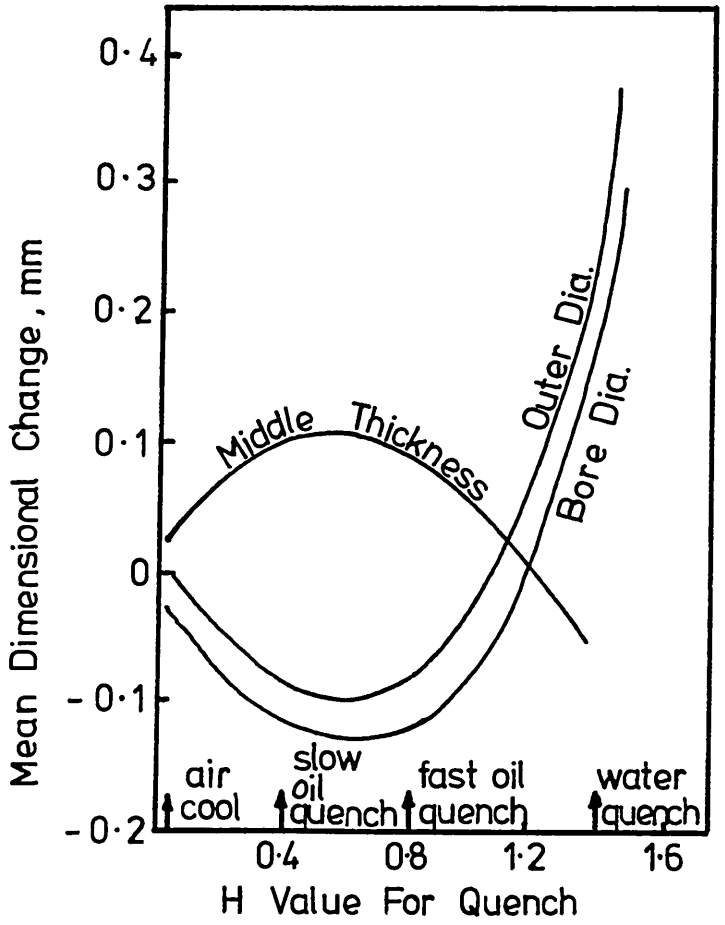
0·4
0·3
0·2
0·1
0
-0·1
-0·2
Mean Dimensional Change, mm
Middle Thickness
Outer Dia.
Bore Dia.
air cool
slow oil quench
fast oil quench
water quench
0·4
0·8
1·2
1·6
H Value For Quench

FIGURE 2.18

POSITIONS OF DISTORTION MEASUREMENT ON A PLATE OF EN30B STEEL[49]

FIGURE 2.19

THROUGH THICKNESS DISTORTION OF A QUENCHED EN30B PLATE[49]

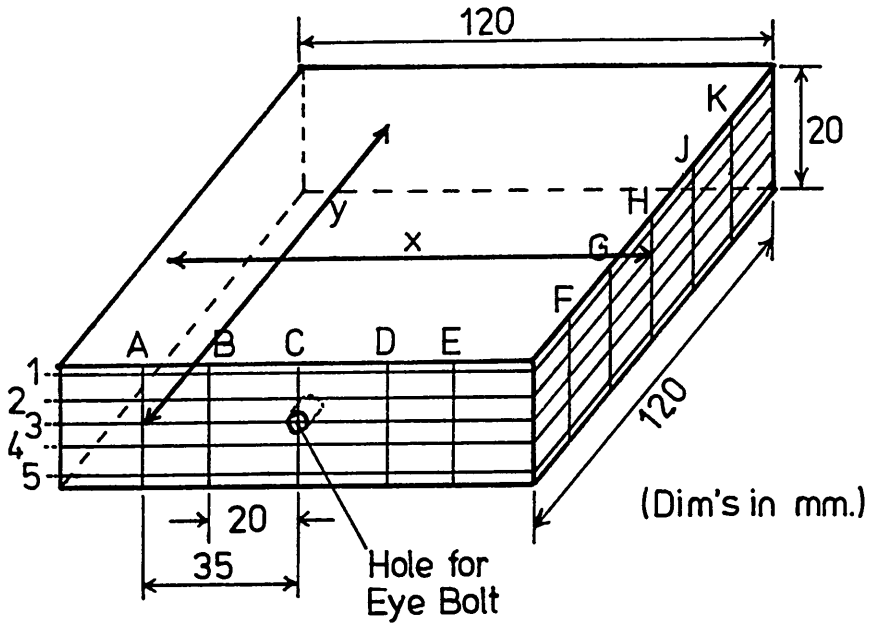
120
20
K
J
H
G
F
y
x
A
B
C
D
E
1
2
3
4
5
120
20
35
Hole for
Eye Bolt
(Dim's in mm.)

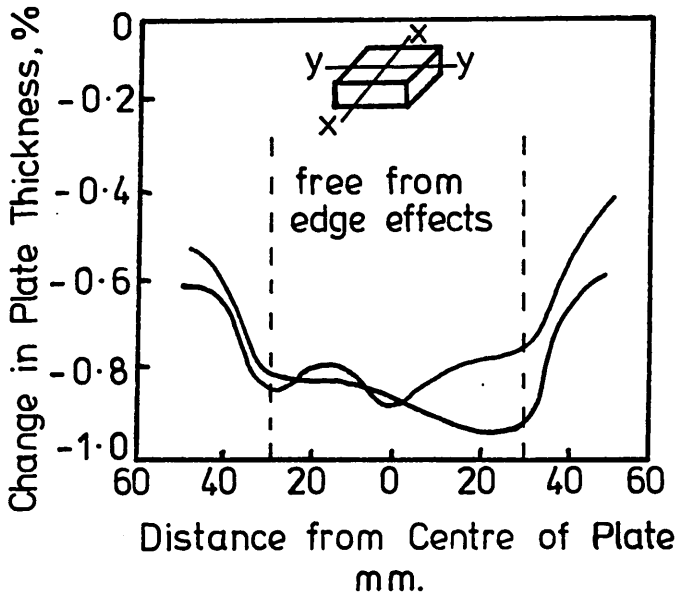
Change in Plate Thickness, %
0
-0·2
-0·4
-0·6
-0·8
-1·0
x
y
y
x
free from
edge effects
60
40
20
0
20
40
60
Distance from Centre of Plate
mm.

FIGURE 2.20

SURFACE BOUNDARY CONDITION USED BY FLETCHER[57] FOR TEMPERATURE ANALYSIS

FIGURE 2.21

STRAIN INDUCED BY CHANGE OF TEMPERATURE DISTRIBUTION[69]

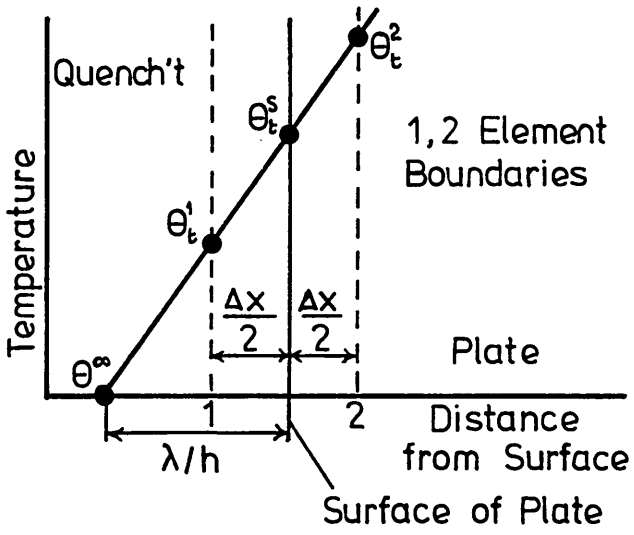
Quench't
Temperature
θ_t^2
θ_t^s
θ_t^1
θ^∞
1,2 Element Boundaries
$\frac{\Delta x}{2}$
$\frac{\Delta x}{2}$
Plate
1
2
Distance from Surface
λ/h
Surface of Plate

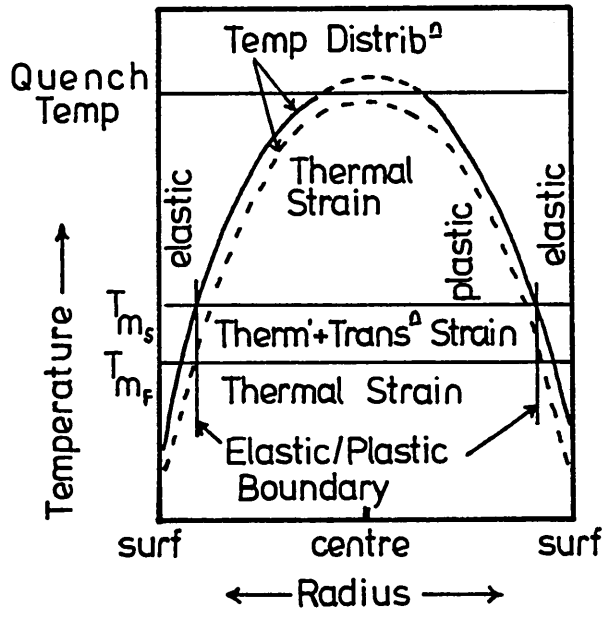
Temp Distrib^n
Quench Temp
Thermal Strain
elastic
plastic
elastic
Temperature
T_{m_s}
Therm'+Trans^n Strain
T_{m_F}
Thermal Strain
Elastic/Plastic Boundary
surf
centre
surf
Radius

FIGURE 2.22

CALCULATED RESIDUAL STRESSES IN CARBURISED PLATE OF SAE 1321 WITH DIFFERENT SURFACE CARBON CONTENTS[70]

(Constant case depths)

FIGURE 2.23

RELATIONSHIP BETWEEN STRESS AND STRAIN IN A 20mm THICK, OIL QUENCHED EN30B PLATE[49]

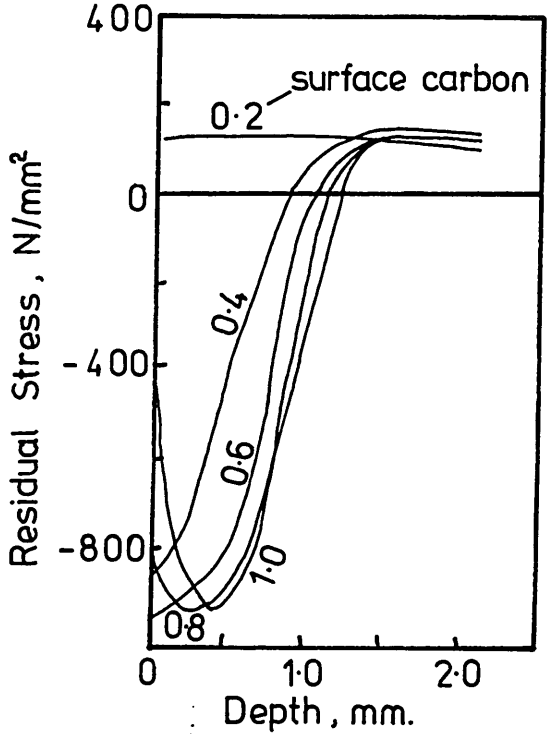
400
0
-400
-800
surface carbon
0·2
0·4
0·6
0·8
1·0
Residual Stress, N/mm²
0
1·0
2·0
Depth, mm.

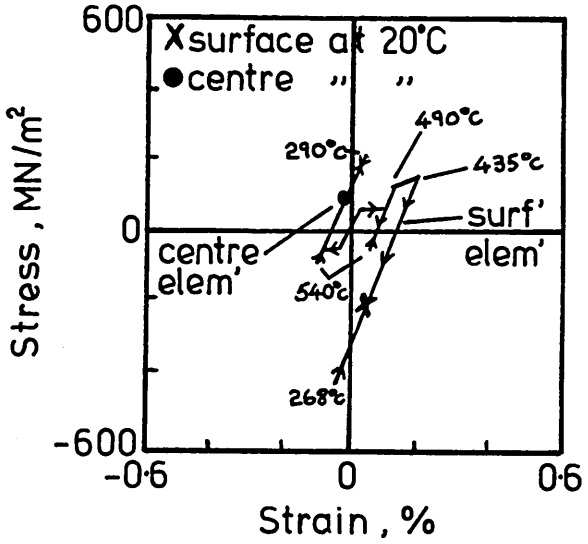
600
-600
X surface at 20°C
● centre " "
290°C
490°C
435°C
surf' elem'
centre elem'
540°C
268°C
Stress, MN/m²
-0·6
0
0·6
Strain, %

FIGURE 2.24

COMPARISON OF CALCULATED AND EXPERIMENTAL RESIDUAL STRESSES IN A WATER QUENCHED EN30B PLATE

FIGURE 2.25

COMPARISON OF CALCULATED AND EXPERIMENTAL RESIDUAL STRESSES IN AN OIL QUENCHED EN30B PLATE

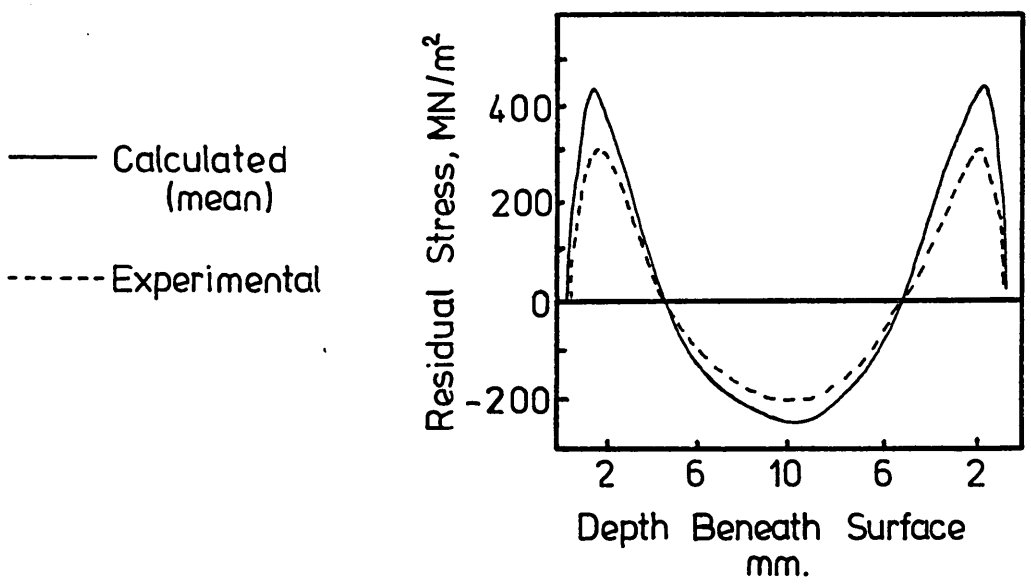
Calculated (mean)
Experimental
Residual Stress, MN/m²
400
200
0
-200
2
6
10
6
2
Depth Beneath Surface mm.

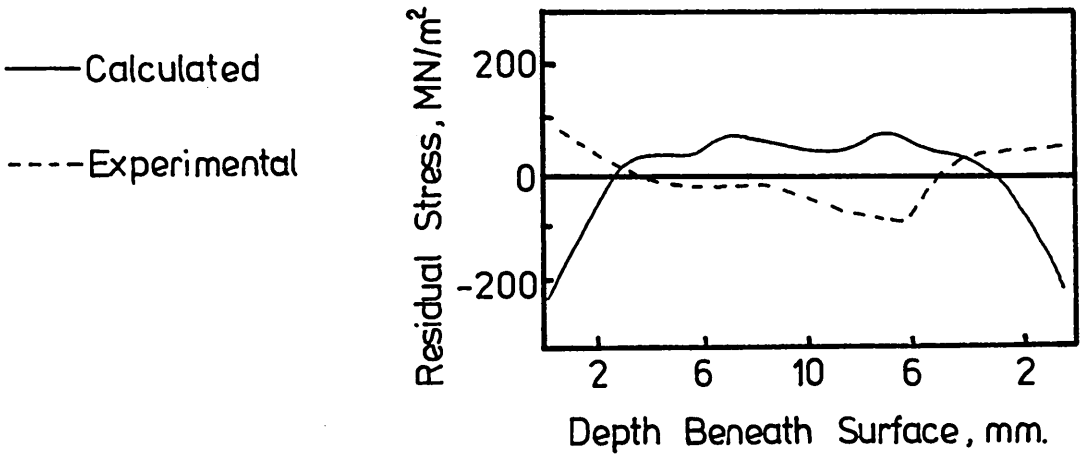
Calculated
Experimental
Residual Stress, MN/m²
200
0
-200
2
6
10
6
2
Depth Beneath Surface, mm.

FIGURE 2.26

THE END EFFECT IN A SEMI-INFINITE RECTANGLE WITH A PARABOLIC LOAD[76]

FIGURE 2.27

DECAY OF FORCE FROM THE END OF A ROD (X = 0) OF DIAMETER 2B

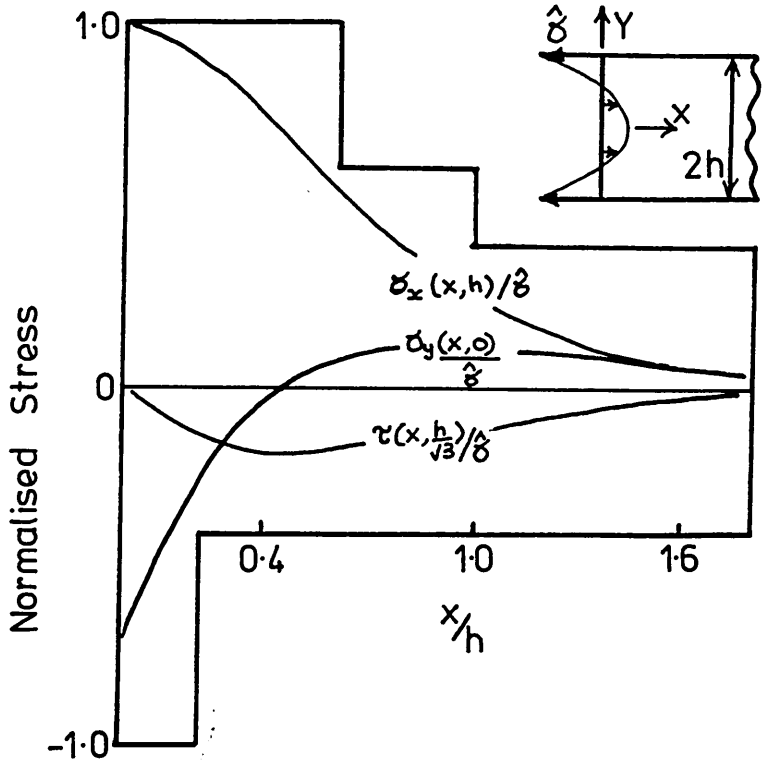

$$\frac{F_s}{F} = \exp -[2{\cdot}15(x/2b)]$$

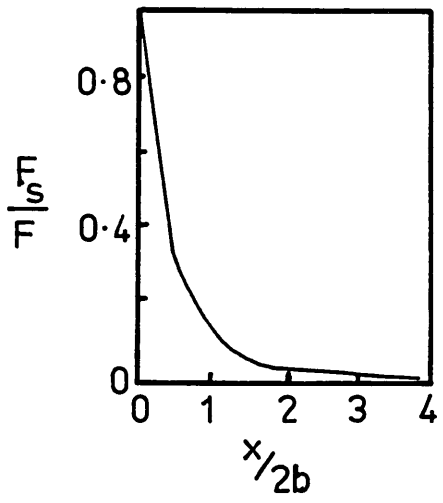

FIGURE 2.28

FINITE ELEMENT THERMAL ANALYSIS
RESULTS FOR THE HEATING OF THE
SURFACE OF A SEMI-INFINITE SOLID[94]

FIGURE 2.29

STABILITY OF TEMPERATURE DISTRIBUTIONS
PREDICTED BY THE FINITE ELEMENT METHOD
WITH RESPECT TO THE TIME STEP USED

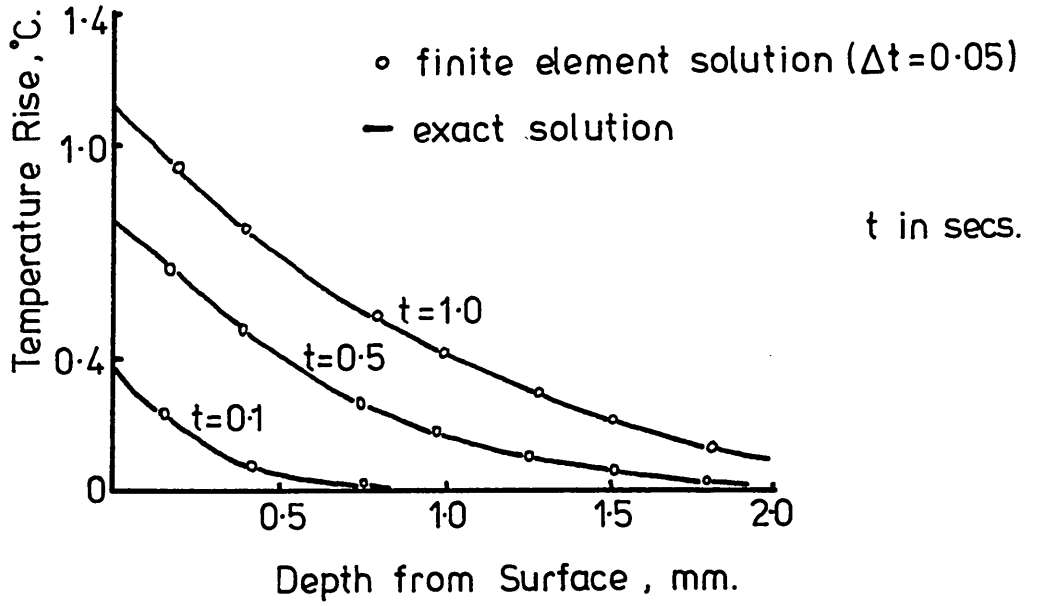
Temperature Rise, °C.
1·4
1·0
0·4
0
o finite element solution (Δt=0·05)
— exact solution
t in secs.
t=1·0
t=0·5
t=0·1
0·5
1·0
1·5
2·0
Depth from Surface, mm.

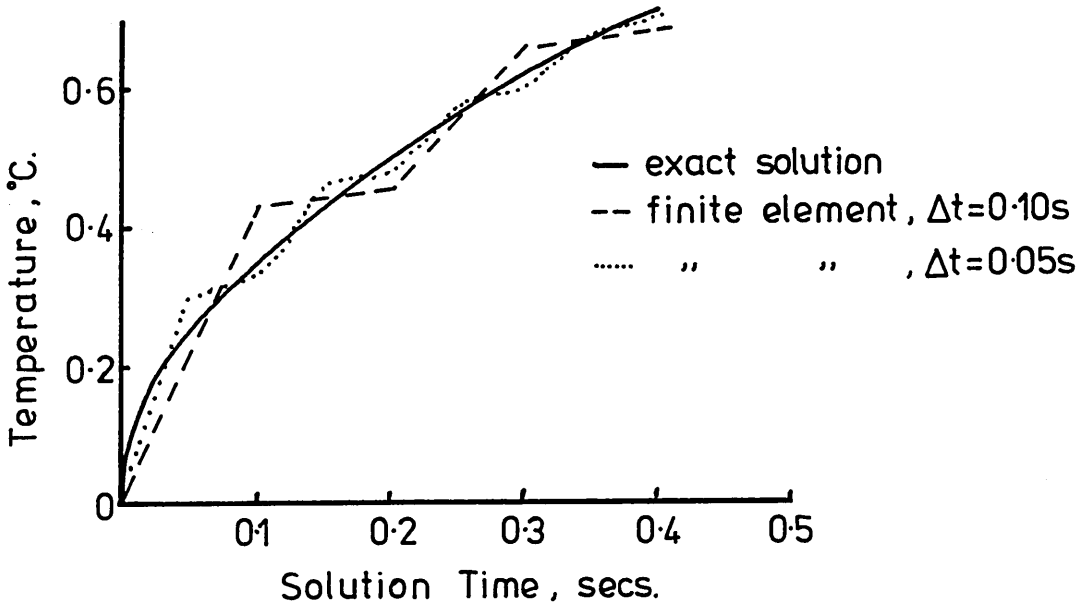
Temperature, °C.
0·6
0·4
0·2
0
— exact solution
-- finite element, Δt=0·10s
..... ,, ,, , Δt=0·05s
0·1
0·2
0·3
0·4
0·5
Solution Time, secs.

FIGURE 2.30

FINITE ELEMENT ANALYSIS OF HEAT REMOVAL AT A CIRCULAR HOLE IN AN INFINITE PLATE[95]

(α = Surface Heat Transfer Coefficient)

a) Mesh Idealisation

b) Variation of Surface Temperature with Time

—— Exact Solution

• • • • • Mesh A & C

▫ ▫ ▫ ▫ Mesh B

× × × × All Meshes

(a.)

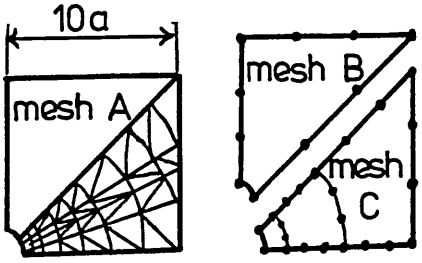

(b.)

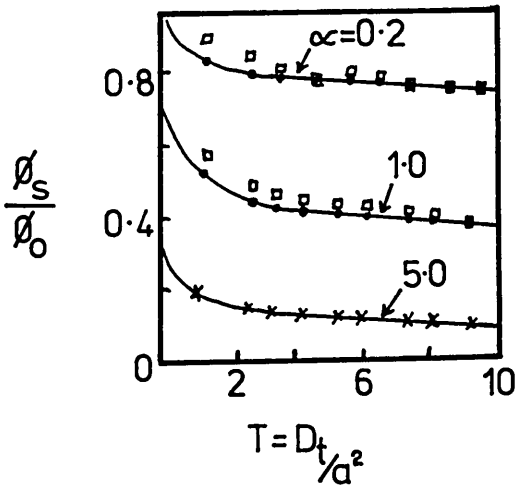

Mesh	Total Degrees of Freedom
A	49
B	12
C	28

FIGURE 2.31

THE EFFECT OF TEMPERATURE VARIATION ON THE END OF A PLATE[102]

FIGURE 2.32

AXISYMMETRIC MESH USED BY TOSHIOKA[103] TO MODEL A ROUND BAR

—— Exact Energy Solution

—×— Finite Element Method,
Constant Temp/Element

• Variable Temp/Element

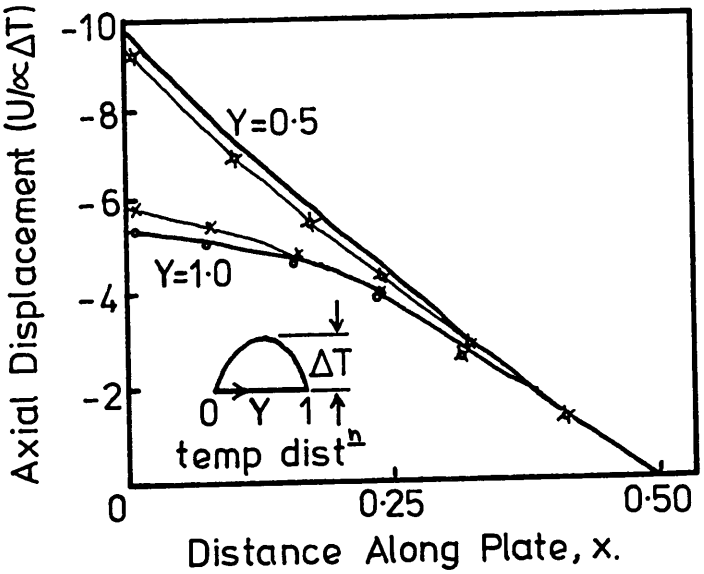

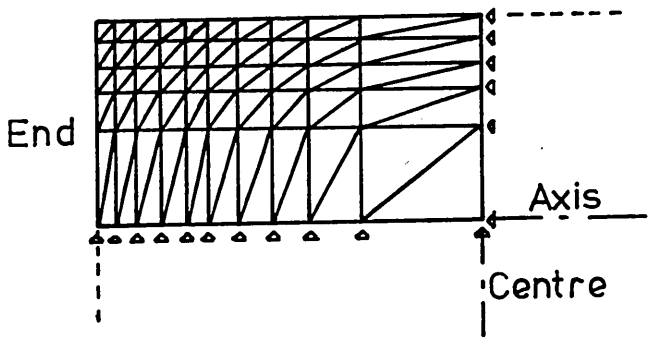

FIGURE 2.33

RADIAL DISTORTION IN VERTICALLY QUENCHED (WATER) STEEL BARS[103]

Steel	C	Si	Mn	P	S	Ni	Cr	Mo
S38C	0.37	0.27	0.76	0.016	0.033	0.053	0.14	0.029
SNCM8	0.39	0.27	0.77	0.015	0.031	1.73	0.80	0.170

FIGURE 2.34

AXISYMMETRIC MESH USED BY TAIRA AND INOUE[105] FOR THE ANALYSIS OF A CYLINDER

--- 850°C water quench, theoretical

—— " " " , experimental

····· 650°C " " , "

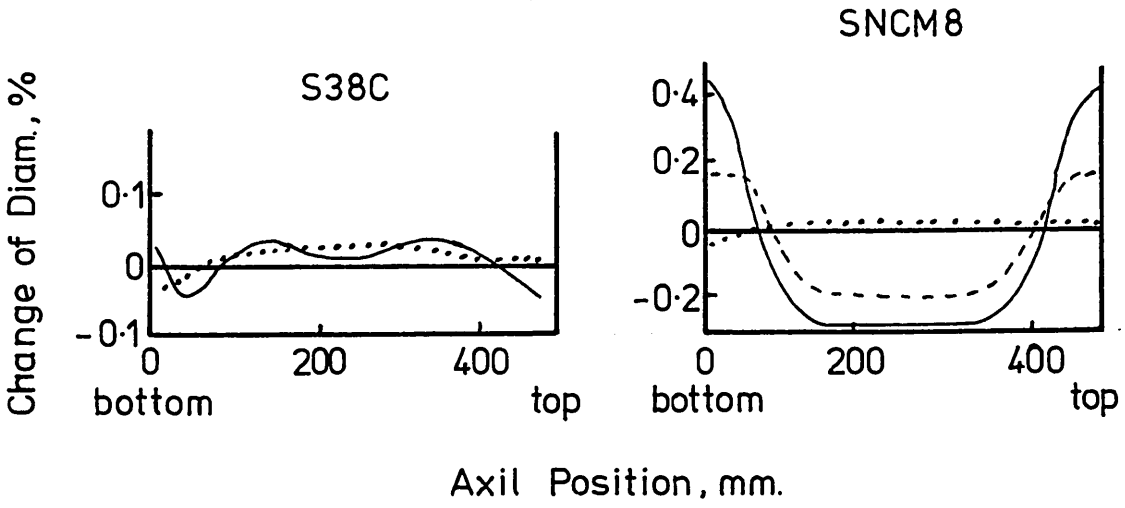

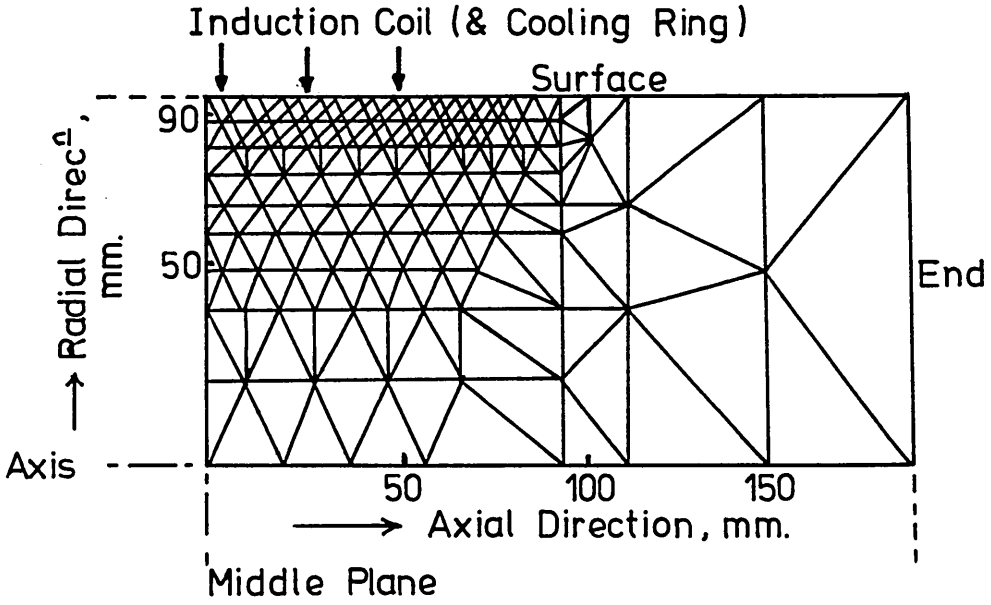

FIGURE 2.35

THEORETICAL AND EXPERIMENTAL RESULTS FOR RESIDUAL STRESSES IN A WATER QUENCHED CYLINDER[7]

FIGURE 2.36

DEFORMATION OF A CYLINDER SPECIMEN[108]
original quarter cylinder = 120 X 62.5 mm

x • o Experimental

—— Theoretical

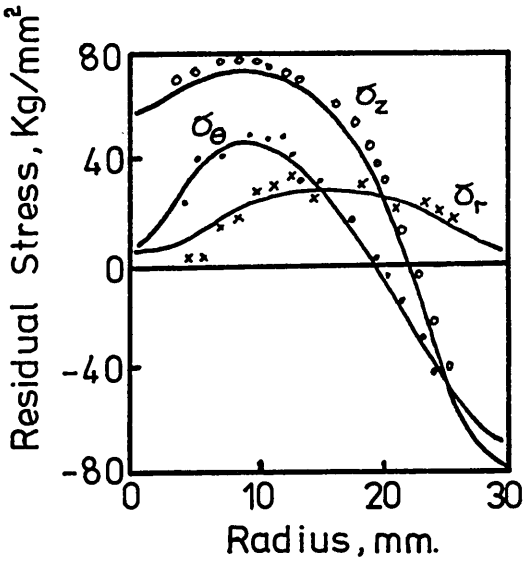

– – – Calculated

• • • • • Measured

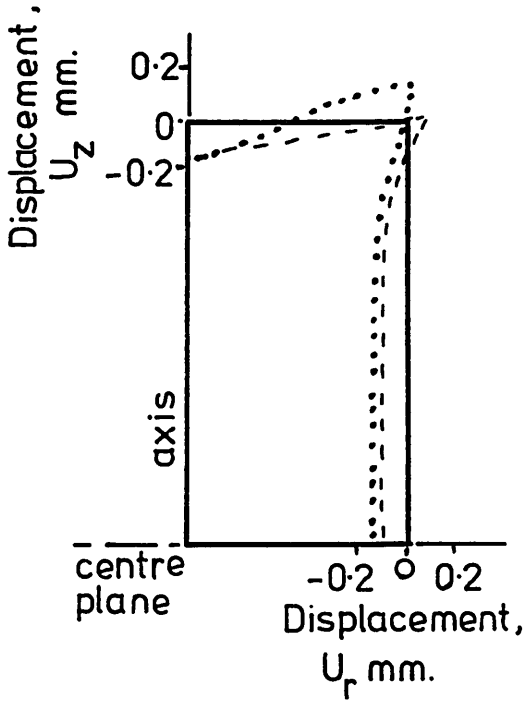

FIGURE 3.1-1

METROLOGY MEASURING POINTS ON
PLATE SAMPLES

FIGURE 3.1-2

CALCULATING THE PLATE THICKNESS
BY DIAL GAUGE READINGS

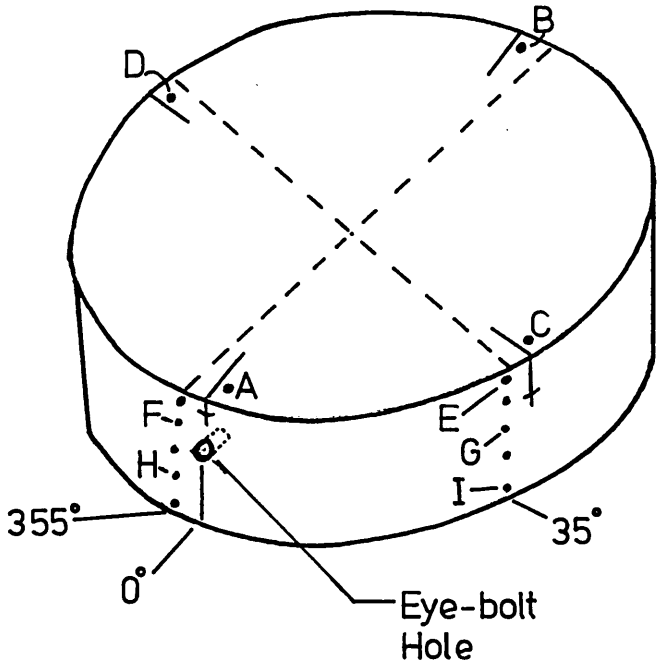
B
D
C
A
F
E
G
H
I
355°
35°
0°
Eye-bolt
Hole

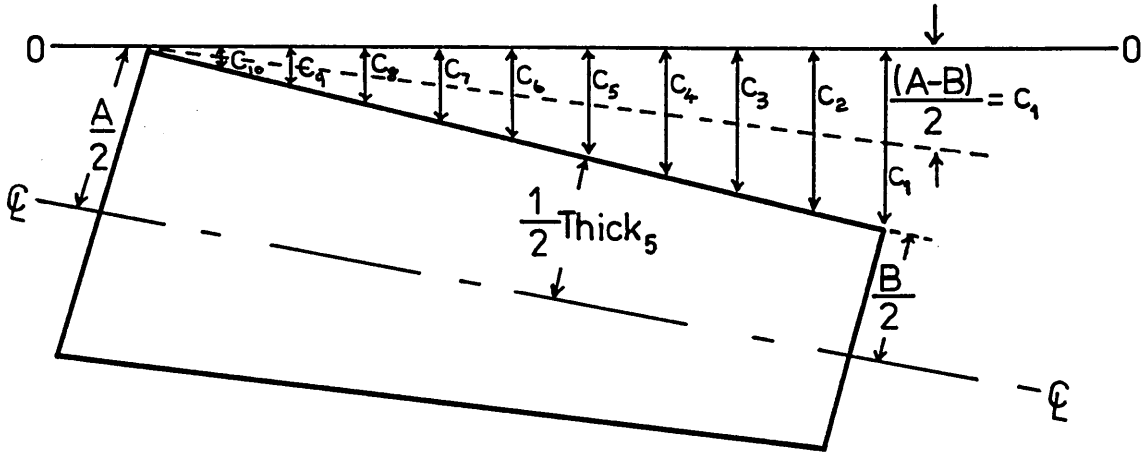
0
0
C_{10}
C_9
C_8
C_7
C_6
C_5
C_4
C_3
C_2
C_1
$\frac{(A-B)}{2} = C_1$
$\frac{A}{2}$
$\frac{1}{2}$ Thick$_5$
$\frac{B}{2}$
℄
℄

FIGURE 3.1-3

EXPERIMENTAL PLATE AND
MOUNTING FRAME

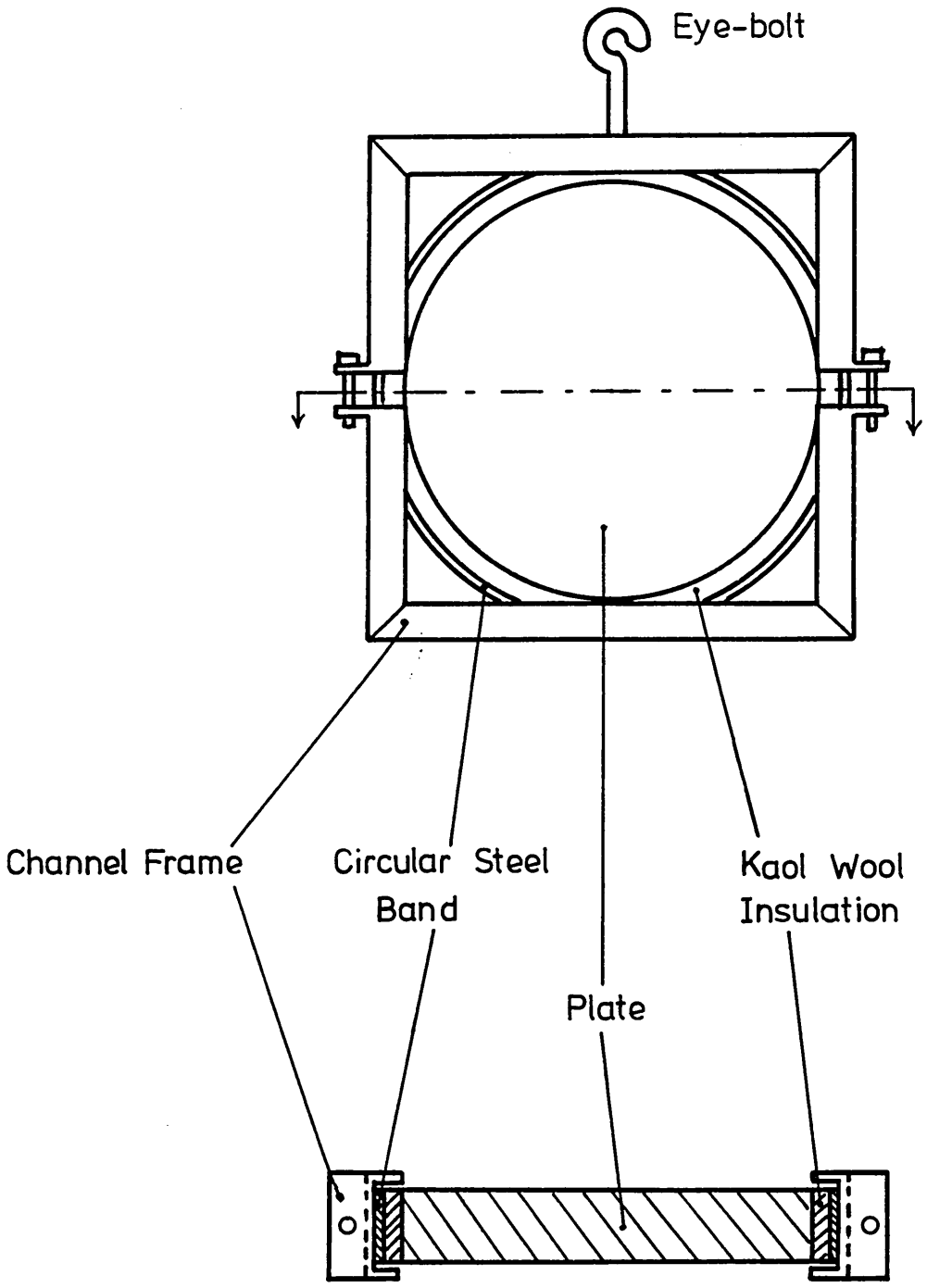
Eye-bolt
Channel Frame
Circular Steel Band
Kaol Wool Insulation
Plate

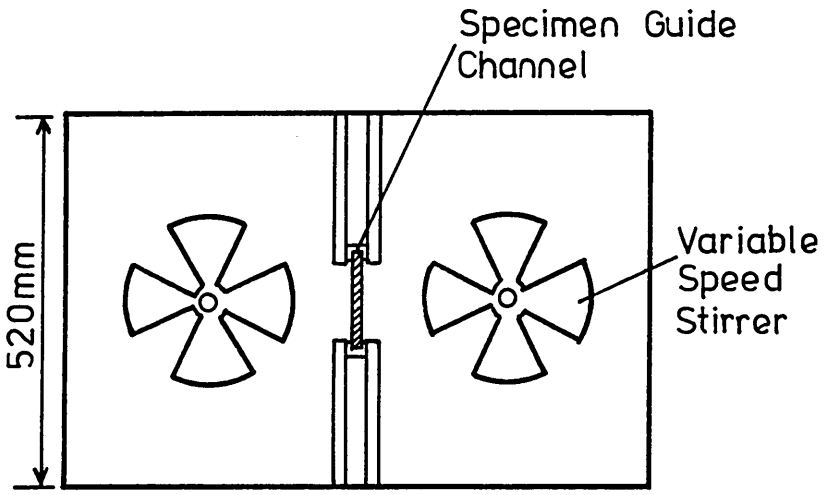
Specimen Guide
Channel
520mm
Variable
Speed
Stirrer

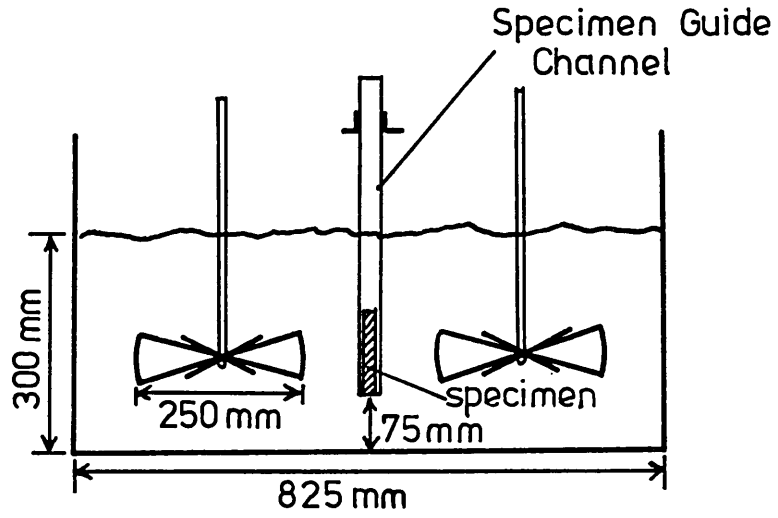
Specimen Guide
Channel
300 mm
250 mm
specimen
75mm
825 mm

FIGURE 3.2-1

MICROSECTIONS TAKEN FROM EN30B STEEL PLATE SAMPLES

FIGURE 3.2-2

READING POSITIONS FOR HARDNESS TRAVERSES ON ANNEALED AND QUENCHED EN30B STEEL PLATE SAMPLES

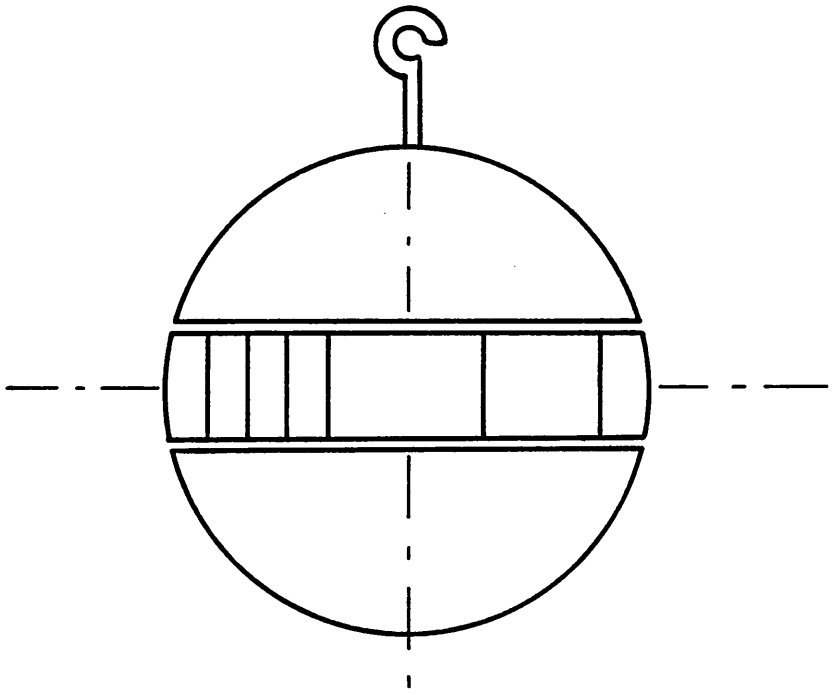

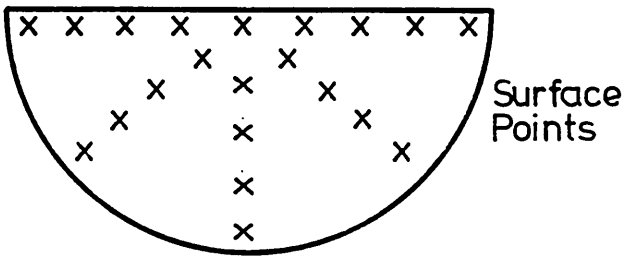
Surface
Points

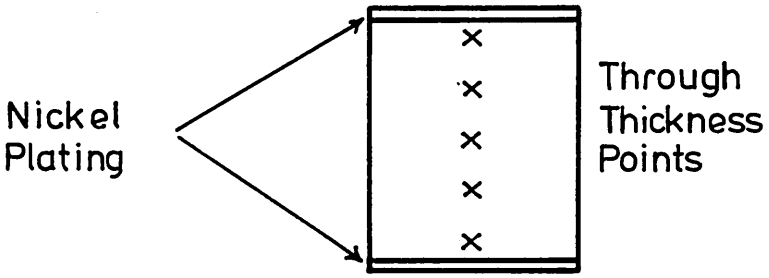
Nickel
Plating
Through
Thickness
Points

FIGURE 3.3-1

STRAIN - GAUGE ROSETTE POSITIONS ON THE EDGE OF THE EXPERIMENTAL PLATE

Rosette CA is below the centre plane
" CB is on " " "
" DB is above " " "
" AD is on " " "

FIGURE 3.3-2

A STRAIN - GAUGE ROSETTE

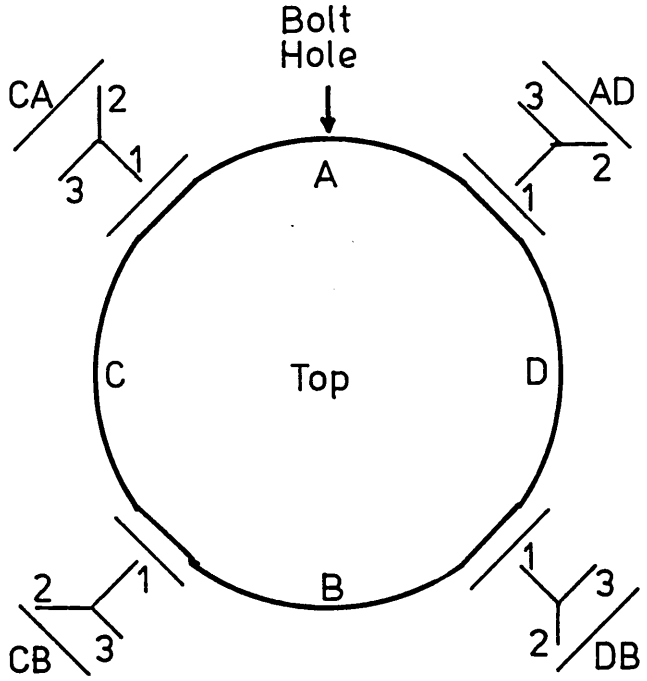

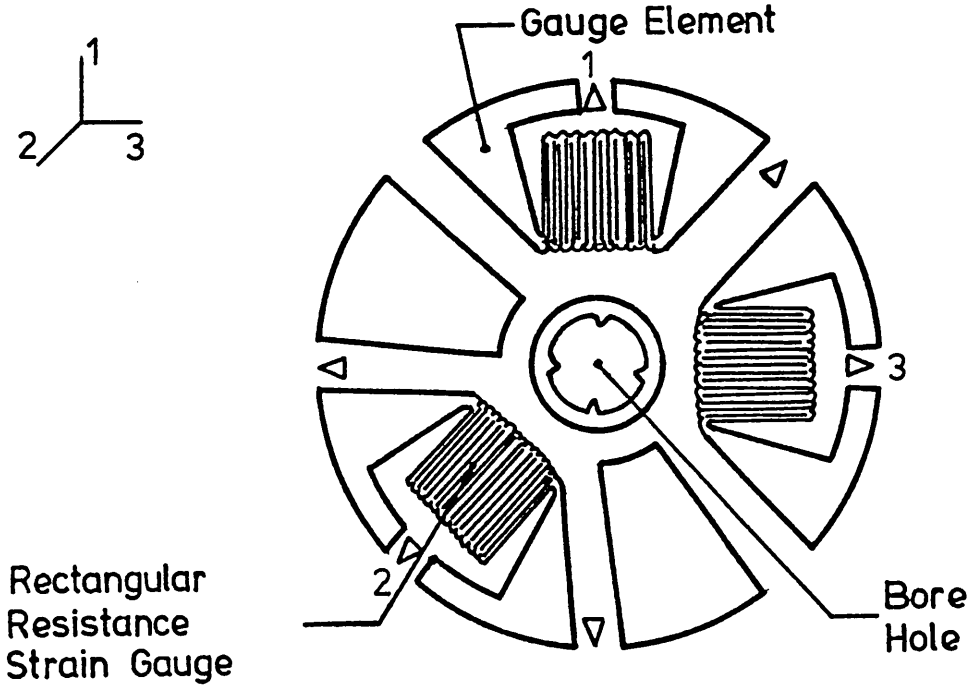

Rectangular
Resistance
Strain Gauge

FIGURE 4.1-1

STRESS FIELD IN POLAR SPACE
where R, Z and H are external forces

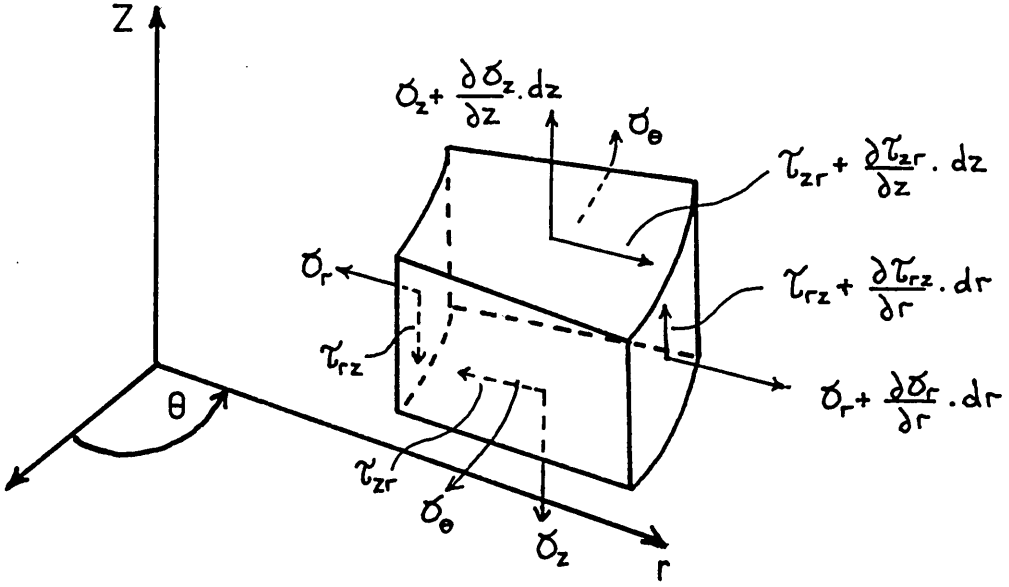

A. Equilibrium Equations

$$\frac{\partial \sigma_r}{\partial r} + \boxed{\frac{1}{r}\frac{\partial \tau_{r\theta}}{\partial \theta}} + \frac{\partial \tau_{rz}}{\partial z} + \frac{\sigma_r - \sigma_\theta}{r} + \boxed{R} = 0 \qquad \text{a.)}$$

$$\frac{\partial \tau_{rz}}{\partial r} + \boxed{\frac{1}{r}\frac{\partial \tau_{\theta z}}{\partial \theta}} + \frac{\partial \sigma_z}{\partial z} + \frac{\tau_{rz}}{r} + \boxed{Z} = 0 \qquad \text{b.)}$$

$$\boxed{\frac{\partial \tau_{r\theta}}{\partial r} + \frac{1}{r}\frac{\partial \sigma_\theta}{\partial \theta} + \frac{\partial \tau_{z\theta}}{\partial z} + \frac{2\tau_{r\theta}}{r} + H = 0}$$

B. Strain-Displacement Relations

$$\varepsilon_{rr} = \frac{\partial u}{\partial r} \quad ; \quad \varepsilon_{zz} = \frac{\partial w}{\partial z} \quad ; \quad \varepsilon_{\theta\theta} = \frac{u}{r} + \boxed{\frac{1}{r}\frac{\partial v}{\partial \theta}}$$

$$\varepsilon_{r\theta} = \frac{1}{2}\left(\boxed{\frac{1}{r}\frac{\partial u}{\partial \theta}} + \frac{\partial v}{\partial r} - \frac{v}{r}\right) = 0 \quad ; \quad \varepsilon_{rz} = \frac{1}{2}\left(\frac{\partial u}{\partial z} + \frac{\partial w}{\partial r}\right)$$

$$\varepsilon_{z\theta} = \frac{1}{2}\left(\frac{\partial v}{\partial z} + \boxed{\frac{1}{r}\frac{\partial w}{\partial \theta}}\right) = 0$$

FIGURE 4.1-1 (CONTINUED)

STRESS FIELD IN POLAR SPACE

C. Compatibility Equations

$$\nabla^2\sigma_r - \frac{2}{r^2}(\sigma_r - \sigma_\theta) + \frac{1}{1+\nu}\frac{\partial^2\Theta}{\partial r^2} = 0 \qquad \text{c.)}$$

$$\nabla^2\sigma_\theta + \frac{2}{r^2}(\sigma_r - \sigma_\theta) + \frac{1}{1+\nu}\frac{1}{r}\frac{\partial\Theta}{\partial r} = 0 \qquad \text{d.)}$$

$$\nabla^2\sigma_z + \frac{1}{1+\nu}\frac{\partial^2\Theta}{\partial z^2} = 0 \qquad \text{e.)}$$

$$\tau_{rz} - \frac{1}{r^2}\tau_{rz} + \frac{1}{1+\nu}\frac{\partial^2\Theta}{\partial r\,\partial z} = 0 \qquad \text{f.)}$$

, where Θ is the sum of the three normal components of stress and ∇^2 is a stress function operator as defined below ;

$$\nabla^2 = \frac{\partial^2}{\partial r^2} + \frac{1}{r}\frac{\partial}{\partial r} + \frac{\partial^2}{\partial z^2}$$

FIGURE 4.2-1

LINEARLY BIASED COLUMN MESH OF EX16 ELEMENTS, USED FOR TEMPERATURE ANALYSIS

(Nodal points only shown for element number 1.)

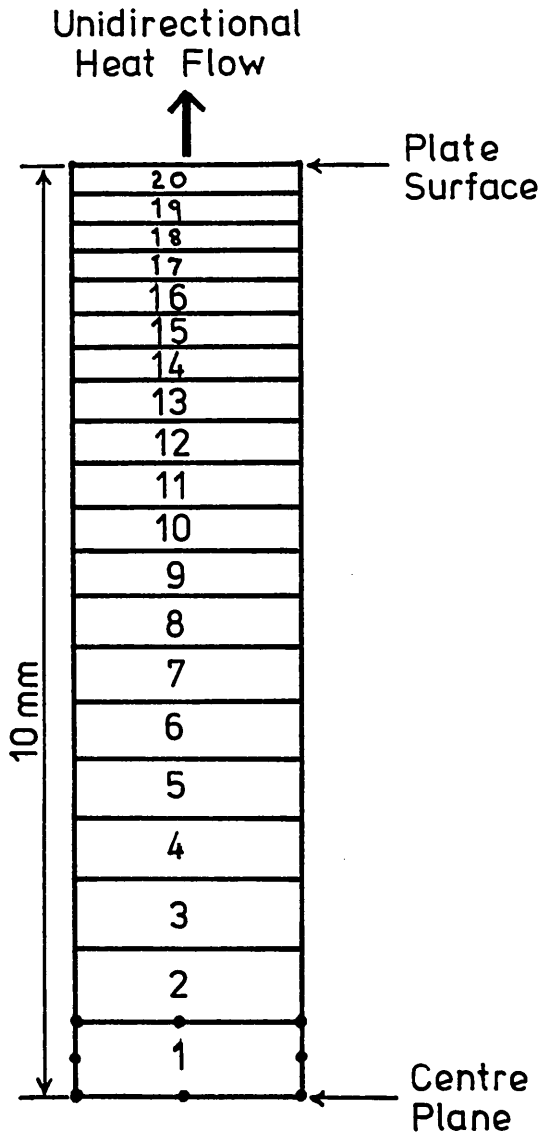

• Nodal Points

FIGURE 4.3-1

ELASTIC PROPERTY DATA OF
EN30B STEEL

TPs are the temperature points for property input data to the finite element model (Linear Interpolation)

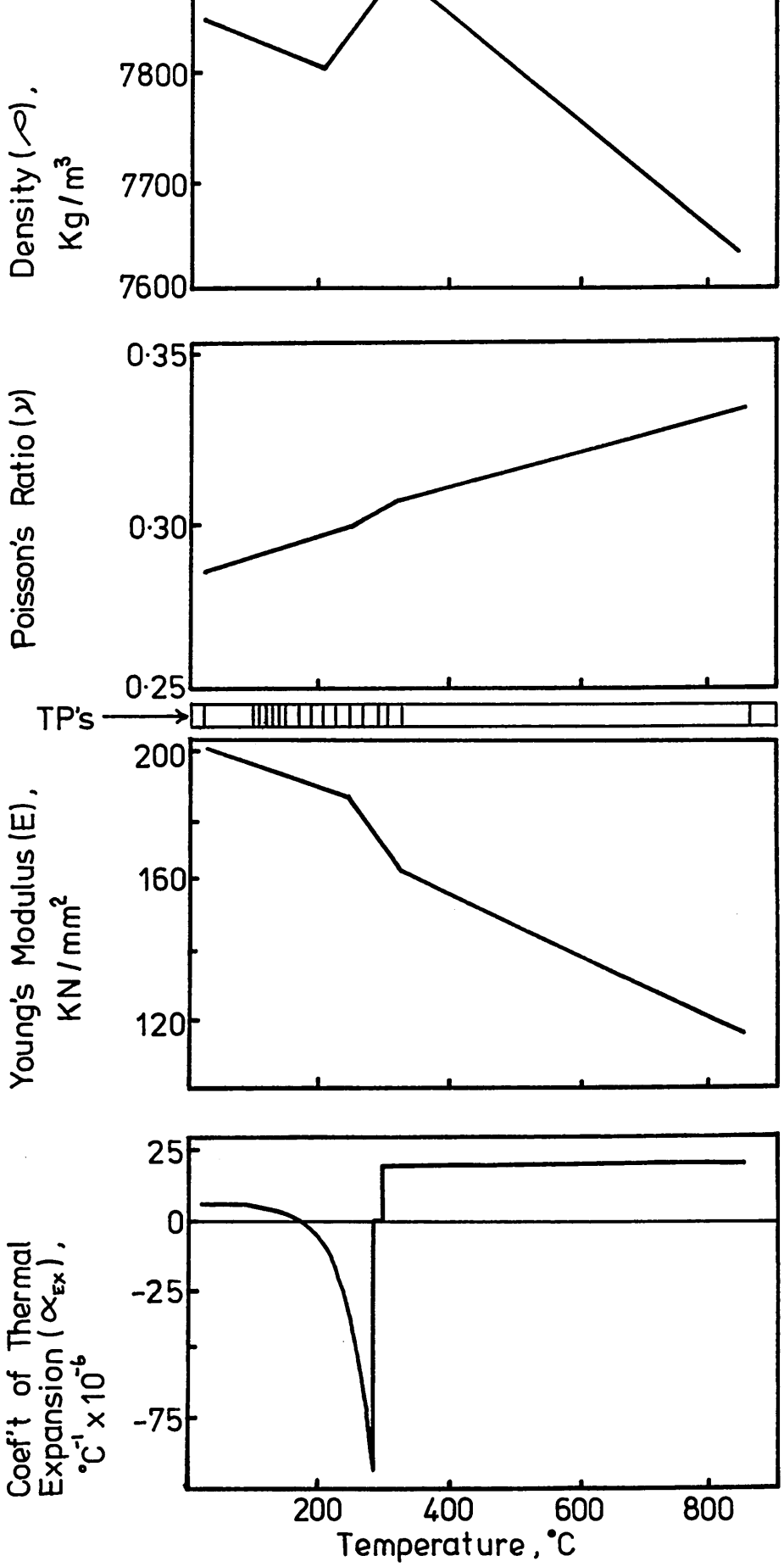
Density (ρ), Kg/m³
7800
7700
7600
Poisson's Ratio (ν)
0·35
0·30
0·25
TP's
Young's Modulus (E), KN/mm²
200
160
120
Coef't of Thermal Expansion (α_ex), °C⁻¹ x 10⁻⁶
25
0
-25
-75
200
400
600
800
Temperature, °C

FIGURE 4.3-2

PLASTIC PROPERTY DATA FOR
EN30B STEEL[1]

a) Work Hardening Coefficients

b) Flow Stress

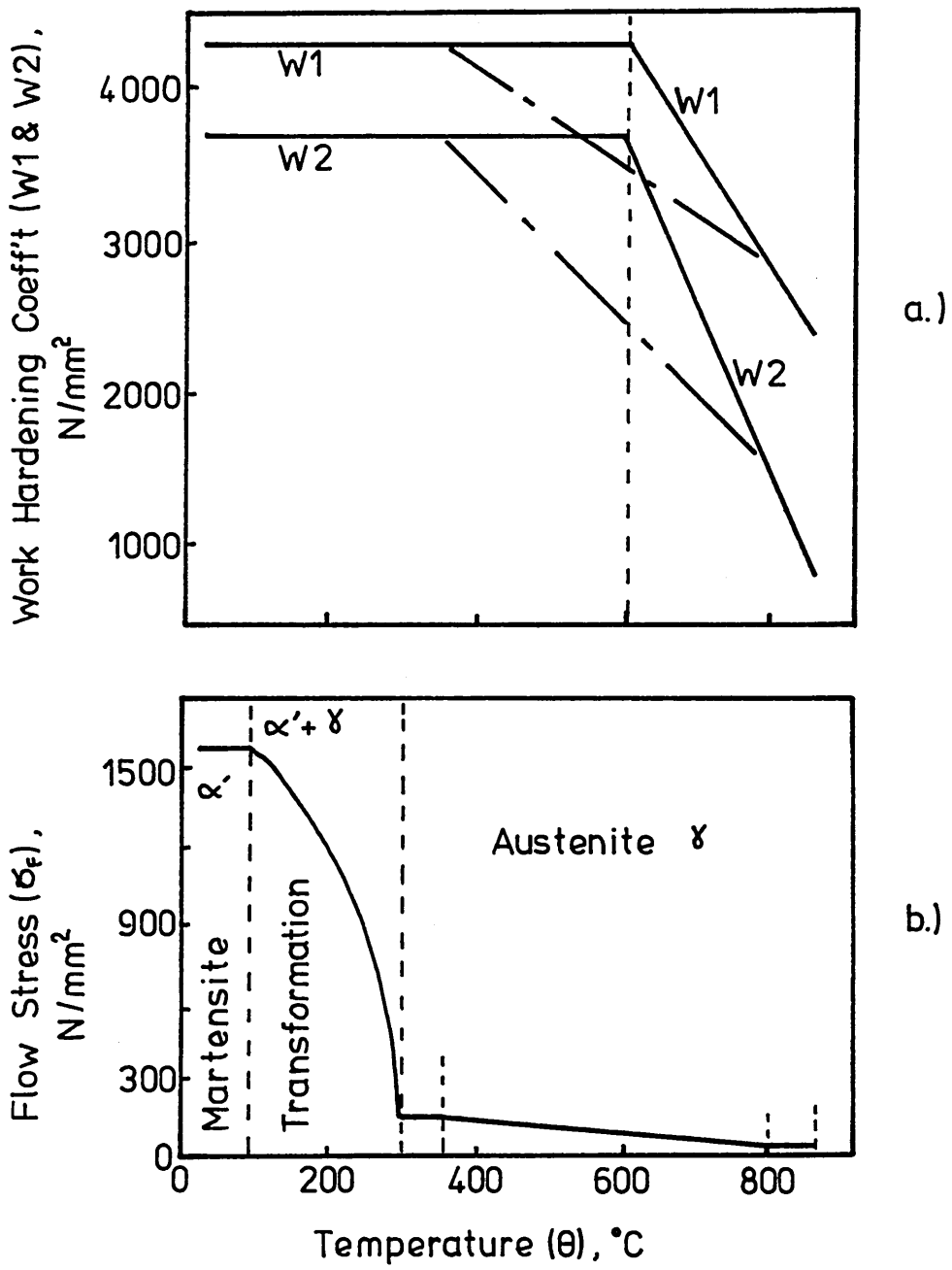
Work Hardening Coeff't (W1 & W2), N/mm²
4000
3000
2000
1000
W1
W2
W1
W2
a.)
Flow Stress (σ_f), N/mm²
1500
900
300
0
α'
α'+ γ
Austenite γ
Martensite
Transformation
0
200
400
600
800
Temperature (θ), °C
b.)

FIGURE 4.3-2 (CONTINUED)

PLASTIC PROPERTY DATA FOR
EN30B STEEL.

c) Work Hardening Curve Data
Employed in the Finite Element
Analysis

c.)

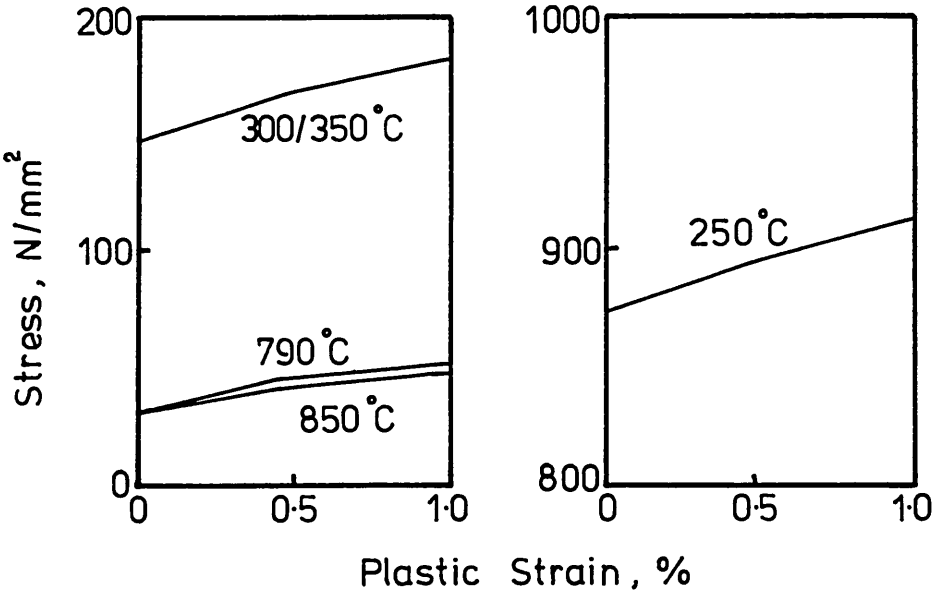
200
100
0
1000
900
800
300/350°C
790°C
850°C
250°C
0
0·5
1·0
Stress, N/mm²
Plastic Strain, %

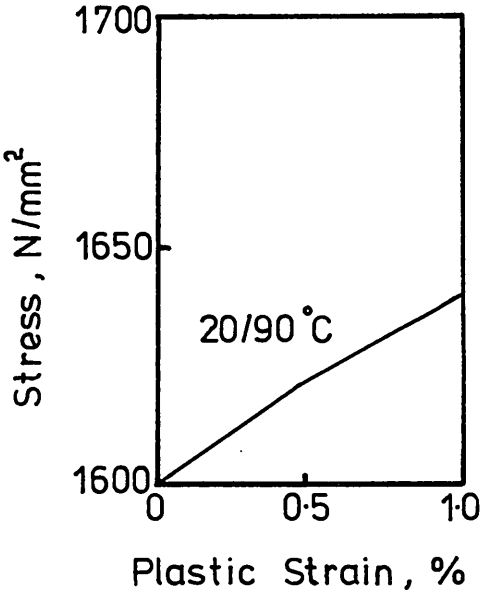
1700
1650
1600
20/90°C
0
0·5
1·0
Stress, N/mm²
Plastic Strain, %

FIGURE 4.3-3

FINITE ELEMENT MESHING OF THE UPPER QUADRANT OF THE PLATE STRUCTURE

The model shown has a mesh of axisymmetric elements with a linear bias towards the surface and edge.

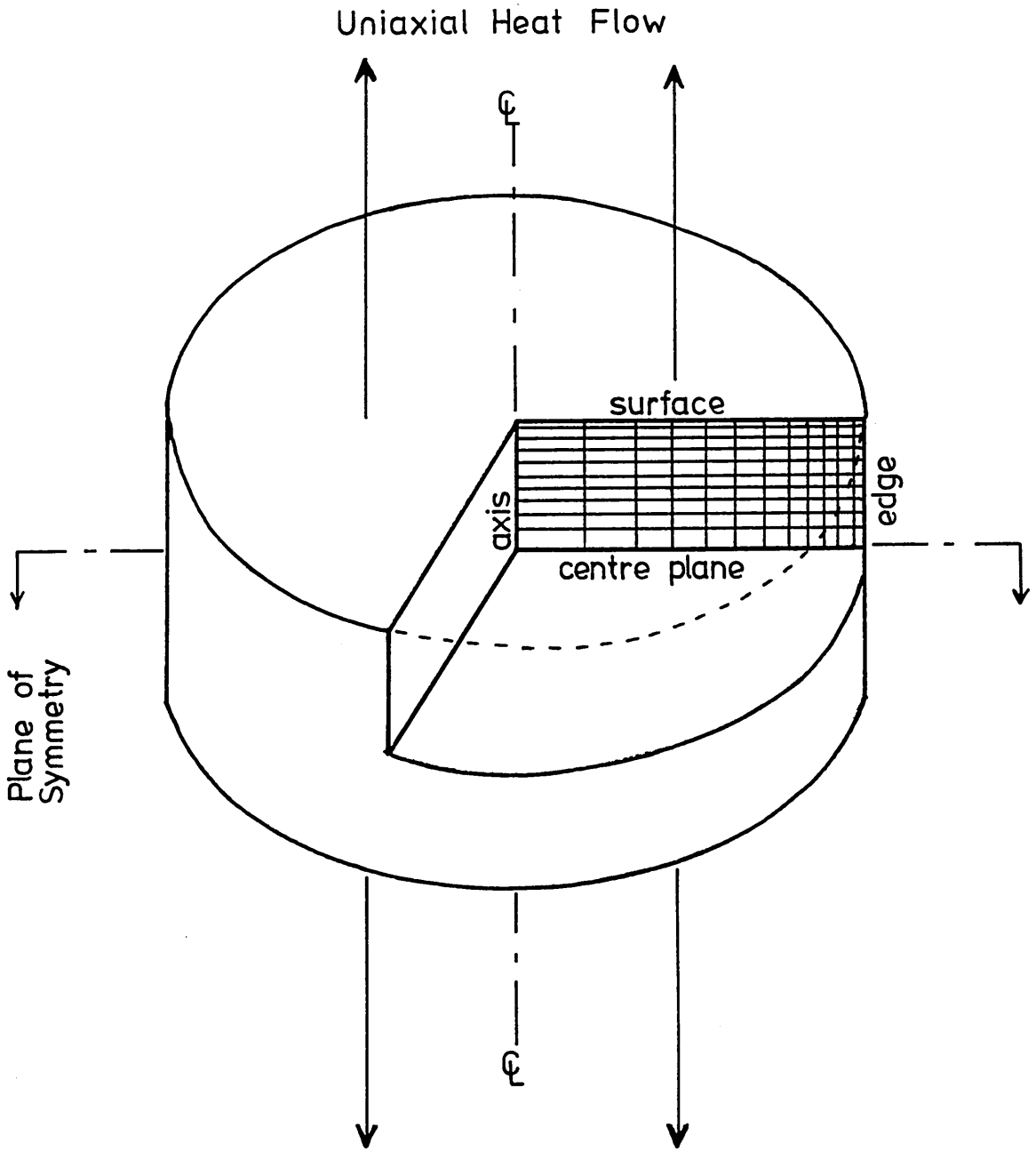
Uniaxial Heat Flow
surface
axis
edge
centre plane
Plane of Symmetry

FIGURE 4.3-4

A COARSE MODEL OF THE UPPER QUADRANT OF A PLATE STRUCTURE USING THREE-DIMENSIONAL FINITE ELEMENTS

Each vertical block is subdivided into 4 solid elements (as shown for one block)

60 elements

FIGURE 4.3-5

A REFINED MODEL OF THE UPPER QUADRANT OF A PLATE STRUCTURE USING THREE-DIMENSIONAL FINITE ELEMENTS

Each vertical block is subdivided into 4 solid elements (as shown for one block)

224 elements

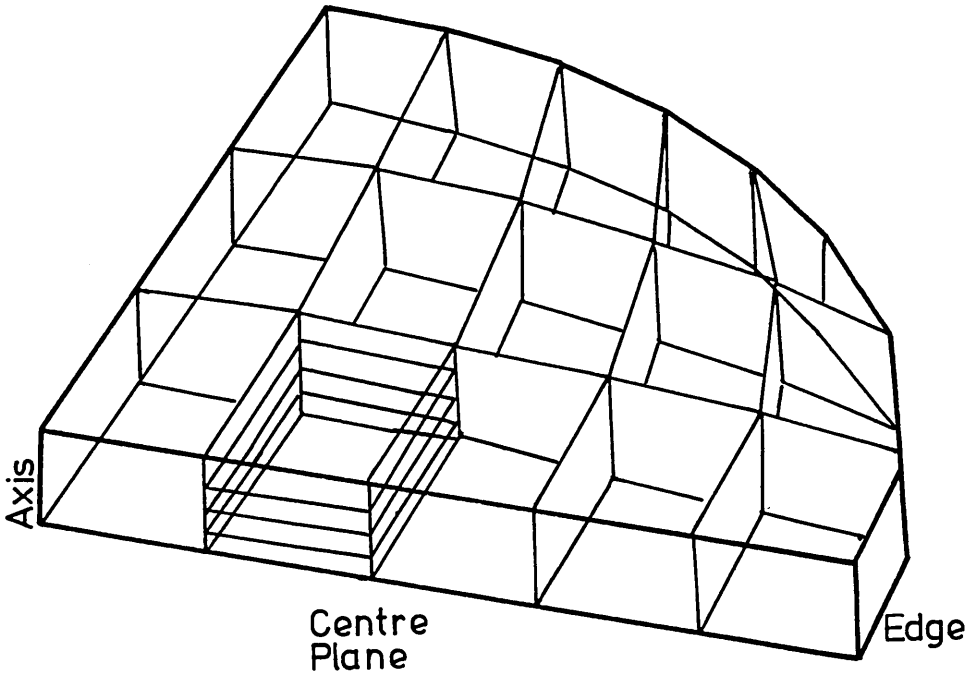
Axis
Centre
Plane
Edge

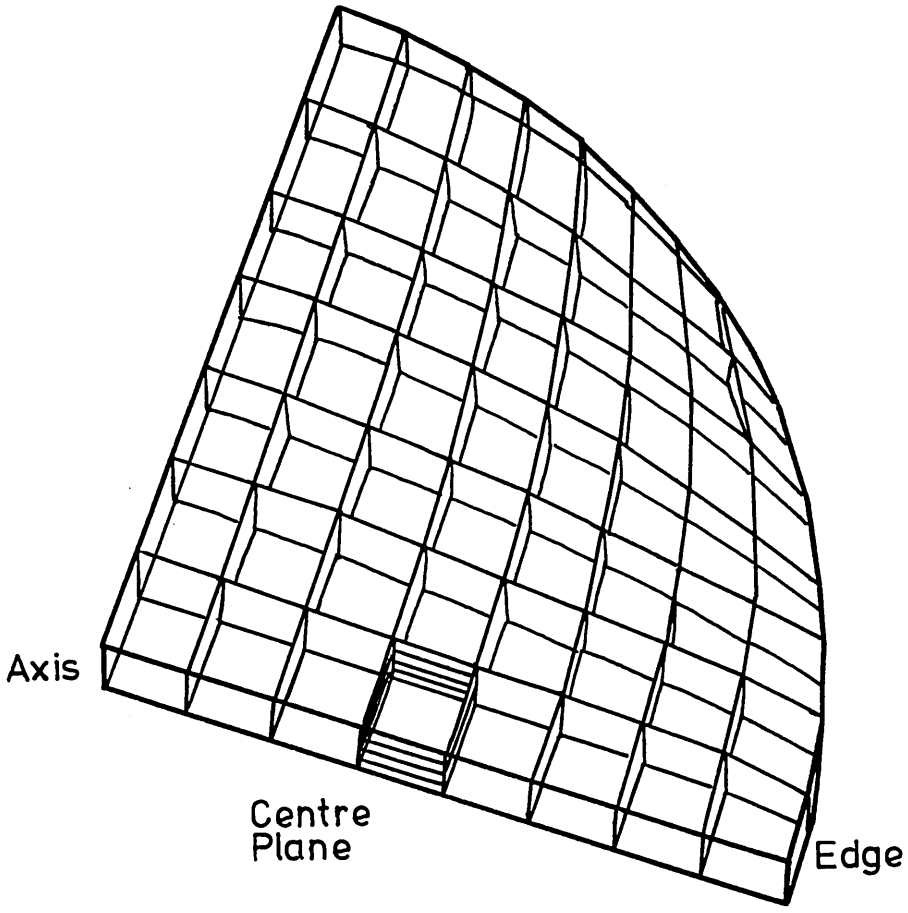
Axis
Centre
Plane
Edge

FIGURE 4.3-6

A 5° WEDGE MESH (B) USED TO MODEL A SEGMENT OF THE PLATE. A 2:1 ELEMENT BIAS AGAINST THE SURFACE AND EDGE IS SHOWN

55 elements

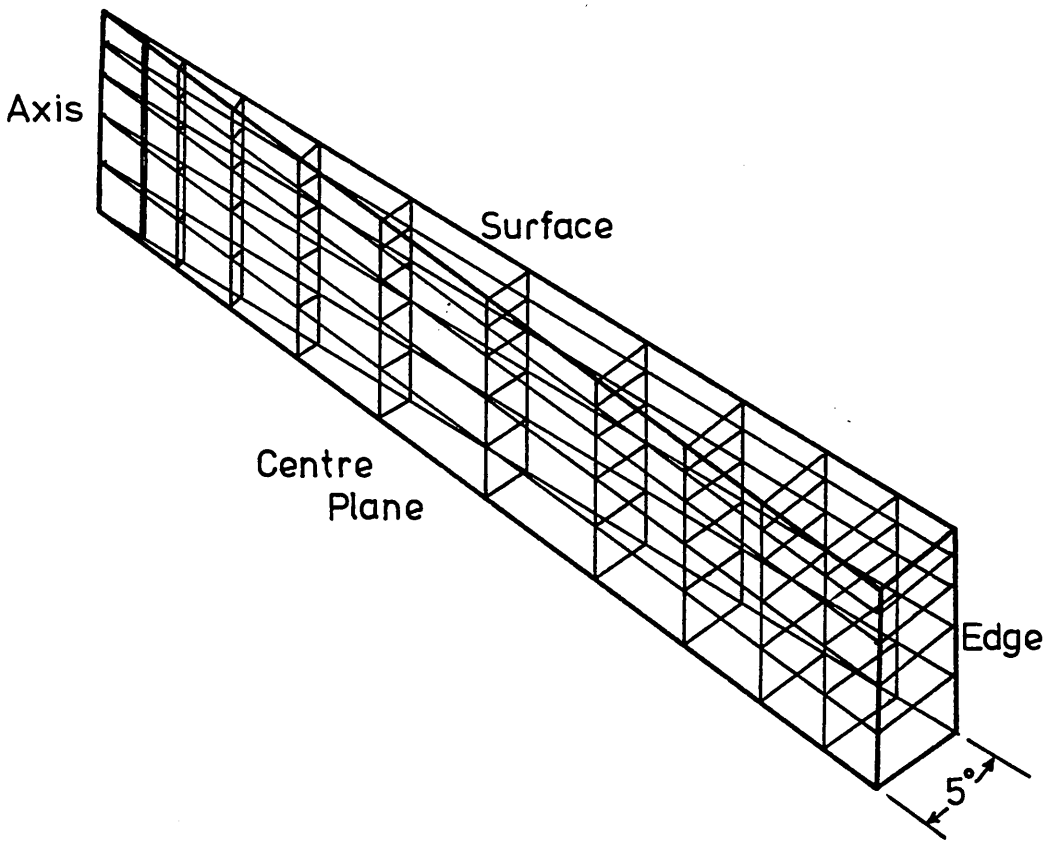
Axis
Surface
Centre
Plane
Edge
5°

FIGURE 4.3-7

AXISYMMETRIC MESH (E) OF EX16 ELEMENTS

Model Size = 3.75 x 10.0 mm
Mesh = 10 x 12 elements
120 elements
405 nodes

FIGURE 4.3-8

AXISYMMETRIC MESH OF TRIANGULAR ELEMENTS

Model Size = 3.75 x 10.0 mm
Mesh = 10 element rows x 10
element columns
200 elements
441 nodes

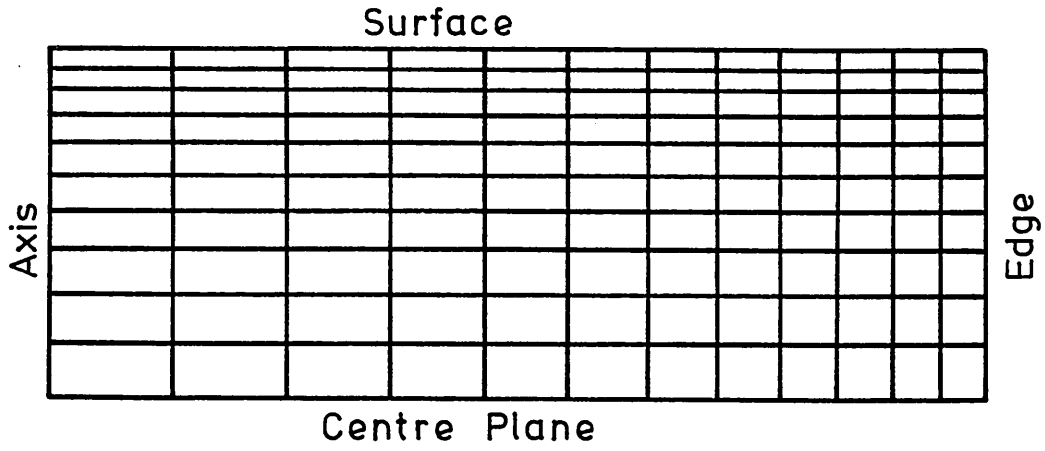
Surface
Axis
Edge
Centre Plane

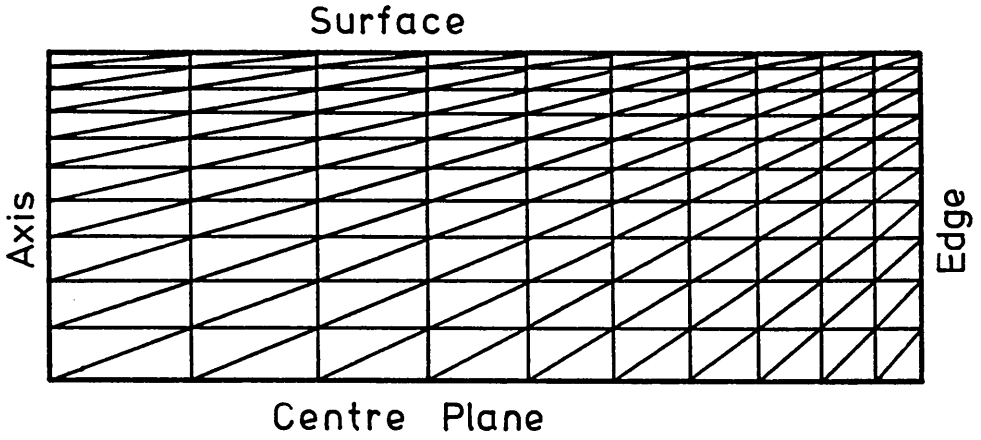
Surface
Axis
Edge
Centre Plane

FIGURE 4.3-9

AXISYMMETRIC MESH(F) OF EX16 ELEMENTS, CHOSEN AS THE OPTIMUM MODEL FOR THE UNIDIRECTIONAL HEAT FLOW - RESIDUAL STRESS ANALYSIS

Model Size = 10 x 30 mm radius
Mesh = 10 x 15 (6:1 bias)
Elements = 150
Nodes = 501

A - Node number 1 in element 1 (centre of plate)
B - " " 31 " " 15
C - " " 471 " " 136
D - " " 501 " " 150 (corner of plate)

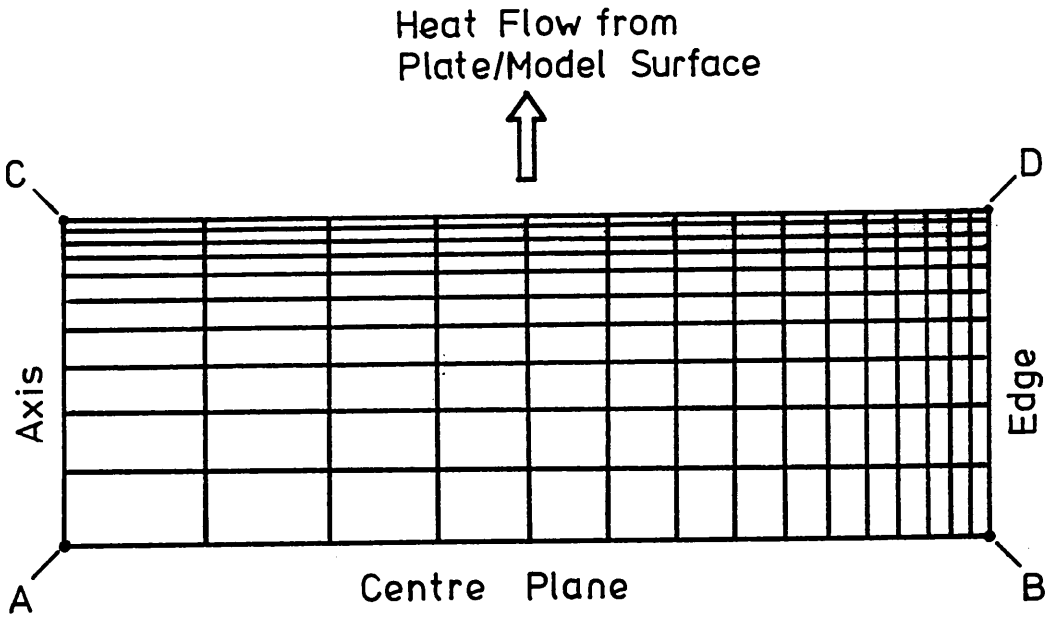
Heat Flow from
Plate/Model Surface
C
D
Axis
Edge
A
Centre Plane
B

FIGURE 5.1-1

EXPERIMENTALLY DETERMINED THROUGH-THICKNESS DISTORTIONS IN A WATER QUENCHED EN30B STEEL

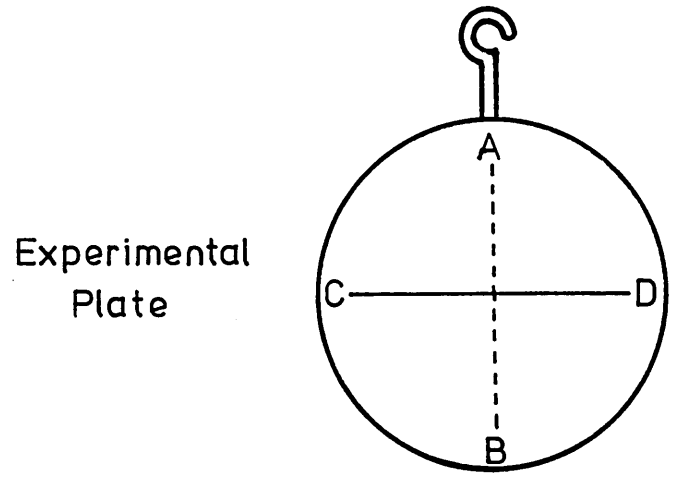
Experimental
Plate
A
B
C
D

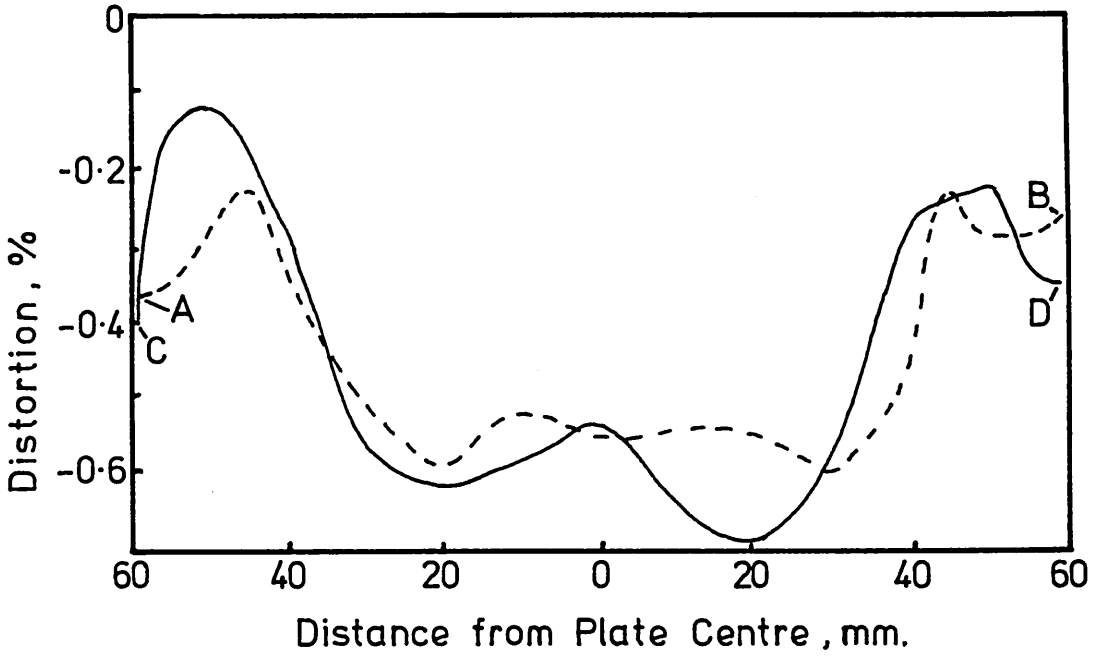
0
-0·2
-0·4
-0·6
Distortion, %
A
B
C
D
60
40
20
0
20
40
60
Distance from Plate Centre, mm.

FIGURE 6.1-1

PREDICTED TEMPERATURE PROFILES FOR THE UNIDIRECTIONAL HEAT FLOW CASE OF A WATER QUENCHED EN30B STEEL PLATE (20 mm THICK)

a) COOLING CURVES FOR POINTS ON THE PLATE AXIS

Node 1 : centre
Node 95 : 7 mm from the surface
Node 283 : 3 mm from the surface
Node 471 : surface

b) TEMPERATURE GRADIENTS ALONG THE PLATE AXIS AT VARIOUS TIMES, EARLY IN THE QUENCH

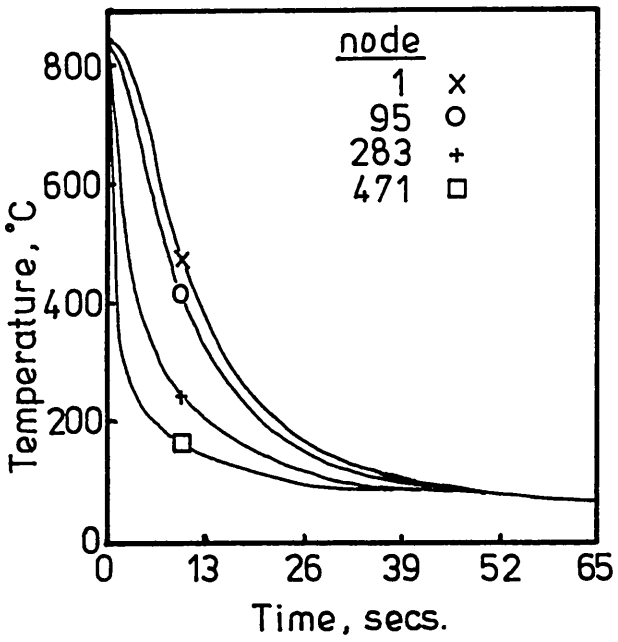
node
1 x
95 o
283 +
471 □
800
600
400
200
0
Temperature, °C
0
13
26
39
52
65
Time, secs.

a.)

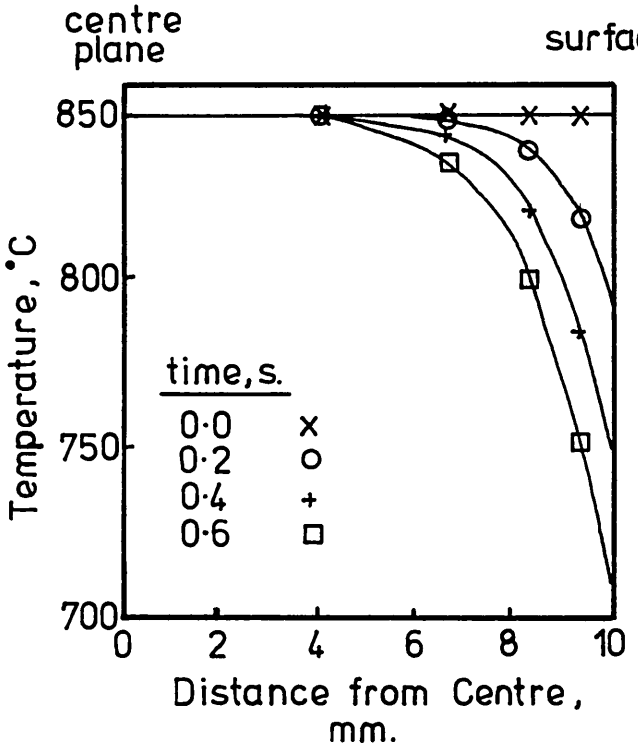
centre plane
surface
850
800
750
700
Temperature, °C
time, s.
0·0 x
0·2 o
0·4 +
0·6 □
0
2
4
6
8
10
Distance from Centre, mm.

b.)

FIGURE 6.1-2a

PREDICTED THERMAL CHARACTERISTICS FOR A WATER QUENCHED, 20 mm THICK PLATE OF EN30B STEEL

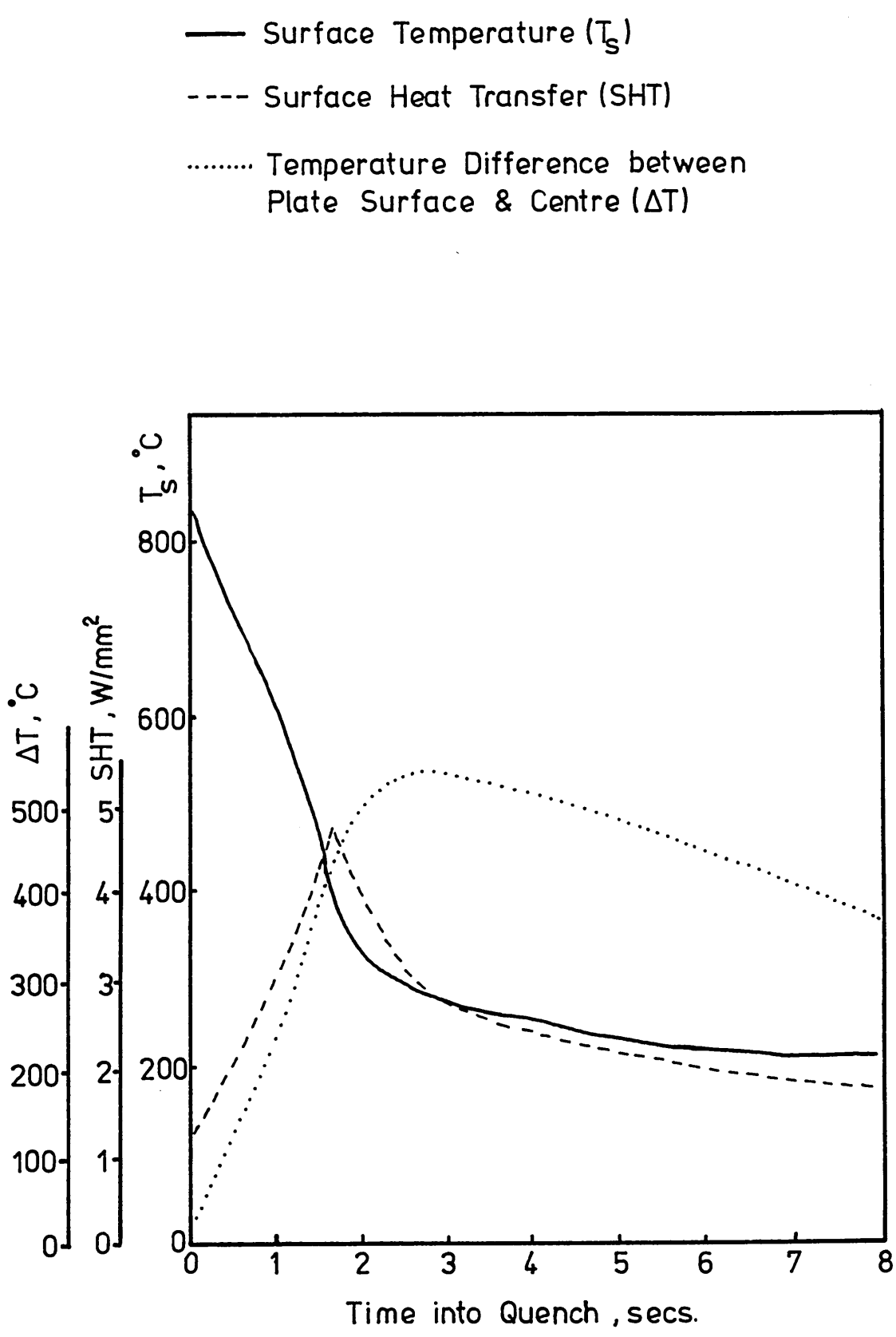
Surface Temperature (T_s)
Surface Heat Transfer (SHT)
Temperature Difference between Plate Surface & Centre (ΔT)
T_s, °C
800
600
400
200
0
ΔT, °C
500
400
300
200
100
0
SHT, W/mm²
5
4
3
2
1
0
0
1
2
3
4
5
6
7
8
Time into Quench, secs.

FIGURE 6.1-2b

TRANSIENT TEMPERATURE PROFILES ALONG THE AXIS OF A WATER QUENCHED, 20 mm THICK EN30B STEEL PLATE, AS PREDICTED BY THE FINITE ELEMENT PROGRAMME

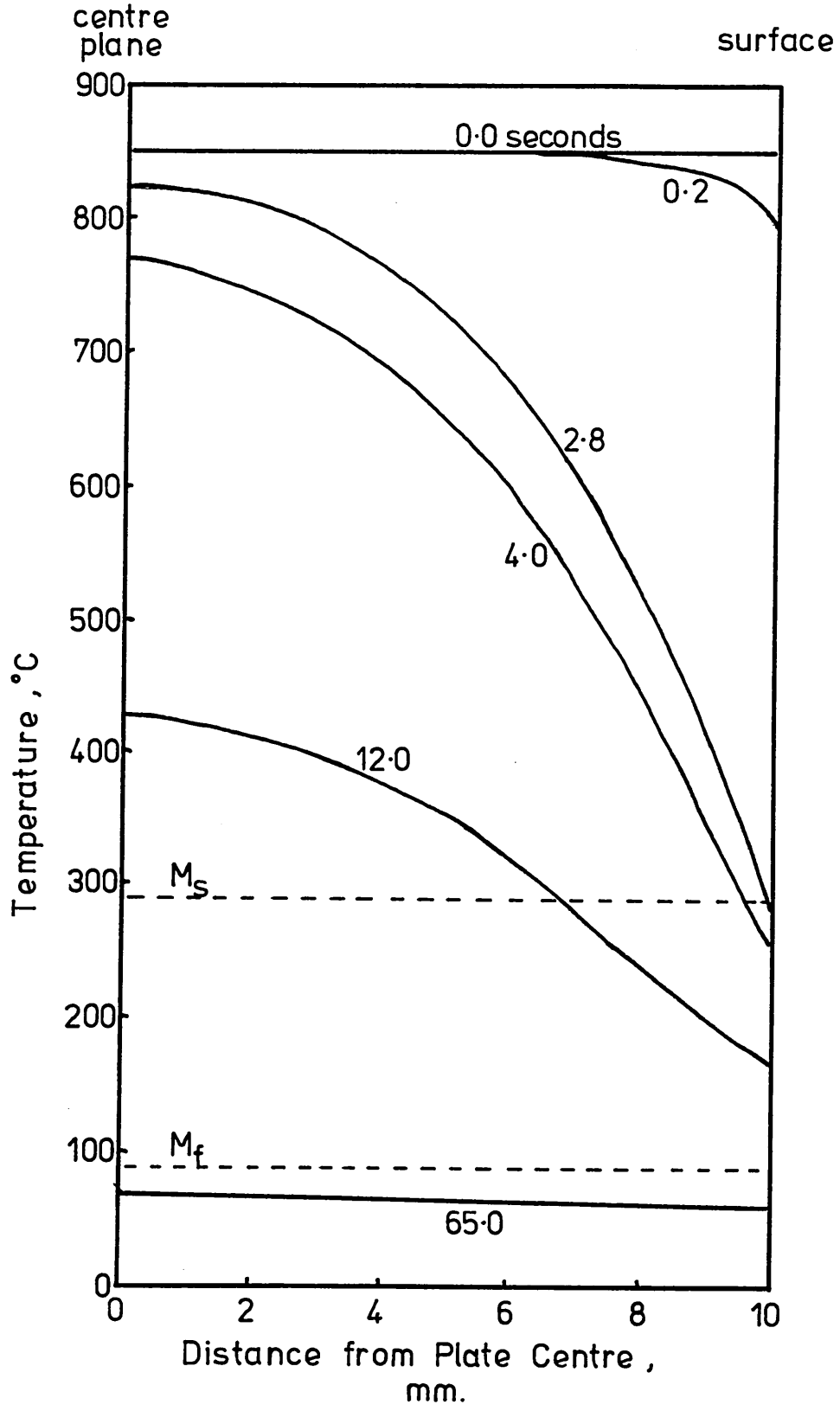
centre plane
surface
900
800
700
600
500
400
300
200
100
0
0·0 seconds
0·2
2·8
4·0
12·0
M_s
M_f
65·0
Temperature, °C
0
2
4
6
8
10
Distance from Plate Centre, mm.

FIGURE 6.2-1

DISTRIBUTION OF STRESS ALONG THE AXIS OF THE PLATE (NODE 1 TO 471) AT 0.02 SECONDS INTO THE UNIDIRECTIONAL WATER QUENCH ANALYSIS

FIGURE 6.2-2

DISTRIBUTION OF RADIAL STRESS (N/mm^2) AT 0.02 SECONDS INTO THE UNIDIRECTIONAL WATER QUENCH ANALYSIS

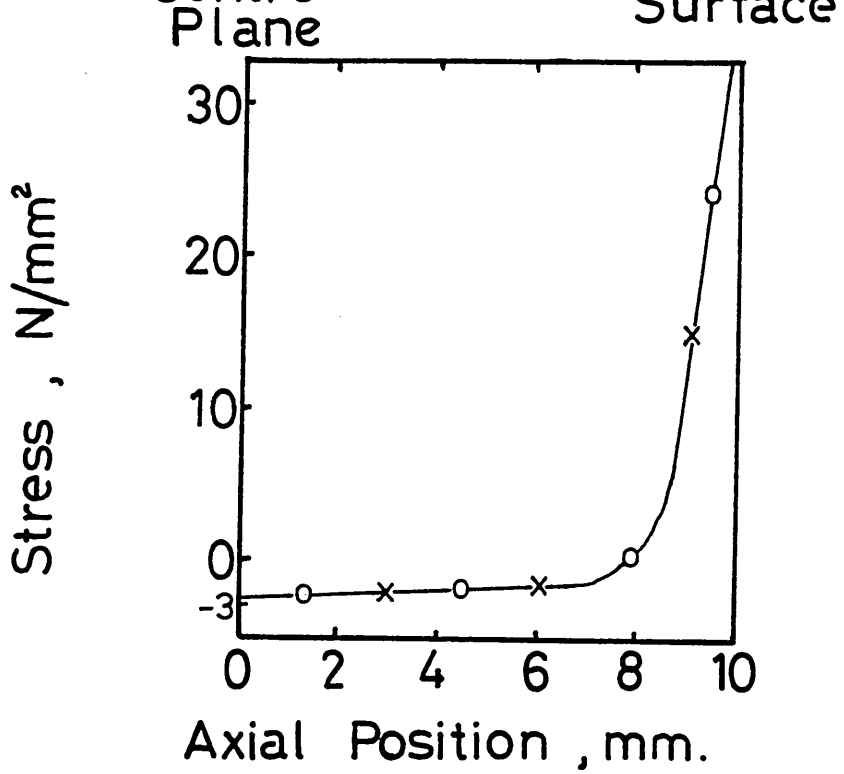

× Radial

o Hoop

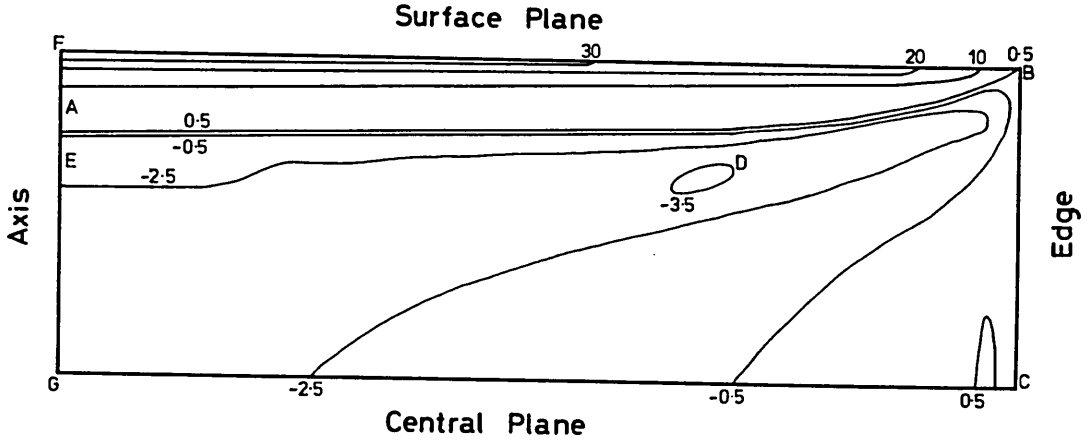

FIGURE 6.2-3

DISTRIBUTION OF STRESS ALONG THE
SURFACE OF THE PLATE (NODE 471 TO 501)
AT 0.02 SECONDS INTO THE UNIDIRECTIONAL
WATER QUENCH ANALYSIS

FIGURE 6.2-4

DISTRIBUTION OF STRESS ALONG THE
CENTRAL PLANE OF THE PLATE (NODE 1 TO 31)
AT 0.02 SECONDS INTO THE UNIDIRECTIONAL
WATER QUENCH ANALYSIS

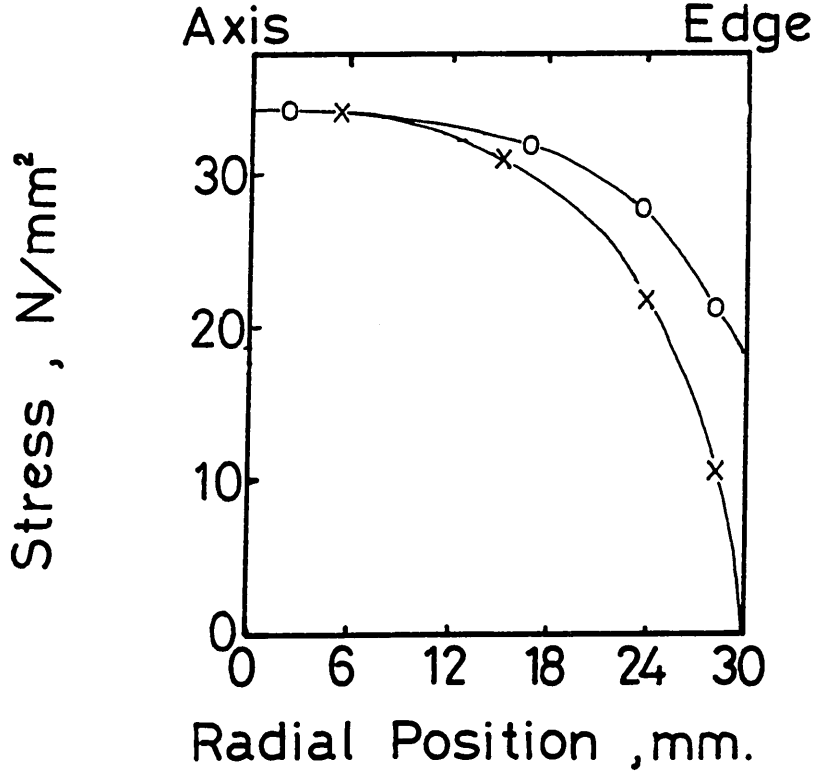

× Radial
o Hoop
+ Axial

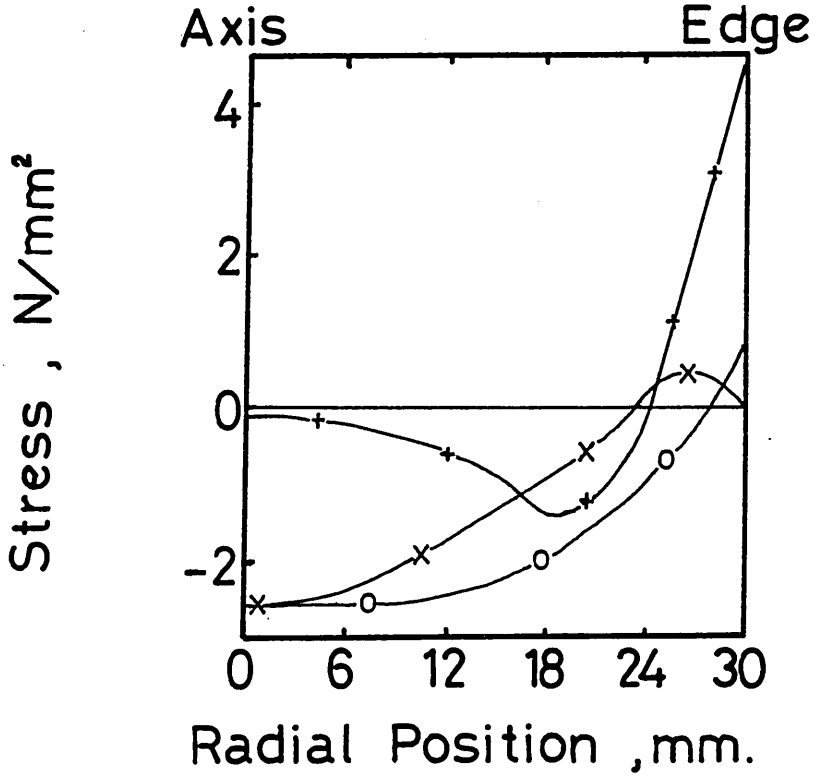

FIGURE 6.2-5

DISTRIBUTION OF HOOP STRESS (N/mm^2) AT 0.02 SECONDS INTO THE UNIDIRECTIONAL WATER QUENCH ANALYSIS

FIGURE 6.2-6

DISTRIBUTION OF AXIAL STRESS (N/mm^2) AT 0.02 SECONDS INTO THE UNIDIRECTIONAL WATER QUENCH ANALYSIS

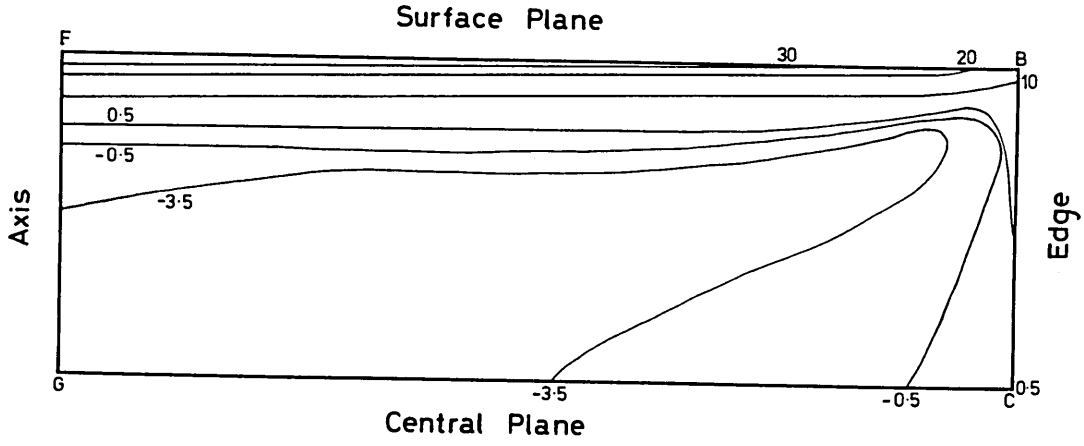
Surface Plane
F
30
20
B
10
0·5
-0·5
-3·5
Axis
Edge
G
-3·5
-0·5
C
0·5
Central Plane

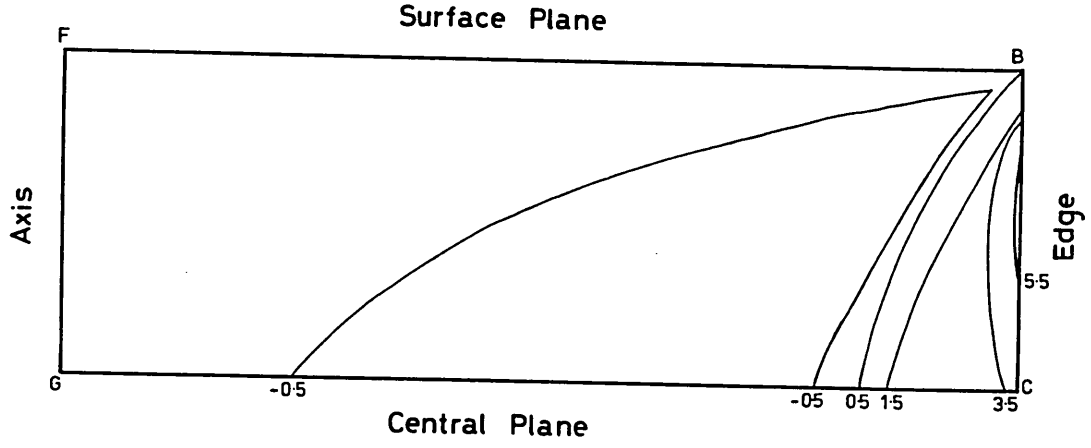
Surface Plane
F
B
Axis
Edge
5·5
G
-0·5
-0·5
0·5
1·5
3·5
C
Central Plane

FIGURE 6.2-7

DISTRIBUTION OF SHEAR STRESS (N/mm^2)
AT 0.02 SECONDS INTO THE UNIDIRECTIONAL
WATER QUENCH ANALYSIS

FIGURE 6.2-8

DISTRIBUTION OF EQUIVALENT STRESS
(N/mm^2) at 0.02 SECONDS INTO THE
UNIDIRECTIONAL WATER QUENCH ANALYSIS

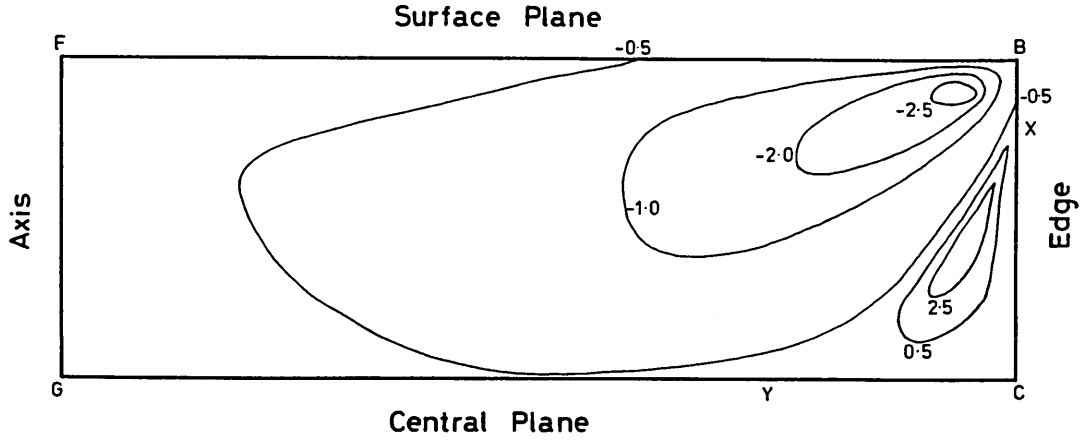
Surface Plane
F
-0·5
B
-0·5
-2·5
X
-2·0
-1·0
Axis
Edge
2·5
0·5
G
Y
C
Central Plane

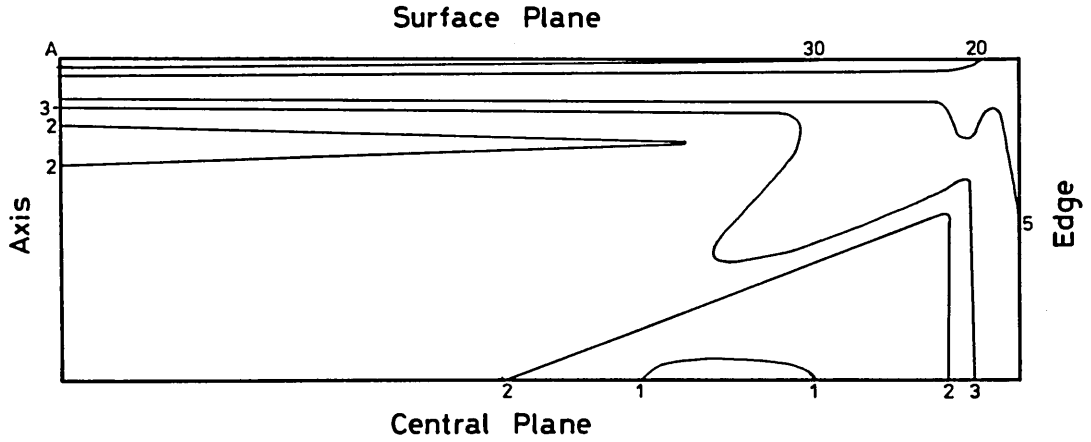
Surface Plane
A
30
20
3
2
2
Axis
5
Edge
2
1
1
2
3
Central Plane

FIGURE 6.2-9

DISTRIBUTION OF STRESS ALONG THE PLATE SURFACE (NODE 471 TO 501) AT 0.2 SEONDS INTO THE UNIDIRECTIONAL WATER QUENCH ANALYSIS

FIGURE 6.2-10

DISTRIBUTION OF RADIAL STRESS (N/mm^2) AT 0.2 SECONDS INTO THE UNIDIRECTIONAL WATER QUENCH ANALYSIS

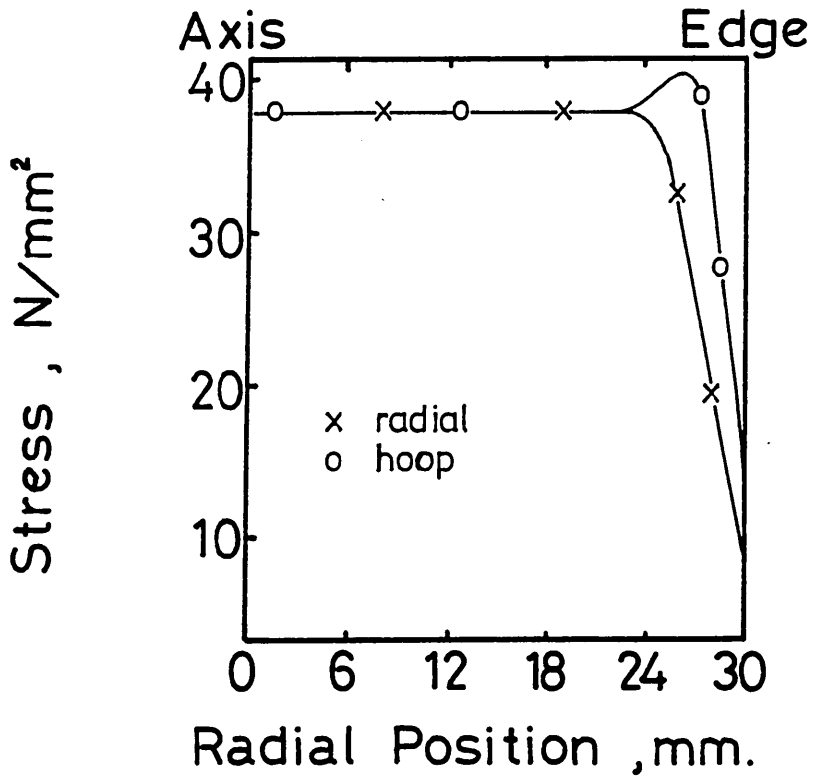
Axis
Edge
40
30
20
10
Stress , N/mm²
x radial
o hoop
0 6 12 18 24 30
Radial Position , mm.

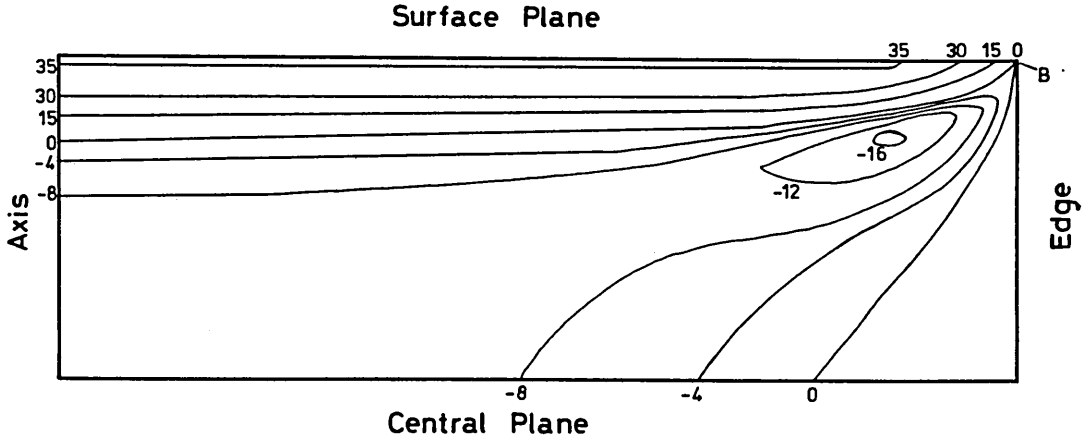
Surface Plane
35 30 15 0
B
35
30
15
0
-4
-8
-16
-12
Axis
Edge
-8 -4 0
Central Plane

FIGURE 6.2-11

DISTRIBUTION OF HOOP STRESS (N/mm^2)
AT 0.2 SECONDS INTO THE UNIDIRECTIONAL
WATER QUENCH ANALYSIS

FIGURE 6.2-12

DISTRIBUTION OF AXIAL STRESS (N/mm^2)
AT 0.2 SECONDS INTO THE UNDIRECTIONAL
WATER QUENCH ANALYSIS

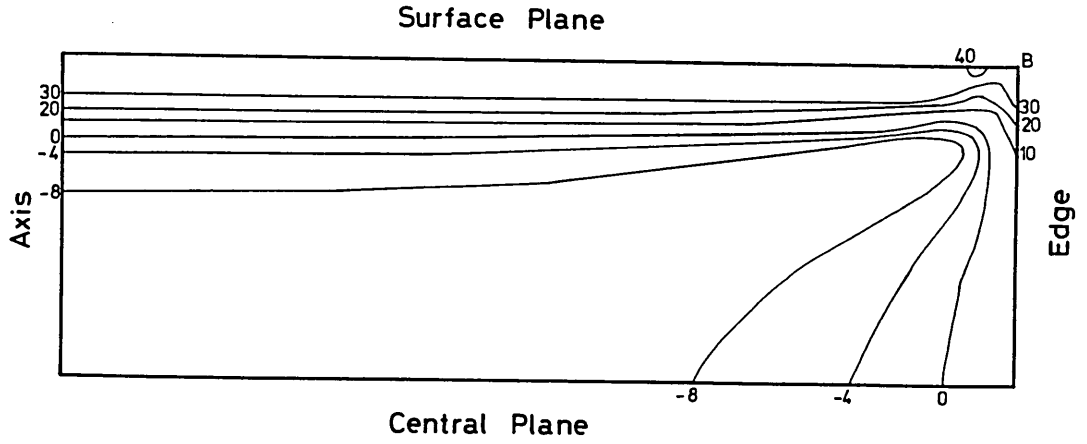
Surface Plane
40
B
30
20
0
-4
-8
30
20
10
Axis
Edge
-8
-4
0
Central Plane

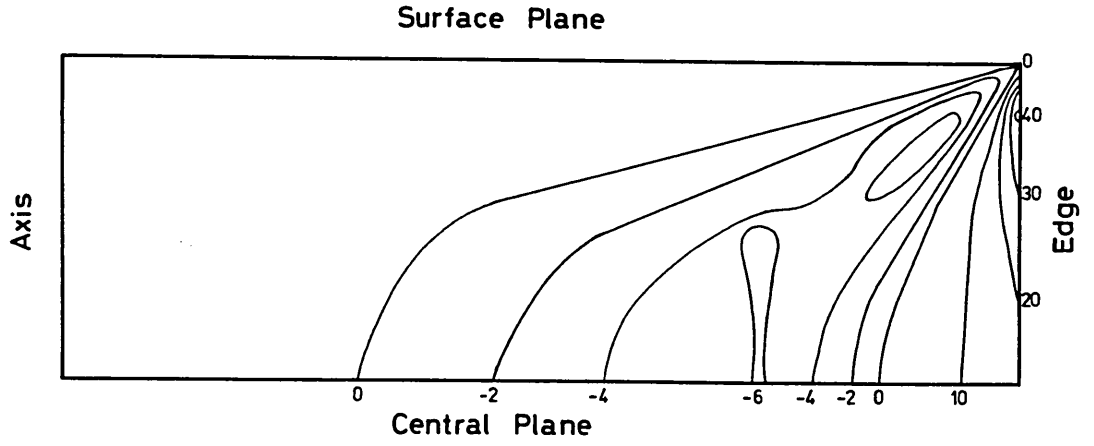
Surface Plane
0
40
30
20
Axis
Edge
0
-2
-4
-6
-4
-2
0
10
Central Plane

FIGURE 6.2-13

DISTRIBUTION OF SHEAR STRESS (N/mm^2)
AT 0.2 SECONDS INTO THE UNIDIRECTIONAL
WATER QUENCH ANALYSIS

FIGURE 6.2-14a

PROPAGATION OF PLASTIC ZONES UP TO
0.6 SECONDS INTO THE UNIDIRECTIONAL
WATER QUENCH ANALYSIS

P : Plastic
E : Elastic

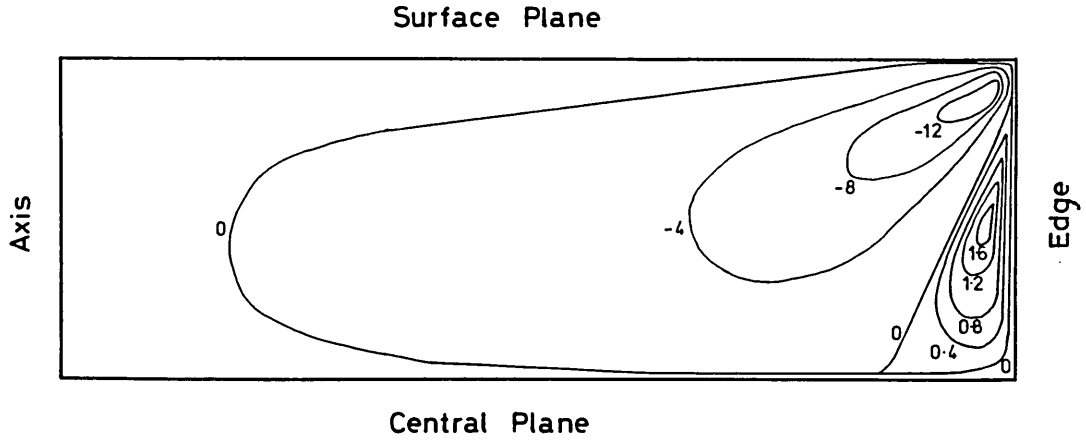
Surface Plane
Axis
Edge
0
-4
-8
-12
1·6
1·2
0·8
0·4
0
0
Central Plane

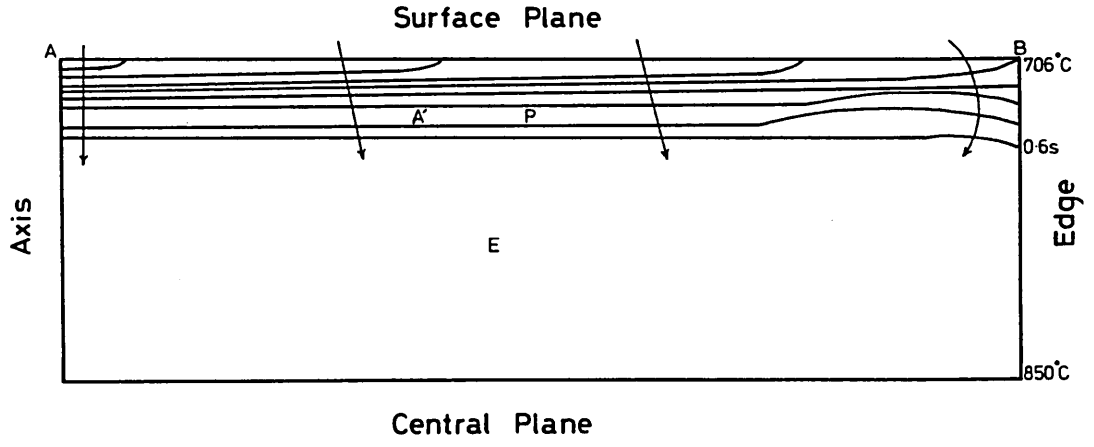
Surface Plane
A
B
706°C
A'
P
0·6s
Axis
E
Edge
850°C
Central Plane

FIGURE 6.2-14b

PROPAGATION OF PLASTIC ZONES AT
0.8 SECONDS INTO THE UNIDIRECTIONAL
WATER QUENCH ANALYSIS

P : Plastic
E : Elastic

FIGURE 6.2-14c

PROPAGATION OF PLASTIC ZONES AT
1.0 SECOND INTO THE UNIDIRECTIONAL
WATER QUENCH ANALYSIS

P : Plastic
E : Elastic

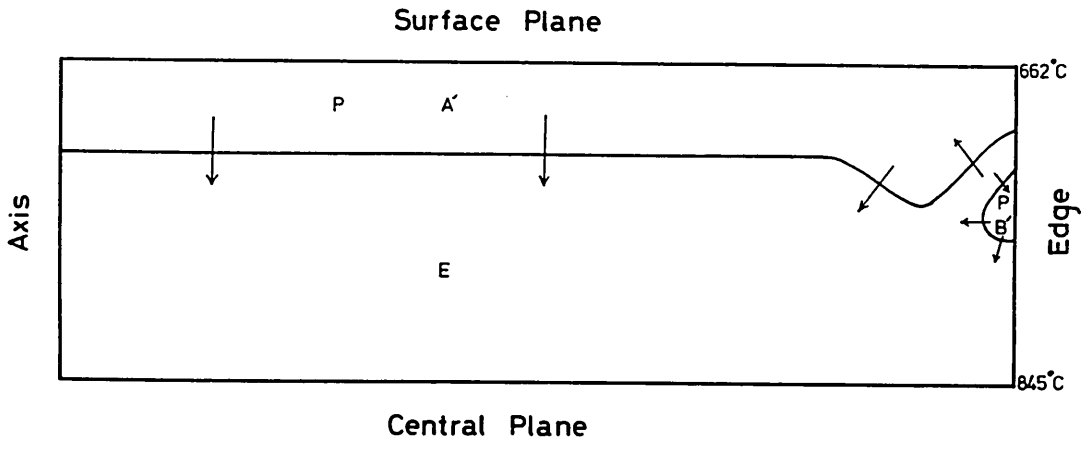
Surface Plane
662°C
P
A´
Axis
Edge
P
B´
E
845°C
Central Plane

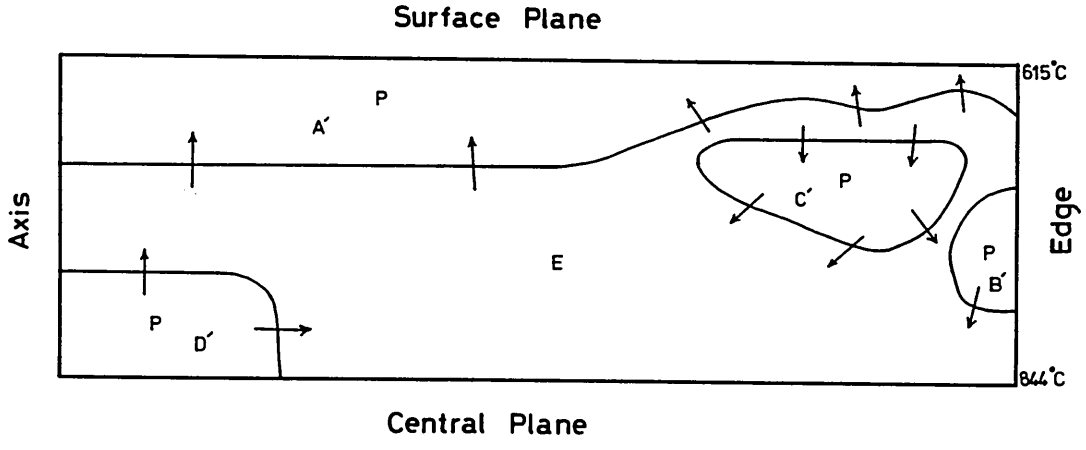
Surface Plane
615°C
P
A´
C´
P
Axis
Edge
E
P
B´
P
D´
844°C
Central Plane

FIGURE 6.2-14d

PROPAGATION OF PLASTIC ZONES AT
1.2 SECONDS INTO THE UNIDIRECTIONAL
WATER QUENCH ANALYSIS

P : Plastic
E : Elastic

FIGURE 6.2-14e

PROPAGATION OF PLASTIC ZONES FROM 1.4
TO 3.0 SECONDS INTO THE UNIDIRECTIONAL
WATER QUENCH ANALYSIS

P : Plastic
E : Elastic

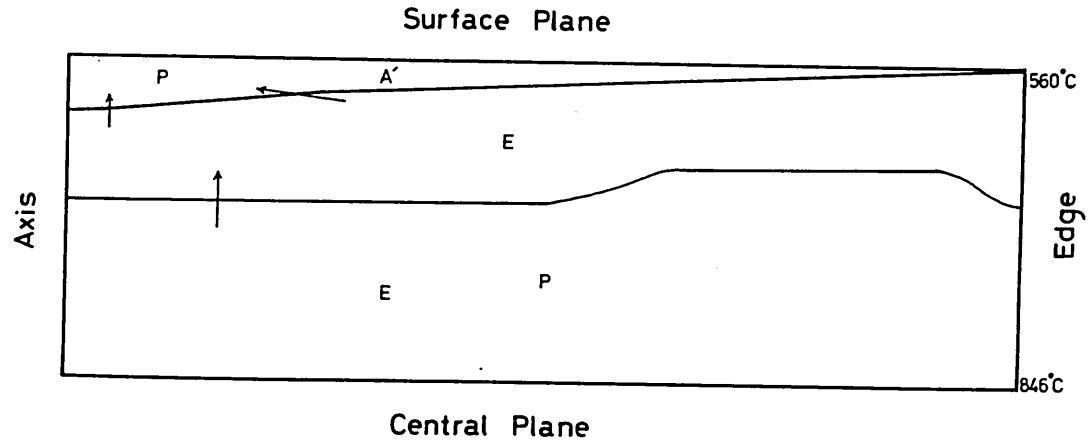
Surface Plane
P
A´
560°C
E
Axis
Edge
E
P
846°C
Central Plane

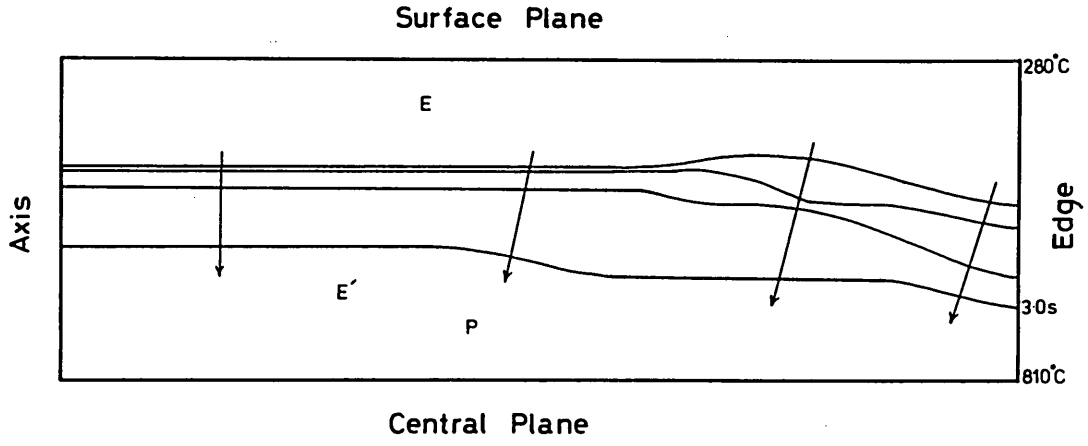
Surface Plane
280°C
E
Axis
Edge
E´
P
3·0s
810°C
Central Plane

FIGURE 6.2-15

a) DISTRIBUTION OF STRESS ALONG THE AXIS OF THE PLATE (NODE 1 TO 471) AT 2.6 SECONDS INTO THE UNIDIRECTIONAL WATER QUENCH ANALYSIS

b) DISTRIBUTUION OF STRESS ALONG THE SURFACE OF THE PLATE (NODE 471 TO 501) AT 2.6 SECONDS INTO THE UNIDIRECTIONAL WATER QUENCH ANALYSIS

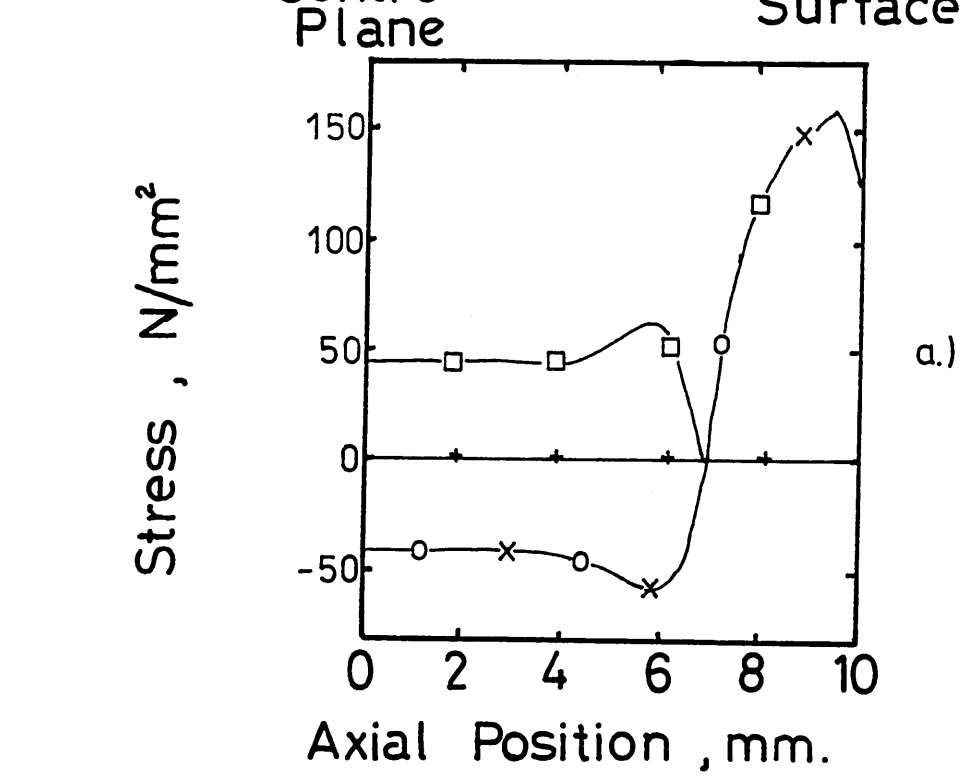

× Radial
o Hoop
+ Axial
□ Equiv't

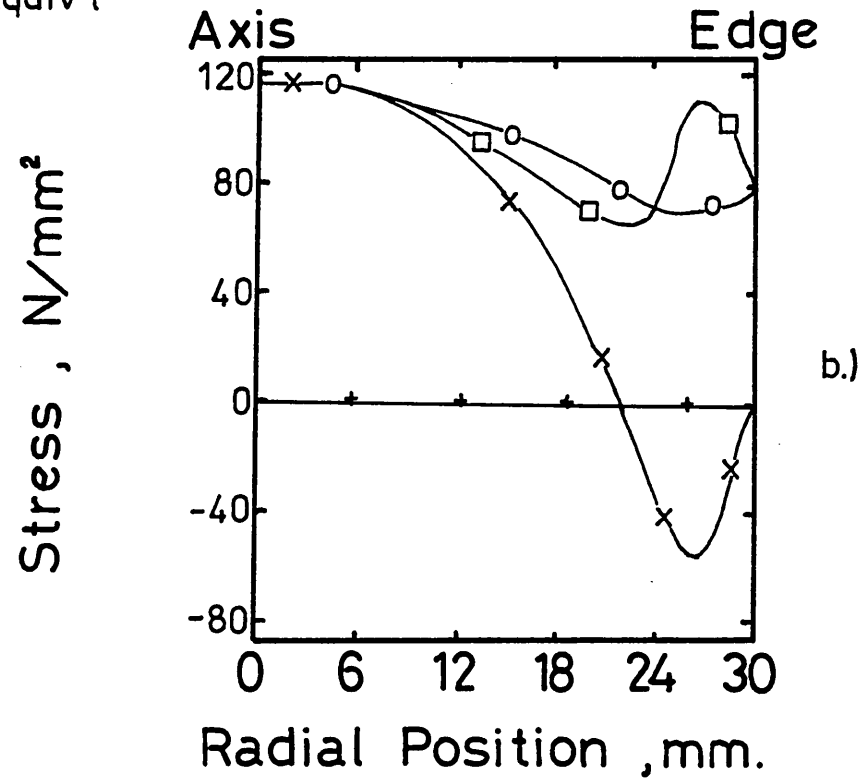

FIGURE 6.2-15 (CONTINUED)

c) DISTRIBUTION OF STRESS ALONG THE CENTRAL PLANE OF THE PLATE (NODE 1 TO 31) AT 2.6 SECONDS INTO THE UNIDIRECTIONAL WATER QUENCH ANALYSIS

d) DISTRIBUTION OF STRESS ALONG THE EDGE OF THE PLATE (NODE 31 TO 501) AT 2.6 SECONDS INTO THE UNIDIRECTIONAL WATER QUENCH ANALYSIS

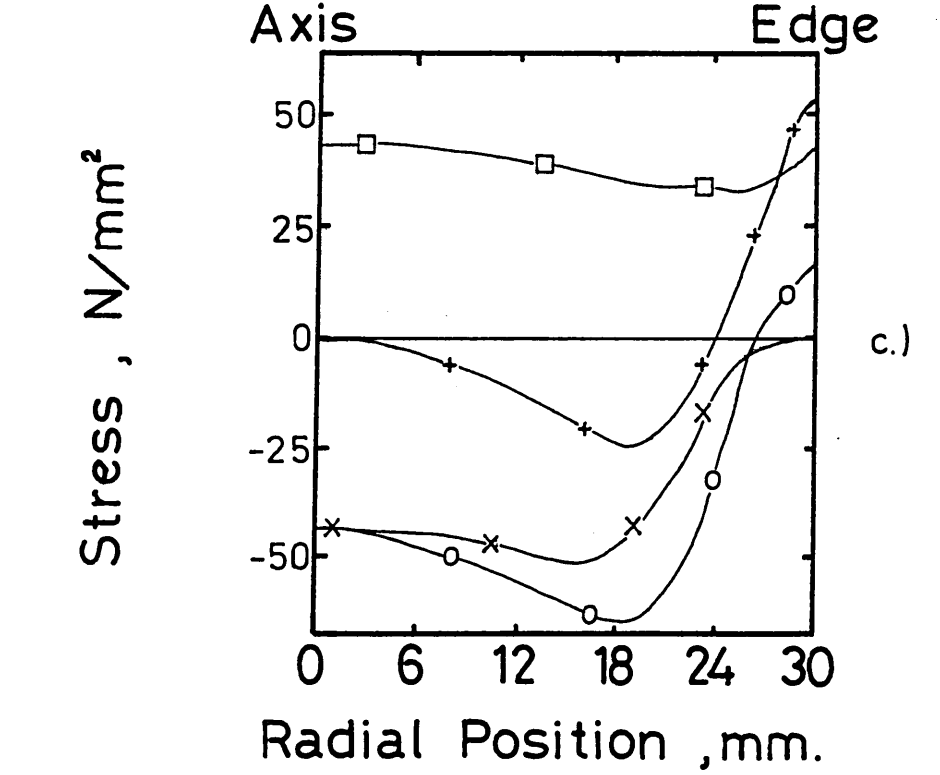

× Radial
o Hoop
+ Axial
□ Equiv't

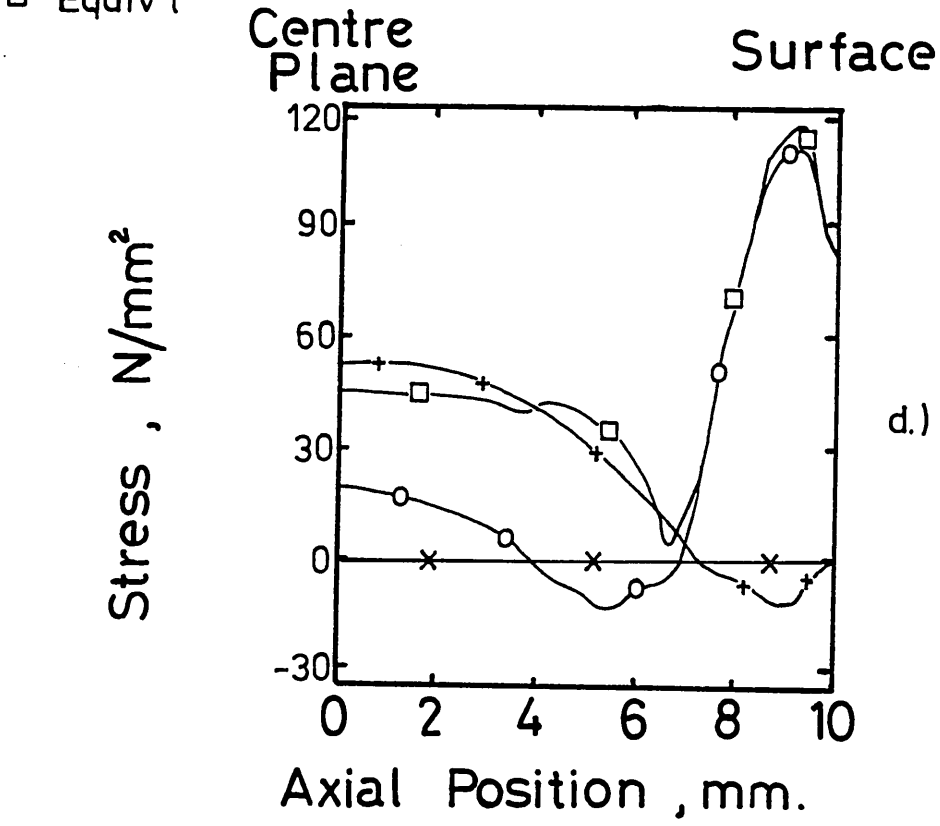

FIGURE 6.2-16

a) DISTRIBUTION OF STRESS ALONG THE AXIS OF THE PLATE (NODE 1 TO 471) AT 4.0 SECONDS INTO THE UNIDIRECTIONAL WATER QUENCH ANALYSIS

b) DISTRIBUTION OF STRESS ALONG THE CENTRAL PLANE OF THE PLATE (NODE 1 TO 31) AT 4.0 SECONDS INTO THE UNIDIRECTIONAL WATER QUENCH ANALYSIS

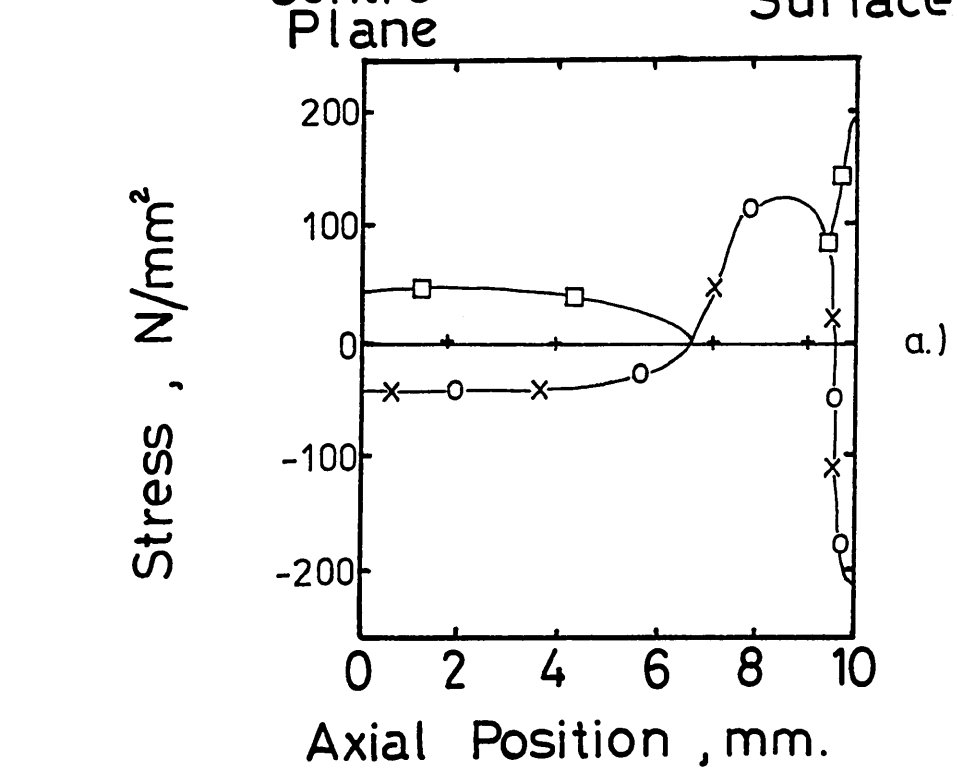

× Radial
o Hoop
+ Axial
□ Equiv't

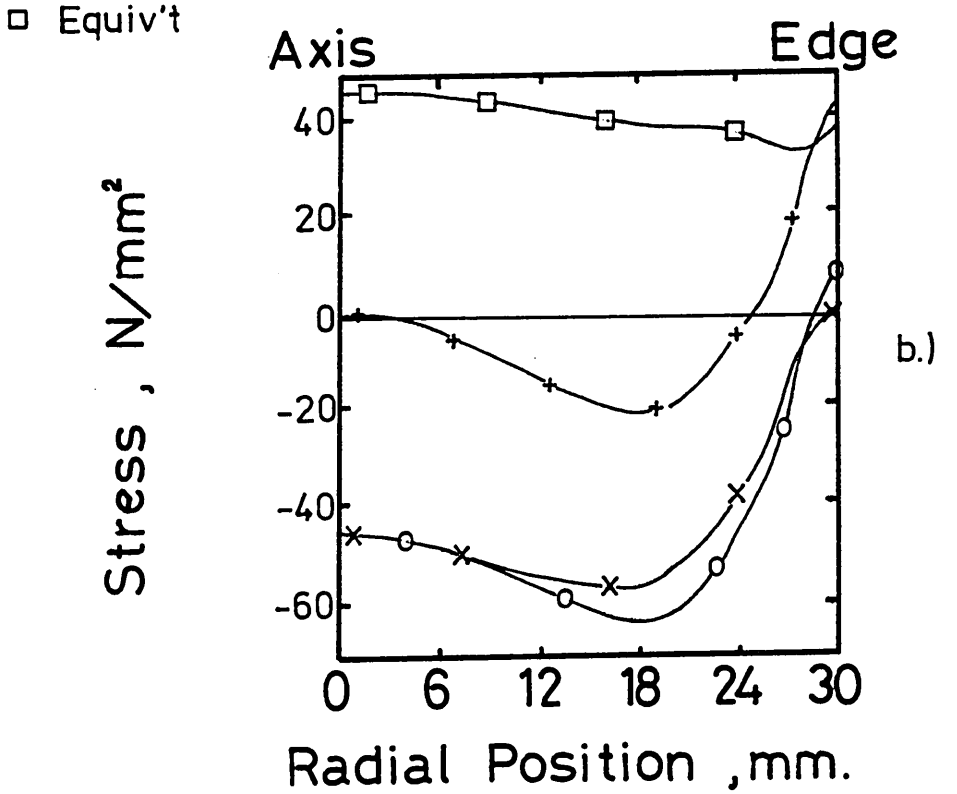

FIGURE 6.2-16 (Continued)

c) DISTRIBUTION OF STRESS ALONG THE SURFACE OF THE PLATE (NODE 471 TO 501) AT 4.0 SECONDS INTO THE UNIDIRECTIONAL WATER QUENCH ANALYSIS

FIGURE 6.2-17

PROPAGATION OF PLASTIC ZONES FROM 3.2 TO 3.6 SECONDS INTO THE UNIDIRECTIONAL WATER QUENCH ANALYSIS

P : Plastic

E : Elastic

× Radial

o Hoop

\+ Axial

□ Equiv't

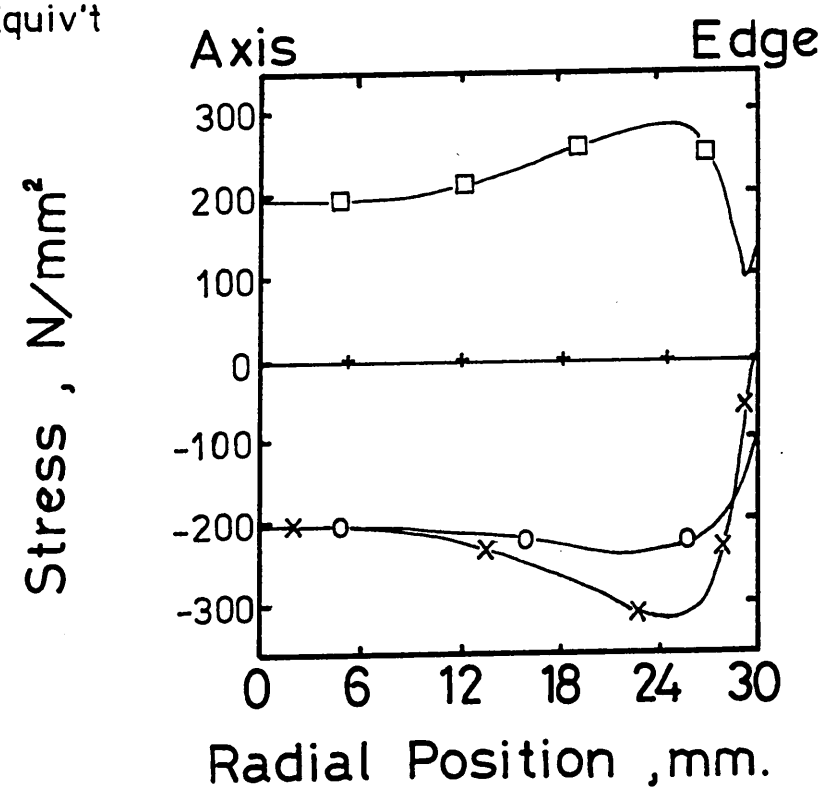

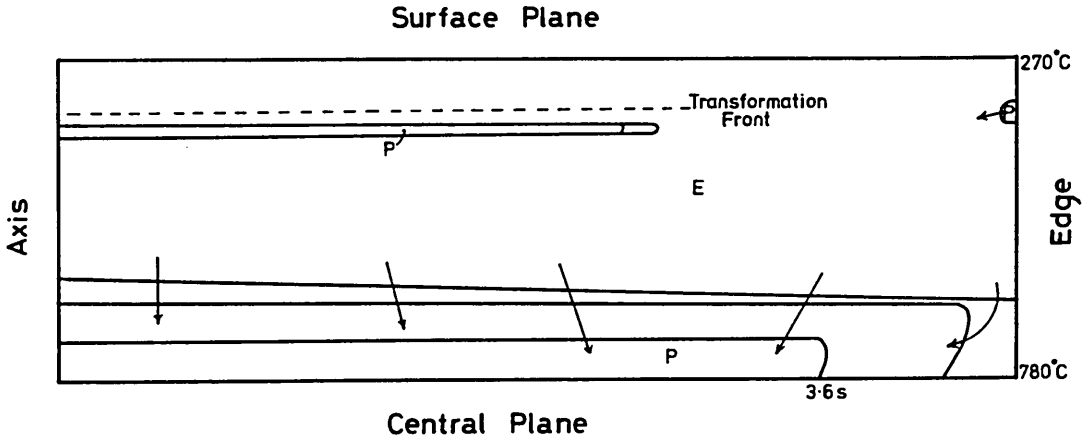

FIGURE 6.2-18

DISTRIBUTION OF RADIAL STRESS (N/mm^2)
AT 4.0 SECONDS INTO THE UNIDIRECTIONAL
WATER QUENCH ANALYSIS

FIGURE 6.2-19

DISTRIBUTION OF HOOP STRESS (N/mm^2)
AT 4.0 SECONDS INTO THE UNIDIRECTIONAL
WATER QUENCH ANALYSIS

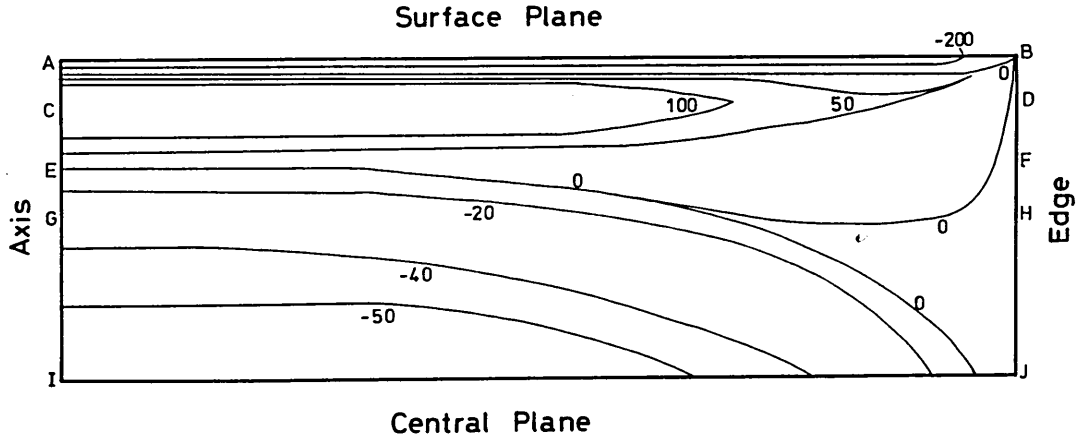
Surface Plane
-200
A
B
0
C
100
50
D
E
F
0
G
-20
0
H
Axis
Edge
-40
0
-50
I
J
Central Plane

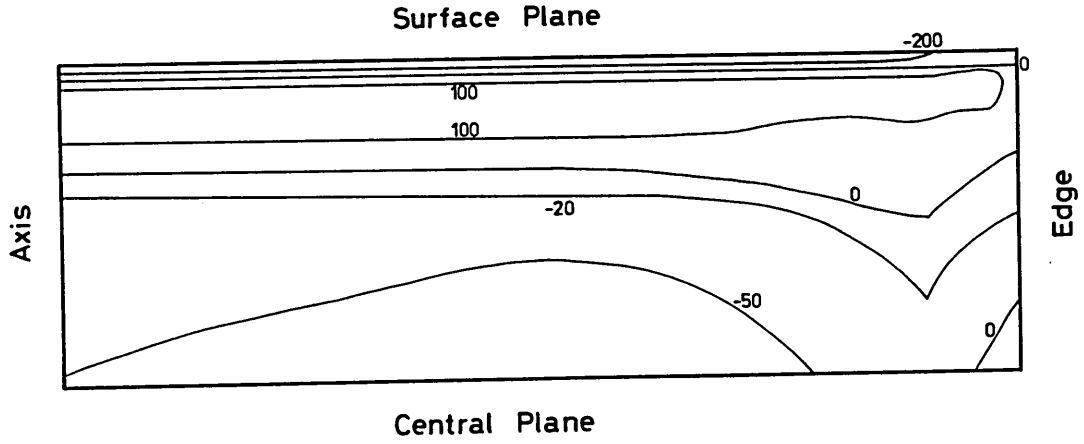
Surface Plane
-200
0
100
100
0
-20
Axis
Edge
-50
0
Central Plane

FIGURE 6.2-20

DISTRIBUTION OF AXIAL STRESS (N/mm^2)
AT 4.0 SECONDS INTO THE UNIDIRECTIONAL
WATER QUENCH ANALYSIS

FIGURE 6.2-21

DISTRIBUTION OF EQUIVALENT STRESS (N/mm^2)
AT 4.0 SECONDS INTO THE UNIDIRECTIONAL
WATER QUENCH ANALYSIS

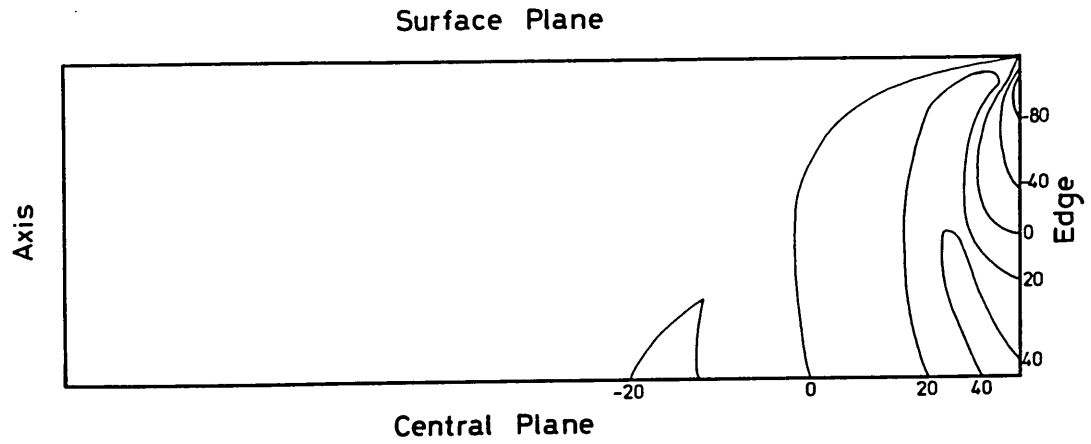
Surface Plane
Axis
Edge
80
40
0
20
40
-20
0
20
40
Central Plane

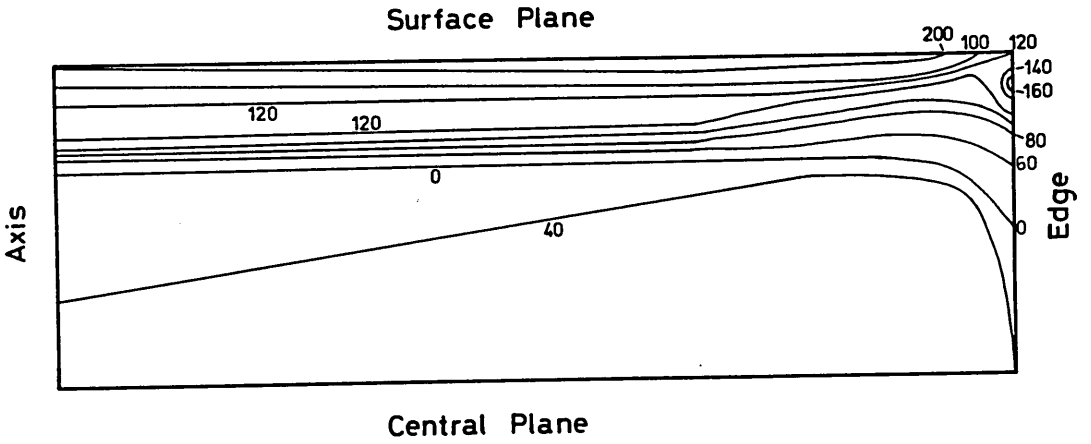
Surface Plane
Axis
Edge
200
100
120
140
160
120
120
80
60
0
40
0
Central Plane

FIGURE 6.2-22a

PROPAGATION OF PLASTIC ZONES FROM 3.8 TO 9.6 SECONDS INTO THE UNIDIRECTIONAL WATER QUENCH ANALYSIS

P : Plastic
E : Elastic

FIGURE 6.2-22b

PROPAGATION OF PLASTIC ZONES FROM 10.0 TO 13.2 SECONDS INTO THE UNIDIRECTIONAL WATER QUENCH ANALYSIS

P : Plastic
E : Elastic

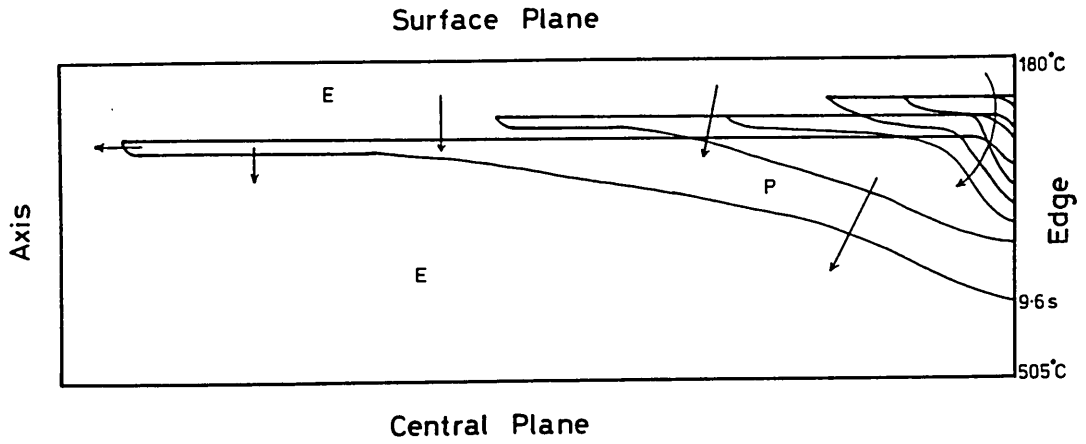
Surface Plane
E
P
E
Axis
Edge
180°C
9·6s
505°C
Central Plane

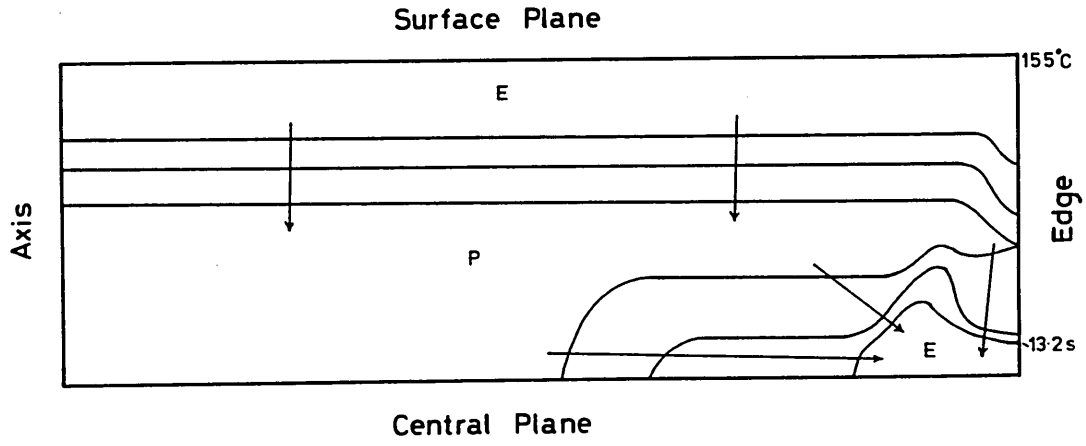
Surface Plane
E
P
E
Axis
Edge
155°C
13·2s
Central Plane

FIGURE 6.2-23

a) DISTRIBUTION OF STRESS ALONG THE AXIS OF THE PLATE (NODE 1 TO 471) AT 12.0 SECONDS INTO THE UNIDIRECTIONAL WATER QUENCH ANALYSIS

b) DISTRIBUTION OF STRESS ALONG THE CENTRAL PLANE OF THE PLATE (NODE 1 TO 31) AT 12.0 SECONDS INTO THE UNIDIRECTIONAL WATER QUENCH ANALYSIS

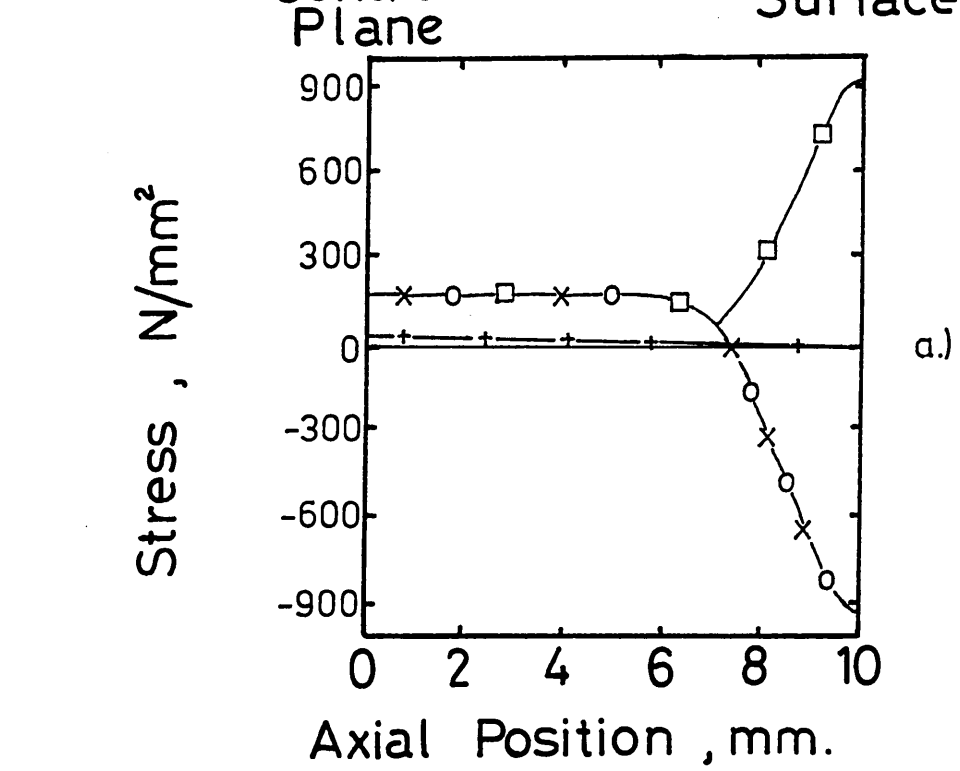

× Radial
o Hoop
+ Axial
□ Equiv't

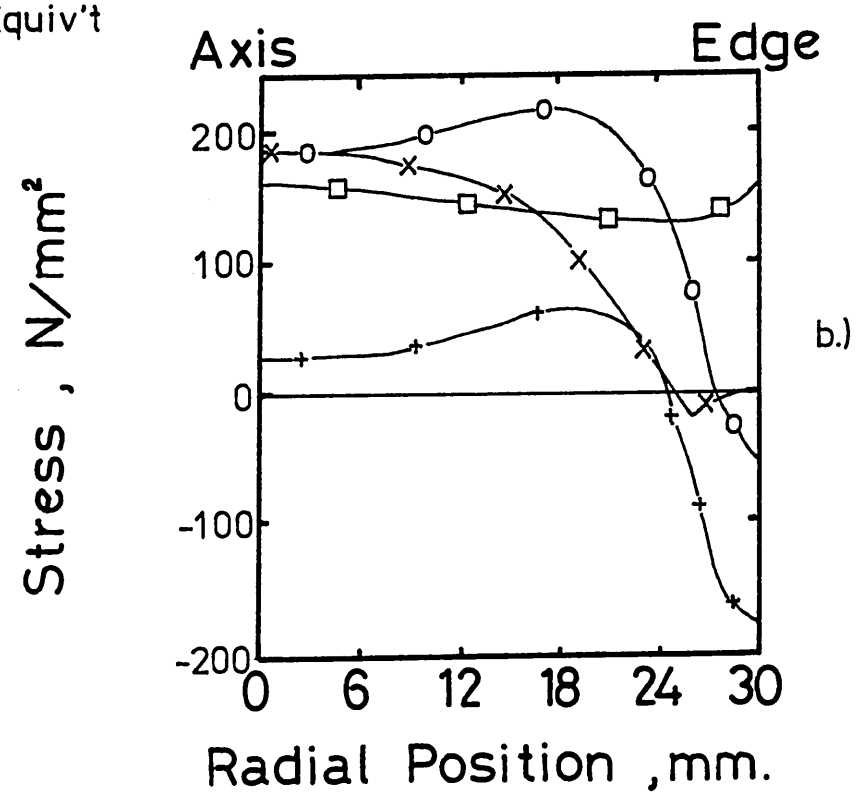

FIGURE 6.2-23 (Continued)

c) DISTRIBUTION OF STRESS ALONG THE SURFACE OF THE PLATE (NODE 471 TO 501) AT 12.0 SECONDS INTO THE UNIDIRECTIONAL WATER QUENCH ANALYSIS

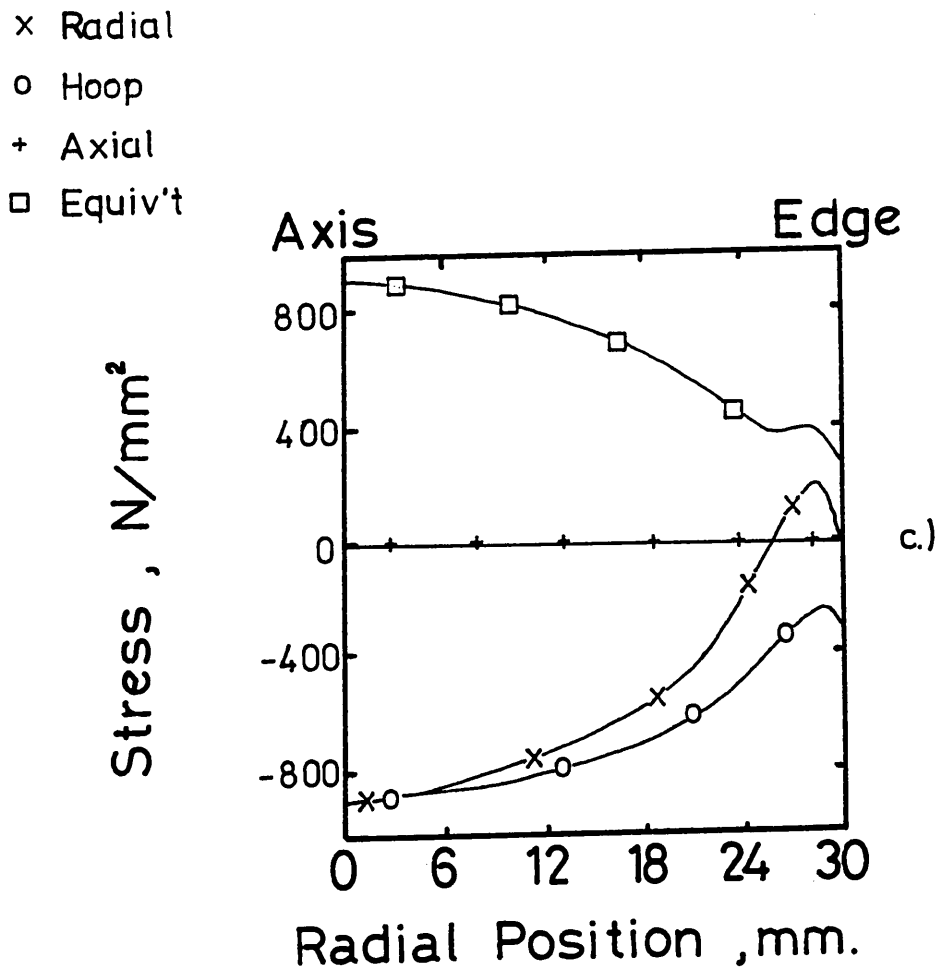
× Radial
o Hoop
+ Axial
□ Equiv't
Axis
Edge
800
400
0
-400
-800
Stress , N/mm²
0
6
12
18
24
30
Radial Position , mm.
c.)

FIGURE 6.2-24

DISTRIBUTION OF RADIAL STRESS (N/mm^2)
AT 12.0 SECONDS INTO THE UNIDIRECTIONAL
WATER QUENCH ANALYSIS

FIGURE 6.2-25

DISTRIBUTION OF HOOP STRESS (N/mm^2)
AT 12.0 SECONDS INTO THE UNIDIRECTIONAL
WATER QUENCH ANALYSIS

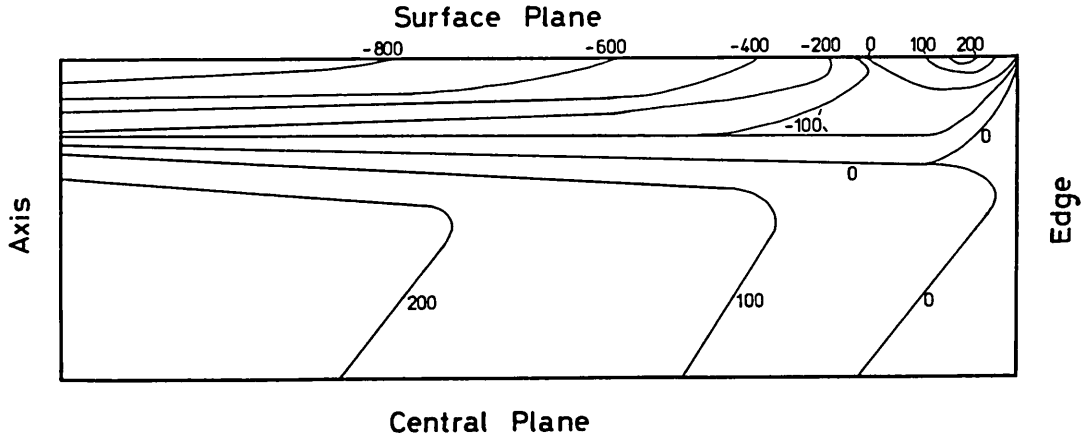
Surface Plane
-800
-600
-400
-200
0
100
200
-100
0
0
200
100
0
Axis
Edge
Central Plane

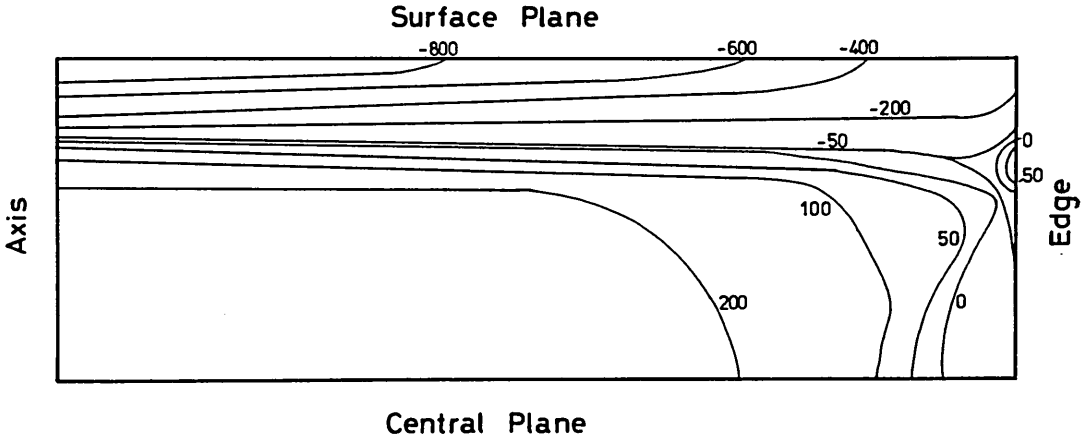
Surface Plane
-800
-600
-400
-200
-50
0
50
100
50
200
0
Axis
Edge
Central Plane

FIGURE 6.2-26

DISTRIBUTION OF AXIAL STRESS (N/mm^2)
AT 12.0 SECONDS INTO THE UNIDIRECTIONAL
WATER QUENCH ANALYSIS

FIGURE 6.2-27

DISTRIBUTION OF EQUIVALENT STRESS (N/mm^2)
AT 12.0 SECONDS INTO THE UNIDIRECTIONAL
WATER QUENCH ANALYSIS

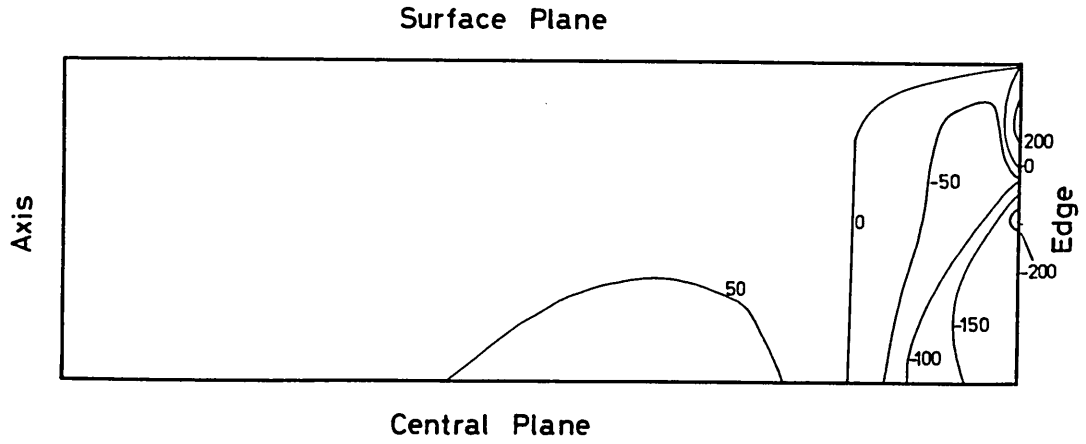
Surface Plane
Axis
Edge
Central Plane
200
0
-50
0
-200
50
-150
-100

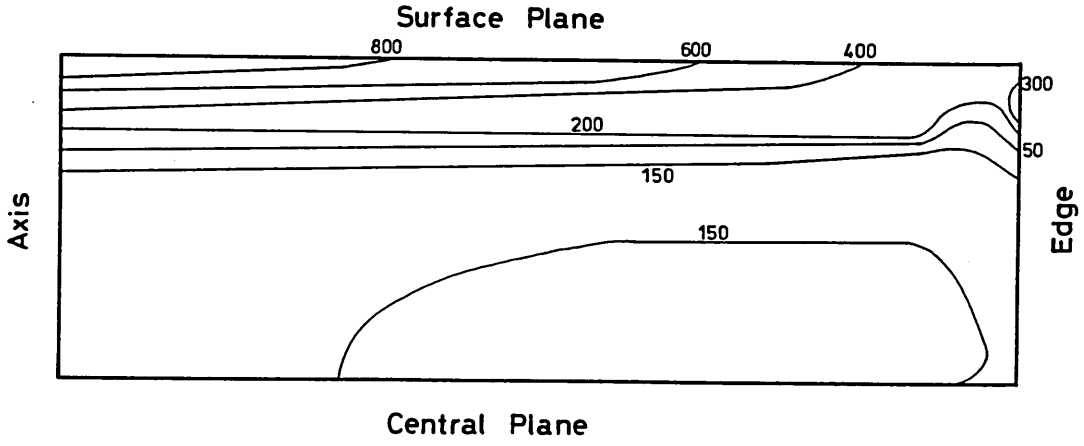
Surface Plane
800
600
400
300
200
50
150
150
Axis
Edge
Central Plane

FIGURE 6.2-28

a) DISTRIBUTION OF RESIDUAL STRESS ALONG THE AXIS OF THE PLATE (NODE 1 TO 471) AT 65.0 SECONDS INTO THE UNIDIRECTIONAL WATER QUENCH ANALYSIS

b) DISTRIBUTION OF RESIDUAL STRESS ALONG THE SURFACE OF THE PLATE (NODE 471 TO 501) AT 65.0 SECONDS INTO THE UNIDIRECTIONAL WATER QUENCH ANALYSIS

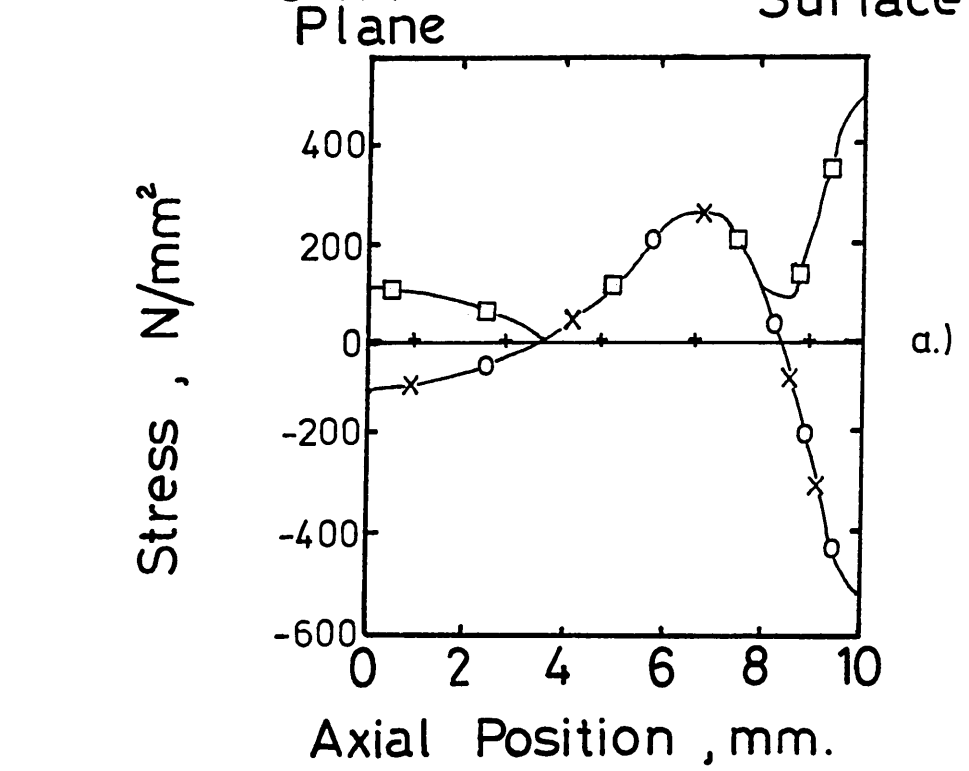

× Radial
o Hoop
+ Axial
□ Equiv't

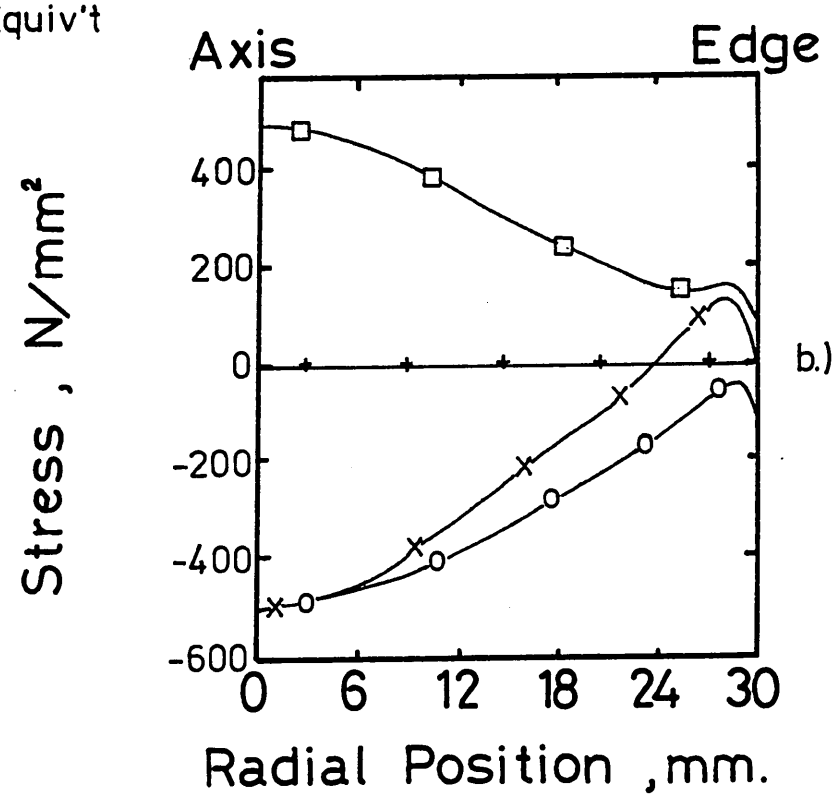

FIGURE 6.2-28 (Continued)

c) DISTRIBUTION OF RESIDUAL STRESS ALONG THE CENTRAL PLANE OF THE PLATE (NODE 1 TO 31) AT 65.0 SECONDS INTO THE UNIDIRECTIONAL WATER QUENCH ANALYSIS

FIGURE 6.2-29

DISTRIBUTION OF RESIDUAL RADIAL STRESS (N/mm^2) AT 65.0 SECONDS INTO THE UNIDIRECTIONAL WATER QUENCH ANALYSIS

× Radial

o Hoop

\+ Axial

□ Equiv't

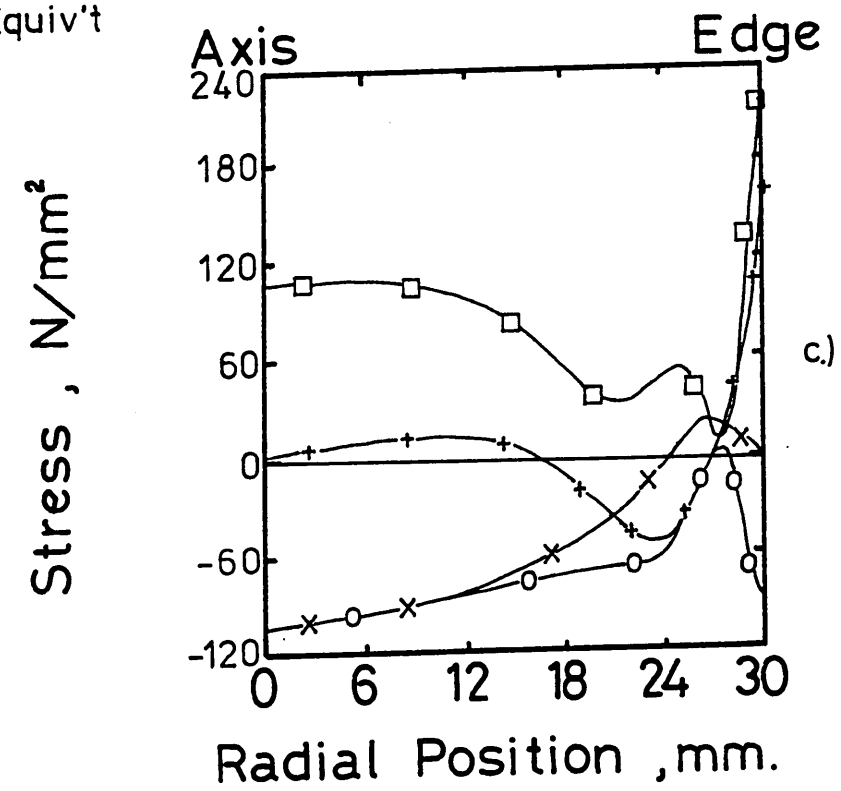

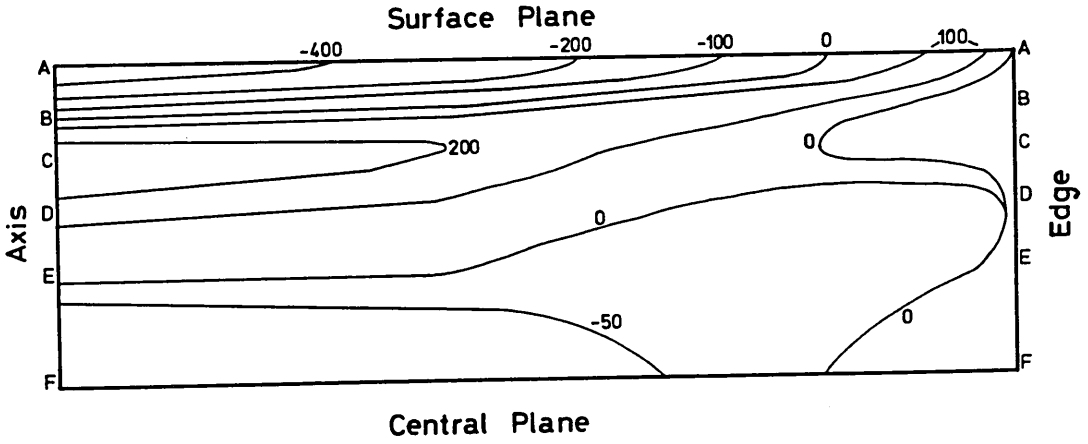

FIGURE 6.2-30

DISTRIBUTION OF RESIDUAL HOOP STRESS (N/mm^2)
AT 65.0 SECONDS INTO THE UNIDIRECTIONAL
WATER QUENCH ANALYSIS

FIGURE 6.2-31

DISTRIBUTION OF RESIDUAL AXIAL STRESS (N/mm^2)
AT 65.0 SECONDS INTO THE UNIDIRECTIONAL
WATER QUENCH ANALYSIS

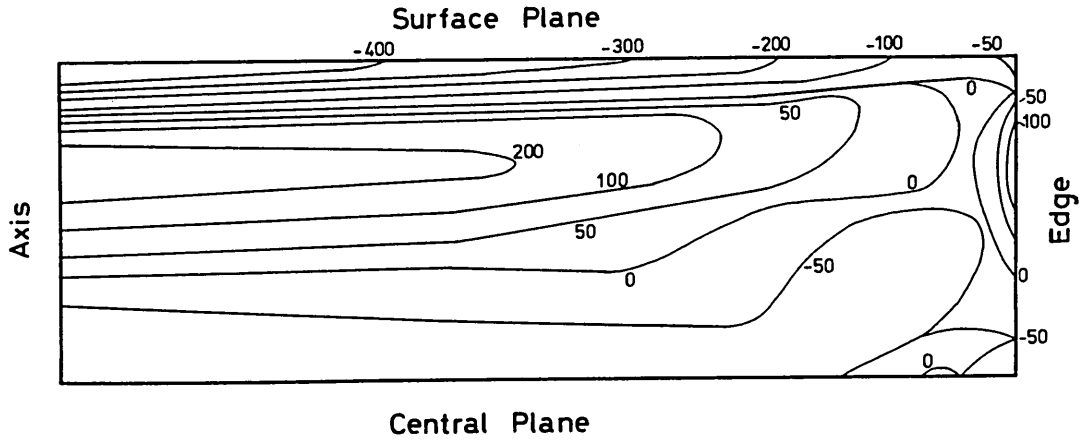
Surface Plane
-400
-300
-200
-100
-50
0
50
200
100
50
0
-50
0
-50
100
0
0
-50
Axis
Edge
Central Plane

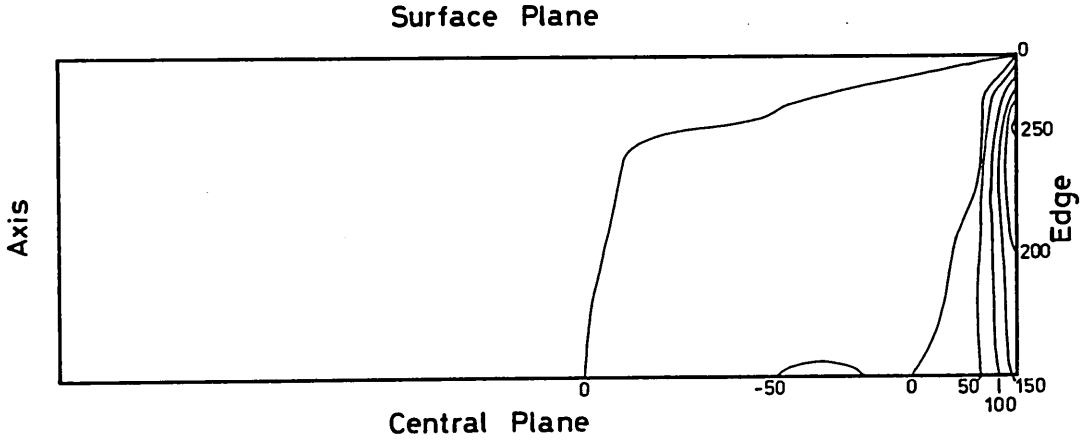
Surface Plane
0
250
200
150
100
0
-50
0
50
Axis
Edge
Central Plane

FIGURE 6.2-32

DISTRIBUTION OF RESIDUAL SHEAR STRESS (N/mm^2)
AT 65.0 SECONDS INTO THE UNIDIRECTIONAL
WATER QUENCH ANALYSIS

FIGURE 6.2-33

DISTRIBUTION OF EQUIVALENT STRESS (N/mm^2)
AT 65.0 SECONDS INTO THE UNIDIRECTIONAL
WATER QUENCH ANALYSIS

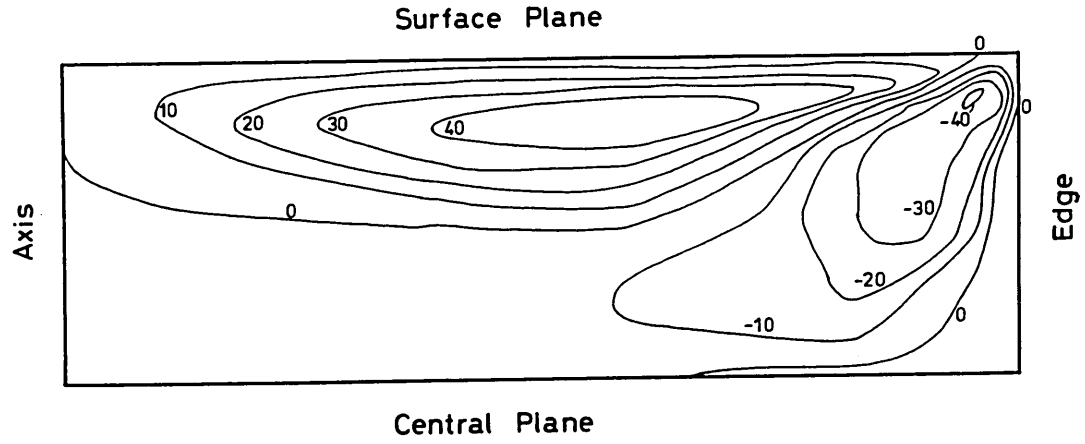
Surface Plane
0
10
20
30
40
-40
0
0
-30
-20
-10
0
Axis
Edge
Central Plane

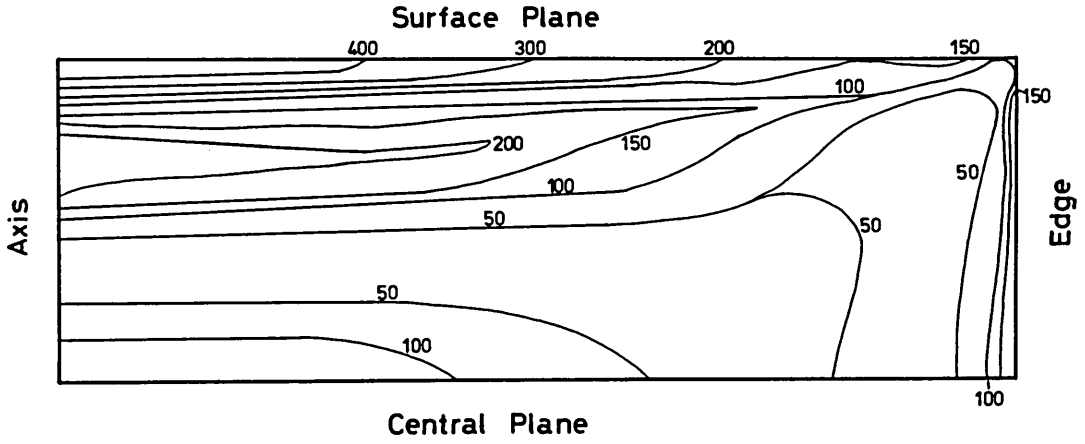
Surface Plane
400
300
200
150
100
150
200
150
100
50
50
50
50
100
100
Axis
Edge
Central Plane

FIGURE 6.2-34

RELATIONSHIP BETWEEN STRESS AND STRAIN AT THE CENTRE AND SURFACE OF A UNIDIRECTIONAL WATER QUENCHED 20 mm THICK PLATE.

..... Node 1/Radial, Hoop

_____ Node 471/Radial, Hoop

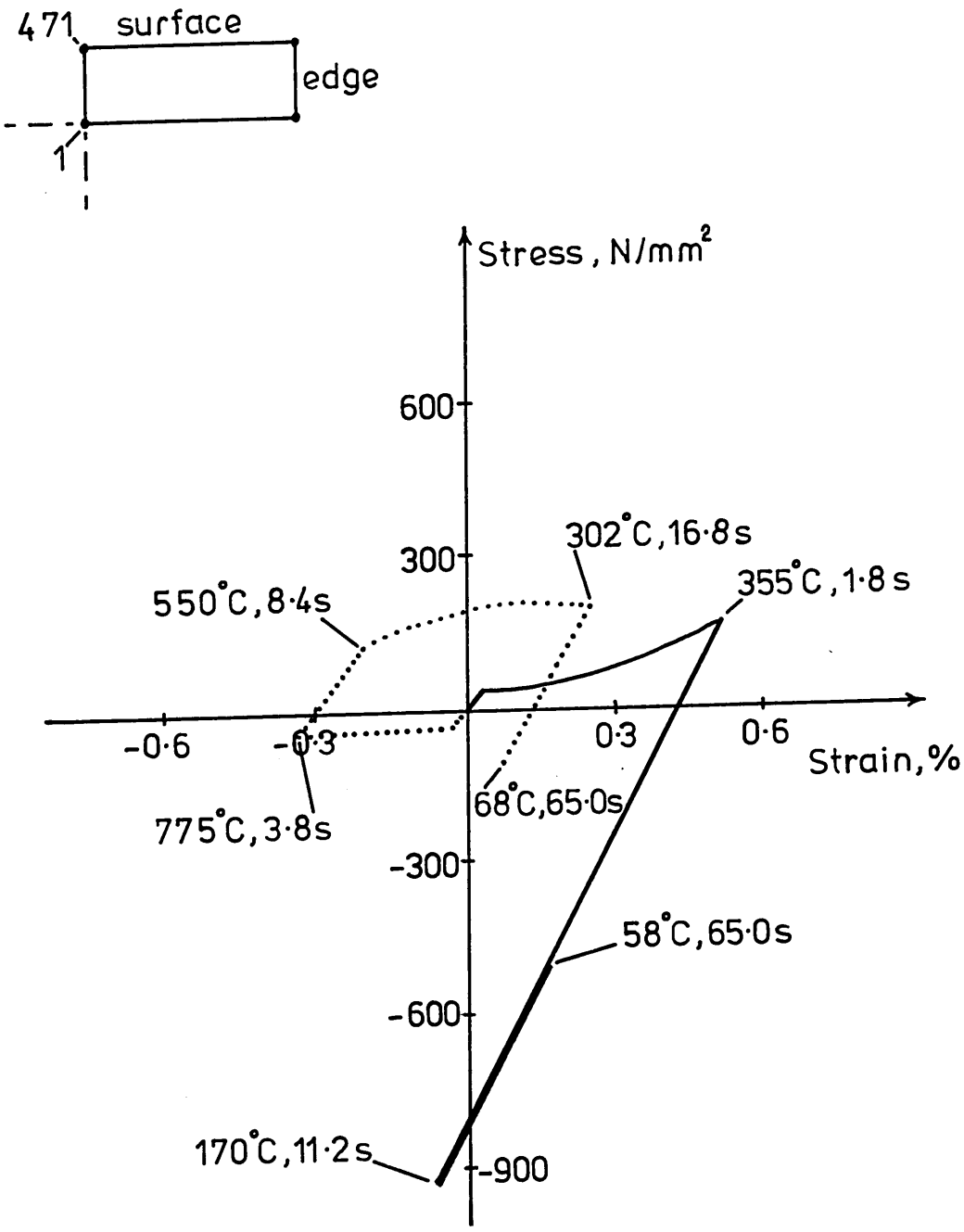
471
surface
edge
1
Stress, N/mm²
600
300
-300
-600
-900
302°C, 16·8s
355°C, 1·8s
550°C, 8·4s
-0·6
-0·3
0·3
0·6
Strain, %
68°C, 65·0s
775°C, 3·8s
58°C, 65·0s
170°C, 11·2s

FIGURE 6.2-35

RELATIONSHIP BETWEEN STRESS AND STRAIN AT THE CORNER OF A UNIDIRECTIONAL WATER QUENCHED 20 mm THICK PLATE

..... Node 501/Hoop

FIGURE 6.2-36

RELATIONSHIP BETWEEN STRESS AND STRAIN AT THE MID-EDGE POSITION OF A UNIDIRECTIONAL WATER QUENCHED 20 mm THICK PLATE

_____ Node 31/Axial

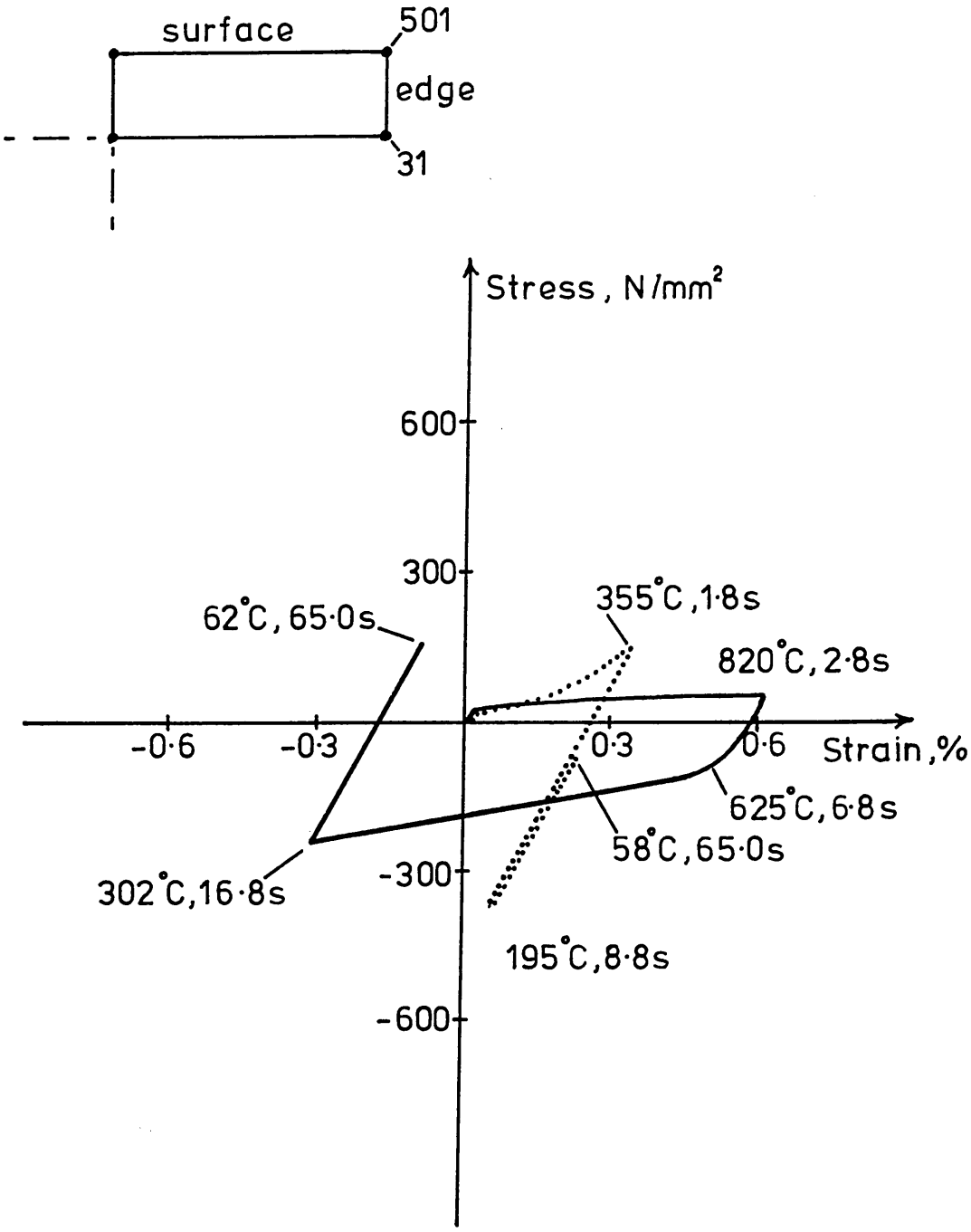
surface
501
edge
31
Stress, N/mm²
600
300
-300
-600
-0·6
-0·3
0·3
0·6
Strain,%
62°C, 65·0s
355°C, 1·8s
820°C, 2·8s
625°C, 6·8s
58°C, 65·0s
302°C, 16·8s
195°C, 8·8s

FIGURE 6.3-1

DETERMINATION OF EDGE CORRECTION FACTORS FROM THE FINITE ELEMENT MODEL, WHICH CAN BE APPLIED TO THE RESULTS OF AN INFINITE PLATE MODEL

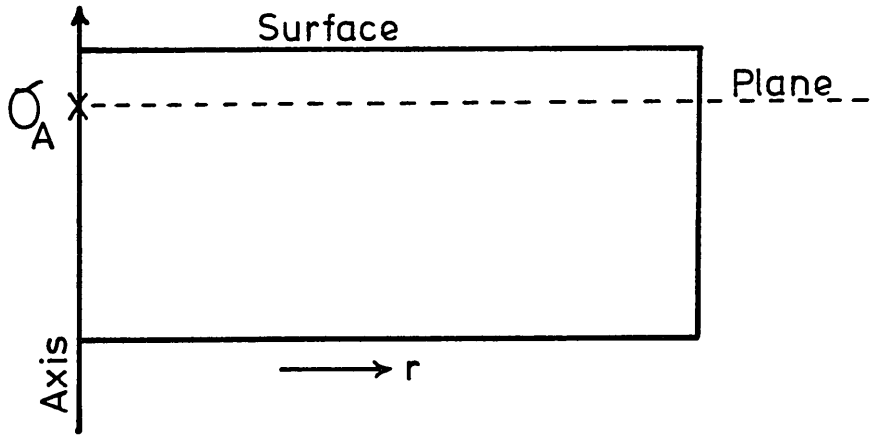

$$\text{Mean Stress on Plane} = \frac{\sum_o^r \sigma}{n} = \hat{\sigma}$$

, where $n = N^o$ of summed stress points.

$$\text{EDGE CORRECTION FACTOR} = \frac{\hat{\sigma}}{\sigma_A}$$

FIGURE 6.4-1

TEMPERATURE PROFILES FOR THE TWO-DIMENSIONAL (HEAT FLOW) WATER QUENCH MODEL

a) COOLING CURVES FOR THE FOUR CORNERS OF THE PLATE MODEL

Node 1 is the plate centre
Node 35 is the mid-edge of the plate
Node 690 is the mid-surface of the plate
Node 724 is the plate corner

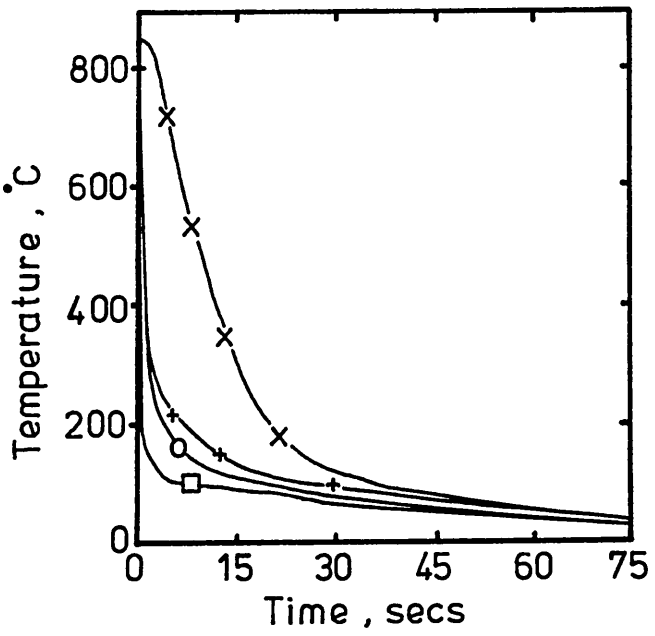

a.)

x	Node	1
o	"	35
+	"	690
□	"	724

FIGURE 6.4-1 (Continued)

TEMPERATURE PROFILES FOR THE TWO-DIMENSIONAL (HEAT FLOW) WATER QUENCH MODEL

b) TEMPERATURE GRADIENTS ALONG THE AXIS OF THE PLATE

c) TEMPERATURE GRADIENTS ALONG THE CENTRAL PLANE OF THE PLATE

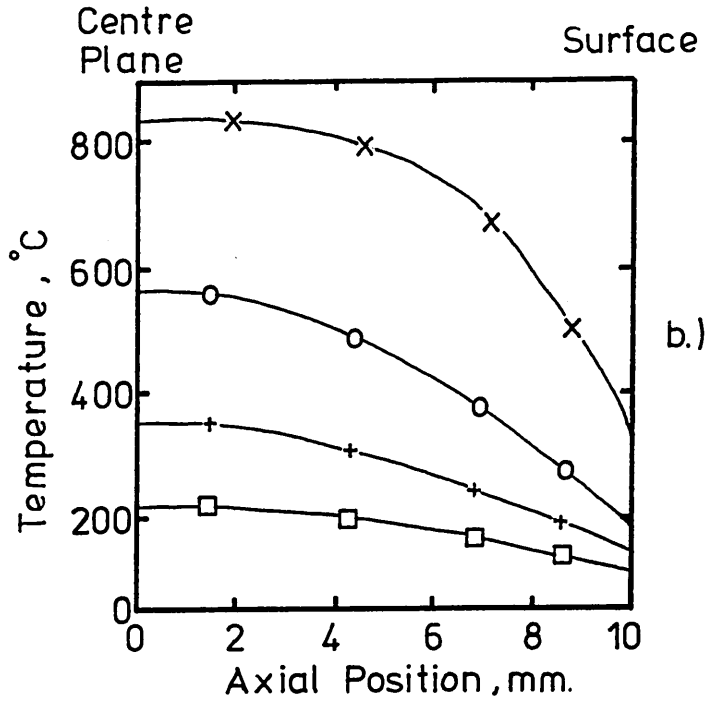

b.)

Time

x 2 seconds

o 8 "

+ 14 "

□ 20 "

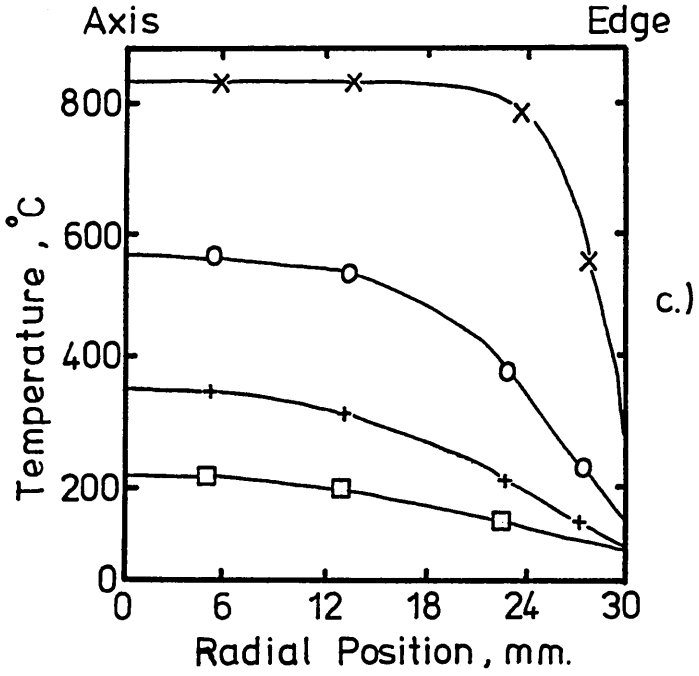

c.)

FIGURE 6.4-1 (Continued)

TEMPERATURE PROFILES FOR THE TWO-DIMENSIONAL (HEAT FLOW) WATER QUENCH MODEL

d) TEMPERATURE GRADIENTS ALONG THE EDGE OF THE PLATE

e) TEMPERATURE GRADIENTS ALONG THE SURFACE OF THE PLATE

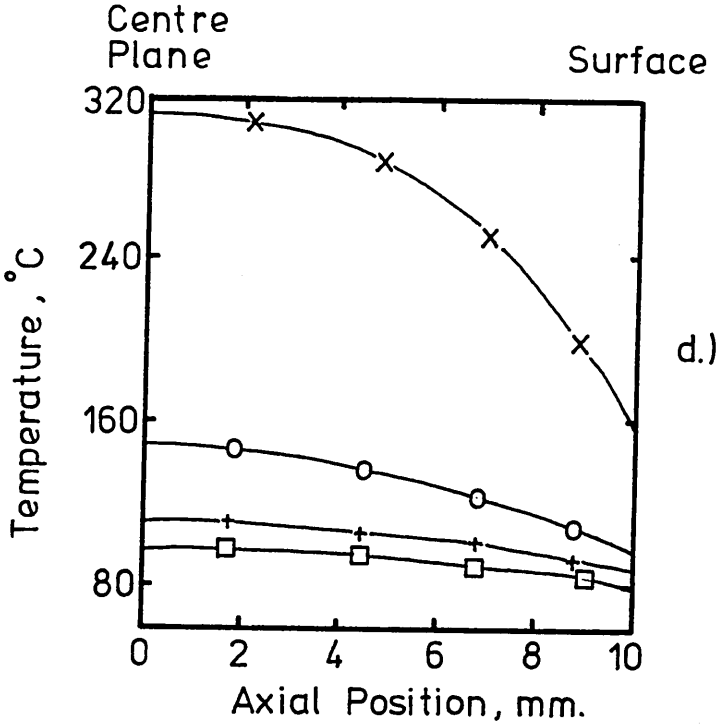

d.)

Time

x 2 seconds

o 8 "

+ 14 "

□ 20 "

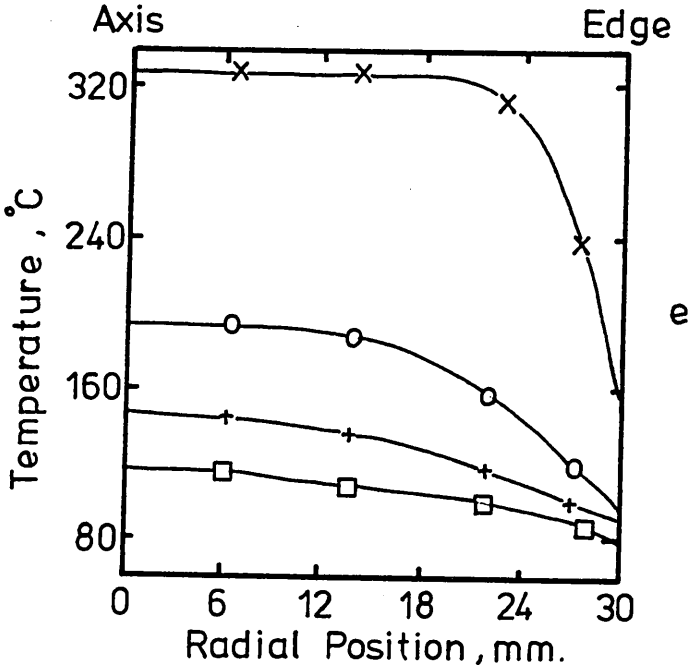

e.)

FIGURE 6.4-2

a) DISTRIBUTION OF STRESS ALONG THE AXIS OF THE PLATE AT 0.005 SECONDS INTO THE TWO-DIMENSIONAL (HEAT FLOW) WATER QUENCH ANALYSIS

b) DISTRIBUTION OF STRESS ALONG THE SURFACE OF THE PLATE AT 0.005 SECONDS INTO THE TWO-DIMENSIONAL (HEAT FLOW) WATER QUENCH ANALYSIS

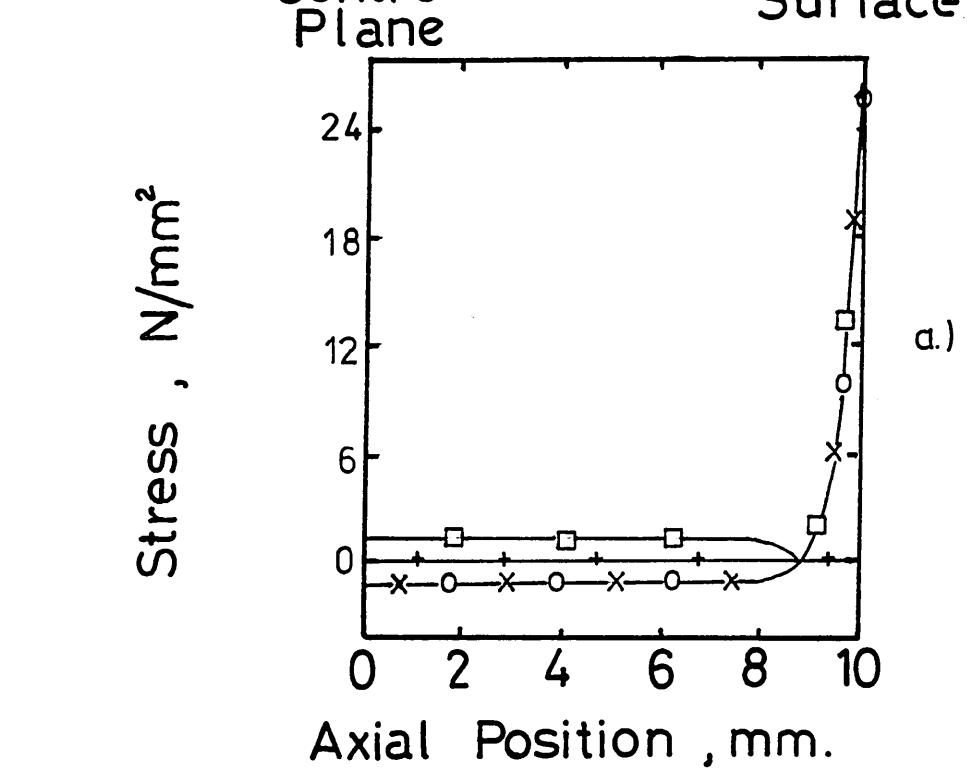

× Radial
o Hoop
+ Axial
□ Equiv't

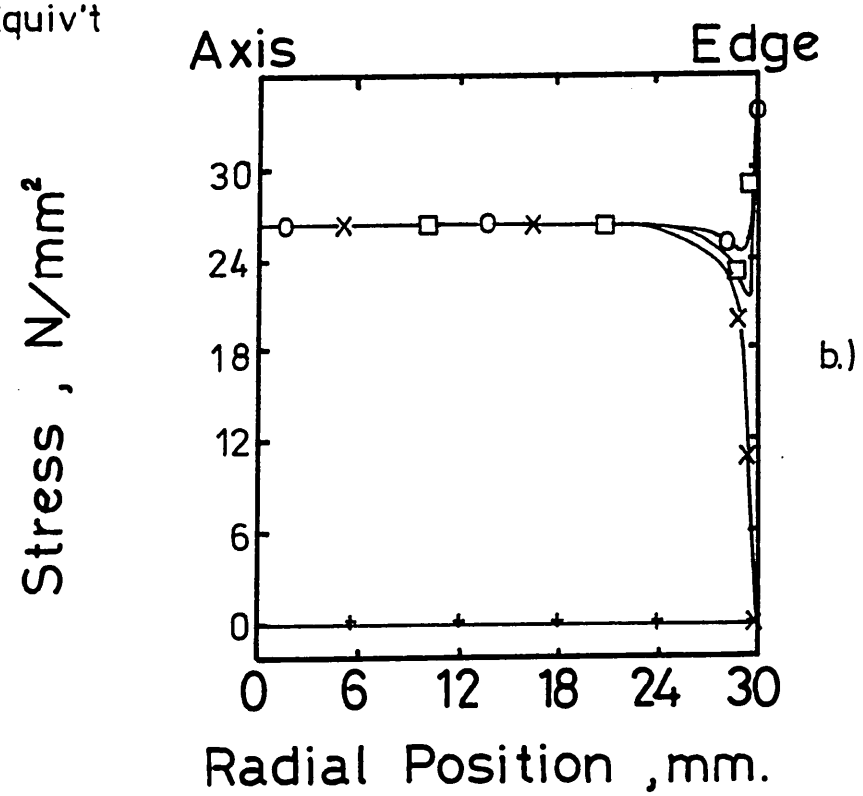

FIGURE 6.4-2 (Continued)

c) DISTRIBUTION OF STRESS ALONG THE CENTRAL PLANE OF THE PLATE AT 0.005 SECONDS INTO THE TWO-DIMENSIONAL (HEAT FLOW) WATER QUENCH ANALYSIS

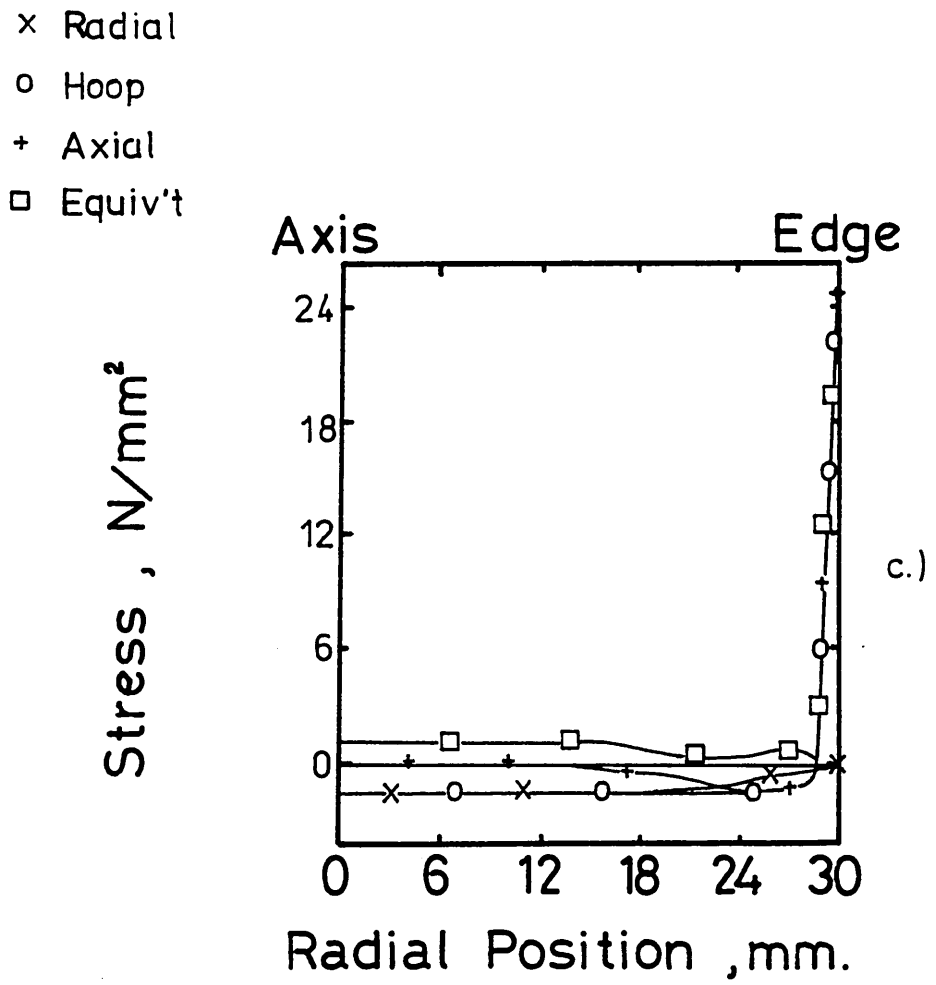
× Radial
o Hoop
+ Axial
□ Equiv't
Axis
Edge
Stress , N/mm²
24
18
12
6
0
0 6 12 18 24 30
Radial Position , mm.
c.)

FIGURE 6.4-3

a) DISTRIBUTION OF STRESS ALONG THE AXIS OF THE PLATE AT 0.25 SECONDS INTO THE TWO-DIMENSIONAL (HEAT FLOW) WATER QUENCH ANALYSIS

b) DISTRIBUTION OF STRESS ALONG THE SURFACE OF THE PLATE AT 0.25 SECONDS INTO THE TWO-DIMENSIONAL (HEAT FLOW) WATER QUENCH ANALYSIS

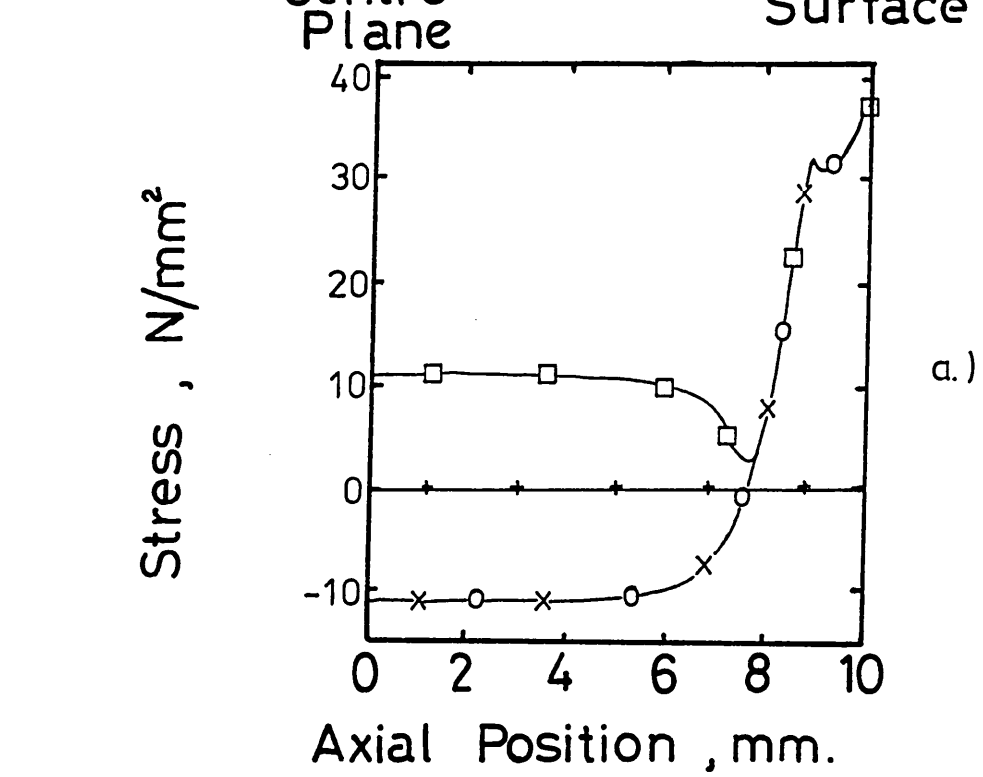

× Radial
o Hoop
+ Axial
□ Equiv't

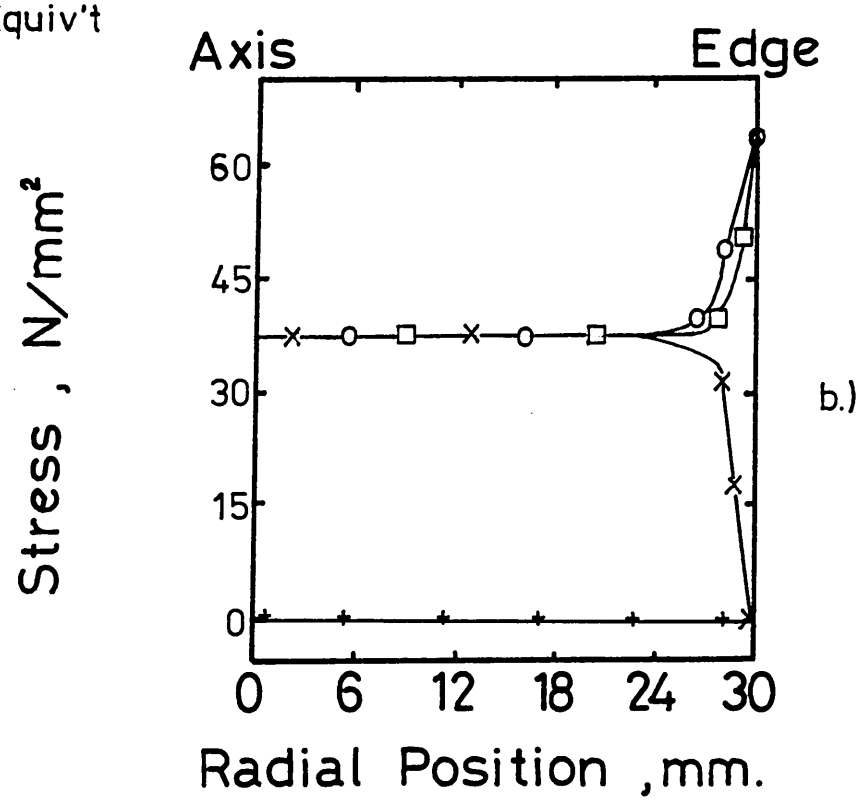

FIGURE 6.4-3 (Continued)

c) DISTRIBUTION OF STRESS ALONG THE CENTRAL PLANE OF THE PLATE AT 0.25 SECONDS INTO THE TWO-DIMENSIONAL (HEAT FLOW) WATER QUENCH ANALYSIS

d) DISTRIBUTION OF STRESS ALONG THE EDGE OF THE PLATE AT 0.25 SECONDS INTO THE TWO-DIMENSIONAL (HEAT FLOW) WATER QUENCH ANALYSIS

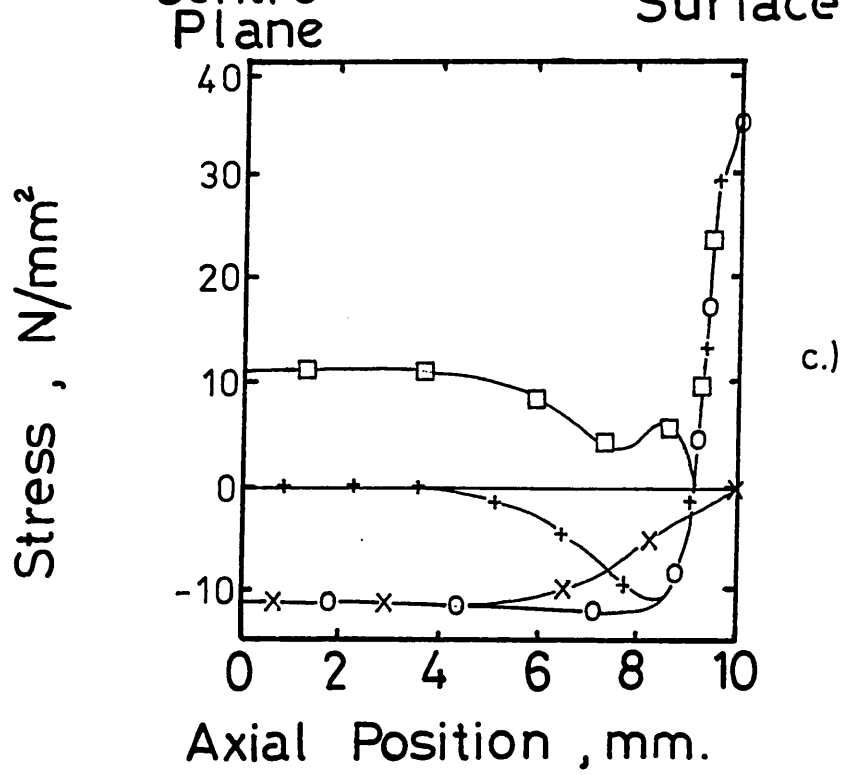

× Radial
o Hoop
+ Axial
□ Equiv't

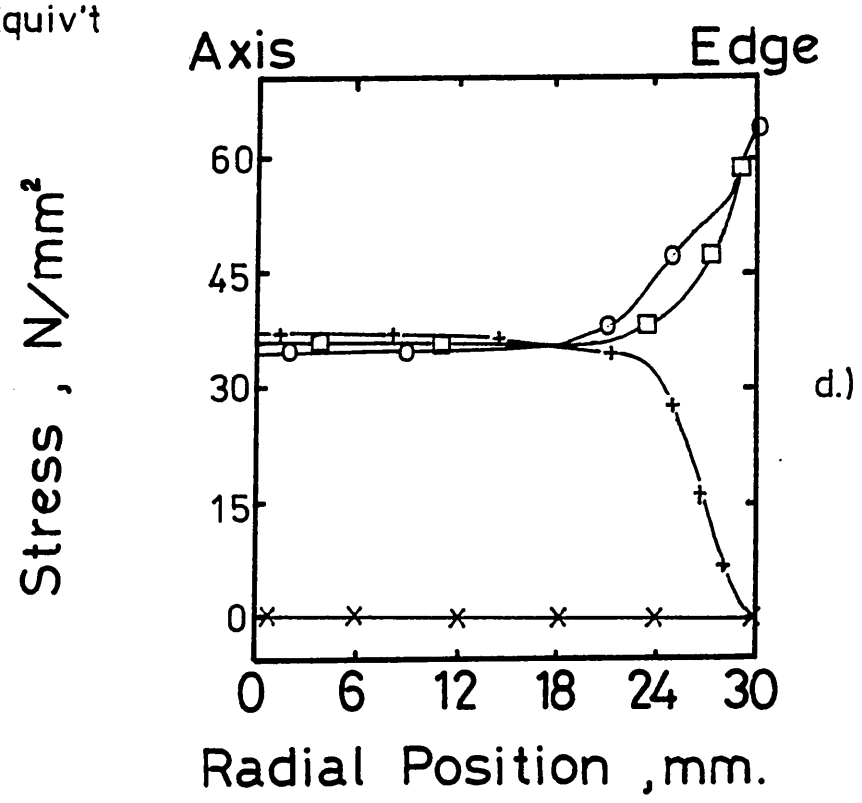

FIGURE 6.4-4

a) DISTRIBUTION OF STRESS ALONG THE AXIS OF THE PLATE AT 1.0 SECOND INTO THE TWO-DIMENSIONAL (HEAT FLOW) WATER QUENCH ANALYSIS

b) DISTRIBUTION OF STRESS ALONG THE SURFACE OF THE PLATE AT 1.0 SECOND INTO THE TWO-DIMENSIONAL (HEAT FLOW) WATER QUENCH ANALYSIS

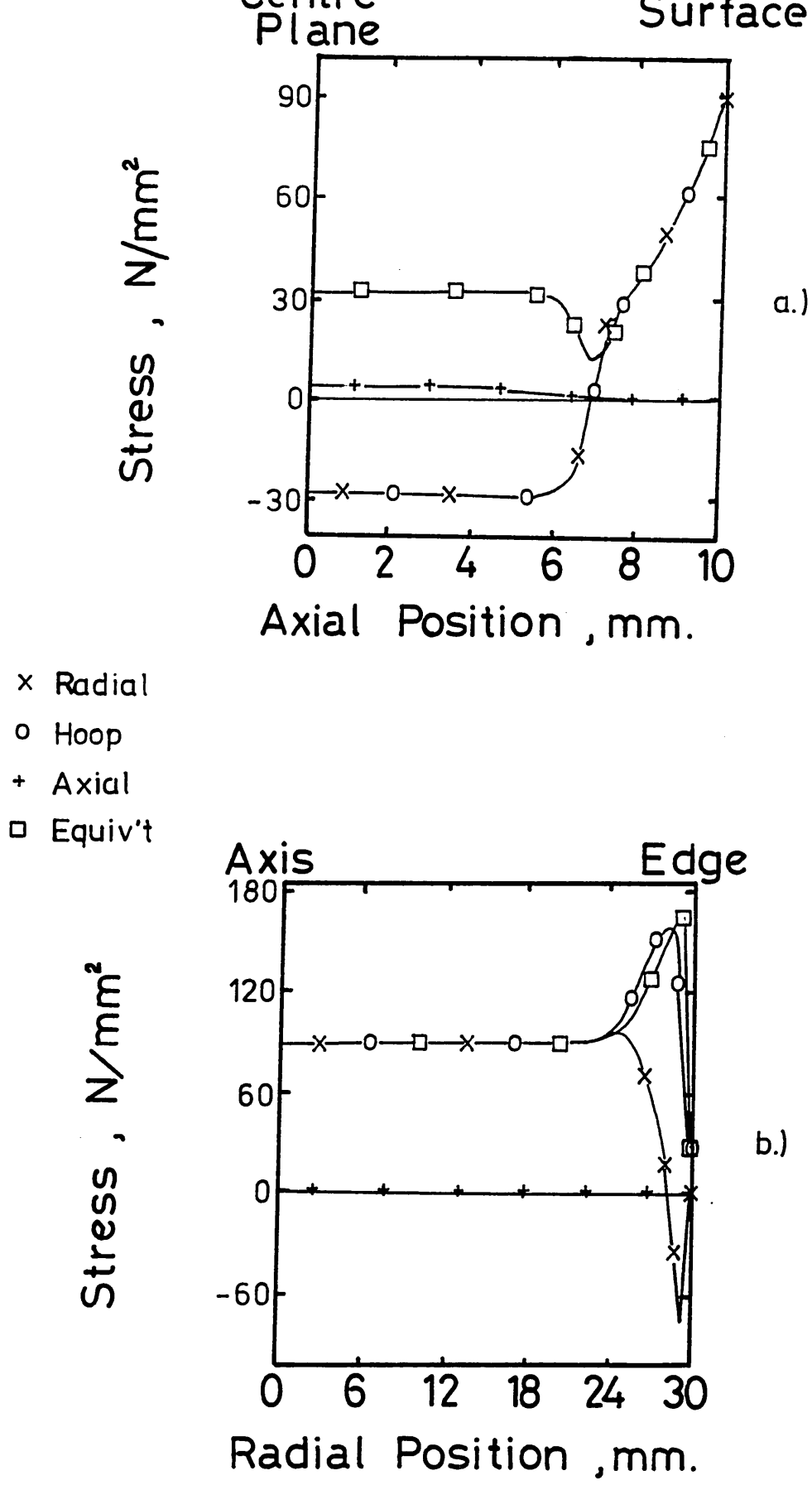
Centre Plane
Surface
90
60
30
0
-30
Stress , N/mm²
0 2 4 6 8 10
Axial Position , mm.
a.)
× Radial
o Hoop
+ Axial
□ Equiv't
Axis
Edge
180
120
60
0
-60
Stress , N/mm²
0 6 12 18 24 30
Radial Position , mm.
b.)

FIGURE 6.4-4 (Continued)

c) DISTRIBUTION OF STRESS ALONG THE CENTRAL PLANE OF THE PLATE AT 1.0 SECOND INTO THE TWO-DIMENSIONAL (HEAT FLOW) WATER QUENCH ANALYSIS

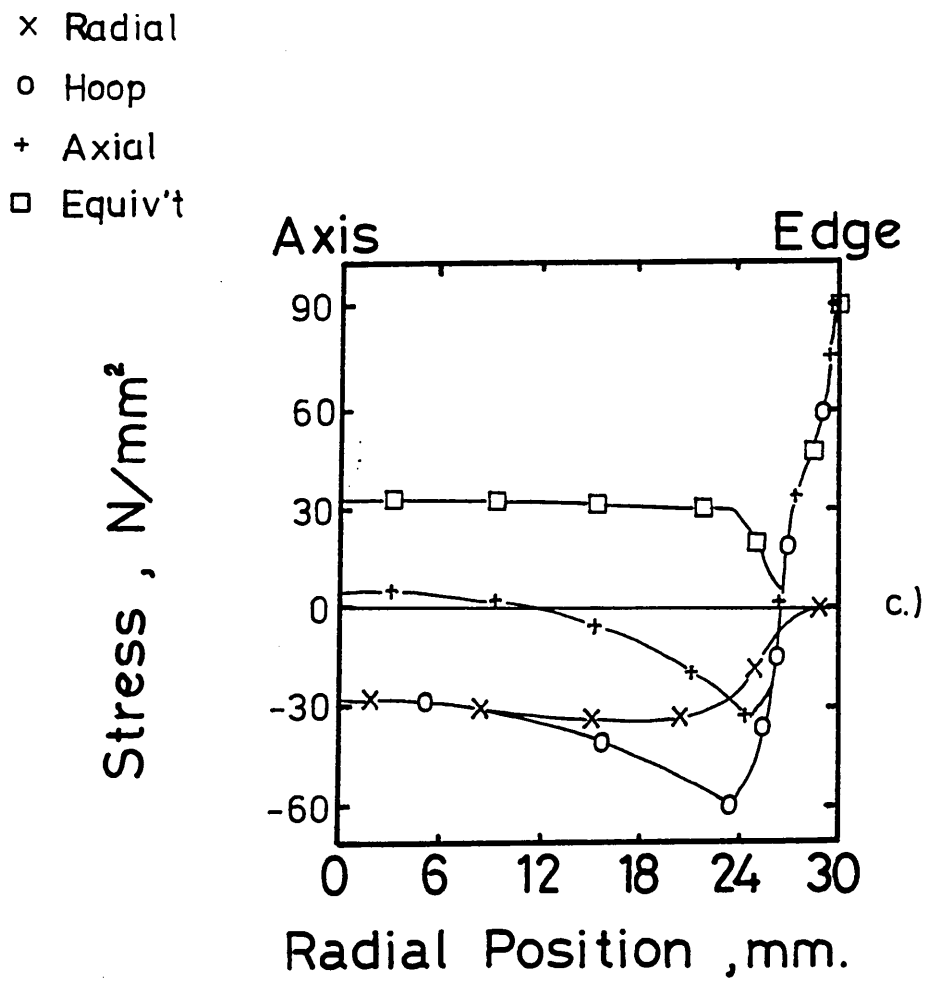
× Radial
o Hoop
+ Axial
□ Equiv't
Axis
Edge
90
60
30
0
-30
-60
0
6
12
18
24
30
Stress , N/mm²
Radial Position , mm.
c.)

FIGURE 6.4-5

a) DISTRIBUTION OF STRESS ALONG THE AXIS OF THE PLATE AT 2.0 SECONDS INTO THE TWO-DIMENSIONAL (HEAT FLOW) WATER QUENCH ANALYSIS

b) DISTRIBUTION OF STRESS ALONG THE SURFACE OF THE PLATE AT 2.0 SECONDS INTO THE TWO-DIMENSIONAL (HEAT FLOW) WATER QUENCH ANALYSIS

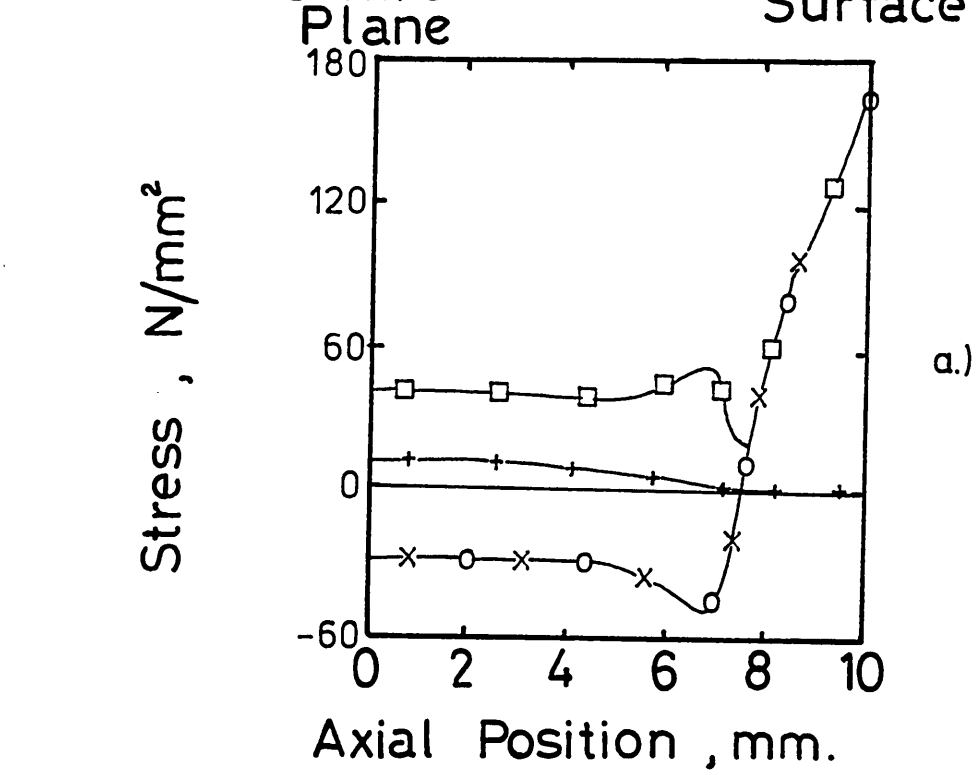

a.)

× Radial
o Hoop
+ Axial
□ Equiv't

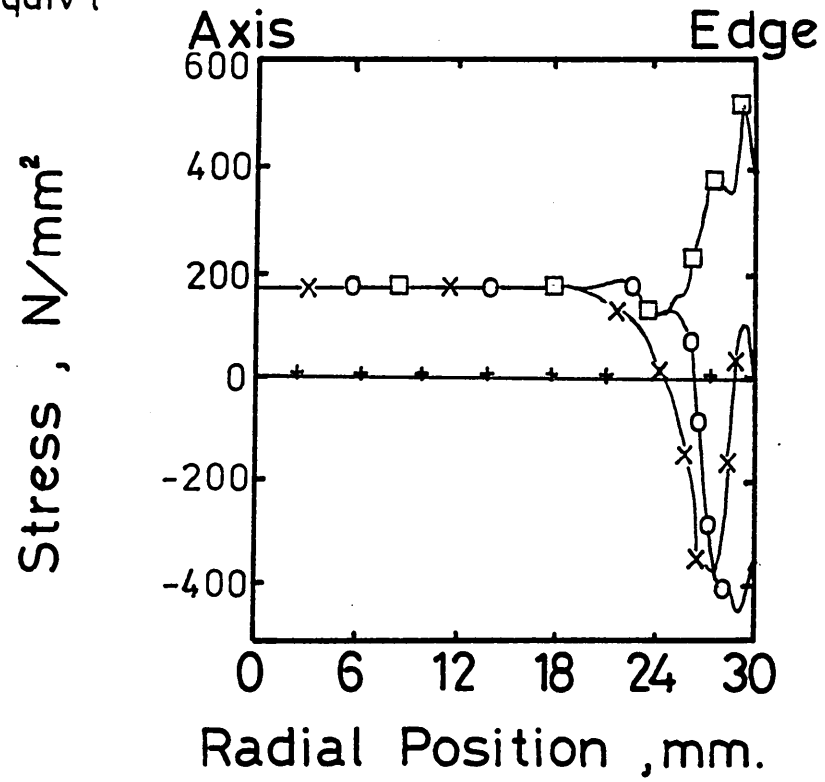

b.)

FIGURE 6.4-5 (Continued)

c) DISTRIBUTION OF STRESS ALONG THE CENTRAL PLANE OF THE PLATE AT 2.0 SECONDS INTO THE TWO-DIMENSIONAL (HEAT FLOW) WATER QUENCH ANALYSIS

d) DISTRIBUTION OF STRESS ALONG THE EDGE OF THE PLATE AT 2.0 SECONDS INTO THE TWO-DIMENSIONAL (HEAT FLOW) WATER QUENCH ANALYSIS

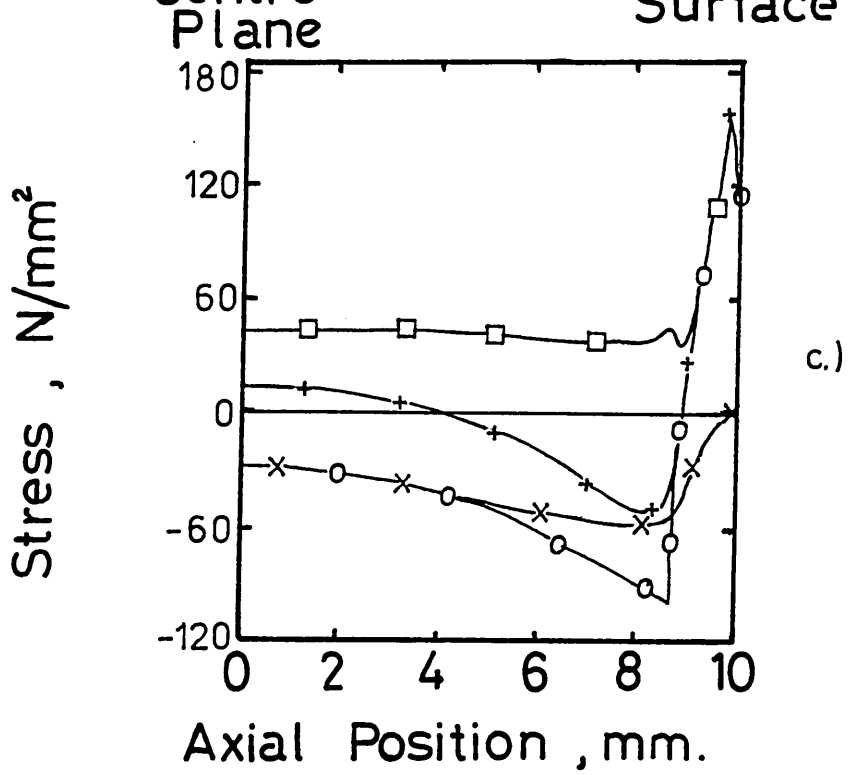

× Radial
o Hoop
+ Axial
□ Equiv't

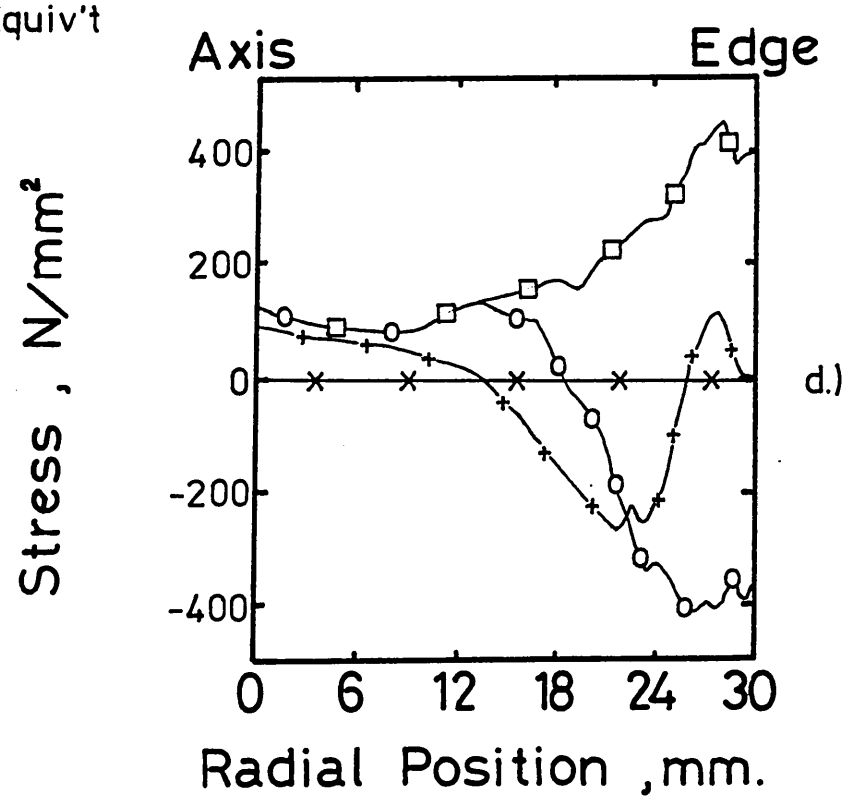

FIGURE 6.4-6

a) DISTRIBUTION OF STRESS ALONG THE AXIS OF THE PLATE AT 5.6 SECONDS INTO THE TWO-DIMENSIONAL (HEAT FLOW) WATER QUENCH ANALYSIS

b) DISTRIBUTION OF STRESS ALONG THE SURFACE OF THE PLATE AT 5.6 SECONDS INTO THE TWO-DIMENSIONAL (HEAT FLOW) WATER QUENCH ANALYSIS

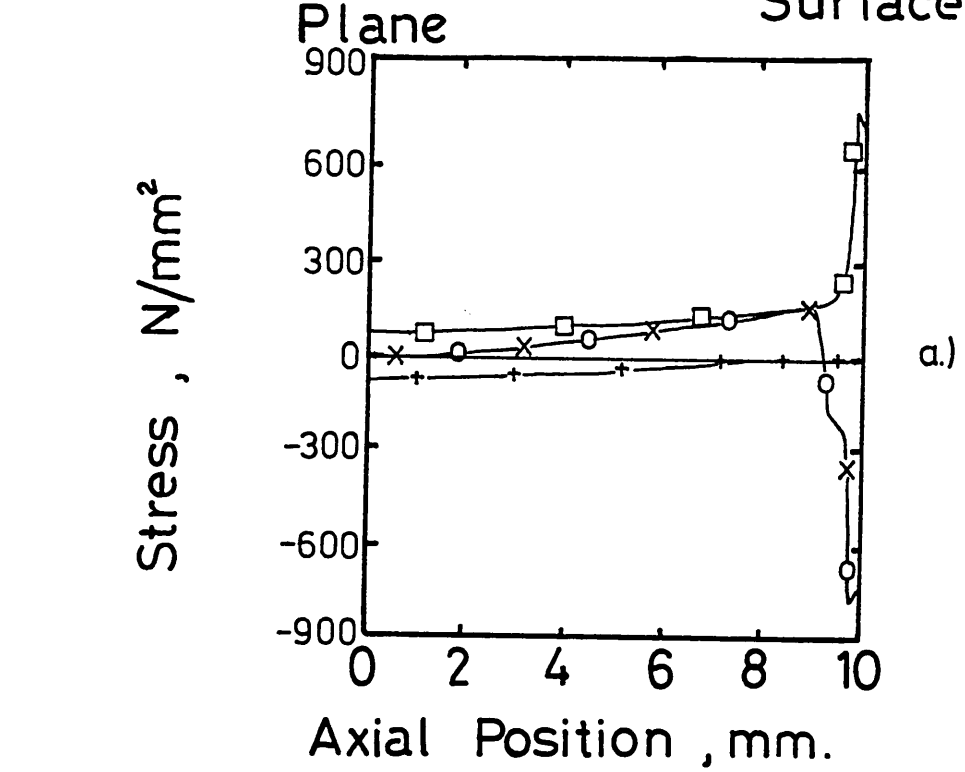

× Radial
o Hoop
+ Axial
□ Equiv't

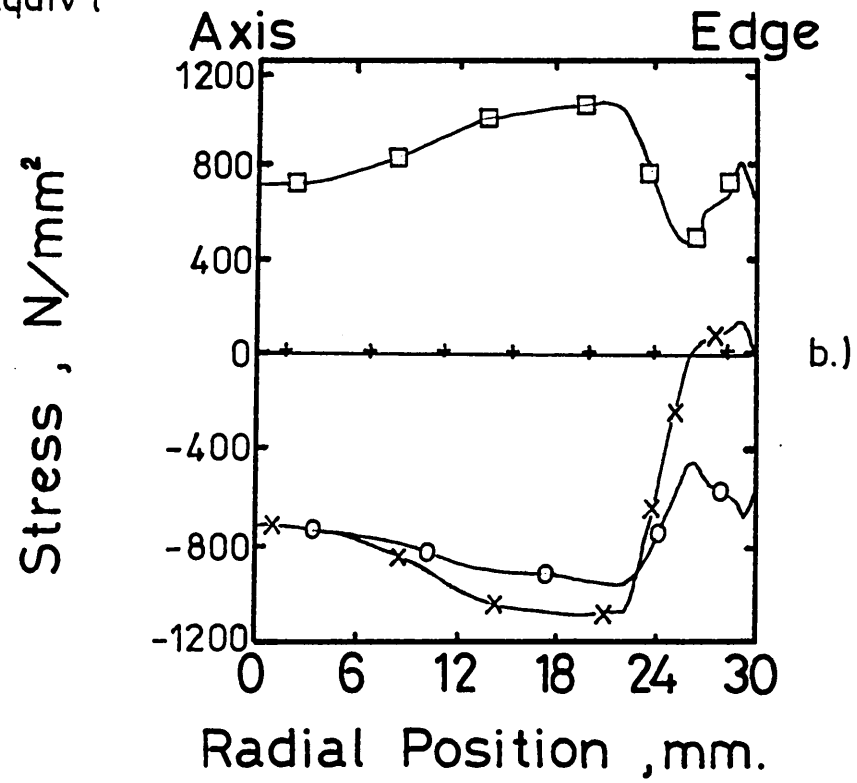

FIGURE 6.4-6 (Continued)

c) DISTRIBUTION OF STRESS ALONG THE CENTRAL PLANE OF THE PLATE AT 5.6 SECONDS INTO THE TWO-DIMENSIONAL (HEAT FLOW) WATER QUENCH ANALYSIS

d) DISTRIBUTION OF STRESS ALONG THE EDGE OF THE PLATE AT 5.6 SECONDS INTO THE TWO-DIMENSIONAL (HEAT FLOW) WATER QUENCH ANALYSIS

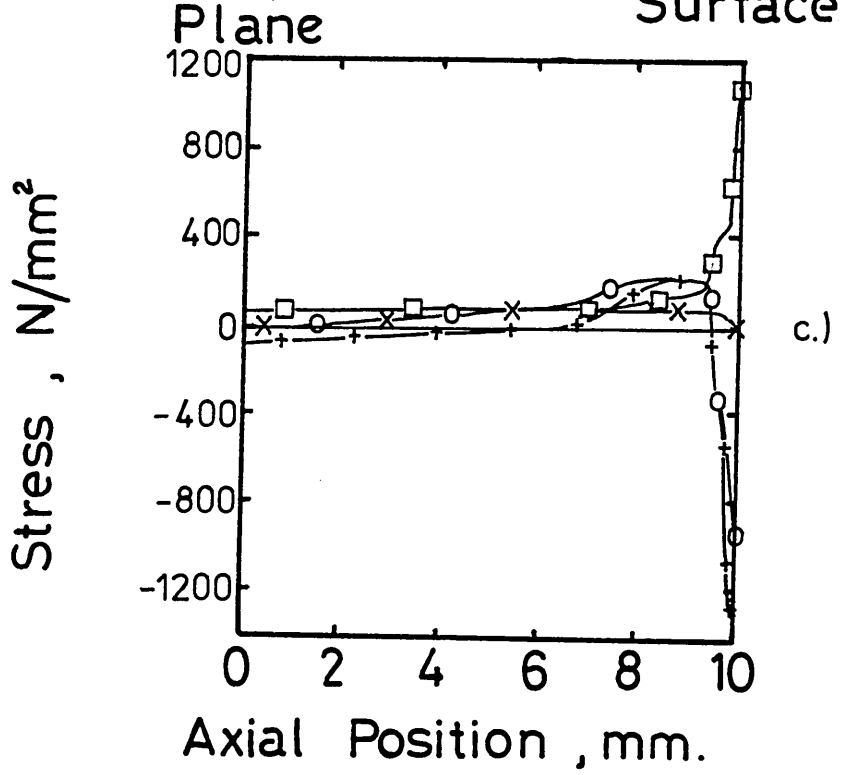

× Radial
o Hoop
+ Axial
□ Equiv't

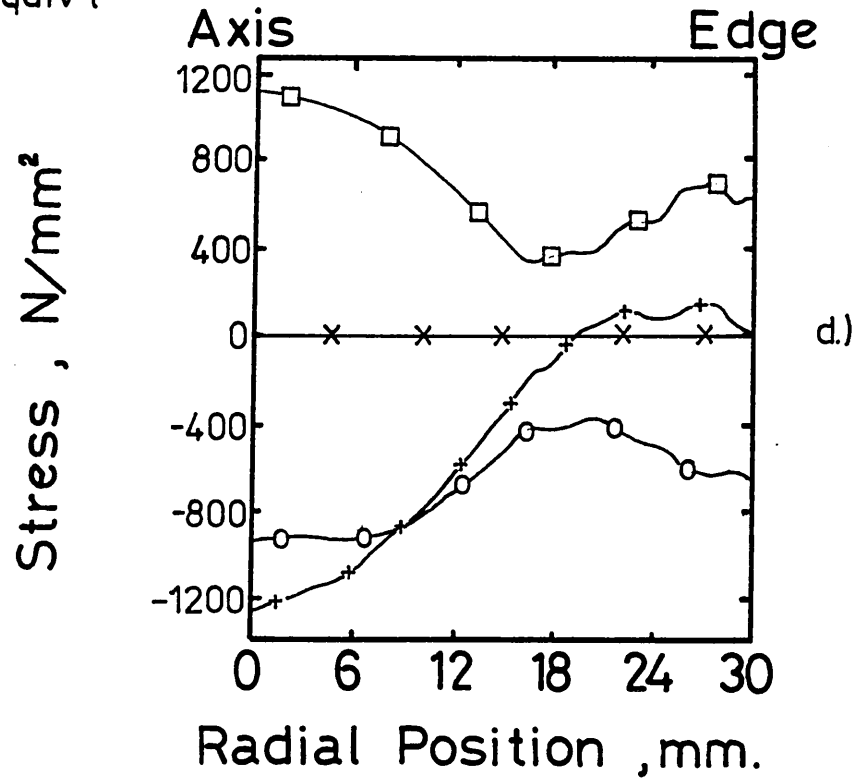

FIGURE 6.4-7

a) DISTRIBUTION OF STRESS ALONG THE AXIS OF THE PLATE AT 9.8 SECONDS INTO THE TWO-DIMENSIONAL (HEAT FLOW) WATER QUENCH ANALYSIS

b) DISTRIBUTION OF STRESS ALONG THE SURFACE OF THE PLATE AT 9.8 SECONDS INTO THE TWO-DIMENSIONAL (HEAT FLOW) WATER QUENCH ANALYSIS

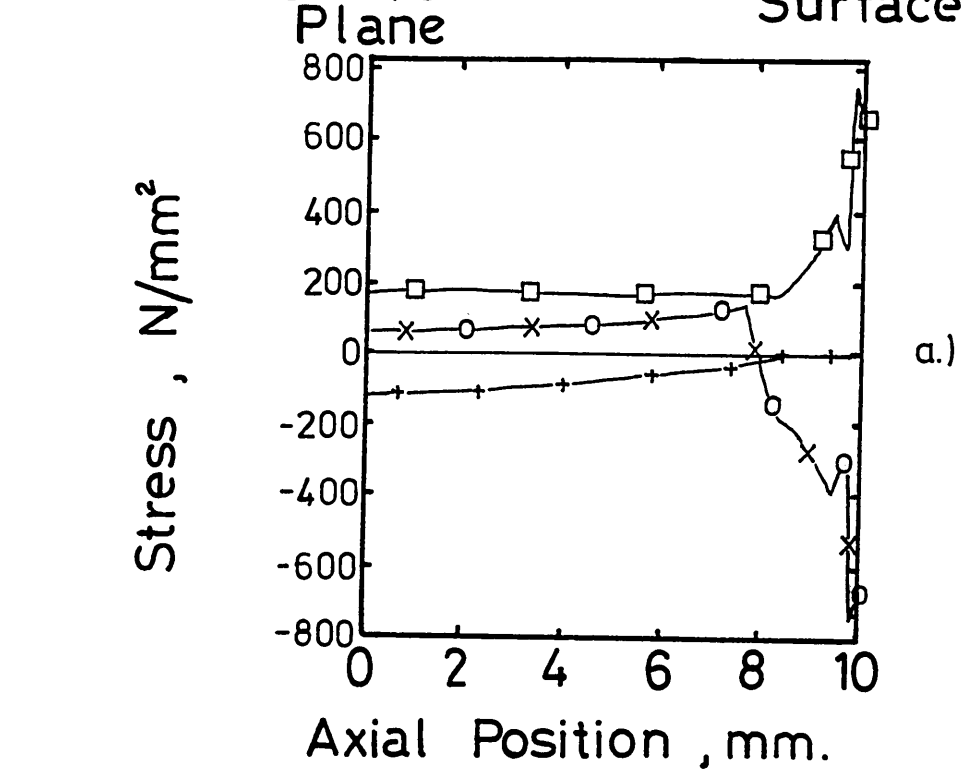

× Radial
o Hoop
+ Axial
□ Equiv't

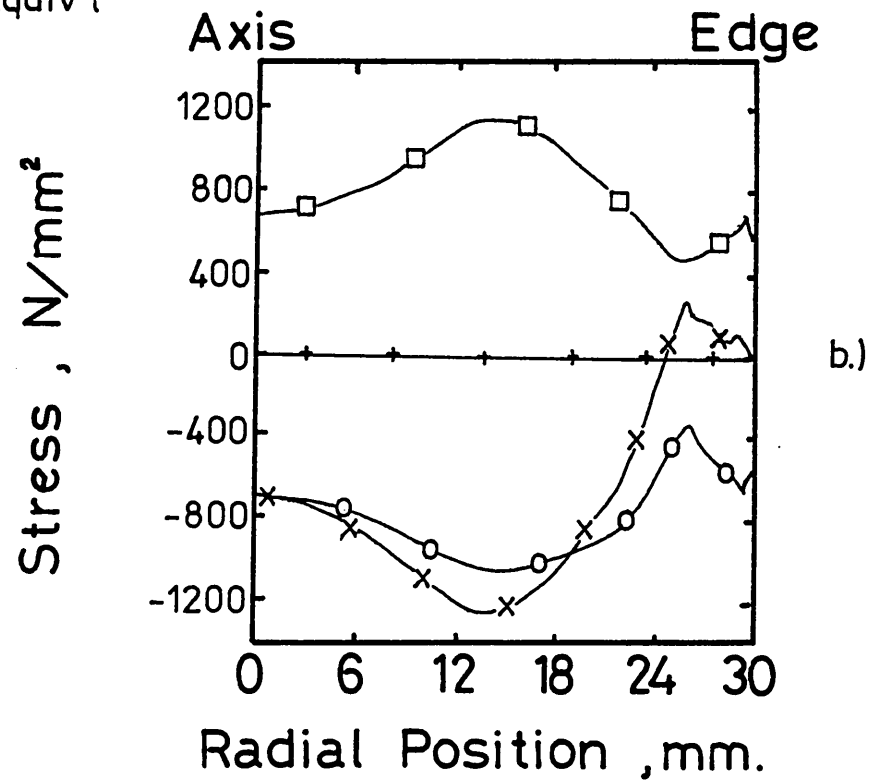

FIGURE 6.4-7 (Continued)

c) DISTRIBUTION OF STRESS ALONG THE CENTRAL PLANE OF THE PLATE AT 9.8 SECONDS INTO THE TWO-DIMENSIONAL (HEAT FLOW) WATER QUENCH ANALYSIS

d) DISTRIBUTION OF STRESS ALONG THE EDGE OF THE PLATE AT 9.8 SECONDS INTO THE TWO-DIMENSIONAL (HEAT FLOW) WATER QUENCH ANALYSIS

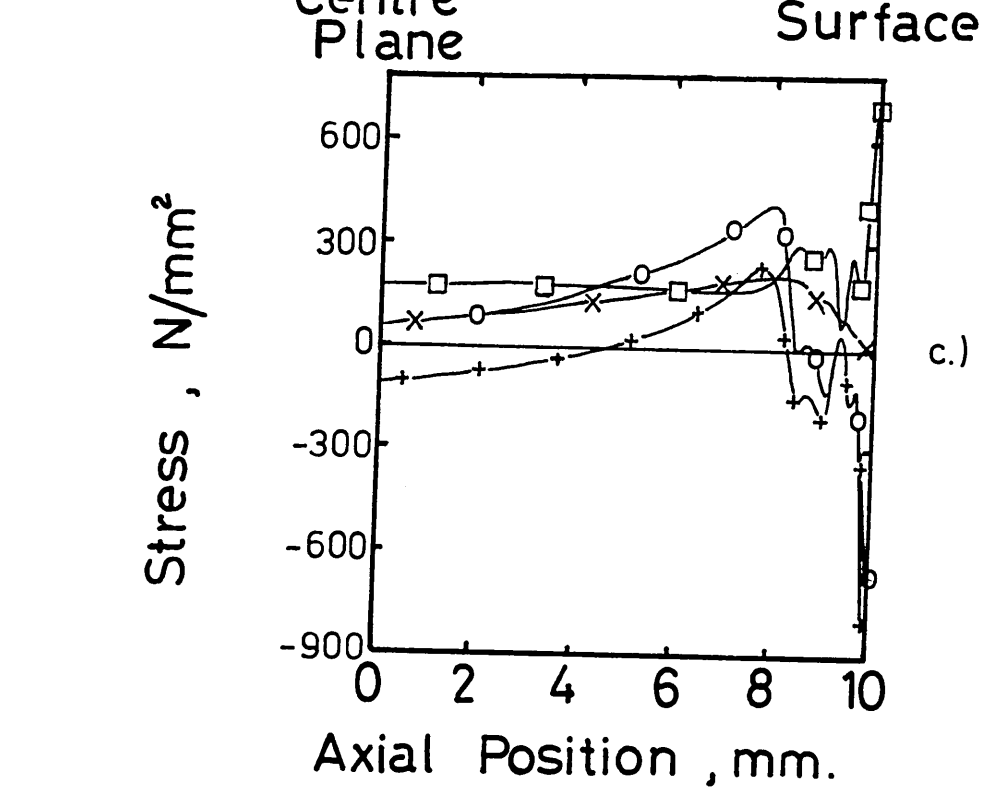

× Radial
o Hoop
+ Axial
□ Equiv't

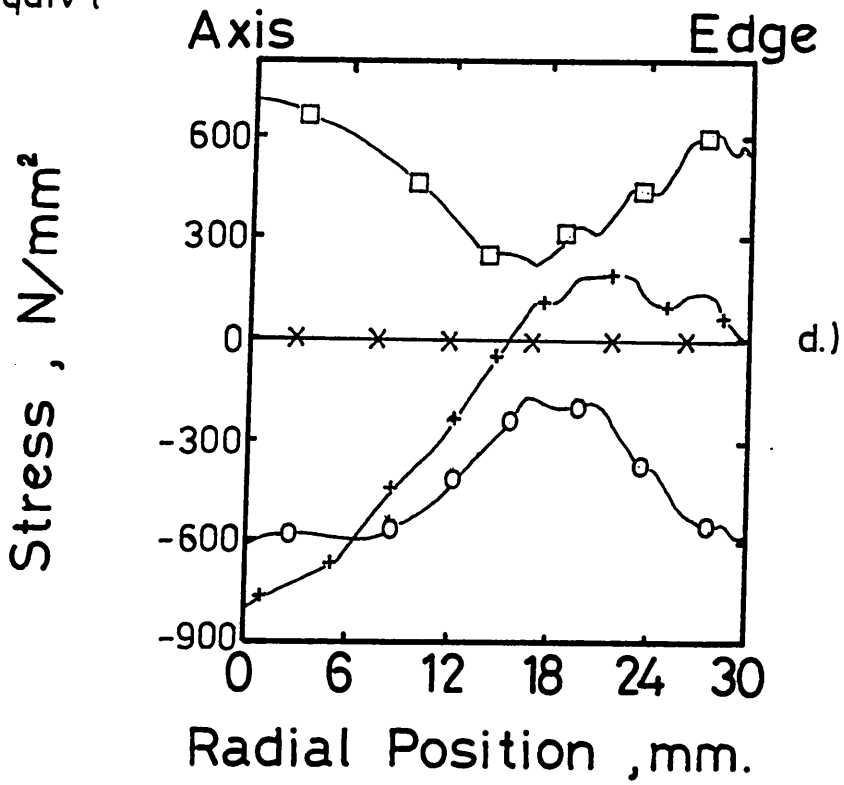

FIGURE 6.5-1

a) DISTRIBUTION OF STRESS ALONG THE AXIS OF A 30 mm RADIUS PLATE AT 0.02 SECONDS INTO THE UNIDIRECTIONAL WATER QUENCH ANALYSIS

b) DISTRIBUTION OF STRESS ALONG THE EDGE OF A 30 mm RADIUS PLATE AT 0.02 SECONDS INTO THE UNIDIRECTIONAL WATER QUENCH ANALYSIS

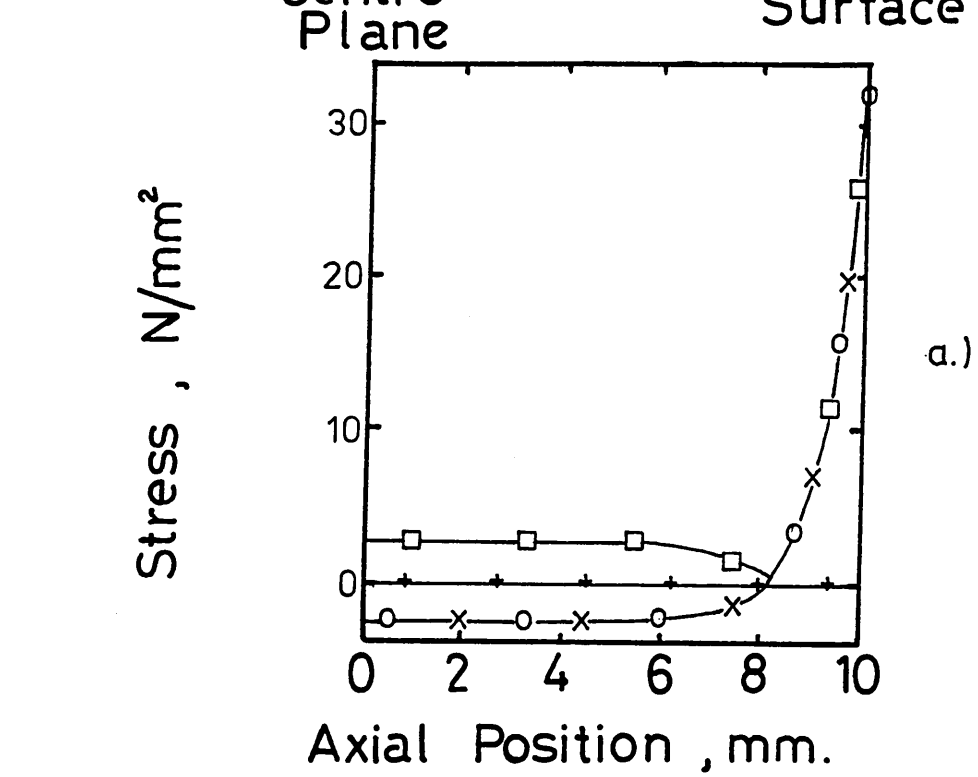

× Radial
o Hoop
+ Axial
□ Equiv't

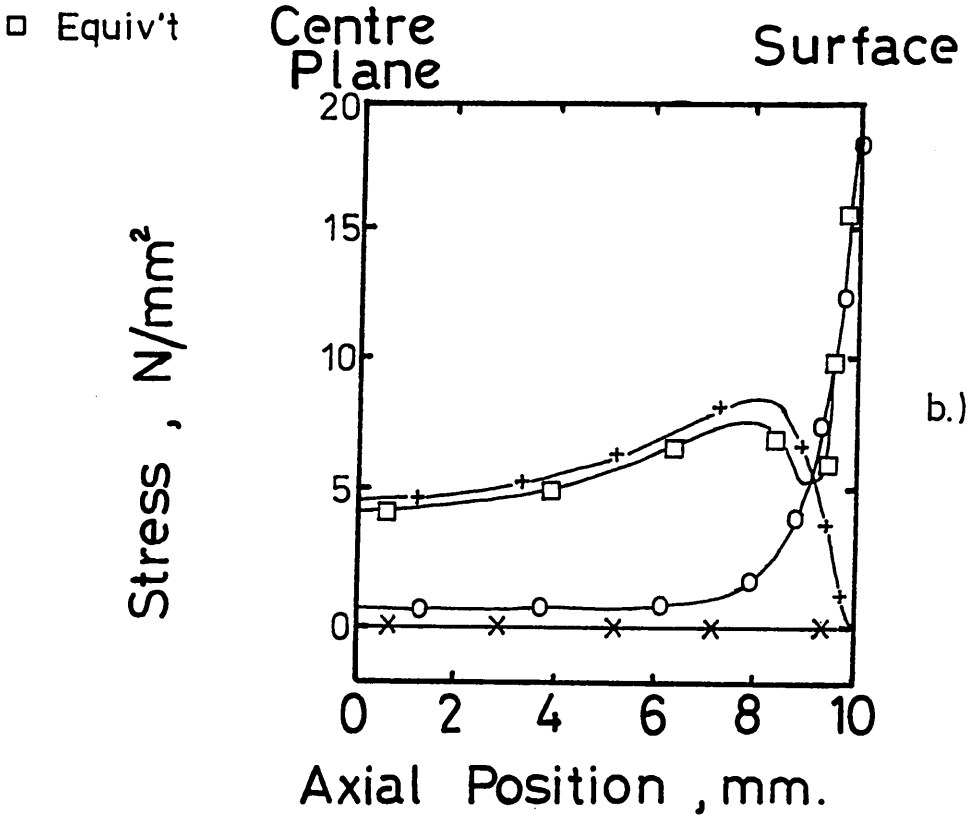

FIGURE 6.5-1 (Continued)

c) DISTRIBUTION OF STRESS ALONG THE SURFACE OF A 30 mm RADIUS PLATE AT 0.02 SECONDS INTO THE UNIDIRECTIONAL WATER QUENCH ANALYSIS

d) DISTRIBUTION OF STRESS ALONG THE CENTRAL PLANE OF A 30 mm RADIUS PLATE AT 0.02 SECONDS INTO THE UNIDIRECTIONAL WATER QUENCH ANALYSIS

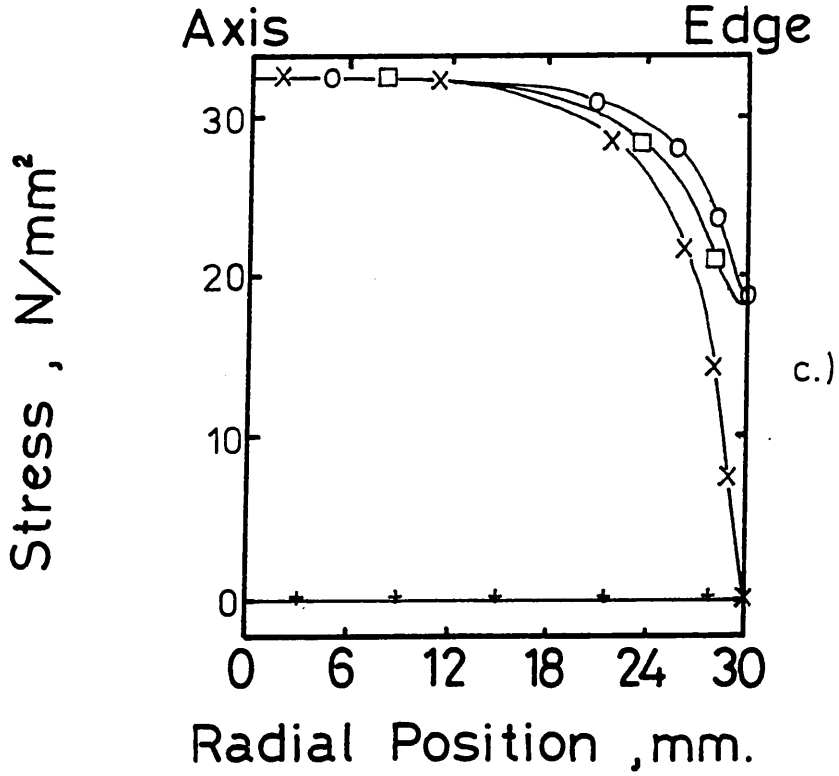

c.)

× Radial
o Hoop
+ Axial
□ Equiv't

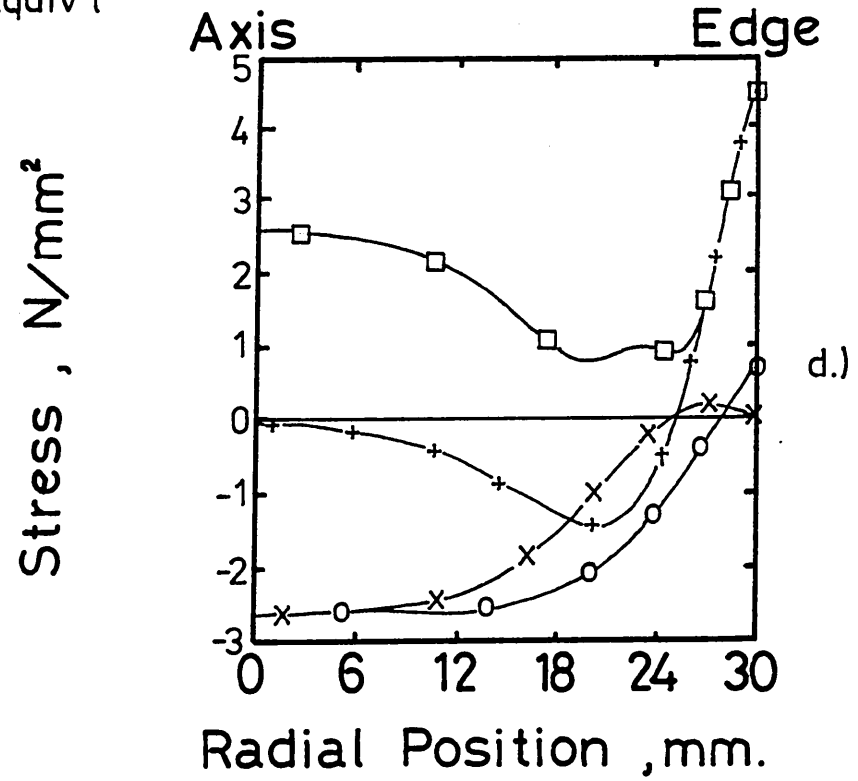

d.)

FIGURE 6.5-2

a) DISTRIBUTION OF STRESS ALONG THE AXIS OF A 30 mm RADIUS PLATE AT 0.2 SECONDS INTO THE UNIDIRECTIONAL WATER QUENCH ANALYSIS

b) DISTRIBUTION OF STRESS ALONG THE EDGE OF A 30 mm RADIUS PLATE AT 0.2 SECONDS INTO THE UNIDIRECTIONAL WATER QUENCH ANALYSIS

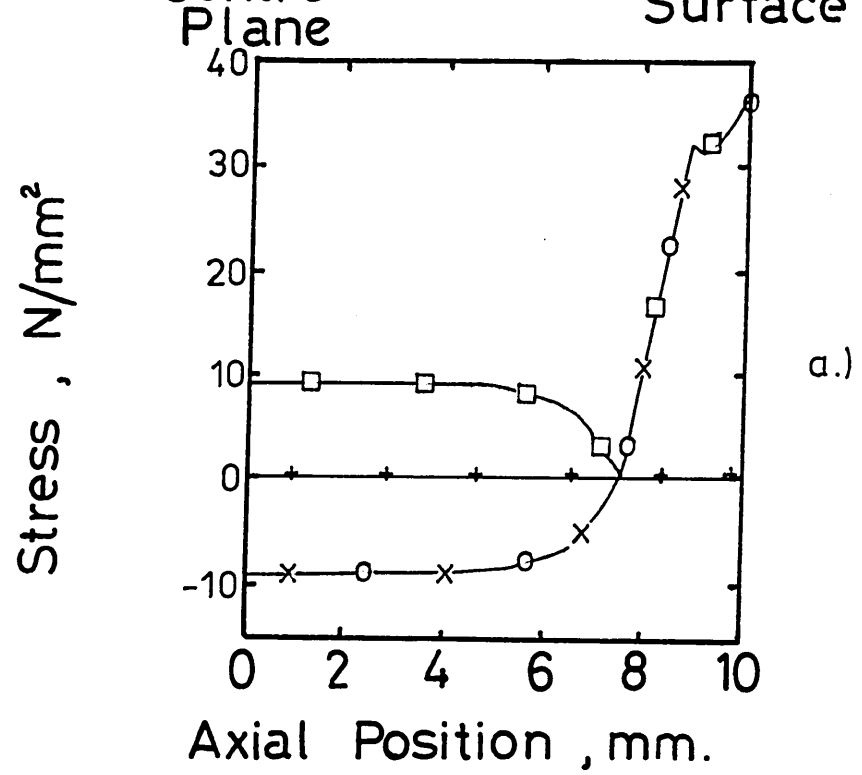

× Radial
o Hoop
+ Axial
□ Equiv't

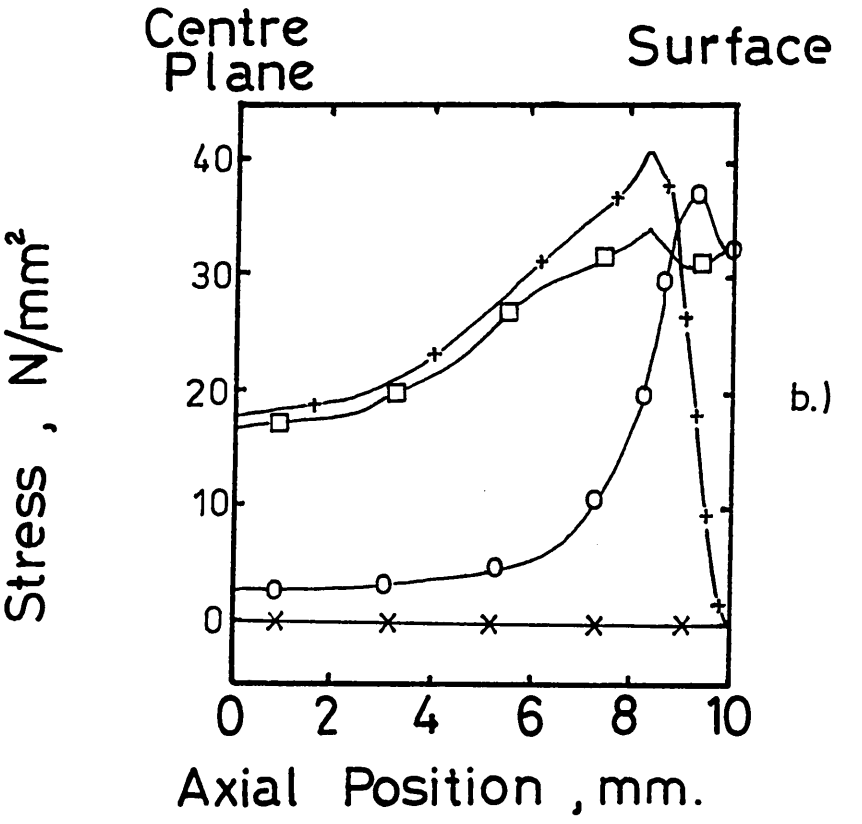

FIGURE 6.5-2 (Continued)

c) DISTRIBUTION OF STRESS ALONG THE SURFACE OF A 30 mm RADIUS PLATE AT 0.2 SECONDS INTO THE UNIDIRECTIONAL WATER QUENCH ANALYSIS

d) DISTRIBUTION OF STRESS ALONG THE CENTRAL PLANE OF A 30 mm RADIUS PLATE AT 0.2 SECONDS INTO THE UNIDIRECTIONAL WATER QUENCH ANALYSIS

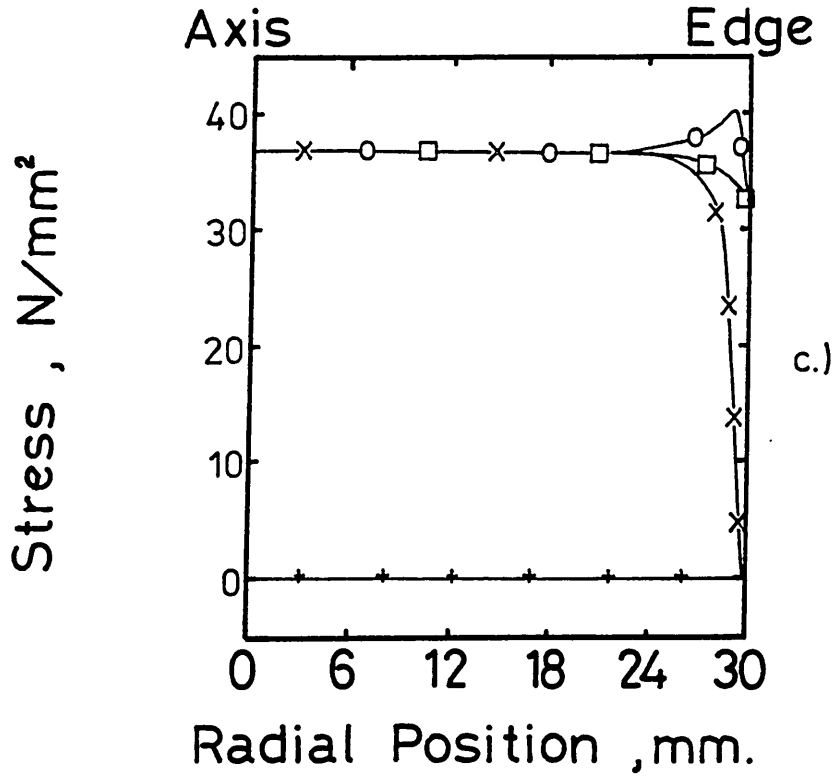

× Radial
o Hoop
+ Axial
□ Equiv't

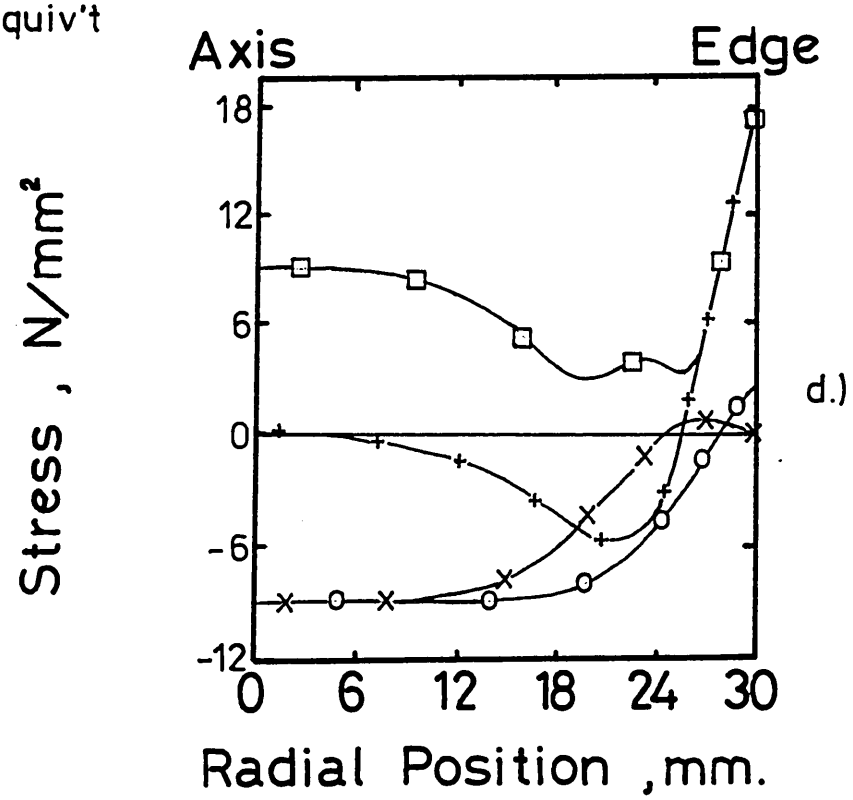

FIGURE 6.5-3

a) DISTRIBUTION OF STRESS ALONG THE SURFACE OF A 60 mm RADIUS PLATE AT 0.02 SECONDS INTO THE UNIDIRECTIONAL WATER QUENCH ANALYSIS

b) DISTRIBUTION OF STRESS ALONG THE CENTRAL PLANE OF A 60 mm RADIUS PLATE AT 0.02 SECONDS INTO THE UNIDIRECTIONAL WATER QUENCH ANALYSIS

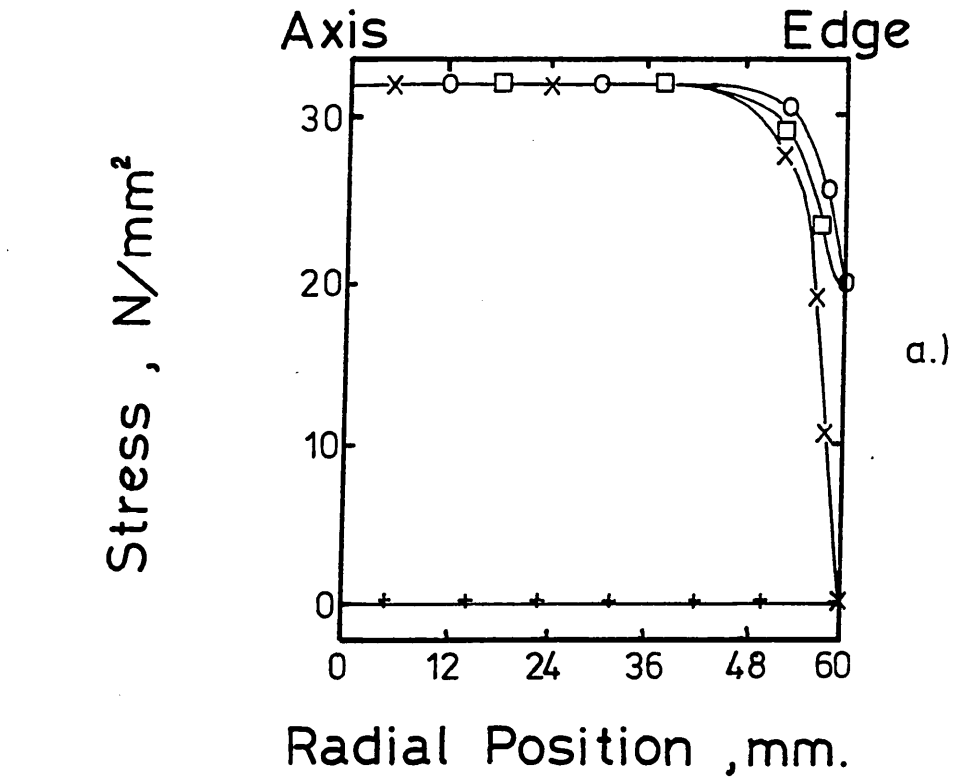

× Radial
o Hoop
+ Axial
□ Equiv't

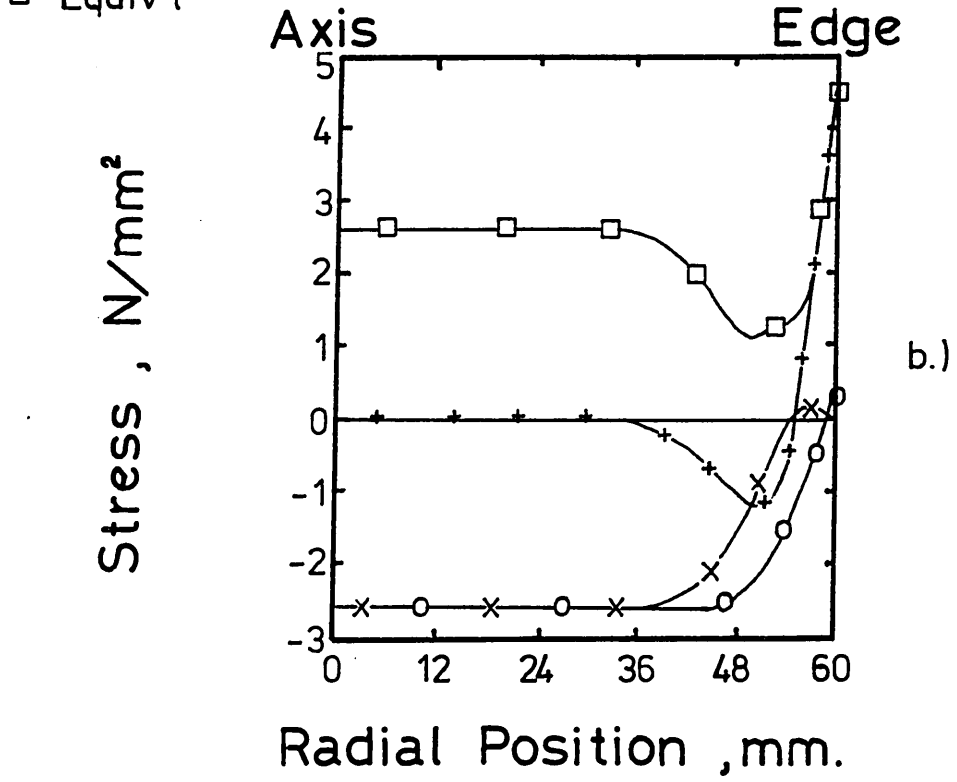

FIGURE 6.5-4

a) DISTRIBUTION OF STRESS ALONG THE SURFACE OF A 60 mm RADIUS PLATE AT 0.2 SECONDS INTO THE UNIDIRECTIONAL WATER QUENCH ANALYSIS

b) DISTRIBUTION OF STRESS ALONG THE CENTRAL PLANE OF A 60 mm RADIUS PLATE AT 0.2 SECONDS INTO THE UNIDIRECTIONAL WATER QUENCH ANALYSIS

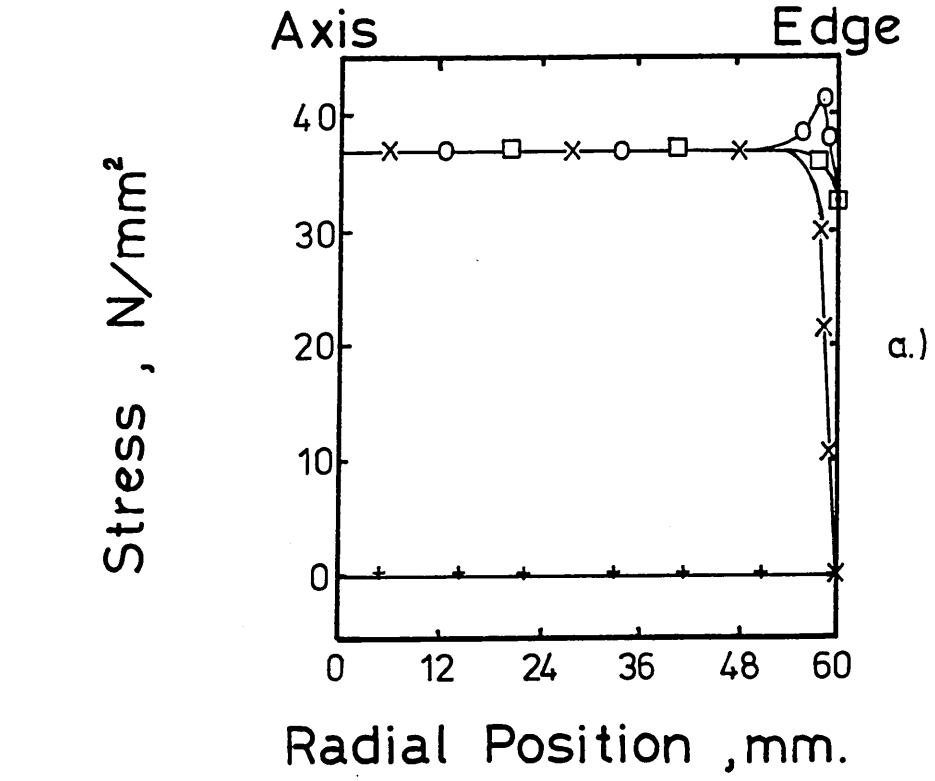

× Radial
o Hoop
+ Axial
□ Equiv't

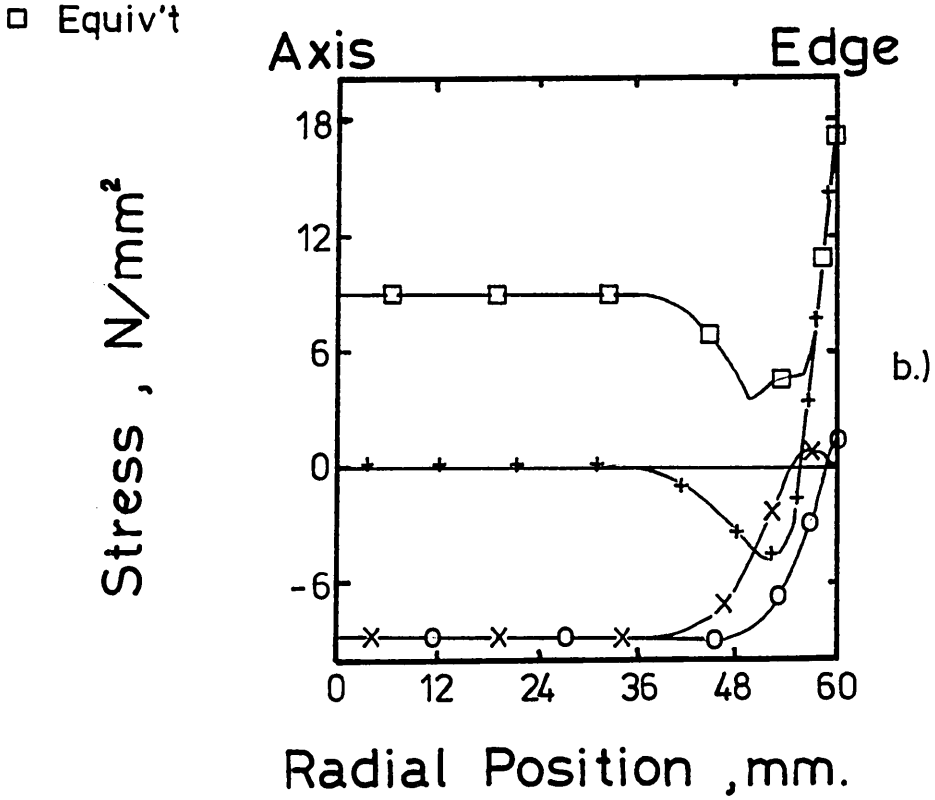

FIGURE 6.5-5

a) DISTRIBUTION OF STRESS ALONG THE SURFACE OF A 15 mm RADIUS PLATE AT 0.02 SECONDS INTO THE UNIDIRECTIONAL WATER QUENCH ANALYSIS

b) DISTRIBUTION OF STRESS ALONG THE CENTRAL PLANE OF A 15 mm RADIUS PLATE AT 0.02 SECONDS INTO THE UNIDIRECTIONAL WATER QUENCH ANALYSIS

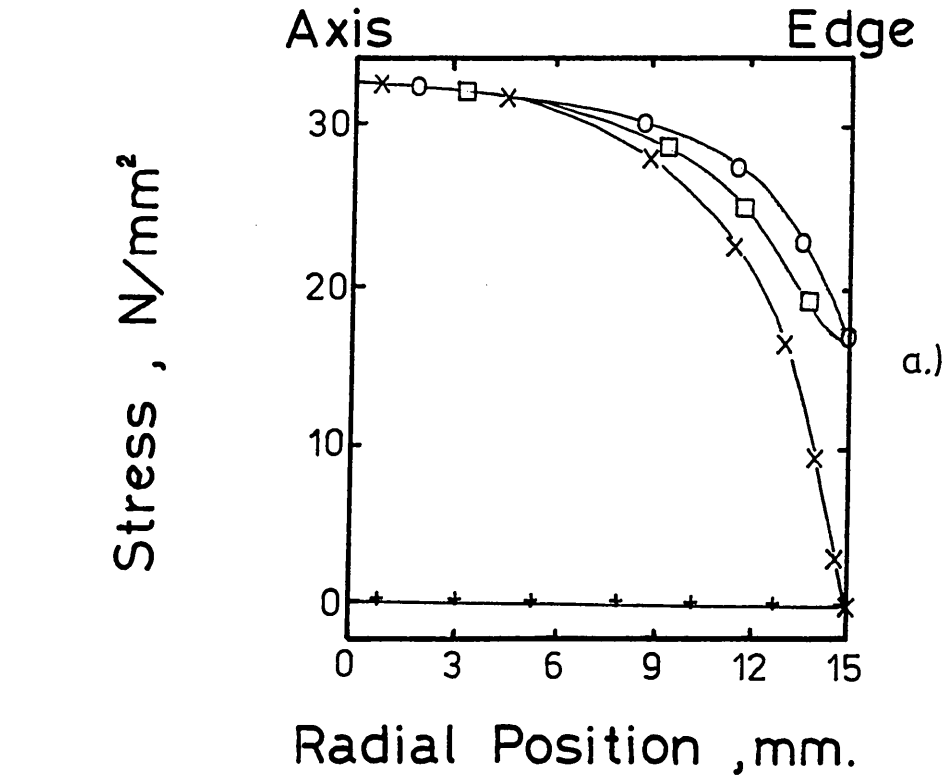

× Radial
o Hoop
+ Axial
□ Equiv't

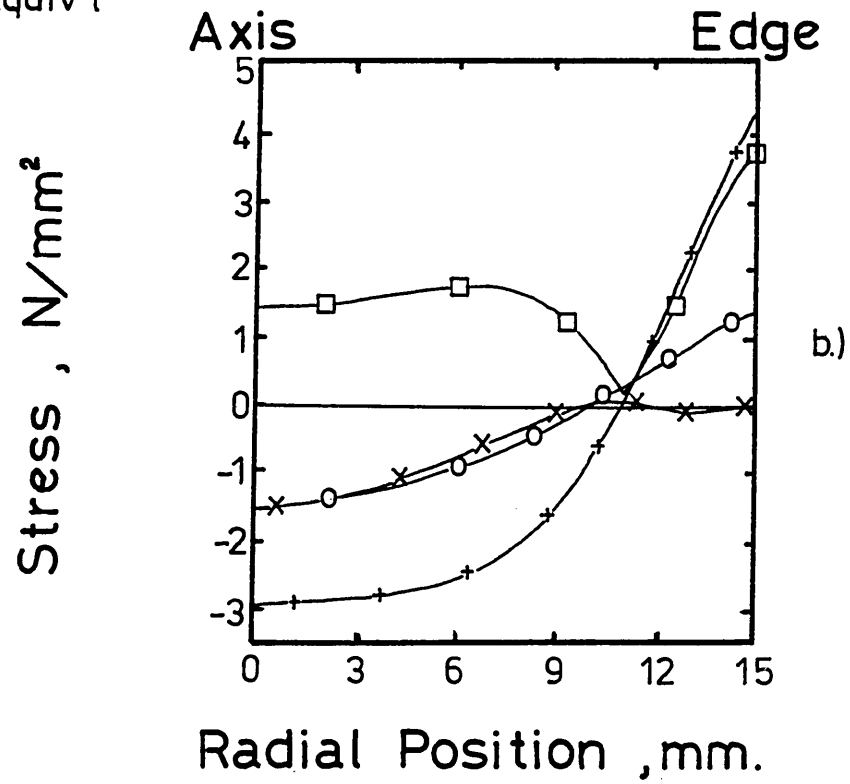

FIGURE 6.5-6

a) DISTRIBUTION OF STRESS ALONG THE SURFACE OF A 15 mm RADIUS PLATE AT 0.02 SECONDS INTO THE UNIDIRECTIONAL WATER QUENCH ANALYSIS

b) DISTRIBUTION OF STRESS ALONG THE CENTRAL PLANE OF A 15 mm RADIUS PLATE AT 0.2 SECONDS INTO THE UNIDIRECTIONAL WATER QUENCH ANALYSIS

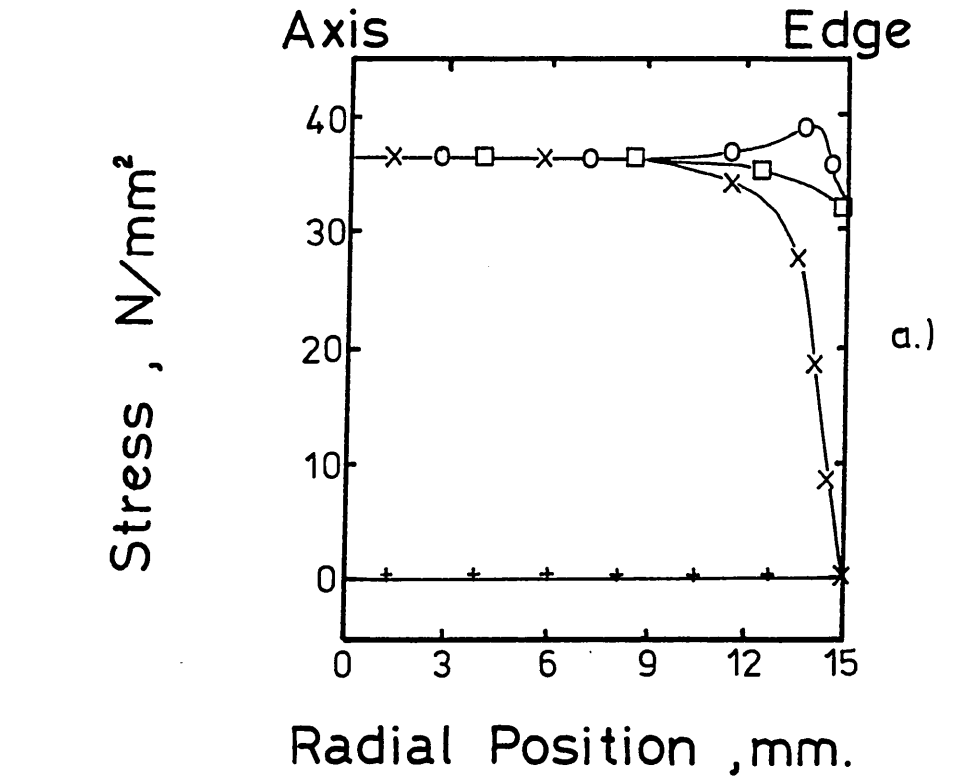

× Radial
o Hoop
+ Axial
□ Equiv't

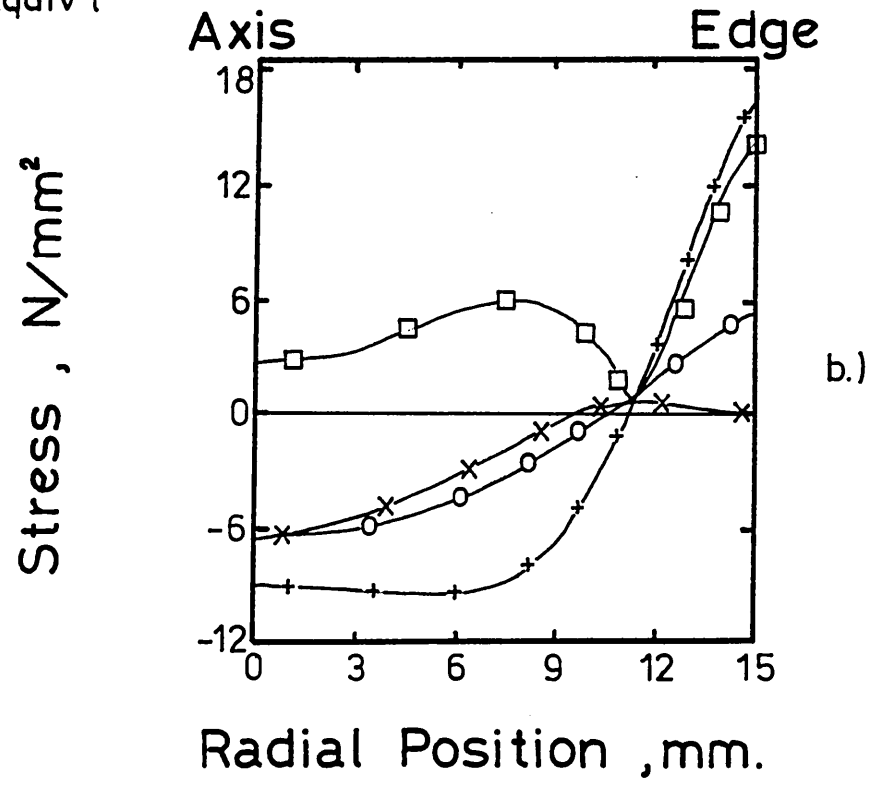

FIGURE 6.5-7

a) DISTRIBUTION OF STRESS ALONG THE EDGE OF A 2 mm RADIUS HOLE IN THE CENTRE OF A 32 mm RADIUS PLATE AT 0.2 SECONDS INTO THE UNIDIRECTIONAL WATER QUENCH ANALYSIS

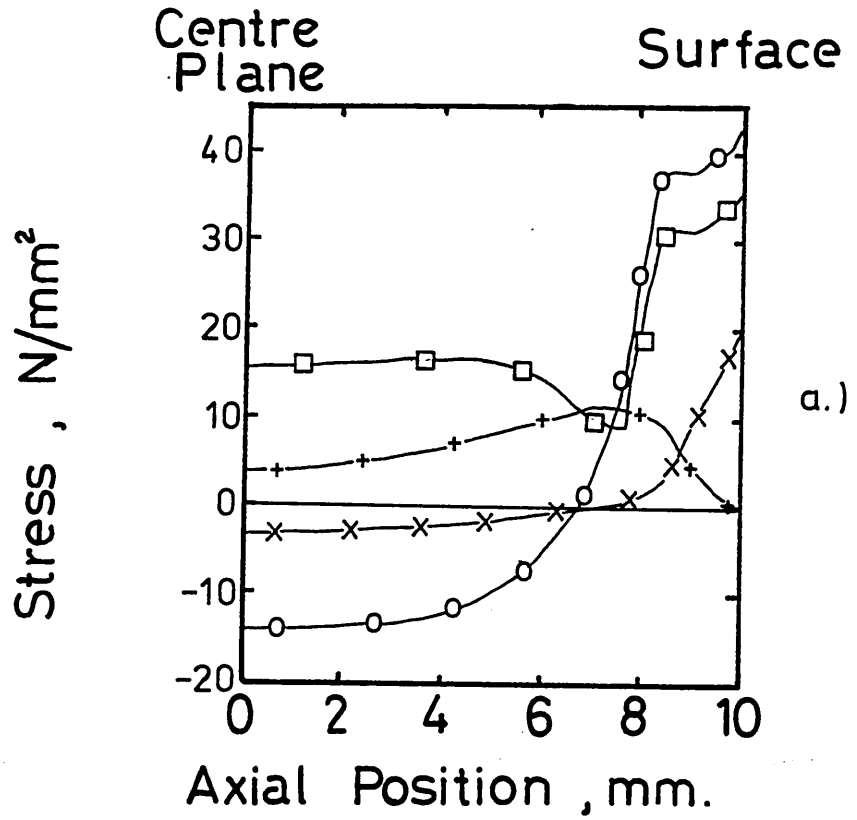
Centre Plane
Surface
Stress , N/mm²
40
30
20
10
0
-10
-20
0
2
4
6
8
10
Axial Position , mm.
a.)
× Radial
o Hoop
+ Axial
□ Equiv't

FIGURE 6.5-7 (Continued)

b) DISTRIBUTION OF STRESS ALONG THE SURFACE OF A 32 mm RADIUS PLATE (WITH A 2 mm RADIUS CENTRAL HOLE) AT 0.2 SECONDS INTO THE UNIDIRECTIONAL WATER QUENCH ANALYSIS

c) DISTRIBUTION OF STRESS ALONG THE CENTRAL PLANE OF A 32 mm RADIUS PLATE (WITH A 2 mm RADIUS CENTRAL HOLE) AT 0.2 SECONDS INTO THE UNIDIRECTIONAL WATER QUENCH ANALYSIS

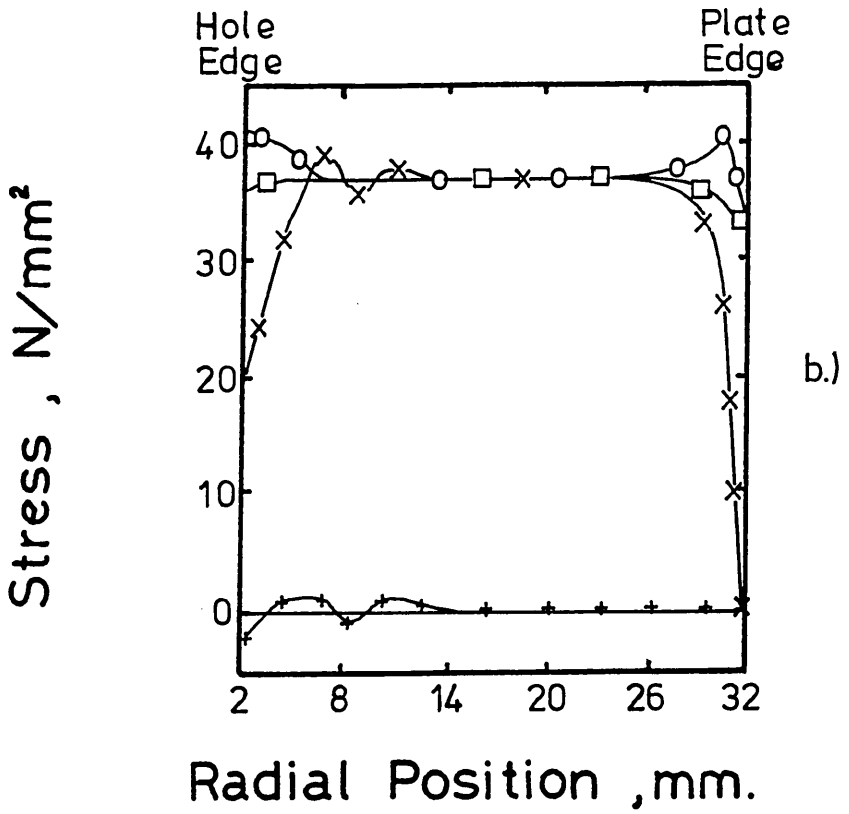

b.)

× Radial
o Hoop
+ Axial
□ Equiv't

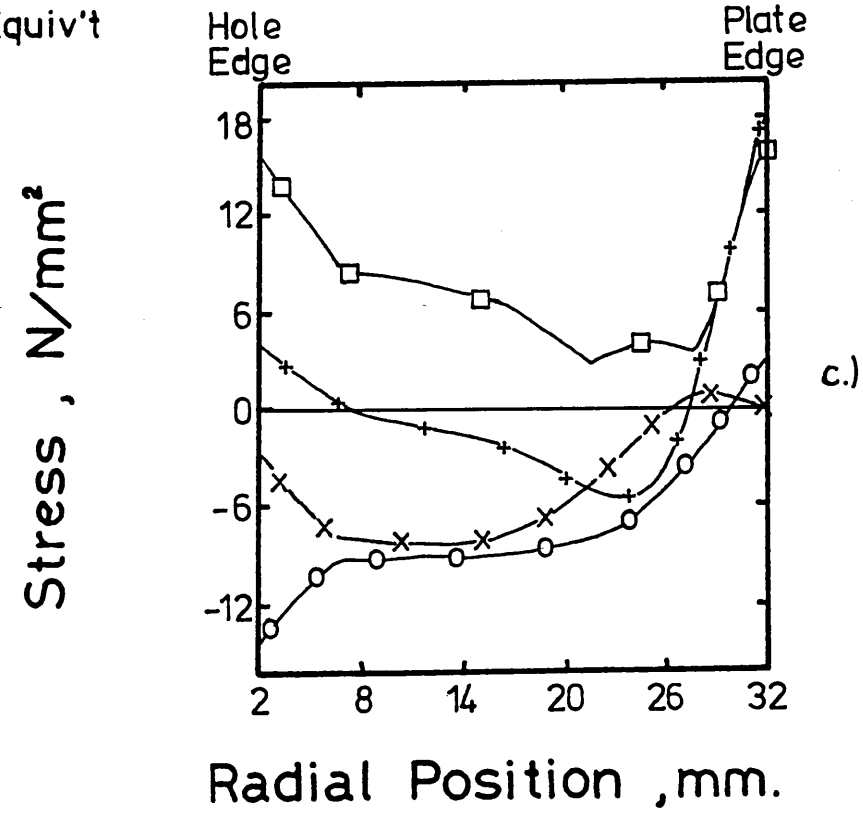

c.)

FIGURE 7.2-1

MODIFICATION OF THE EDGE EFFECTED ZONE (EEZ) BY PLASTICITY

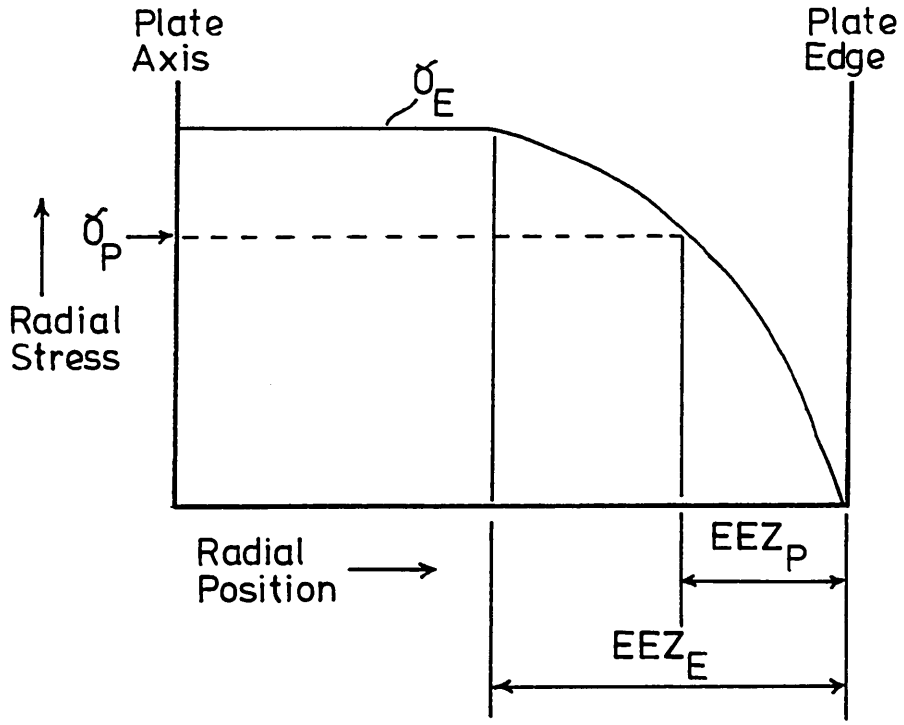

E - Elastic

P - Plastic

FIGURE 7.5-1

COMPARISON OF RESIDUAL STRESS RESULTS ALONG THE PLATE AXIS BETWEEN FINITE ELEMENT AND FINITE DIFFERENCE MODELS, ACCOMPANIED BY EXPERIMENTAL DATA FROM PREVIOUS WORK

(20 mm thick, water quenched plates)

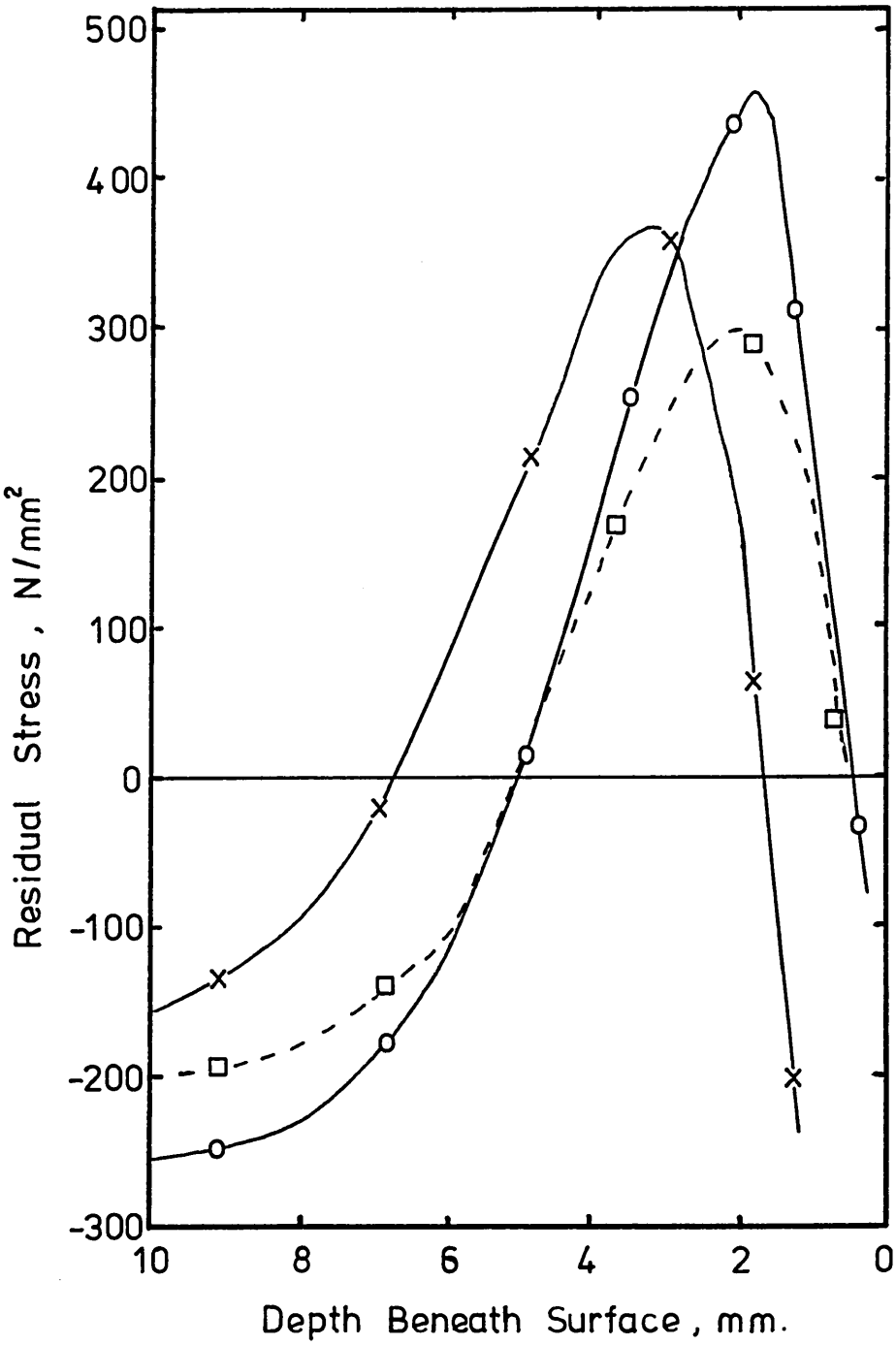

—o— Average Infinite Plate Results[49]

—×— Corrected Finite Model Results (factor, 1·5625)

--□-- Corrected Experimental Stress[49]

FIGURE 7.6-1

VARIATION OF EDGE CORRECTION FACTOR WITH TIME,
FOR A WATER QUENCHED 20 mm THICK PLATE

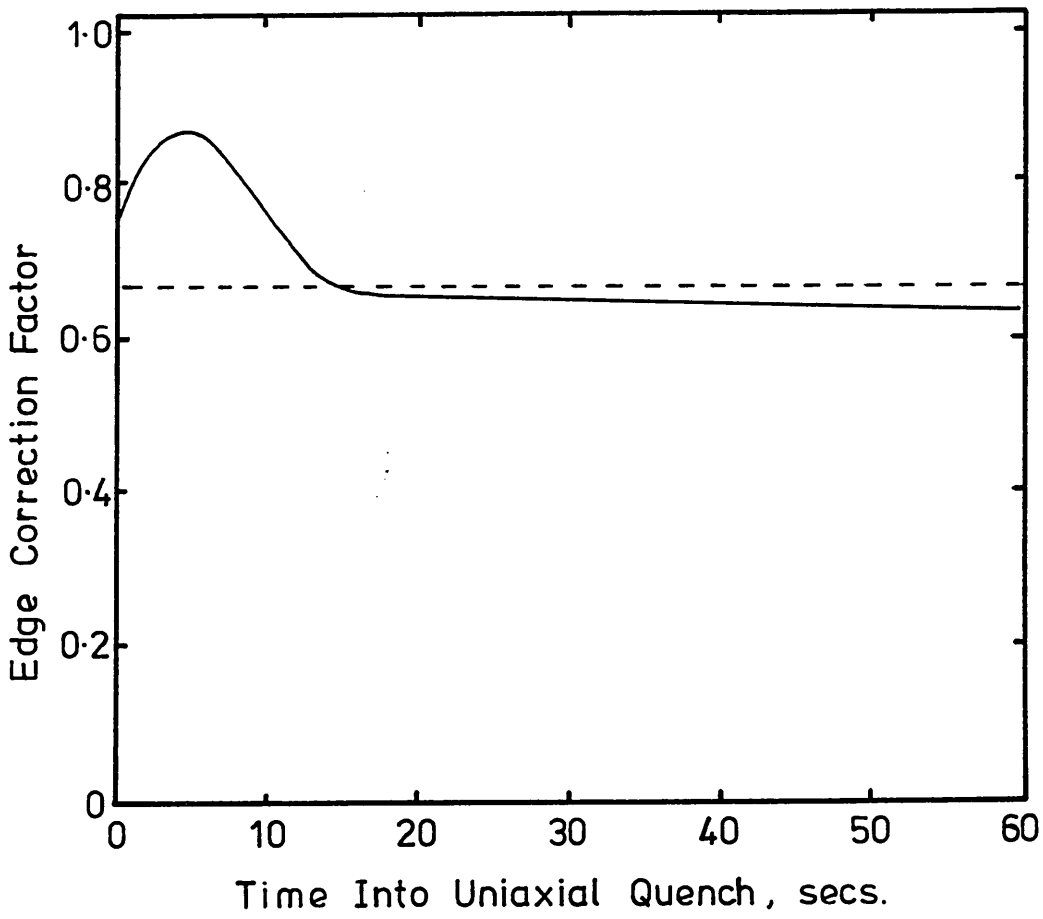

—— Calculated from the finite element model.

---- Saint Venant Principle.

FIGURE 7.6-2

EFFECT OF EDGE CORRECTION FACTORS ON THE DISTRIBUTION OF STRESS NEAR TO THE PLATE EDGE

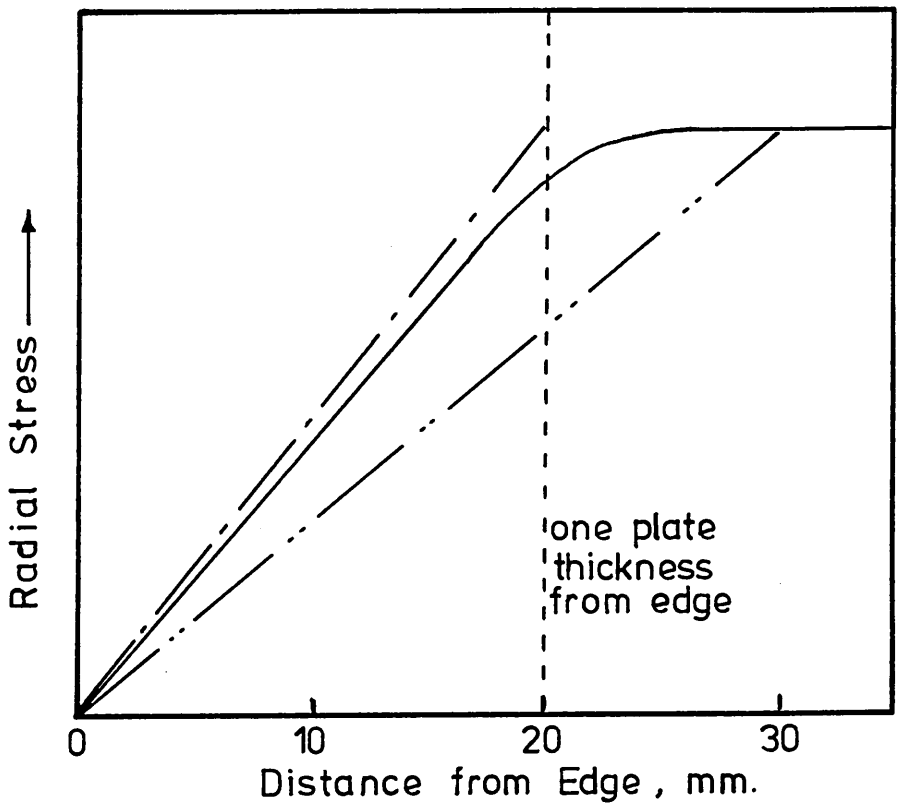

——— Factor 0·64, Finite element.

-—·— " 0·67, Saint Venant.

--—··— " 0·50, Fletcher & Price[49]

FIGURE 7.6-3

VARIATION OF EDGE CORRECTION FACTOR (ECF) FOR
IN-PLANE STRESSES WITH CIRCULAR PLATE GEOMETRY

x-x ECF based on Saint Venants Principle (Type 1)
o-o ECF derived from the finite element model (Type 1)
+-+ ECF based on Fletcher and Price[49] (Type 1)
□-□ ECF based on Saint Venants Principle (Type 2)

where, Type 1 is a linear derivation
Type 2 is an area derivation

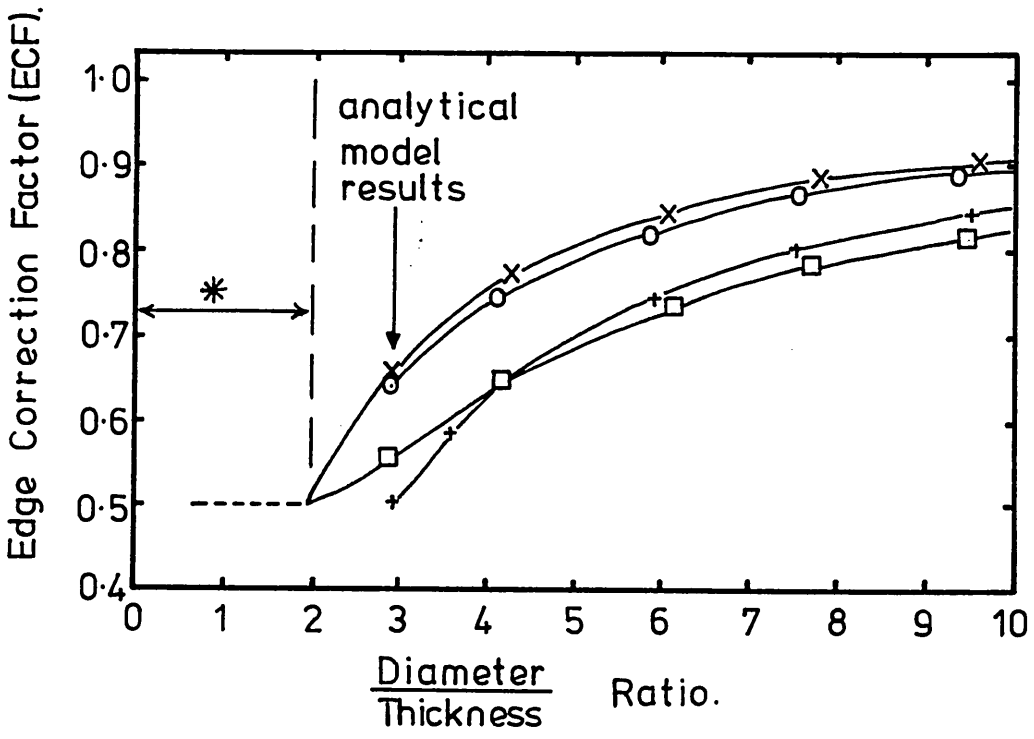

* Edge effected region penetrated to plate axis.

Reprinted from

MATERIALS SCIENCE AND TECHNOLOGY

Incorporating Metal Science and Metals Technology

THE INSTITUTE OF METALS
1 CARLTON HOUSE TERRACE LONDON SW1Y 5DB

7. S. DENIS, A. SIMON, and G. BECK: in Proc. Conf. on 'Eigenspannungen', Karlsruhe, April 1983, Deutsche Gesellschaft für Metalkunde, 211.
8. S. DENIS, A. SIMON, and G. BECK: *Härterei-Tech. Mitt.*, 1982, **36**, 18.
9. T. ERICSSON: in 'Hardenability concepts', (ed. D. V. Doane and J. S. Kirkaldy), 579; 1977, Warrendale, Pa, The Metallurgical Society of AIME.
10. S. SJÖSTRÖM: Doctoral thesis, University of Linköping, 1982.
11. H. FUJIO, T. AIDA, and Y. MASUMOTO: *Bull. Jpn Soc. Mech. Eng.*, 1977, **20**, 1655.
12. Y. DESALOS, J. GUISTI, and F. GUNSBERG: 'Déformations et contraintes lors du traitement thermique de pièces en acier', Report no. RE902, Institut de Recherches de la Sidérurgie Française, Germain-en-laye, 1982.
13. R. F. PRICE and A. J. FLETCHER: *Met. Technol.*, 1980, **7**, 203.
14. Internal report, British Steel Corporation, Swinden Laboratories.
15. G. W. GREENWOOD and R. M. JOHNSON: *Proc. R. Soc.*, 1965, **A283**, 403.
16. F. ABBASI and A. J. FLETCHER: *Mater. Sci. Technol.*, this issue, 830.

Appendix

The deviatoric stress and strain are given by

$$s_{ij} = \boldsymbol{\sigma}_{ij} - \delta_{ij}\sigma \quad \text{and} \quad e_{ij} = \boldsymbol{\varepsilon}_{ij} - \delta_{ij}\varepsilon$$

Under uniaxial conditions,

$$\varepsilon = \tfrac{1}{3}\varepsilon_{xx}(1-2\nu) \quad \text{and} \quad \sigma = \tfrac{1}{3}\sigma_{xx}$$

In the case of the Maxwell body,

$$\dot{e}_{ij} = \frac{\dot{s}_{ij}}{2\mu} + \frac{s_{ij}}{2\eta}$$

Hence

$$\frac{2(1+\nu)\dot{\varepsilon}_{xx}}{3} = \frac{\dot{\sigma}_{xx}}{3\mu} + \frac{\sigma_{xx}}{3\eta}$$

In the case of a stress-relaxation test, $\dot{\varepsilon}_{xx} = 0$. Therefore

$$\frac{\dot{\sigma}_{xx}}{3\mu} + \frac{\sigma_{xx}}{3\eta} = 0$$

On integration,

$$\ln \sigma_{xx} = \frac{-\mu t \ln (\sigma_{xx})_0}{\eta}$$

or

$$\frac{\sigma_{xx}}{(\sigma_{xx})_0} = \exp(-\mu t/\eta)$$

In the case of the Kelvin body,

$$2\eta\dot{e}_{ij} + 2\mu e_{ij} = s_{ij}$$

The same procedure as that detailed above gives $\sigma_{xx} = 2\mu\varepsilon_{xx}(1+\nu)$ when the conditions of the stress-relaxation tests are applied. The standard linear solid is described by

$$\dot{e}_{ij} + \lambda e_{ij} = \frac{\dot{s}_{ij}}{2\mu} + \frac{s_{ij}}{2\eta}$$

which becomes under uniaxial conditions

$$\dot{\varepsilon}_{xx} + \lambda\varepsilon_{xx} = \frac{\dot{\sigma}_{xx}}{2\mu(1+\nu)} + \frac{\sigma_{xx}}{2\eta(1+\nu)}$$

On integration

$$\frac{\sigma_{xx}}{(\sigma_{xx})_0} = \left[1 - \frac{2\lambda\eta(1+\nu)}{E}\right]\exp(-\mu t/\eta) + \frac{2\lambda\eta(1+\nu)}{E}$$

which gives, with the selection of suitable values of the constants, the best fit with the experimental stress-relaxation curves over the complete ranges of time and temperature examined.

Effect of free edge on thermal stresses in quenched steel plates

A finite-element technique has been used to examine the effect of the edge on the generation of thermal stress in a water-quenched circular plate of a steel of high hardenability. This allows results obtained using an infinite-plate model to be applied to finite bodies, where the stress distribution is influenced by the presence of a free edge. The radial residual stress begins to fall towards zero at a point about one-and-a-half plate thicknesses from the free edge. The variation in the stress in this part of the plate was complex and was accompanied by the development of an axial stress which was compressive up to a point close to the edge, where it became tensile. The variation in the hoop stress resembled that in the radial stress, but tensile values were always obtained at points on the edge. The mean value of the radial and hoop stresses in the edge-affected region was 75% of the stresses formed in the interior of the plate. This provides a suitable conversion factor when finite bodies are involved. *MST/5*

A. J. Fletcher
C. Lewis

 The authors are in the Department of Metallurgy, Sheffield City Polytechnic.

Introduction

The use of mathematical models to follow the creation of thermal stress during the quenching of steel components is complex, with the result that most work in this field has concerned relatively simple geometrical shapes, particularly cylinders, where the assumption of a plane-strain condition allows considerable simplification of the calculations. However, actual components generally have more complex shapes and the presence of unloaded edges causes substantial modification of the stress distribution near the edge. There have been few detailed investigations concerning the effect of the edge on the stress distribution in a component, and most have simply used the principle of Saint Venant to limit the edge-affected region to a distance from the edge equal to the fundamental dimension of the component[1] (for example, thickness in the case of a plate or disc). von Mises[2] suggested that in many components this was an underestimate of the effect of the edge, although it was probably a suitable criterion in the case of thin plates and long cylinders. The most complete study of the stress distribution close to a free edge was made by Horvay,[3,4] who showed that stresses would be generated perpendicular to the radial direction. However, the work was limited to an elastic analysis, whereas the thermal-stress calculations considered here require plasticity to be included. The only technique capable of handling such complex calculations is the finite-element method, which has been applied mainly to the mid-sections of cylinders.[5–8] The distortion of specimens studied by Toshioka[8] implies that the edge effect extends for a distance less than the diameter of the cylinder.

It is essential to have information about the effect of the edge on the stress distribution if reliable predictions are to be made about the stresses generated in components other than those of the most simple shapes. Even the stress distributions in discs of plate-shaped objects are much affected by the presence of a free edge, although a relatively simple plane-stress model will be possible at points well away from the circumference.† A plane-stress model has been used in conjunction with a suitable correction factor to compare the predicted residual-stress distribution in quenched plates with those obtained by experiment.[9] Two such factors have been used previously and each assumed a linear reduction in the stresses in the plane of the plate, beginning at a distance from the edge equal to either one or one-and-a-half plate thicknesses. These distances were based on Saint Venant's principle[1] in the first case, and experimental measurements of the point at which the faces of a quenched plate were no longer parallel in the second.[9] It was assumed in the latter case that changes in the thickness of the plate indicate a departure from the plane-stress condition as a consequence of the proximity of the unloaded edge.

As an alternative to the methods described above, the stress distribution in the edge-affected region may be obtained by the appropriate two- or three-dimensional calculation, the complexity of which requires the use of a finite-element technique. The whole period of the quench must be split into a series of very small time steps and the calculation repeated at each step, making even the two-dimensional problem discussed below very long and very expensive. It is unlikely that such calculations can be used widely to determine the thermal stresses set up in industrial quenching operations, but the present results are very useful as a check on whether the correction factors used in conjunction with a much simpler plane-stress model are valid. They also provide a valuable insight into the generation of thermal stress near a free edge, which may give an indication of what can be expected in bodies with a variety of different geometries.

On account of the large amount of data generated during the complete quench, this paper includes only the results pertaining to the very early stages of the quench, to the point just beyond the first appearance of plastic flow. This allows the effect of the edge on the stress distribution to be considered without the complications attendant upon the growth of the plastic zone, the reversal of the thermal stress, and the transformation of the austenite to martensite. These aspects are to be considered separately.[10]

Method of calculation

Both the temperature distribution and the associated thermal stresses were obtained by the use of the Bersafe finite-element program, developed by the Central Electricity Generating Board Laboratories, Berkeley. It was assumed that heat flow occurred only out of the faces of the plate; that is, the edges were assumed to be perfectly insulated.

The calculation of the temperature distribution during the quench used the Berkeley program FLHE which involved a Crank–Nicolson solution to the transient heat conduction equation. The basic element used to produce

† Subsequently referred to as the edge, in contrast to the plate faces, which are called surfaces.

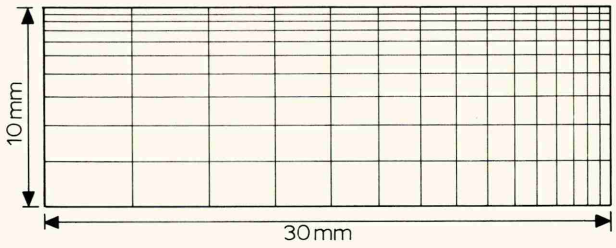

1 Mesh of single quadrant on plate

the mesh was an axisymmetric isoparametric element with four corner nodes, four midside nodes, and with a shape function that allowed a quadratic temperature variation in any plane. In view of the symmetry of the heat flow and the geometry of the disc-shaped specimen, it was necessary to consider only a single quadrant of a radial section, as shown in Fig. 1. The diameter of the disc was 60 mm and its thickness was 10 mm. This ensured that the central axis of the disc was outside the region of the specimen where the stress was influenced by the free edge at the circumference.

The size of mesh and the amount of bias required to establish instability was obtained by trial and error; the maximum mesh size at which satisfactory results were obtained is shown in Fig. 1. Although the unidirectional heat flow required bias only in the axial direction, the subsequent stress analysis required bias towards the edge as well. There was a relatively severe restriction on both the number of elements and Gauss points allowed during the plasticity stage of the calculation, so the mesh distribution shown in Fig. 1 is a compromise between the maintenance of stability in the calculation, the permitted number of elements and nodes, and the requirement that the aspect ratio of any element should not exceed 6. The temperatures obtained during the first three time intervals were used to obtain a weighted average of the intermediate value by means of the equation

$$\theta_t^* = \tfrac{1}{4}(\theta_{t-1} + 2\theta_t + \theta_{t+1})$$

where the subscripts refer to the time interval and the asterisk to the weighted average. The same equation was then used for every other set of three consecutive temperatures until the whole quenching period had been covered. The same procedure was subsequently used in the stress analysis. In order that the mesh of a single quadrant should be representative of the thermal stress generation processes in the whole structure, it was necessary that there should be zero radial displacement for any node that lay on the plate axis and that there should be zero axial displacement for any node that lay in the plane of symmetry of the plate (the central plane).

Plastic flow was initiated at an early stage in the quench, and the mechanical and physical properties of the material varied markedly as the temperature fell. Therefore the complete stress-generation process required a total of 52 elastic–plastic calculations in sequence, with 10 thermal loading increments of equal size in each calculation. The results reported here refer only to the first calculation, which covered only the first 0·2 s of the quench. Even so, this time was sufficient to generate plastic flow in some parts of the plate. Equilibrium was attained at each load step, and the iterative process by which this was achieved was continued until the residual load was 1% of the load increment. (Details of the method by which the plasticity calculation was carried out in the Bersafe program have been given by Hellen *et al.*[11])

Conditions at the central axis of the plate approximated very closely to the plane-stress conditions of an infinite plate subject to a unidirectional heat flow. Therefore, the results obtained previously[9] with identical data and an infinite-plate model provide a useful comparison with the present calculation. Provided the temperature distributions were identical, the level of agreement between the two sets of results was very good, although in the later stages of the quench a small discrepancy appeared in the two sets of temperatures obtained at the same time.

Table 1 Composition of 835 M30 (En 30B) steel, wt-%

C	Si	Mn	Cr	Mo	Ni	Fe
0·30	0·42	0·72	1·25	0·23	4·83	Bal.

Mechanical and thermal property data

The properties used were those of an air-hardening steel 835 M30 (En 30B), the composition of which is given in Table 1. The dilatometry data, the uniaxial relationships between stress and strain at the temperatures under consideration, and the surface heat transfer coefficients were obtained during an earlier investigation,[9,12] while the thermal conductivity, Young's modulus, and Poisson ratio data were obtained from a similar material.[13] The constraints of the program limited the relationships between stress and strain to 7 curves with 20 data points each. The Bersafe program did not allow the use of both a plasticity and a viscous-flow calculation, so the latter was excluded. The surface heat transfer coefficients were those pertaining to a water-quenched plate.[12]

Results

The effect of a free edge on the distribution of stress in a quenched plate is most readily examined in the very early stages of the quench, before the complications produced by

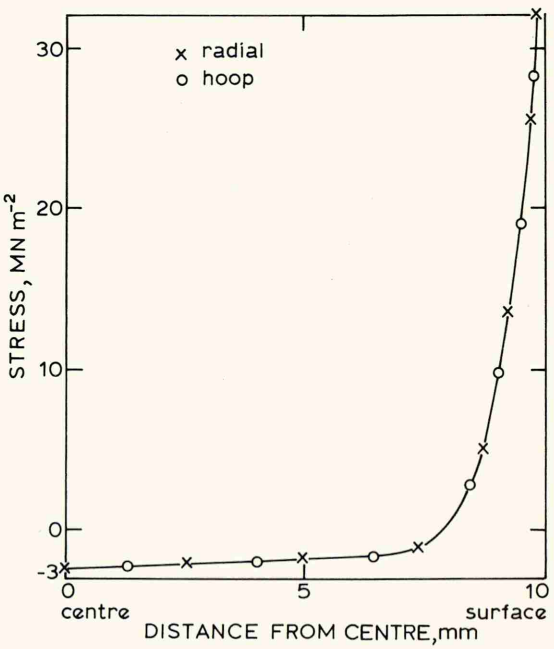

2 Relationship between stress and perpendicular distance from surface outside edge-affected region of plate (0·02 s)

plastic flow and stress reversals have appeared. Thus, the results shown in Figs. 2–9 are those obtained at the first incremental point of the loading sequence of the first calculation. This occurred after only 0·02 s, when the surface and centre temperatures were 840 and 850°C respectively. Well away from the edge (that is, one-and-a-half plate thicknesses distant) the stress distribution is identical to that predicted by the infinite-plate plane-stress model, in which a relatively large radial stress exists at the surface and a smaller compressive radial stress occurs towards the centre.

As the edge is approached these stresses decay until, at the edge, they become zero. The equations of equilibrium are

$$\frac{\partial \sigma_r}{\partial r} + \frac{\partial \tau}{\partial z} + \frac{\sigma_r - \sigma_\theta}{r} = 0$$

$$\frac{\partial \sigma_z}{\partial z} + \frac{\partial \tau}{\partial r} + \frac{\sigma_z}{r} = 0$$

where σ_r, σ_θ, and σ_z are the normal stresses in the radial (r), hoop (θ), and axial (z) directions, respectively, and τ is the shear stress in a radial section. As is clear from these equations, the decay is accompanied by changes in the hoop stress as well as the development of axial and shear stresses. These changes are considered just after the start of the quench when all the stresses are elastic.

RADIAL STRESS

Figure 3 shows that the rate of decay of the radial stress depends on position within the plate. At the surface this stress begins to decay at about one-and-a-half times the plate thickness from the edge; the initial rate of decay is small but it becomes progressively greater as the edge is approached (Fig. 4). In a direction just below but parallel to the surface, the tensile radial stress well away from the edge (GF in Fig. 3) is lower than at the surface, but the rate of decay is unchanged. Consequently the stress becomes zero some distance from the edge (at a point on AB in Fig. 3), after which it becomes slightly compressive before returning to zero (at a point on BC). The stress reversal becomes more pronounced as the distance of the section from the surface increases, and the magnitude of the maximum compressive stress may be greater than the original tensile stress present before the start of the decay process (compare points D and E). The tendency for the stress to become more negative during the approach to the edge persists even when the original stress (on line GF) is also negative. Therefore, in such cases there is an initial increase, rather than a decay, in the radial stress. Eventually, at a point very close to BC, the radial stress falls abruptly to zero, to comply with the boundary conditions at the free edge (Fig. 3).

Along lines close and parallel to the centreline, the compressive stress decays steadily but reaches zero a short distance from the edge. It then becomes slightly positive, before returning again to zero at the edge itself (Fig. 5).

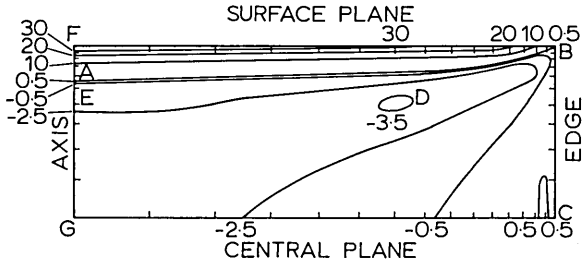

3 Distribution of radial stress near edge (0·02 s)

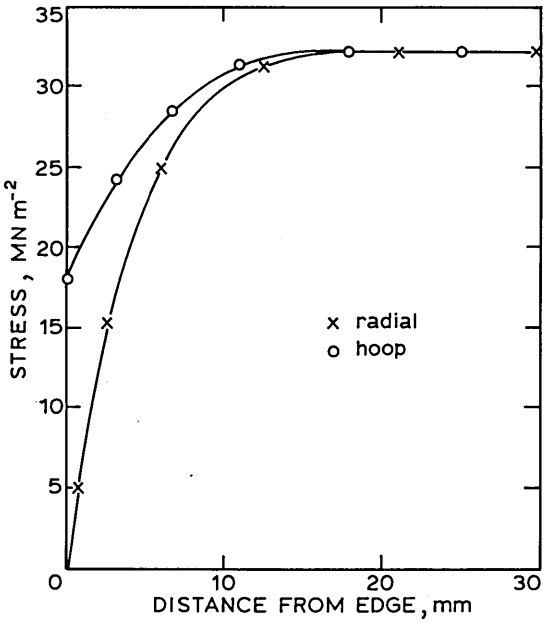

4 Distribution of stress along surface of plate (0·02 s)

This set of very complex results is the consequence of several factors:

(i) the requirement that the radial stress reaches zero at all points on the edge (BC)

(ii) the marked variation in the level of stress found at points well away from the edge (for example, GF in Fig. 3) before decay begins, with a consequent variation in the amount of decay required as the edge is approached

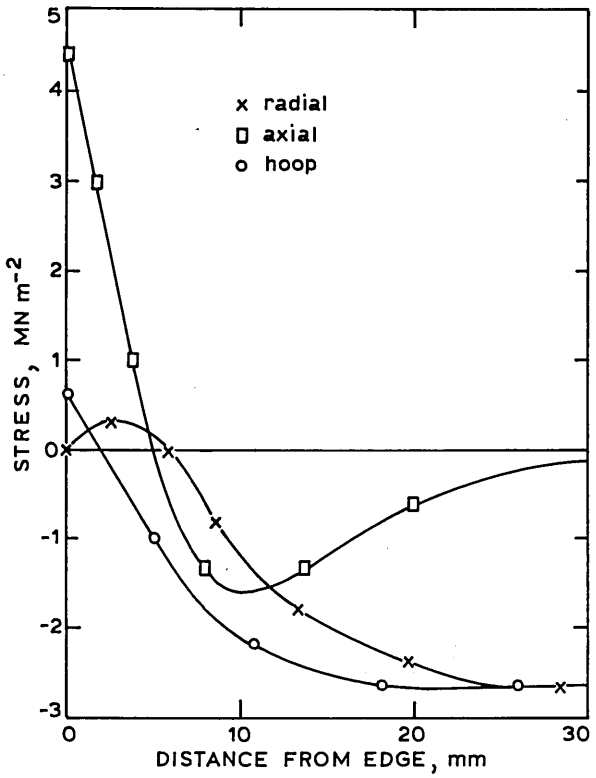

5 Distribution of stress along central plane of plate (0·02 s)

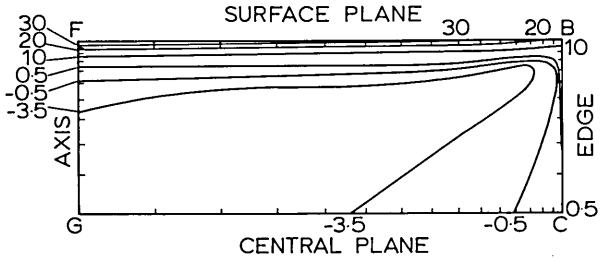

6 Distribution of hoop stress near edge (0·02 s)

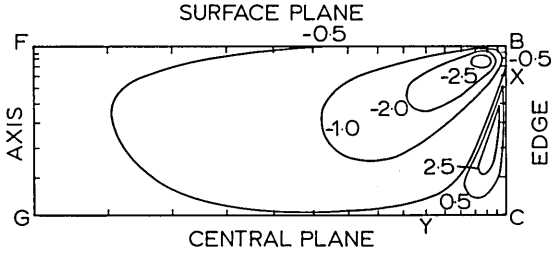

8 Distribution of shear stress near edge (0·02 s)

(iii) the requirement that the net force on any section perpendicular to the surface must be zero; this would account for the stress reversals associated with most longitudinal sections and the delay in the decay process in sections close to the midplane between surface and centre

(iv) the requirement that the rate at which the radial stress decays is related to other stress components through the equations of equilibrium.

HOOP STRESS

At points on GF in Fig. 3 the radial and the hoop stresses are equal (Fig. 2). As the radial stress decays towards the edge, the hoop stress changes in a similar but not identical fashion (*see* Fig. 6), although there is no requirement for the latter to reach zero at the edge. However, the equation of equilibrium shows that the rate of change in the radial stress is related to either the development of a difference between the hoop and radial stresses or the development of a shear stress gradient perpendicular to the surface. Hence, there is usually a small discrepancy between the hoop and radial stresses present at each point (*see* e.g. Figs. 4 and 5). In addition, the net hoop force on any radial section must be zero. Thus, over most of the section there is a net compressive force which has to be compensated for by tensile forces at all points along the edge. At the corner B this stress is substantial, since the hoop stress at the surface never falls to less than half its value at F.

Despite the differences already mentioned, the overall pattern of hoop stress resembles quite closely the corresponding radial-stress distribution (compare Figs. 5 and 6).

AXIAL STRESS

Under the plane-stress conditions found more than one-and-a-half times the plate thickness from the edge (along FG), there is zero axial stress at all points (Fig. 7). Likewise, there can be no axial stress normal to the plate surface which is not constrained. Over most of the section a small compressive axial stress is generated, which gradually becomes more negative towards the central plane. There is, however, a requirement that the net axial force on any section parallel to the surface plane must be zero, so a limited region of relatively high tensile stress exists close to the edge. A typical example of the change in axial stress as the edge is approached is shown in Fig. 5, which refers to the central plane of the plate.

There is a further constraint on the axial stress since the central plane is a plane of symmetry and must not therefore be subject to a net bending moment. The difference in length of lines parallel to the plate surface induced by the temperature gradient could be accommodated by the bending of the whole quarter-plate section shown in Fig. 1, particularly at points close to the edge, where such accommodation is not produced by radial stresses. Therefore the axial stresses produced along the central plane (CG) must be such as to maintain continuity with the plate on the other side of the plane; that is, the axial stresses must prevent any bending of the central plane that might be produced as a consequence of the thermal gradient perpendicular to the surface.

SHEAR STRESS

Over most of the edge-affected region the shear stress is compressive, but immediately adjacent to the edge there is a thin wedge-shaped region where the shear stress is tensile (Fig. 8). The apex of this wedge is on the edge close to the junction B with the surface. The regions of most intense shear are also close to the edge, with the most compressive stress adjacent to the junction and the most tensile stress in a lens-shaped region in the centre of the above-mentioned wedge. The shear stresses at points well away from the edge (on FG) and at points along the central plane are zero, as are the same stresses at points at the surface and edge, except immediately adjacent to the corner B. A line along which the stress is zero occurs between X and Y in Fig. 8.

EQUIVALENT STRESS

Although at this stage in the quench the deformation of the plate is elastic at all points, the variation in equivalent stress within the plate is a useful indication of the points at which plastic flow would be generated. For an infinite plate the maximum equivalent stress would be at the surface, and this is true also over much of the edge-affected region of a finite plate. However, in the latter case the surface equivalent stress falls to about half its original value by the time the junction with the edge is reached (Fig. 9). With minor variations, this stress falls rapidly as the perpendicular distance from the surface is increased. Therefore

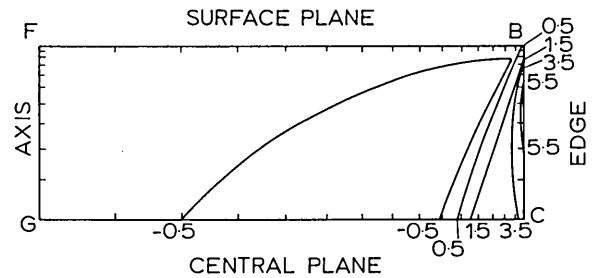

7 Distribution of axial stress near edge (0·02 s)

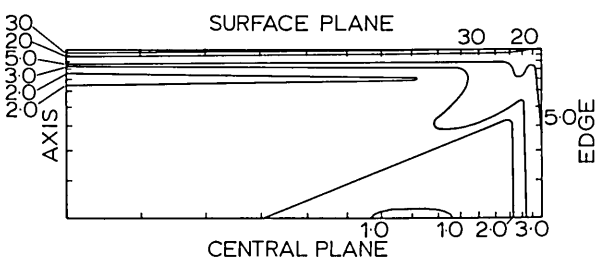

9 Distribution of equivalent stress near edge (0·02 s)

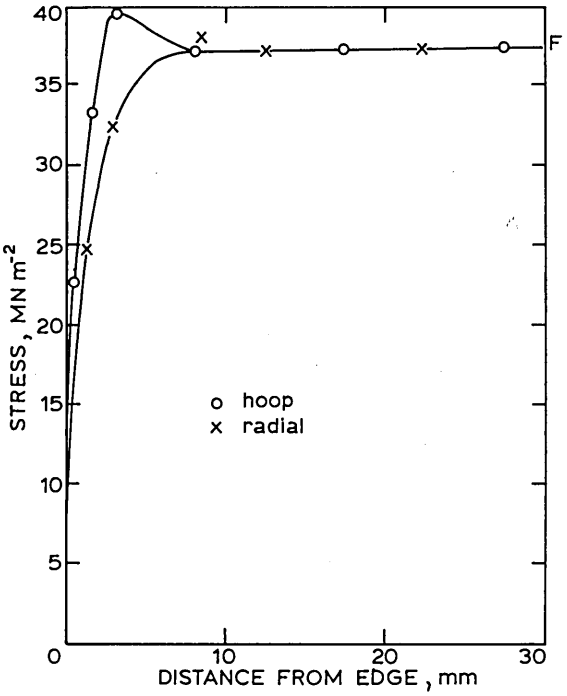

10 Distribution of stress along surface of plate (0·02 s)

one would expect the onset of plastic flow to occur at a point on the surface at least one plate thickness from the edge and at a value of equivalent stress identical to that predicted by an infinite-plate model.

ONSET OF PLASTIC FLOW

As the temperature gradient increases the general level of stress rises, although the pattern of stress distribution is very similar to that obtained at the shorter time. However, after 0·2 s the yield stress is exceeded and flow occurs in the vicinity of the plate surface between the points X and F in Fig. 10. The surface and centre temperatures are now 792 and 850°C, respectively. Flow occurs first at F, but the plastic zone then spreads quickly along the surface as far as X; at the same time it moves a short distance inward from the surface towards the central plane.

The consequence of the onset of plastic flow is to maintain the stress found well away from the edge at the value required to cause flow until a point relatively close to the edge is reached, with a consequent delay in the decay of the radial stress (Fig. 10). At the same time, the hoop stress rises slightly before returning to approximately its original value at the edge (Fig. 10). Apart from the overall increase in stress already referred to, the pattern of stress distribution is virtually unchanged by the onset of plastic flow, which is at this stage confined to a small region near the surface.

Comparison of calculated and experimentally determined thermal stresses

The distribution of thermal stresses may be calculated relatively easily by the use of an infinite-plate model.[9] However, the results of such calculations should not be applied to real components without taking into account the change in stress in the vicinity of the free edge. The two-dimensional finite-element calculation described here is an extremely long and costly operation and is not feasible as an everyday technique. Therefore there is a need for a correction factor with which to convert the more easily obtained infinite-plate results into average values applicable to a finite body. It is evident that the stress distributions described above are very complex, and the correction factor will depend on the depth below the surface of the plate at which the stress variation is considered.

Table 2 Correction factors in edge-affected region

Distance from surface, mm	Stress 30 mm from edge, MN m⁻²	Average radial stress in edge-affected region (30 mm from edge)		Average hoop stress in edge-affected region (30 mm from edge)
9·61	−2·7 centre	0·54		0·65
8·70	−2·7	0·56		0·67
7·79	−2·7	0·58		0·70
6·89	−2·7	0·64		0·73
5·98	−2·7	0·70		0·77
5·07	−2·7	0·73		0·85
4·15	−2·4	0·76		0·88
3·25	−2·0	1·20		1·50
2·26	−0·5	0·30		...
1·35	4·0	0·60		0·82
0·45	22·0 surface	0·74		0·91
Mean		0·67		0·84
Overall mean			0·75	
Value used by Fletcher and Price[9]			0·50	
Value obtained using Saint Venant's principle			0·67	

Table 2 gives the ratio of the average stress in the edge-affected region to the stress one-and-a-half plate thicknesses from the edge as a function of depth below the plate surface. It is evident that the mean ratio for the whole section is reasonably close to that obtained over large areas of the plate and could form a suitable basis for a single correction factor. At the points at which there are major discrepancies between the actual and the mean ratios the initial stresses tend to be close to zero, so that the inaccuracy resulting from such discrepancies is not very significant. Table 2 also gives the corresponding ratios considered by Fletcher and Price,[9] which were derived by assuming that the in-plane stress fell linearly to zero and that the regions affected by the stress decay were either one plate thickness (Saint Venant's principle) or one-and-a-half plate thicknesses away from the edge. The latter was the distance from the edge beyond which the two faces of a

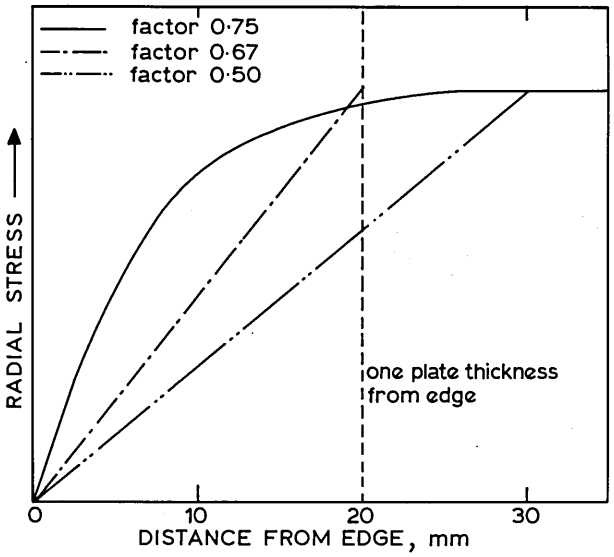

11 Effect of correction factors on distribution of radial stress near edge

quenched plate were parallel; that is, there was no further change in thickness as a consequence of variations in stress near the edge. The results given in Table 2 suggest an average correction factor that is considerably higher than that used by Fletcher and Price,[9] although it is only slightly higher than that obtained by the use of Saint Venant's principle. The distance from the edge at which the stresses in the plane of the plate begin to decay is in agreement with previously published results,[9] but the present work has shown that these stresses do not decay at a uniform rate as the edge is approached. Figure 11 compares a typical relationship between stress and distance from the edge at a correction factor of 0·75 with those obtained by using either Saint Venant's principle or the factor suggested by Fletcher and Price.[9]

The present calculations, of course, refer to the early stages of the quench, so that the use of these correction factors to modify residual-stress distributions requires information on any change in the factors as the quench continues. The development of the zone of plastic flow and the stress reversals later in the quench produce complex changes in the stress distribution near the edge. These changes and their effect on the correction factors referred to above are discussed elsewhere.[10]

Conclusion

The results of the finite-element calculation described in this paper show that the stresses present in a circular disc during the early stages of a quench in water vary in a very complex manner as the unloaded circumference of the disc is approached. The average level of the stresses in the plane of the plate is about 75% of the stresses formed in the interior of the body. This is significantly higher than previous estimates would suggest.

Acknowledgments

The authors wish to thank the Science and Engineering Research Council for the award of a grant which enabled the work to be carried out. Thanks are also due to Dr B. Hudson of AERE Harwell, and the staff of the finite-element groups at both the Rutherford and Appleton Laboratories, Chilton, and the CEGB Laboratories, Berkeley, for helpful discussions and advice.

References

1. J. N. GOODIER: *Philos. Mag.*, 1937, **23**, 607.
2. R. von MISES: *Bull. Am. Math. Soc.*, 1945, **52**, 555.
3. G. HORVAY and N. Y. SCHENECTADY: *J. Appl. Mech.*, 1953, **20**, 87.
4. G. HORVAY: *J. Mech. Phys. Solids*, 1957, **5**, 77.
5. S. TAIRA, T. INOUE, and H. UEDA: in Proc. 14th Jap. Congr. on Materials Research, Kyoto, 1970, 165.
6. T. INOUE and K. TANAKA: *Int. J. Mech. Sci.*, 1975, **17**, 361.
7. S. SJÖSTRÖM: Thesis, University of Linköping, 1982.
8. Y. TOSHIOKA: *Tetsu-to-Hagané (J. Iron Steel Inst. Jpn)*, 1976, **62**, 1756.
9. A. J. FLETCHER and R. F. PRICE: *Met. Technol.*, 1981, **8**, 427.
10. A. J. FLETCHER and C. LEWIS: unpublished work.
11. T. K. HELLEN, W. G. GALLUZZO, and A. P. KFOURI: *Int. J. Mech. Sci.*, 1977, **19**, 209.
12. R. F. PRICE and A. J. FLETCHER: *Met. Technol.*, 1980, **7**, 203.
13. British Steel Corporation, Swinden Laboratories, Internal Reports.

Numerical calculations of residual-stress relaxation in quenched plates

Methods of thermal stress relief such as stretching and compression are compared for different thermal and mechanical properties during quenching. The heat equation for a simple geometric model, such as an infinite plate, is solved with an experimental surface conductance and a step-by-step method of determining the temperature field in the thickness of the plate. This field is introduced as data for the uncoupled thermal elastic–plastic model for quenching. In the calculation of the plastic-strain path, the thermal and mechanical properties are considered as temperature dependent for a homogeneous and isotropic material. Good agreement is found between the calculated residual stresses and experimental values for an aluminium alloy and a stainless steel. The predicted residual-stress distributions and strain history are then used as data for the numerical simulation of stress-relief methods with an incremental integration of the Prandtl–Reuss equation. This analysis allows the observation of the effects of small variations in mechanical properties during quenching on the residual-stress field after mechanical stress relief and the theoretical comparison of different processes.

MST/6

J. C. Boyer
M. Boivin

 The authors are in the Laboratoire de Mécanique des Solides, Institute National des Sciences Appliquées de Lyon, Villeurbanne, France.

List of symbols

A	thermal diffusivity
e	thickness of plate
E	Young's modulus
$\bar{h}$	surface heat transfer coefficient
H'	strain hardening coefficient
S	reduced deviatoric stress
t	time
T	temperature of point in plate
T_s	temperature of plate surface
T_∞	temperature of cooling fluid
x_i	coordinates of point in plane ($i = 1, 2, 3$)
α_i	coordinates of centre of yield surface in deviatoric stress space ($i = 1, 2, 3$)
β_n	roots of equation (4)
ε^{el}	elastic strain
ε^{pl}	plastic strain
$\bar{\varepsilon}^{pl}$	equivalent plastic strain
ε^{tot}	total strain
λ	linear thermal expansion coefficient
ν	Poisson's ratio
σ	principal stress
$\bar{\sigma}$	equivalent stress
$\bar{\sigma}_f$	flow stress
$\bar{\sigma}_y$	yield stress

Subscripts

1, 2	components of quantity in x_1 and x_2 directions

Introduction

A mixed method is proposed for calculating with a desktop computer the internal stresses and strains in a thick plate after quenching and relaxation by stretching and compression. The technique allows the use of various hardening and constitutive laws for the different processes. The material is assumed to be homogeneous, isotropic, and without phase transformation. Applications of the method for two materials, a stainless steel and an aluminium alloy, are compared with experimental data.

Quenching model

The geometric structure is an infinite plate with heat flow only in a direction perpendicular to the longitudinal plane, taken as the x_3 direction (Fig. 1).[1] Thermomechanical coupling is neglected. The field of thermal stress is evaluated step by step using a well known solution of the equations for transient heat conduction in an infinite plate.[2]

For each time interval dt, the temperature distribution is obtained from the solution of the heat equation

$$\frac{\partial T}{\partial t} = A\frac{\partial^2 T}{\partial x_3^2} \qquad (1)$$

where A is the constant thermal diffusivity calculated with the mean temperature in the thickness of the plate at the beginning of the time interval. The boundary conditions describing the heat flow on the faces of the plate are

$$(\pm)\frac{\partial T}{\partial x_3} + \bar{h}(T_s - T_\infty) = 0 \quad \text{at} \quad x_3 = (\pm)\tfrac{1}{2}e \qquad (2)$$

where the surface heat transfer coefficient $\bar{h}$ is considered to be constant during the infinitesimal time interval dt for constant surface temperature T_s in a cooling fluid at constant T_∞ during quenching. The temperature at the end of the interval dt is given by

$$T(x_3, t) = T_\infty + 2\sum_{n=1}^{\infty} \exp(-A\beta_n^2 t)\frac{(\bar{h}^2+\beta_n^2)\cos(\beta_n x_3)}{\frac{1}{2}(\beta_n^2+\bar{h}^2)e+\bar{h}} \times \int_0^{e/2} [T(x_3, t-dt) - T_\infty]\cos\beta_n x_3\, dx_3 \qquad (3)$$

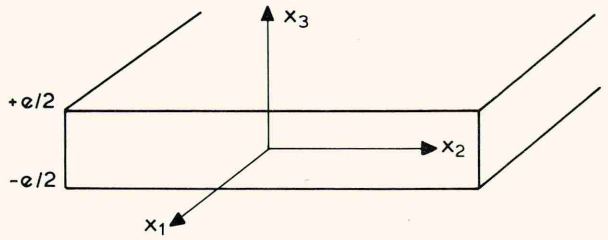

1 Coordinate system for infinite plate of thickness *e*